Doctoral Dissertations   Dissertations and Theses

March 2020

MOLECULAR DESIGN OF ORGANIC SEMICONDUCTORS FOR INTERFACIAL AND EMISSIVE MATERIAL APPLICATIONS

Marcus David Cole
University of Massachusetts Amherst

MOLECULAR DESIGN OF ORGANIC SEMICONDUCTORS FOR INTERFACIAL AND
EMISSIVE MATERIAL APPLICATIONS

A Dissertation Presented

by

MARCUS DAVID COLE

Submitted to the Graduate School of

the University of Massachusetts Amherst in partial fulfillment

of the requirements for the degree of

DOCTOR OF PHILOSOPHY

February 2020

Polymer Science & Engineering Department

MOLECULAR DESIGN OF ORGANIC SEMICONDUCTORS FOR INTERFACIAL AND
EMISSIVE MATERIAL APPLICATIONS

A Dissertation Presented

by

Marcus David Cole

Approved as to style and content by:

_____

Todd Emrick, Chair

_____

Michael Barnes, Member

_____

Ryan Hayward, Member

_____

E. Bryan Coughlin, Department Head
Polymer Science and Engineering

DEDICATION

To James and Vincent, whom I hope I have made proud

ACKNOWLEDGMENTS

for being encouraging voices as I progressed through my doctoral work. Also, a special thank you to my fraternity brother Ryan Handley for your undying support.

This experience would not have been possible without the love and support of my family. I would like to thank my loving sister Deona and my parent Dave and Patrina for always believing in me and keeping me in their thoughts and prayers. I also like to thank my many uncles, aunts and cousins who have offered their support in a multitude of ways. I would like to give a special thank you to my grandmothers, Helen and Agnes, who have always urged me to believe in myself and have supported all of my goals. Finally, I would like to thank my loving partner Anna Klebanowska. I never imagined meeting someone with whom I connect with so deeply and honestly. You are gift that I will forever be grateful for.

ABSTRACT

MOLECULAR DESIGN OF ORGANIC SEMICONDUCTORS FOR INTERFACIAL AND
EMISSIVE MATERIAL APPLICATIONS

MARCUS D. COLE, B.S., UNIVERSITY OF SOUTH CAROLINA COLUMBIA

M.S., UNIVERSITY OF MASSACHUSETTS AMHERST

Ph.D, UNIVERSITY OF MASSACHUSETTS AMHERST

Directed by: Professor Todd Emrick

This dissertation describes the synthesis and characterization of functional
optoelectronically active materials. Synthetic techniques were used to prepare polymers containing
perylene diimide (PDI) or tetraphenylethylene (TPE) moieties in the polymer backbone. PDI-
based structures were prepared with embedded cationic or zwitterionic moieties intended to tailor
organic/inorganic interfaces in thin film photovoltaic devices. The aggregation-induced emission
(AIE)-active TPE polymers were synthesized to study how AIE properties evolve in π-conjugated
polymers. The syntheses discussed here focused on modulation of molecular architecture to give
rise to materials with tailored optoelectronic properties.

Chapter 1 provides a brief overview of the field of organic electronics and the key concepts
underpinning this thesis research. Chapter 2 describes the synthesis of PDI-containing polyionenes
and linear polymer zwitterions. Dual-functional PDI monomers containing tertiary amines at the
imide position, and bulky bromide or phenyl groups at the aromatic core, afforded reactive and
high solubility monomers. Polymers with ammonium bromide and sulfobetaine functionality in
the backbone were prepared by reacting PDI monomers with the appropriate electrophiles. By

controlling PDI content, macromolecular structures with tunable PDI-PDI interactions were achieved and studied spectroscopically. Chapter 3 focuses on integration of novel PDI-based materials into organic and perovskite solar cells as interfacial layers. The interfacial properties, morphology, and device enhancement were studied as a function of PDI incorporation in the polymer backbone. Trends in electronic properties and device performance were correlated to polymer structure and revealed a strong dependence on the selection of cationic *vs.* zwitterionic functionality. The PDI-containing polymers were found to enhance photovoltaic device performance, despite not being continuous conjugated structures, but rather having conjugated molecular segments in the polymer backbone. The effective work function modification of metal cathodes and energy level overlap with perovskite active layer permitted enhanced device performance when tertiary amine-functionalized PDI small molecules were incorporated into devices. Chapter 4 centers on the synthesis and characterization of conjugated polymers containing TPE. The optical properties of these materials were adjusted by controlling extent of vinylene groups in the polymer backbone. These vinylene-containing TPE polymers exhibited similar optical and electronic properties to poly(phenylene vinylene) (PPV) while maintaining the desirable AIE properties of TPE. Moreover, by controlling the mole percent of TPE in PPV copolymers aggregation-caused quenching (ACQ) was attenuated without perturbation of PPV's optical properties. Finally, Chapter 5 projects an outlook of the discussed research. Emphasis is given to where research focus should be oriented to advance the technology beyond the academic space. The aim of this chapter is to highlight the impact of this work and its relationship to bringing the science closer to the general public. The experimental procedures of the materials synthesis, characterization, and device fabrication are then detailed in Chapter 6.

TABLE OF CONTENTS

LIST OF TABLES

LIST OF FIGURES

LIST OF SCHEMES

CHAPTER 1

ORGANIC OPTOELECTRONIC MATERIALS AND THEIR APPLICATIONS

1.1 Overview of organic semiconductors and their applications

Conjugated molecules capable of interacting with the electromagnetic spectrum and/or transporting electrical charges are prevalent throughout nature (Figure 1.1). The cyclic pyrrole tetramer, known as porphyrin, is the photoactive component in chlorophyll and stabilizes iron in heme to transport oxygen in red blood cells. Chromophores such as retinal enable vision as the photosensitive component of photoreceptor cells in the retina of organisms with advanced optical receptors, while other pigments such as beta-carotene and lycopene provide color to food. The electrical and optical properties of these materials arise from the configuration of the π-bonds present in their molecular structure. The alternating δ-bond/π-bond architecture delocalizes electrons through π-orbital overlap, stabilizing these systems due to the availability of resonance structures (Figure 1.2).

(A)   **(B)**   **(C)**
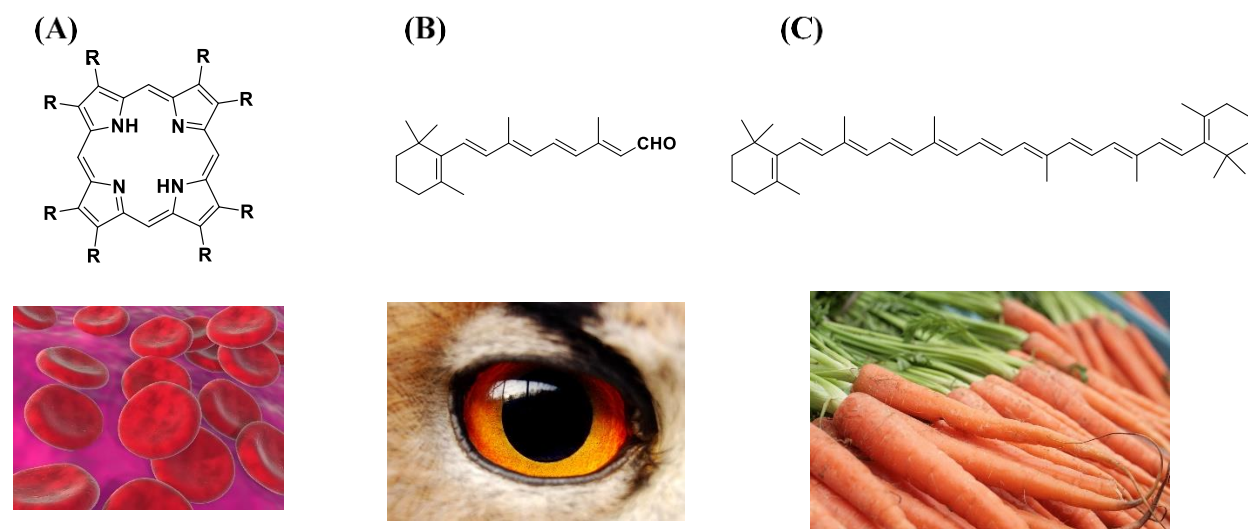
Figure 1. 1. Structures of naturally occurring conjugated structures (A) porphyrin; (B) retinal; and (C) beta-carotene and where they are found.
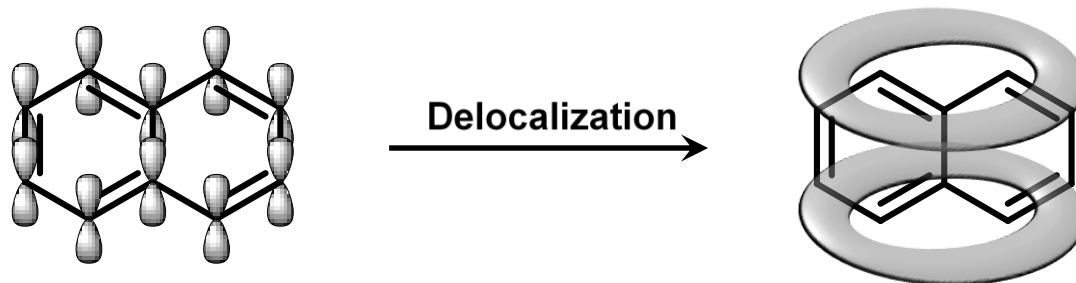
Figure 1. 2. Schematic of delocalization of electrons through π-orbitals in naphthalene

The unique properties of these biological molecules have been harnessed in synthetic structures to develop organic semiconductors. Organic/soft electronics are more versatile when compared to traditional inorganic materials that comprise hard electronics. These organic materials can be processed from solution and modified synthetically with useful functionality. The unique properties of these materials can afford low-cost approaches to fabricate lightweight, thin film devices well-suited for emerging technologies such as wearable electronics and biological sensors.[1] Early work in organic semiconductor synthesis produced polyacetylene[2] and tetrathiafulvene-tetracyanoquinodimethane (TTF-TCNQ) salts[3] which exhibited high conductivities but lacked the necessary solubility and processability for thin film fabrication. The issue of solubility was addressed through the development of polymers containing solubilizing side groups, such as poly(para-phenylene vinylene)[4] and poly(alkylthiophenes).[5] Synthetic advances in recent years have resulted the synthesis of a vast library of conjugated small molecules
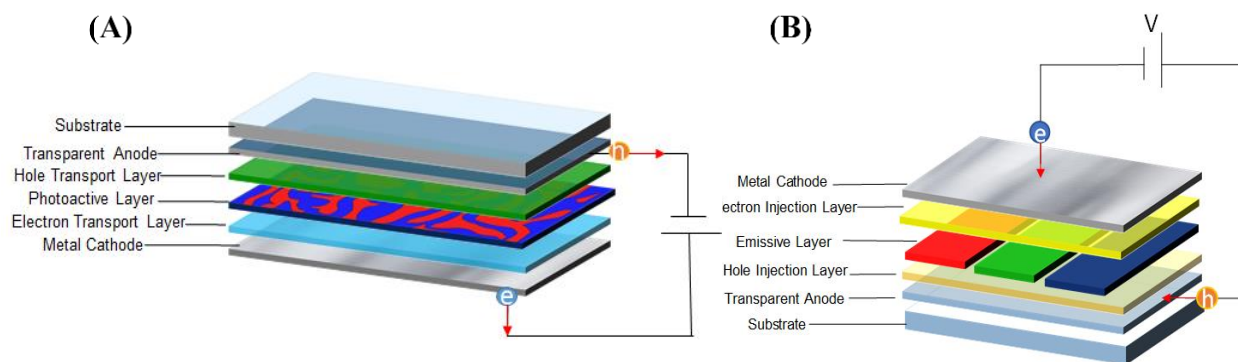
Figure 1. 3. Device architecture of (A) OPV and (B) and OLED devices.

2

and polymers with controllable molecular weights, optoelectronic characteristics, and solution properties. Through these synthetic achievements, solution-processable organic/polymeric semiconductors have been integrated into device architectures such as organic light-emitting diodes (OLEDs) for displays and organic solar cells (OSCs) (Figure 1.3). This thesis work focuses on the synthesis and characterization of novel optoelectronic polymers that represent useful synthetics pathways to materials capable of enhancing the performance of OSC or producing superior emission in the aggregated state.

1.2 Structure property relationship of perylene diimides

Chapter 2 details the synthesis and characterization of perylene diimide (PDI)-based polyionenes and polymer zwitterions. Perylene is a polycyclic aromatic hydrocarbon which is used today as an industrial colorant[6] but lacks solubility in most organic solvents, limiting its utility in thin film electronics. Appending the perylene structure with solubilizing imide groups has proven to be an effective approach to preparing solution processable perylene derivatives (Figure 1.4). PDIs commonly employ bulky substituents at the imide position to achieve optimum
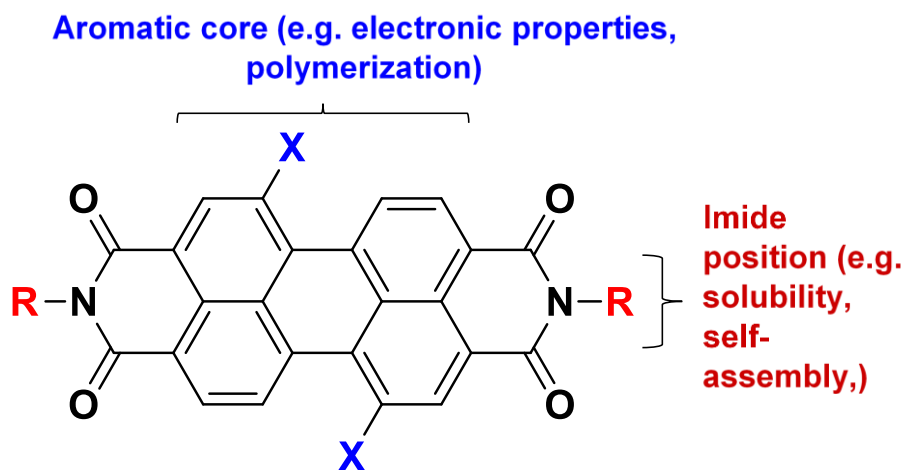
Figure 1. 4. Structure of PDI and the influence of functionality at its imide and aromatic core positions.

3

solubility.[7–9] The two imide groups draw electron density from the aromatic core, resulting in low lying lowest unoccupied molecular orbital (LUMO) (4-5 eV) and highest occupied molecular orbital (HOMO) (6-7 eV). The influence of PDIs energy levels is reflected by its strong electron-accepting behavior. Density-field theory (DFT) calculations have revealed the presence of nodes in the LUMO and HOMO located at the imide nitrogen atoms. [10] This permits modification of the solution properties without significant perturbation of intrinsic photophysical and electronic properties. Due to PDI's structural tunability and high electron affinity, it has found utility as an electron-acceptor in OSCs and active layer in n-type field-effect transistors.[11–14]

In addition to PDI's exceptional optoelectronic properties, its π-π-driven self-assembly into ordered structures is also noteworthy. The assemblies can be modified by introducing functionality with affinities to substrates or solubility properties at the imide group and/or the perylene aromatic core. Hydrogen bonding,[15] electrostatic attraction,[16] co-assembly with other electronically active molecules,[17] and solvent selection[18] have all been shown as methods for
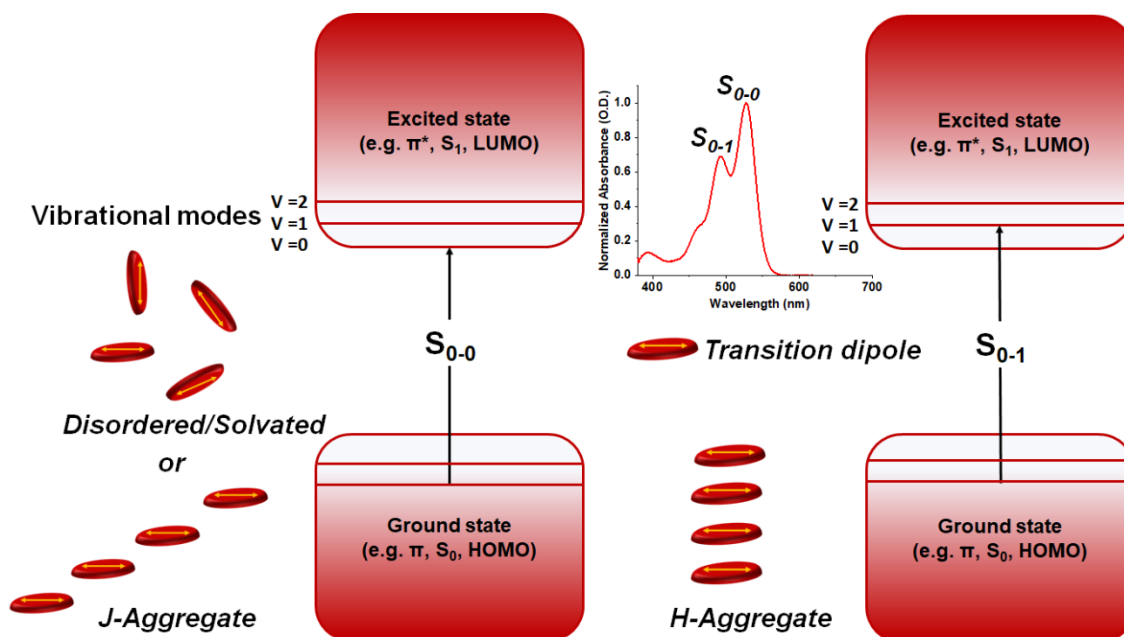
Figure 1. 5. Electronic and vibronic transition in relation to spectral features afforded by transition dipole coupling.

controlling PDI assembly morphology. These PDI assemblies have been reported to form a variety of structures including, nanowires, fibrils, sheets, and nanotubes.[19–21] PDIs exhibit distinct absorption and photoluminescent spectral features, which arise due to interaction of the PDI transition dipole with the local electronic environment. Transition dipoles couple π-conjuaged structures, such as PDIs, to the electromagnetic spectrum and other electronically-active molecules, allowing for absorption of photons of a specific energy or through-space interactions, respectively. In dilute solutions PDI small molecules are freely dispersed; as such, there is no overall alignment of the transition dipoles. This is reflected in the absorption spectra, in which the singlet transition from the ground state to the lowest vibronic band of the first excited state (S_{0-0}) is the dominant and is followed by the lower intensity hypsochromic S_{0-1} transition which arises from the population of the higher vibronic state of the first excited state.[22–24] These features also differentiate J-type aggregation, in which the transition dipoles are offset from each other, from co-facial H-type aggregates, in which the transition dipoles are aligned parallel to each other (Figure 1.5). These spectral signatures are further explored in chapter 2 as they relate to polymer composition.

1.3 Interfacial engineering in photovoltaic devices

Organic photovoltaics (OPVs) offer many advantages over traditional silicon based photovoltaic devices. The solution-processable components of OPV devices can be fabricated in high volumes using low temperature processing conditions to realize low-cost systems. Early work in silicon alternatives to harvesting solar energy focused on photogalvanic (PG) cells.[25] PG devices experienced limitations primarily due to the absence of proper charge selectivity for efficient charge extraction.[26] Introduction of electron-donating, mesoporous metal oxides-supported dyes in dye sensitized solar cells (DSSCs) produced moderate charge selectivity, but still suffered from
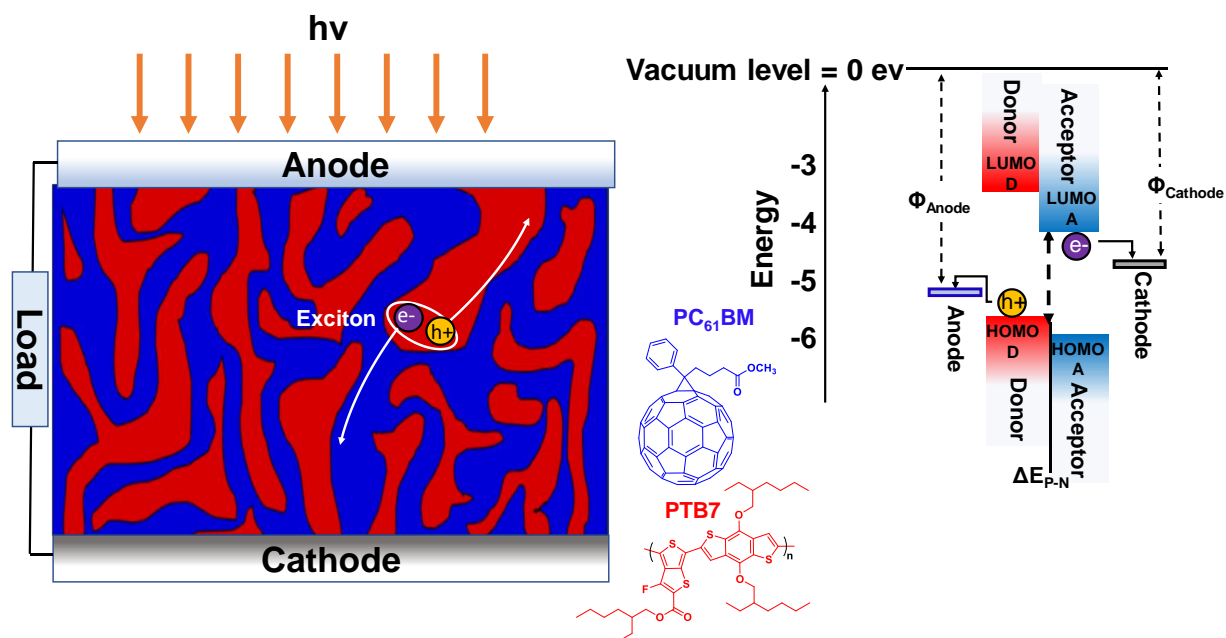
Figure 1. 6. Cross section schematic of photoexcitation in BHJ with electron donor (PTB7) and acceptor (PCBM) structures in a photovoltaic device and energy level diagram of charge extraction.

low power conversion efficiencies and required leachable, liquid electrolyte solutions.[27] The disadvantages of PGs and DSSCs guided further research to develop high performing photovoltaic devices.

Conventional OPV devices are comprised of a photoactive layer containing a p-type electron donor (red), such as poly({4,8-bis[(2-ethylhexyl)oxy]benzo[1,2-*b*:4,5-b′]dithiophene-2,6-diyl}{3-fluoro-2-[(2-ethylhexyl)carbonyl]thieno[3,4-*b*]thiophenediyl}) (PTB7), and an n-type electron acceptor (blue), such as [6,6]-phenyl-C_{61}-butyric acid methyl ester (PCBM), forming a bulk-heterojunction (BHJ) as shown in Figure 1.6. The BHJ is sandwiched between and electrodes which collect charges. Upon photoexcitation an electron-hole pair (i.e., an exciton) is formed in the p-type material. This exciton diffuses to the p-n interface in the BHJ, and under an internal voltage the electron and hole separate into free charge carriers. The BHJ must exhibit sufficient thickness (~50 nm) for maximum light absorption and morphology on the length scale of the

6

exciton's diffusion length (~10 nm) for efficient free charge generation.[28] The holes and electron

travel through the HOMO of the p-type material and LUMO of the n-type material, respectively.

Finally, holes and electrons are collected at the appropriate electrodes to produce a current as

shown in Figure 1.6.

The performance of the device is determined by extracting the photovoltaic metrics: short-

circuit current density (J_{sc}), open-current voltage (V_{oc}), fill-factor (FF), and power conversion

efficiency (PCE) (Figure 1.7). The J_{sc} corresponds to the maximum measurable current in the

absence of an applied bias and is associated with photocurrent generation efficiency. The V_{oc} is

the voltage at which all the charges recombine within the solar cell and are not extracted out into

the external load. The V_{oc} is influenced by several factors, including the energy difference between

the HOMO of the p-type materials and LUMO of the n-type materials (ΔE_{P-N}), light intensity,

exciton recombination, etc.[29] One factor, which is highlighted in this thesis work, is the anode-

cathode work function offset (Φ_{A-C}), which can be tailored by interfacial modification. The FF

reflects the "squareness" of the current density-voltage (J-V) curve and the ratio of the integrated

$$FF = \text{Area X/Area Y} = [V_{mp} * J_{mp}]/[V_{oc} * J_{sc}]$$

$$P_{max} = J_{sc} * V_{oc} * FF$$

$$PCE = P_{max}/P_{in}$$
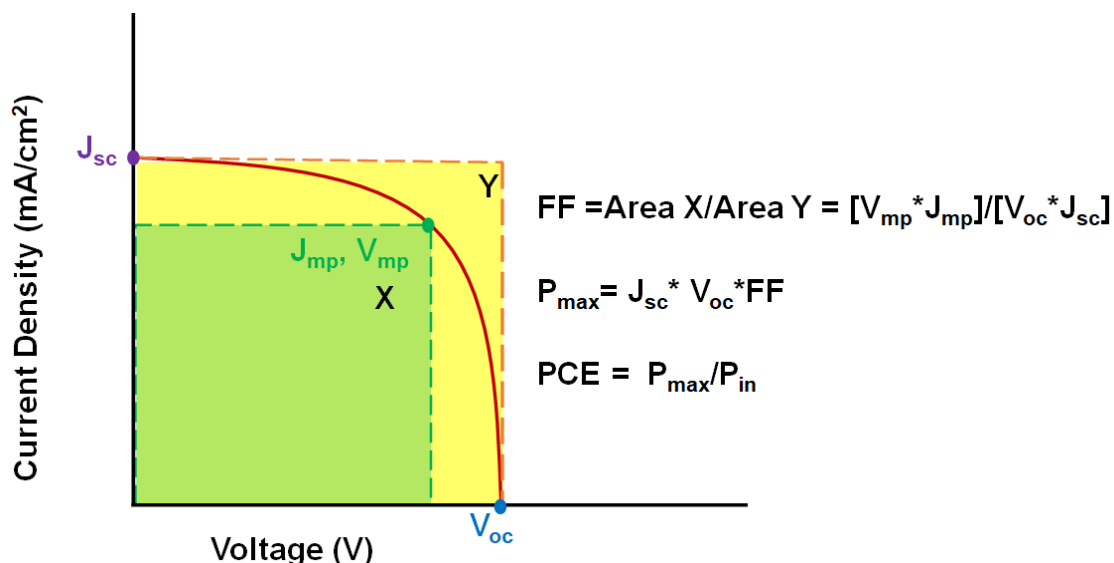
Figure 1. 7. Representative J-V curve of a photovoltaic device and relevant metrics used to determine photovoltaic performance.

area from the J_{sc} and V_{oc} to the current density (J_{mp}) and voltage (V_{mp}) at maximum power output in the J-V (Figure 1.7). The FF is correlated with recombination events in the photovoltaic device. Finally, the PCE is determined by the ratio of the maximum power output (P_m) to the incident power of the light source (P_{in}), as shown in Figure 1.7. Together these photovoltaic metrics provide key information on device performance and how it might be improved by adjusting the materials utilized as active layers or interlayers.

A multi-layered OPV device contains several interfaces at which device failure or enhancement can occur. While the realization of BHJ systems improved donor-acceptor surface area and created desirable length scale for exciton diffusion, this mixed morphology also resurrected contact selectivity issues found in PGs.[30] Methylammonium lead halide ($MAPbX_3$) perovskite solar cells have also become popular as active layer materials. In perovskites, the need for mixed donor-acceptor systems is circumvented due to the ability of perovskites to effectively transport both holes and electrons. While perovskite solar cells (PSCs) have been shown to produce PCE values > 22%[31] they still suffer from limitations in charge selectivity at the electrodes. [32–38] In the absence of charge selective contacts, photocurrent generation is significantly impeded by the recombination of holes and electrons at the active layer/electrode interface.[39,40] Even with the advances in active layer materials and morphology, device performance issues have persisted and must be addressed with novel solutions to achieve high performing and sustainable devices.

Tailoring the organic/inorganic interface of the active layer material with the metal and/or metal oxide electrode is crucial to device performance.[27,41–43] This thesis work will highlight materials for the active layer/cathode interface where it is desirable to introduce materials that can facilitate electron injection and blocks hole transport. Metal oxides such as zinc oxide (ZnO), titanium oxide (TiO_x), niobium oxide (Nb_2O_5), and tin oxide (SnO_2) have been commonly

8
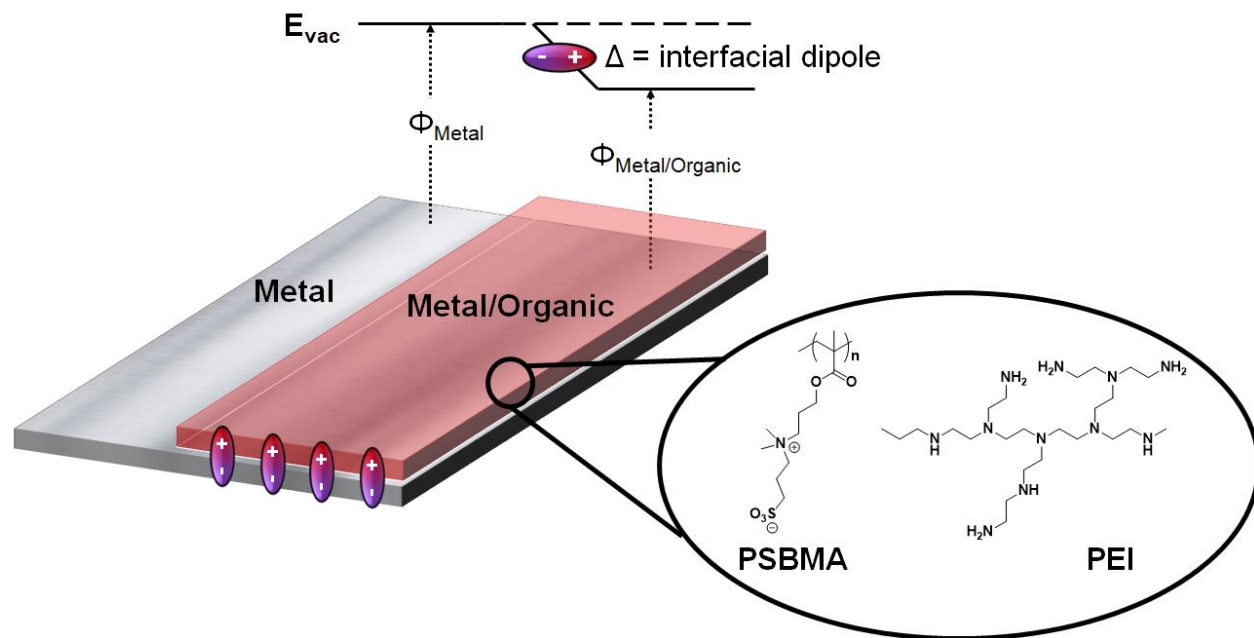
Figure 1. 8. The mechanism of work function modification of a metal substrate by introduction of organic layer with structures capable of producing negative interfacial dipoles.

employed as electron selective layers in OPV[44–47] and perovskite-based devices.[48–53] While these interfacial materials have found some success in improving device performance, they require high temperature processing conditions to form uniform films. An alternative approach is to employ solution processable organic compounds as interfacial layers.

When small molecules and polymers with specific functionalities are coated on inorganic substrates, such as metals and metal oxides, an interfacial dipole (Δ) is induced. While the exact mechanism of the induced Δ is still unclear, electron transfer, fermi-level pinning, or image charge generation have been the prevailing theories behinds its origins.[42,54,55] Interfacial dipole result in a shift in the vacuum level (E_{vac}) (e.g., energy required to eject an electron) at the organic/inorganic interface (Figure 1.8). [41,42,55–57] The changes in the vacuum level can be experimentally observed by modification of the work function (Φ) of the underlying substrate by ultraviolet photoelectron spectroscopy (UPS). UPS provides information on the direction and magnitude of Δ through

9

comparison of the measured Φ of the bare substrate to that of the coated substrate . Lowering the Φ of cathode materials *via* application of a thin organic film reduces the energetic barrier for injection of an electron, which is a desirable attribute for high performing electron-transporting layers (ETLs). Alternatively, low Φ metal electrodes, such as calcium (Ca) and aluminum (Al), can be employed to enhance Φ_{A-C} and improve charge extraction. While low Φ cathodes improve device performance, they are detrimental to device stability due to their propensity to oxidize and degrade over time. Using a high work function metal like silver (Ag) or gold (Au) in the presence of a work function modifying interlayer, a high performing and stable photovoltaic devices can be achieved.

There has been significant work in the establishing structure-property relationships of novel ETL materials. This research has revealed that small molecules and polymers containing functional groups with lone pairs such as tertiary amines and thiols, as well as cations and zwitterions favorably lower the work function of metal cathodes, resulting in enhanced performance and increase stability of organic and perovskite-based photovoltaic devices.[58–63] Beyond work function modification, a high performing ETL must form a uniform film as to prevent short circuiting due to pin holes in the film and facilitate charge transport. The desirable film-forming properties of polymeric structures have made them ideal candidates as interfacial layers. While insulating polymers like polyethyleneimine (PEI)[64] and poly(sulfobetaine methacrylate) (PSBMA)[65] have been shown to enhanced photovoltaic performance due to their ability to preferentially modify the work function of metal cathodes (Figure 1.8), this enhanced performance was observed only in ultra-thin films. A significant decrease in PCE was observed as thickness increases, as charges are unable to penetrate the insulating polymer layer above a critical thickness (~8-10 nm). This thickness intolerance may become a larger issue in high throughput

manufacturing in which interlayer thickness can vary batch-to-batch. Therefore, it was necessary to develop materials with a high thickness tolerance.

Bazan and coworkers previously demonstrated that conjugated polyelectrolytes (CPEs) were able to improve performance of OLEDs over a broad range of thicknesses.[66] Introduction of similar materials to OPV devices as ETLs yielded high efficiency devices that showed good tolerance to interlayer thickness.[67–71]. Similar results were shown in device containing zwitterionic, conjugated small molecules and polymers containing zwitterions, in which the positive and negative charges are covalently linked.[58,62,72,73] In Chapter 3, the work function modification and ETL performance properties of PDI-containing structures are detailed and highlight the importance of compounding charge transport and interfacial tuning properties in charge selective layers.

1.4 Aggregation-induced emission: structures and concepts

Chapter 4 details the syntheses and characterization of tetraphenylethylene (TPE)-containing small molecules and conjugated polymers. The utility of π-conjugated small molecules and polymers extends beyond transportation of charge or energy. These types of materials also are capable of emitting photons to generate light when a stimulus is applied. This stimulus can be the absorption of higher energy photons or application of an electrical potential which promotes an electron from a ground state molecular orbital into an unoccupied molecular orbital (excited state). In conjugated systems the predominant electronic transition is from the ground-state π orbital to an unoccupied π orbital (i.e., π to π*). The excited electron is then able to relax back to the ground state by several different processes (Figure 1.9). Depending on the vibrational state of the excited molecule, internal conversion (IC) takes place, which allows for relaxation to the lowest
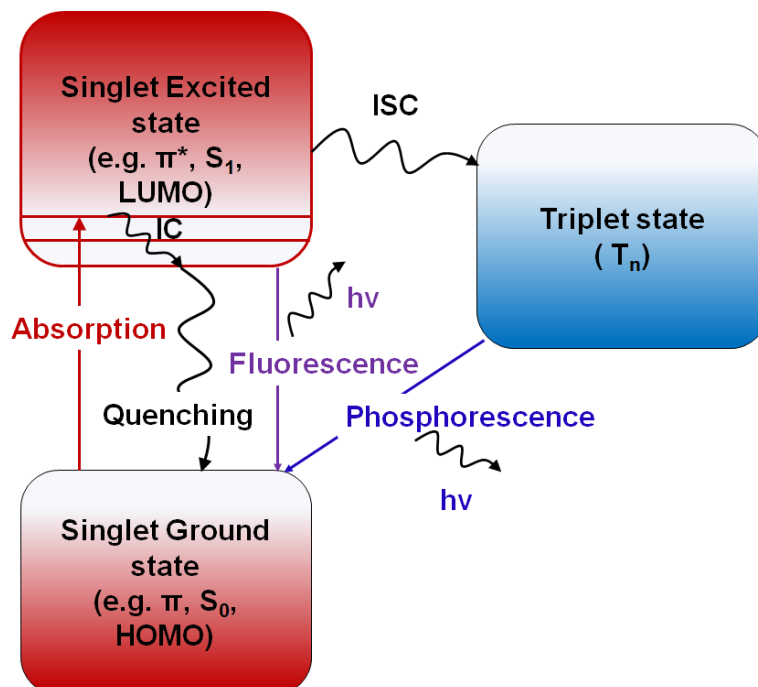
Figure 1. 9. Jablonski diagram of transitions occurring in π-conjugated structures.

vibrational mode of the excited state. Intersystem crossing (ISC) to the "spin-forbidden" triplet state (T_1) then relaxation to S_0 results *via* phosphorescence. Photoluminescence, also known as fluorescence, arises from radiative relaxation from S_1 to S_0 and has become an important analytical tool for monitoring the presence of analytes[74] and molecular processes.[75]

In contrast to radiative relaxation, an excited molecule can relax back to the ground state *via* IC processes (e.g., dissipation of energy through molecular vibration) and/or through energy or electron transfer to its environment. Both processes result in non-radiative relaxation of the excited molecule and compete with the radiative relaxation pathways. Stimulation of non-radiative relaxation is referred to as quenching and drives the "on-off" response in fluorescence sensors. While quenching can be beneficial for certain applications, it is detrimental for efficient luminescence in imaging probes and active layers in OLEDs. These applications require that the conjugated small molecules or polymers maintain their emissive properties following fabrication into nanoparticles or thin films. The planar structure and high affinity to π-π stacking of most

conjugated systems leads to the formation of non-radiative excimers in the aggregated stated, resulting in concentration- or aggregation-caused quenching (ACQ).[76] ACQ is highly sensitive to the orientation of the molecules in the aggregate. For example, the fluorescence of chlorophyll was shown to quench during *in vitro* experiments at concentrations significantly lower than those found *in vivo* in chloroplasts.[77,78] The differences between the *in vivo* and *in vitro* relaxation modes was due to the proximity of chlorophyll molecules in the solution (~10 Å) versus in chlorophyll-containing proteins (~12 Å).[79] Proper spacing of the fluorophores prevents the π-π overlap necessary to form fluorescent trap sites. With a greater understanding of the relationship between molecular architecture and quenching, several approaches have been developed to attenuate ACQ. Methods such as introduction of bulky moieties to interfere with π-π stacking,[80] co-assembly of chromophores,[81] cross-dipole stacking,[82] enhanced intramolecular charge transfer transition by introduction of heteroatoms,[83,84] and formation of emissive J-type aggregates[15,85] have been shown to be effective. A simpler approach to addressing ACQ would be to design structures that exhibit enhanced emission in the aggregated state.
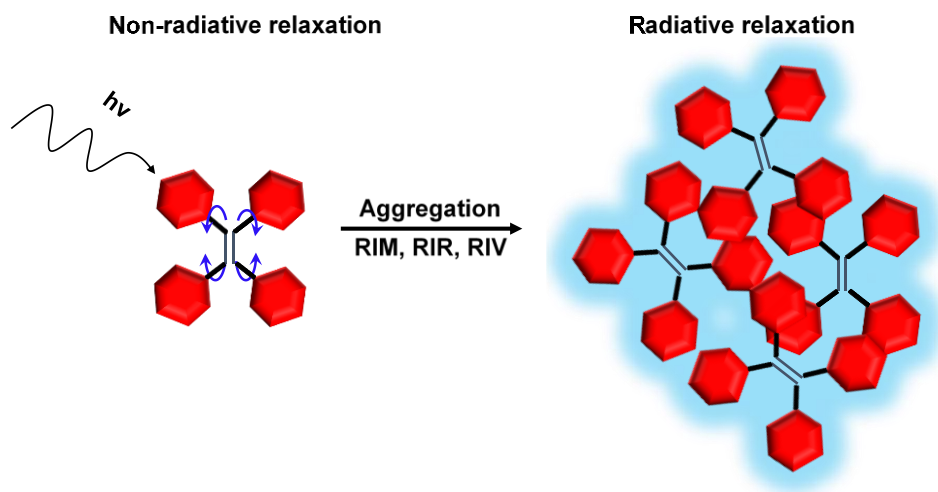
Figure 1. 10. Mechanism of aggregation-induced emission of propeller-like aromatic structures.

13

Aggregation-induced emission (AIE) was first reported by Tang and coworkers in 2001 with hexaphenyl silole (HPS) derivatives.[86] AIE-active molecules, or AIEgens, exhibit distinguishing structural features. Compared to the planar, fused-ring structures susceptible to ACQ such as perylene, AIE-molecules (e.g., TPE and HPS) consist of propeller-like structures with multiple aromatic rings that form randomly oriented structures in the solid-state with inadequate π-π interactions necessary for quenching (Figure 1.10).[86] This difference in structure plays a crucial role in how these types of molecules behave in solution or the aggregated state. In solution, AIEgens exhibit infinitesimal emission due to energy transfer to the surround solvent through molecular motion leading to higher non-radiative relaxation rate relative to the radiative relaxation rate. This can be easily observed in the emittance of solutions of AIEgens in THF:H_2O mixtures (Figure 1.11): as the water content is increased, the hydrophobic fluorophores begin to aggregate resulting in observable emission. The opposite effect is observed in trifluoroethanol
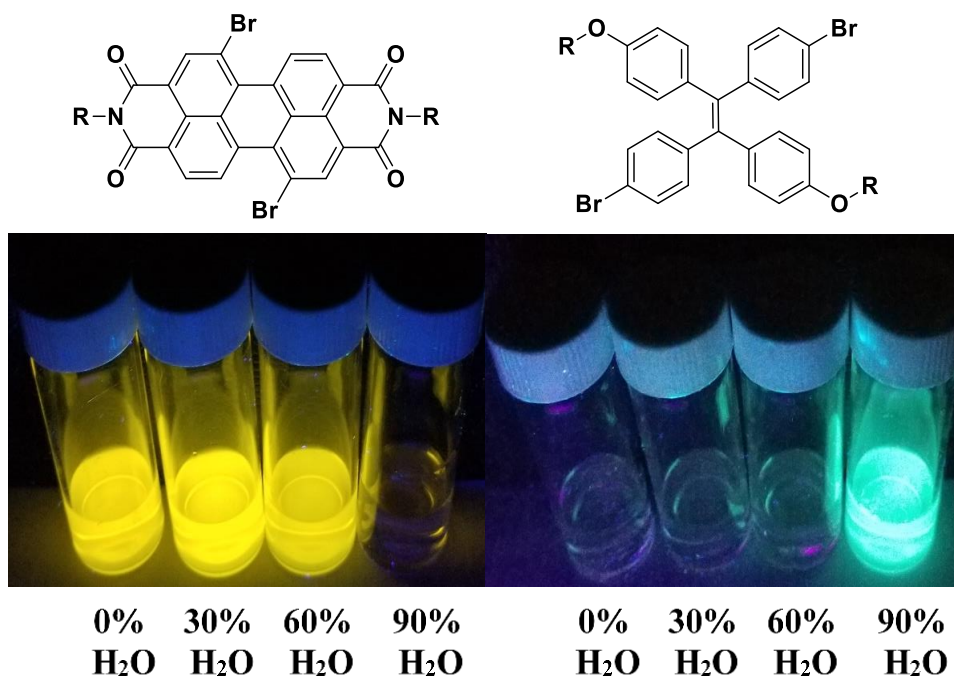
Figure 1. 11. Images of (A) PDI TFE/H2O mixtures and (B) TPE in THF/H2O under 365 nm UV excitation illustrating ACQ and AIE.

14

(TFE):H$_2$O mixtures of PDI. Theoretical modeling and experimental results by Peng and coworkers provided insight to the relationship between the structure of AIE-type molecules and rates of radiative or non-radiative decay under various conditions.[87,88] Their results were in agreement with first principles ideas of freely rotating phenyl rings in AIE compounds leading to the dominant non-radiative relaxation in solution.[89] Further studies by Tang and Wu provided insight to the mechanism of AIE. Firstly, the induced emission was not due to twisted intermolecular charge transfer (TICT) observed in other structures, as the emission and absorption of the AIE-active species were not influence by solvent polarity.[90] Secondly, emission was observed to increase in response to an increase in viscosity and decrease in temperature. Under these conditions the intramolecular rotation and vibration was significantly hindered, resulting in increased radiative relaxation.[90] Finally, it was shown that by preparing structures with hydrogen bonding moieties which hindered intramolecular motion, emission could be achieved.[91] Combined, these results support the proposed mechanisms of restriction of intramolecular motion (RIM) as the source of AIE.

Due to its synthetic accessibility, TPE is an ideal molecular scaffold for developing AIE materials. Integrating TPE into conjugated polymer has realized a versatile class of polymers with applications ranging from polymeric OLEDS to dual-channel fluorescent sensors.[92–94] When TPE was incorporated into these systems, it behaved independently as an AIE-active component rather than in cooperation with the polymeric structure. A greater understanding of molecular design in AIE-active polymers is necessary to fully realize their potential as high performing emitters. One approach to this would be to synthesize TPE within a known polymeric solid-state emitter and study the evolution of the polymer's optoelectronic properties. A promising candidate for this kind of study is PPV, which has been investigated extensively as a solid-state emitter in OLEDs

but still suffers from ACQ.[95–101]   In Chapter 4, the synthesis and characterization of small

molecule precursors and   TPE-containing π-conjugated polymers is discussed.   This work

highlights how AIE can be harnessed within a known solid-state emitter and methods for tailoring

of the TPE optical properties through simple modification of molecular structure.

1.5 Thesis outline

This dissertation thesis discusses the synthesis, characterization, and device integration of

functional PDI- and TPE-containing polymers as interfacial layers in photovoltaic devices and

quench-resistant emissive materials for solid-state emitter applications. Focus is given to

synthesizing polymeric structures with tunable optical and electronic properties via modification

of polymer backbone functionality and monomer solution properties.

In Chapter 2, the molecular design, synthesis, and characterization of PDI-based polymers

are discussed.[102] Two PDI small molecules containing tertiary amines at the imide positions and

bromide or phenyl groups conjugated to the aromatic core were prepared. The moieties introduced

at the aromatic core served two primary functions: 1) to attenuate π-π stacking to improve

monomer and polymer solubility and 2) to modify the optoelectronic properties of the synthesized

compounds. The tertiary amine groups were used to react with α,ω-alkyl dihalides or bis-sultone

monomers, resulting in polymers with ionene or zwitterionic functionality embedded in the

polymer backbone, respectively. The PDI content (mole%) was modulated by controlling the

monomer feed ratio and polymers with targeted 10, 50, and 100 mole% PDI were prepared with

good yield (40-80%) and agreement with targeted PDI incorporation. The solution optical

properties of the resulting polymers were studied by UV-vis absorption and photoluminescence

spectroscopy. The ratio of S_{0-0} to S_{0-1} vibronic bands in the absorption spectra and the

photoluminescence quantum yield were related to PDI content and cationic *vs.* zwitterionic

functionality. The strong dependence of functionality on solution properties observed in these materials and will guide future design of molecules amenable to thin film electronic devices.

In Chapter 3, the efficacy of PDI-containing small molecules and polymers as ETLs is discussed.[103,104] The work function modifier properties were investigated using ultraviolet photoelectron spectroscopy (UPS). Photovoltaic device performance was studied as function of PDI content. The PDI-based polymers were also able to enhance the performance of perovskite-based photovoltaic devices, demonstrating the universal applicability of these novel materials. The results of this study revealed an optimum conjugation density for interlayer performance, which holds the potential for a cost-effective method for designing interfacial materials. Additionally, tertiary amine-containing small molecule PDIs with bromide or phenyl-terpyridyl groups were integrated into perovskite devices. The devices prepared with the PDI-containing ETLs outperformed interlayer free devices as well as devices containing the phenyl-terpyridyl small molecules and exhibited good tolerance to interlayer thickness.

In Chapter 4, focus is given to the synthesis and characterization of TPE-containing conjugated polymers. TPE monomers were designed to contain functionality amenable to palladium (Pd)-catalyzed Suzuki-Miyaura coupling or metal-free Horner-Waddsworth-Emmons polymerizations. The optoelectronic properties of the two sets of polymers were compared to study the effect of backbone chemistry. Additionally, small molecule analogs were synthesized to further analyze the influence of effect of bond rigidity on AIE properties. The structures containing vinylene spacers, effectively acting as poly(para-phenylene vinylene) (PPV) analogs of TPE exhibit strong emission when aggregated in THF:H_2O mixtures, as well as solution emission, in stark contrast to the small molecules. Moreover, by preparing copolymers of PPV with 25 and 50

mole% TPE, ACQ could be mitigated. These results illustrated a simple approach to prepare versatile polymers with both solution and aggregate emission.

In Chapter 5, the results and impact of this work are summarized. The results of this thesis are also examined in the context of the broad and developing field of organic electronics. Additionally, future outlooks of this work are considered with a focus on key modifications necessary for commercialization of thin film photovoltaic devices and novel polymeric materials for solid-state emitters. Finally, in chapter 6 the synthetic methodology and instrumentation employed for this work is documented in detail.

1.6 References

(1)   Garnier, F. Organic-Based Electronics a La Carte. *Acc. Chem. Res.* **1999**, *32* (3), 209–215. https://doi.org/10.1021/ar9800340.

(2)   Shirakawa, H.; Macdiarmid, A. G.; Chiang, C. K.; Fincher Jr., C. R.; Park, Y. W.; Heeger, A. J.; Louis, E. J.; Gau, S. C. Electical Conductivity in Doped Polyacetylene. *Phys. Rev. Lett.* **1977**, *39* (17), 1098–1101. https://doi.org/10.1103/PhysRevLett.39.1098.

(3)   Coleman, L. B.; Cohen, M. J.; Sandman, D. J.; Yamagishi, F. G.; Garito, A. F.; Heeger, A. J. Superconducting Fluctuations and the Peierls Instability in an Organic Solid. *Solid State Commun.* **1973**, *12* (11), 1125–1132. https://doi.org/10.1016/0038-1098(73)90127-0.

(4)   Hsieh, B. R.; Yu, Y.; VanLaeken, A. C.; Lee, H. General Methodology toward Soluble Poly(p -Phenylenevinylene) Derivatives. *Macromolecules* **1997**, *30* (25), 8094–8095. https://doi.org/10.1021/ma9713771.

(5)   Jen, K.; Miller, G. G.; Elsenbaumer, R. L. Highly Conducting, Soluble, and Environmentally-Stable Poly(3-Alkylthiophenes). *J. Chem. Soc. Chem. Commun.* **1986**, *5* (17), 1346. https://doi.org/10.1039/c39860001346.

(6)   Herbst, W.; Hunger, K.; Wilker, G.; Ohleier, H.; Winter, R. *Industrial Organic Pigments*; 2004; Vol. Third Edit. https://doi.org/10.1002/3527602429.

(7)   Yuan, Z.; Lee, S. L.; Chen, L.; Li, C.; Mali, K. S.; De Feyter, S.; Müllen, K. Processable Rylene Diimide Dyes up to 4 Nm in Length: Synthesis and STM Visualization. *Chem. - A Eur. J.* **2013**, *19* (36), 11842–11846. https://doi.org/10.1002/chem.201302086.

(8)   Heek, T.; Nikolaus, J.; Schwarzer, R.; Fasting, C.; Welker, P.; Licha, K.; Herrmann, A.; Haag, R. An Amphiphilic Perylene Imido Diester for Selective Cellular Imaging. *Bioconjug. Chem.* **2013**, *24* (2), 153–158. https://doi.org/10.1021/bc3005655.

(9)   Chen, H. C.; Hsu, C. P.; Reek, J. N. H.; Williams, R. M.; Brouwer, A. M. Highly Soluble Benzo[Ghi]Perylenetriimide Derivatives: Stable and Air-Insensitive Electron Acceptors for Artificial Photosynthesis. *ChemSusChem* **2015**, *8* (21), 3639–3650. https://doi.org/10.1002/cssc.201500950.

(10)   Huang, C.; Barlow, S.; Marder, S. R. Perylene-3,4,9,10-Tetracarboxylic Acid Diimides: Synthesis, Physical Properties, and Use in Organic Electronics. *J. Org. Chem.* **2011**, *76* (8), 2386–2407. https://doi.org/10.1021/jo2001963.

(11)   Chen, H. Z.; Ling, M. M.; Mo, X.; Shi, M. M.; Wang, M.; Bao, Z. Air Stable N-Channel Organic Semiconductors for Thin Film Transistors Based on Fluorinated Derivatives of Perylene Diimides. *Chem. Mater.* **2007**, *19* (4), 816–824. https://doi.org/10.1021/cm062352w.

(12)   Tatemichi, S.; Ichikawa, M.; Koyama, T.; Taniguchi, Y. High Mobility N-Type Thin-Film Transistors Based on N,N′-Ditridecyl Perylene Diimide with Thermal Treatments. *Appl. Phys. Lett.* **2006**, *89* (11), 2004–2007. https://doi.org/10.1063/1.2349290.

(13)   Zhao, D.; Wu, Q.; Cai, Z.; Zheng, T.; Chen, W.; Lu, J.; Yu, L. Electron Acceptors Based on α-Substituted Perylene Diimide (PDI) for Organic Solar Cells. *Chem. Mater.* **2016**, *28* (4), 1139–1146. https://doi.org/10.1021/acs.chemmater.5b04570.

(14)   Zhong, Y.; Trinh, M. T.; Chen, R.; Wang, W.; Khlyabich, P. P.; Kumar, B.; Xu, Q.; Nam, C. Y.; Sfeir, M. Y.; Black, C.; et al. Efficient Organic Solar Cells with Helical Perylene

Diimide Electron Acceptors. *J. Am. Chem. Soc.* **2014**, *136* (43), 15215–15221. https://doi.org/10.1021/ja5092613.

(15)   Kaiser, T. E.; Stepanenko, V.; Würthner, F. Fluorescent J-Aggregates of Core-Substituted Perylene Bisimides: Studies on Structure-Property Relationship, Nucleation-Elongation Mechanism, and Sergeants-and-Soldiers Principle. *J. Am. Chem. Soc.* **2009**, *131* (19), 6719–6732. https://doi.org/10.1021/ja900684h.

(16)   Everett, T. A.; Higgins, D. A. Electrostatic Self-Assembly of Ordered Perylene-Diimide/Polyelectrolyte Nanofibers in Fluidic Devices: From Nematic Domains to Macroscopic Alignment. *Langmuir* **2009**, *25* (22), 13045–13051. https://doi.org/10.1021/la9019298.

(17)   Gebers, J.; Rolland, D.; Marty, R.; Suàrez, S.; Cervini, L.; Scopelliti, R.; Brauer, J. C.; Frauenrath, H. Solubility and Crystallizability: Facile Access to Functionalized π-Conjugated Compounds with Chlorendylimide Protecting Groups. *Chem. - A Eur. J.* **2015**, *21* (4), 1542–1553. https://doi.org/10.1002/chem.201403623.

(18)   Krieg, E.; Shirman, E.; Weissman, H.; Shimoni, E.; Wolf, S. G.; Pinkas, I.; Rybtchinski, B. Supramolecular Gel Based on a Perylene Diimide Dye: Multiple Stimuli Responsiveness, Robustness, and Photofunction. *J. Am. Chem. Soc.* **2009**, *131* (40), 14365–14373. https://doi.org/10.1021/ja903938g.

(19)   Ma, X.; Zhang, Y.; Zhang, Y.; Peng, C.; Che, Y.; Zhao, J. Stepwise Formation of Photoconductive Nanotubes through a New Top-Down Method. *Adv. Mater.* **2015**, *27* (47), 77467751. https://doi.org/10.1002/adma.201503771.

(20)   Wu, H.; Xie, Z.; Xiao, B.; He, Z.; Zhang, W.; Wu, X.; Würthner, F.; Wang, C.; Xie, F.; Liu, L.; et al. Self-Assembled Perylene Bisimide J-Aggregates as Promising Cathode Modifier for Highly Efficient Inverted Polymer Solar Cells. *Mater. Horiz.* **2015**, 514–518. https://doi.org/10.1039/C5MH00056D.

(21)   Chen, Y.; Feng, Y.; Gao, J.; Bouvet, M. Self-Assembled Aggregates of Amphiphilic Perylene Diimide-Based Semiconductor Molecules: Effect of Morphology on Conductivity. *J. Colloid Interface Sci.* **2012**, *368* (1), 387–394. https://doi.org/10.1016/j.jcis.2011.10.076.

(22)   Hestand, N. J.; Spano, F. C. Interference between Coulombic and CT-Mediated Couplings in Molecular Aggregates: H- to J-Aggregate Transformation in Perylene-Based π-Stacks. *J. Chem. Phys.* **2015**, *143* (24), 244707. https://doi.org/10.1063/1.4938012.

(23)   Spano, F. C.; Introduction, I. The Spectral Signatures of Frenkel Polarons in H and J Aggregates. *Acc. Chem. Res.* **2009**, *43* (3), 429–439.

(24)   Siddiqui, S.; Spano, F. H- and J-Aggregates of Conjugated Polymers and Oligomers. *Chem. Phys. Lett.* **1999**, *308* (1–2), 99–105. https://doi.org/10.1016/S0009-2614(99)00577-1.

(25)   Albery, W. J.; Archer, M. D. Optimum Efficiency of Photogalvanic Cells for Solar Energy Conversion. *Nature* **1977**, *270* (5636), 399–402. https://doi.org/10.1038/270399a0.

(26)   Albery, W. J. Development of Photogalvanic Cells for Solar Energy Conversion. *Acc. Chem. Res.* **1982**, *15* (5), 142–148. https://doi.org/10.1021/ar00077a003.

(27)   Ratcliff, E. L.; Zacher, B.; Armstrong, N. R. Selective Interlayers and Contacts in Organic Photovoltaic Cells. *J. Phys. Chem. Lett.* **2011**, *2* (11), 1337–1350. https://doi.org/10.1021/jz2002259.

(28)   Peumans, P.; Yakimov, A.; Forrest, S. R. Small Molecular Weight Organic Thin-Film Photodetectors and Solar Cells. *J. Appl. Phys.* **2003**, *93* (7), 3693–3723. https://doi.org/10.1063/1.1534621.

(29)   Elumalai, N. K.; Uddin, A. Open Circuit Voltage of Organic Solar Cells: An in-Depth Review. *Energy Environ. Sci.* **2016**, *9* (2), 391–410. https://doi.org/10.1039/c5ee02871j.

(30)   Meiss, J.; Riede, M. K.; Leo, K. Towards Efficient Tin-Doped Indium Oxide (ITO)-Free Inverted Organic Solar Cells Using Metal Cathodes. *Appl. Phys. Lett.* **2009**, *94* (1), 013303. https://doi.org/10.1063/1.3059552.

(31)   Yang, W. S.; Park, B.-W.; Jung, E. H.; Jeon, N. J. Iodide Management in Formamidinium-Lead-Halide – Based Perovskite Layers for Efficient Solar Cells. *Science (80-.).* **2017**, *356* (6345), 1376–1379. https://doi.org/10.1126/science.aan2301.

(32)   Yang, G.; Wang, C.; Lei, H.; Zheng, X.; Qin, P.; Xiong, L.; Zhao, X.; Yan, Y.; Fang, G. Interface Engineering in Planar Perovskite Solar Cells: Energy Level Alignment, Perovskite Morphology Control and High Performance Achievement. *J. Mater. Chem. A* **2017**, *5* (4), 1658–1666. https://doi.org/10.1039/C6TA08783C.

(33)   Fakharuddin, A.; Schmidt-Mende, L.; Garcia-Belmonte, G.; Jose, R.; Mora-Sero, I. Interfaces in Perovskite Solar Cells. *Adv. Energy Mater.* **2017**, *7* (22). https://doi.org/10.1002/aenm.201700623.

(34)   Wu, Y.; Chen, W.; Yue, Y.; Liu, J.; Bi, E.; Yang, X.; Islam, A.; Han, L. Consecutive Morphology Controlling Operations for Highly Reproducible Mesostructured Perovskite Solar Cells. *ACS Appl. Mater. Interfaces* **2015**, *7* (37), 20707–20713. https://doi.org/10.1021/acsami.5b05576.

(35)   Liu, Y.; Renna, L. A.; Page, Z. A.; Thompson, H. B.; Kim, P. Y.; Barnes, M. D.; Emrick, T.; Venkataraman, D.; Russell, T. P. A Polymer Hole Extraction Layer for Inverted Perovskite Solar Cells from Aqueous Solutions. *Adv. Energy Mater.* **2016**, 1–7. https://doi.org/10.1002/aenm.201600664.

(36)   Guo, Y.; Sato, W.; Shoyama, K.; Nakamura, E. Sulfamic Acid-Catalyzed Lead Perovskite Formation for Solar Cell Fabrication on Glass or Plastic Substrates. *J. Am. Chem. Soc.* **2016**, *138* (16), 5410–5416. https://doi.org/10.1021/jacs.6b02130.

(37)   Grill, I.; Aygüler, M. F.; Bein, T.; Docampo, P.; Hartmann, N. F.; Handloser, M.; Hartschuh, A. Charge Transport Limitations in Perovskite Solar Cells: The Effect of Charge Extraction Layers. *ACS Appl. Mater. Interfaces* **2017**, acsami.7b09567. https://doi.org/10.1021/acsami.7b09567.

(38)   Saliba, M.; Matsui, T.; Seo, J.-Y.; Domanski, K.; Correa-Baena, J.-P.; Nazeeruddin, M. K.; Zakeeruddin, S. M.; Tress, W.; Abate, A.; Hagfeldt, A.; et al. Cesium-Containing Triple Cation Perovskite Solar Cells: Improved Stability, Reproducibility and High Efficiency. *Energy Environ. Sci.* **2016**, *9* (6), 1989–1997. https://doi.org/10.1039/C5EE03874J.

(39)   Wagenpfahl, A.; Rauh, D.; Binder, M.; Deibel, C.; Dyakonov, V. S-Shaped Current-Voltage Characteristics of Organic Solar Devices. *Phys. Rev. B* **2010**, *82* (11), 115306. https://doi.org/10.1103/PhysRevB.82.115306.

(40)   Wagenpfahl, A.; Deibel, C.; Dyakonov, V. Organic Solar Cell Efficiencies under the Aspect of Reduced Surface Recombination Velocities. *IEEE J. Sel. Top. Quantum Electron.* **2010**, *16* (6), 1759–1763. https://doi.org/10.1109/JSTQE.2010.2042142.

(41)   Ishii, B. H.; Sugiyama, K.; Ito, E.; Seki, K. Energy Level Alignment and Interfacial Electronic Structures at Organic / Metal and Organic / Organic Interfaces **. *Adv. Mater.* **1999**, *11* (8), 605–625. https://doi.org/10.1002/(SICI)1521-4095(199906)11:8<605::AID-ADMA605>3.0.CO;2-Q.

(42)   Ishii, H.; Seki, K. Energy Level Alignment at Organic/Metal Interfaces Studied by UV Photoemission: Breakdown of Traditional Assumption of a Common Vacuum Level at the Interface. *IEEE Trans. Electron Devices* **1997**, *44* (8), 1295–1301. https://doi.org/10.1109/16.605471.

(43)   Yin, Z.; Wei, J.; Zheng, Q. Interfacial Materials for Organic Solar Cells: Recent Advances and Perspectives. *Adv. Sci.* **2016**, *3* (8), 1–37. https://doi.org/10.1002/advs.201500362.

(44)   Mohan, M.; Nandal, V.; Paramadam, S.; Reddy, K. P.; Ramkumar, S.; Agarwal, S.; Gopinath, C. S.; Nair, P. R.; Namboothiry, M. A. G. Efficient Organic Photovoltaics with Improved Charge Extraction and High Short-Circuit Current. *J. Phys. Chem. C* **2017**, *121* (10), 5523–5530. https://doi.org/10.1021/acs.jpcc.7b01314.

(45)   Waldauf, C.; Morana, M.; Denk, P.; Schilinsky, P.; Coakley, K.; Choulis, S. A.; Brabec, C. J. Highly Efficient Inverted Organic Photovoltaics Using Solution Based Titanium Oxide as Electron Selective Contact. *Appl. Phys. Lett.* **2006**, *89* (23), 233517. https://doi.org/10.1063/1.2402890.

(46)   Siddiki, M. K.; Venkatesan, S.; Qiao, Q. Nb 2O 5 as a New Electron Transport Layer for Double Junction Polymer Solar Cells. *Phys. Chem. Chem. Phys.* **2012**, *14* (14), 4682–4686. https://doi.org/10.1039/c2cp22627h.

(47)   Trost, S.; Zilberberg, K.; Behrendt, A.; Riedl, T. Room-Temperature Solution Processed SnOxas an Electron Extraction Layer for Inverted Organic Solar Cells with Superior Thermal Stability. *J. Mater. Chem.* **2012**, *22* (32), 16224–16229. https://doi.org/10.1039/c2jm33445c.

(48)   Ling, X.; Yuan, J.; Liu, D.; Wang, Y.; Zhang, Y.; Chen, S.; Wu, H.; Jin, F.; Wu, F.; Shi, G.; et al. Room-Temperature Processed Nb $_2$ O $_5$ as the Electron-Transporting Layer for Efficient Planar Perovskite Solar Cells. *ACS Appl. Mater. Interfaces* **2017**, *9* (27), 23181–23188. https://doi.org/10.1021/acsami.7b05113.

(49)   Schulze, P. S. C.; Bett, A. J.; Winkler, K.; Hinsch, A.; Lee, S.; Mastroianni, S.; Mundt, L. E.; Mundus, M.; Würfel, U.; Glunz, S. W.; et al. Novel Low-Temperature Process for Perovskite Solar Cells with a Mesoporous TiO2Scaffold. *ACS Appl. Mater. Interfaces* **2017**, *9* (36), 30567–30574. https://doi.org/10.1021/acsami.7b05718.

(50)   Song, S.; Kang, G.; Pyeon, L.; Lim, C.; Lee, G. Y.; Park, T.; Choi, J. Systematically Optimized Bilayered Electron Transport Layer for Highly Efficient Planar Perovskite Solar Cells (η = 21.1%). *ACS Energy Lett.* **2017**, *2* (12), 2667–2673. https://doi.org/10.1021/acsenergylett.7b00888.

(51)   Jeong, I.; Park, Y. H.; Bae, S.; Park, M.; Jeong, H.; Lee, P.; Ko, M. J. Solution-Processed Ultrathin TiO $_2$ Compact Layer Hybridized with Mesoporous TiO $_2$ for High-Performance

Perovskite Solar Cells. *ACS Appl. Mater. Interfaces* **2017**, acsami.7b11901. https://doi.org/10.1021/acsami.7b11901.

(52) Xie, J.; Huang, K.; Yu, X.; Yang, Z.; Xiao, K.; Qiang, Y.; Zhu, X.; Xu, L.; Wang, P.; Cui, C.; et al. Enhanced Electronic Properties of SnO2 *via* Electron Transfer from Graphene Quantum Dots for Efficient Perovskite Solar Cells. *ACS Nano* **2017**, acsnano.7b04070. https://doi.org/10.1021/acsnano.7b04070.

(53) Guo, Z.; Gao, L.; Zhang, C.; Xu, Z.; Ma, T. Low-Temperature Processed Non-TiO $_2$ Electron Selective Layers for Perovskite Solar Cells. *J. Mater. Chem. A* **2018**. https://doi.org/10.1039/C7TA10742K.

(54) Lee, H.; Stephenson, J. C.; Richter, L. J.; McNeill, C. R.; Gann, E.; Thomsen, L.; Park, S.; Jeong, J.; Yi, Y.; DeLongchamp, D. M.; et al. The Structural Origin of Electron Injection Enhancements with Fulleropyrrolidine Interlayers. *Adv. Mater. Interfaces* **2016**, *3* (10), 1500852. https://doi.org/10.1002/admi.201500852.

(55) Van Reenen, S.; Kouijzer, S.; Janssen, R. A. J.; Wienk, M. M.; Kemerink, M. Origin of Work Function Modification by Ionic and Amine-Based Interface Layers. *Adv. Mater. Interfaces* **2014**, *1* (8), 1–11. https://doi.org/10.1002/admi.201400189.

(56) Yang, D. S.; Bilby, D.; Chung, K.; Wenderott, J. K.; Jordahl, J.; Kim, B. H.; Lahann, J.; Green, P. F.; Kim, J. Work Function Modification via Combined Charge-Based Through-Space Interaction and Surface Interaction. *Adv. Mater. Interfaces* **2018**, *5* (15), 1800471. https://doi.org/10.1002/admi.201800471.

(57)   Heimel, G.; Romaner, L.; Zojer, E.; Bredas, J. L. The Interface Energetics of Self-Assembled Monolayers on Metals. *Acc. Chem. Res.* **2008**, *41* (6), 721–729. https://doi.org/10.1021/ar700284q.

(58)   Page, Z. A.; Liu, Y.; Duzhko, V. V.; Thomas, P.; Russell, T. P.; Emrick, T. Fulleropyrrolidine Interlayers: Tailoring Electrodes to Raise Organic Solar Cell Efficiency. *Science (80-.).* **2014**, *346* (6208), 441–446. https://doi.org/10.1126/science.1255826.

(59)   Zhang, Z.-G.; Qi, B.; Jin, Z.; Chi, D.; Qi, Z.; Li, Y.; Wang, J. Perylene Diimides: A Thickness-Insensitive Cathode Interlayer for High Performance Polymer Solar Cells. *Energy Environ. Sci.* **2014**, *7* (6), 1966. https://doi.org/10.1039/c4ee00022f.

(60)   Chang, C. Y.; Chang, Y. C.; Huang, W. K.; Lee, K. T.; Cho, A. C.; Hsu, C. C. Enhanced Performance and Stability of Semitransparent Perovskite Solar Cells Using Solution-Processed Thiol-Functionalized Cationic Surfactant as Cathode Buffer Layer. *Chem. Mater.* **2015**, *27* (20), 7119–7127. https://doi.org/10.1021/acs.chemmater.5b03137.

(61)   Yang, R.; Zhao, Z.; He, J.; Wang, J.; Chen, W.; Wang, N.; Zhang, Y. A Water/Alcohol-Soluble Copolymer Based on Fluorene and Perylene Diimide as a Cathode Interlayer for Inverted Polymer Solar Cells. *J. Mater. Chem. C* **2015**, *3*, 4515–4521. https://doi.org/10.1039/C5TC00450K.

(62)   Liu, Y.; Page, Z.; Ferdous, S.; Liu, F.; Kim, P.; Emrick, T.; Russell, T. Dual Functional Zwitterionic Fullerene Interlayer for Efficient Inverted Polymer Solar Cells. *Adv. Energy Mater.* **2015**, *5* (14), 1–6. https://doi.org/10.1002/aenm.201500405.

(63)   Zhu, Z.; Chueh, C. C.; Lin, F.; Jen, A. K. Y. Enhanced Ambient Stability of Efficient Perovskite Solar Cells by Employing a Modified Fullerene Cathode Interlayer. *Adv. Sci.* **2016**, *3* (9), 1–7. https://doi.org/10.1002/advs.201600027.

(64)   Zhou, Y.; Fuentes-hernandez, C.; Shim, J.; Meyer, J.; Giordano, A. J.; Li, H.; Winget, P.; Papadopoulos, T.; Cheun, H.; Kim, J.; et al. A Universal Method to Produce Low–Work Function Electrodes for Organic Electronics. *Science (80-.).* **2012**, *873* (April), 327–332. https://doi.org/10.1126/science.1218829.

(65)   Lee, H.; Puodziukynaite, E.; Zhang, Y.; Stephenson, J. C.; Richter, L. J.; Fischer, D. a; Delongchamp, D. M.; Emrick, T.; Briseno, A. L. Poly(Sulfobetaine Methacrylate)s as Electrode Modi Fi Ers for Inverted Organic Electronics. *J. Am. Chem. Soc.* **2015**, *137*, 540–549. https://doi.org/10.1021/ja512148d.

(66)   Yang, R.; Wu, H.; Cao, Y.; Bazan, G. C. Control of Cationic Conjugated Polymer Performance in Light Emitting Diodes by Choice of Counterion. *J. Am. Chem. Soc.* **2006**, *128* (45), 14422–14423. https://doi.org/10.1021/ja063723c.

(67)   Subbiah, J.; Mitchell, V. D.; Hui, N. K. C.; Jones, D. J.; Wong, W. W. H. A Green Route to Conjugated Polyelectrolyte Interlayers for High-Performance Solar Cells. *Angew. Chemie - Int. Ed.* **2017**, *56* (29), 8431–8434. https://doi.org/10.1002/anie.201612021.

(68)   Chen, Z.; Hu, Z.; Wu, Z.; Liu, X.; Jin, Y.; Xiao, M. Polyelectrolytes for the Interface Engineering of e Ffi Cient Polymer Solar Cells †. *J. Mater. Chem. A Mater. energy Sustain.* **2017**, *5*, 19447–19455. https://doi.org/10.1039/C7TA05246D.

(69)   Tan, Y.; Chen, L.; Wu, F.; Huang, B.; Liao, Z.; Yu, Z.; Hu, L.; Zhou, Y.; Chen, Y. Regulation of the Polar Groups in N-Type Conjugated Polyelectrolytes as Electron

Transfer Layer for Inverted Polymer Solar Cells. *Macromolecules* **2018**, *51* (20), 8197–8204. https://doi.org/10.1021/acs.macromol.8b01490.

(70)   Kesters, J.; Govaerts, S.; Pirotte, G.; Drijkoningen, J.; Chevrier, M.; Van Den Brande, N.; Liu, X.; Fahlman, M.; Van Mele, B.; Lutsen, L.; et al. High-Permittivity Conjugated Polyelectrolyte Interlayers for High-Performance Bulk Heterojunction Organic Solar Cells. *ACS Appl. Mater. Interfaces* **2016**, *8* (10), 6309–6314. https://doi.org/10.1021/acsami.6b00242.

(71)   Zhang, W.; Li, Y.; Zhu, L.; Liu, X.; Song, C.; Li, X.; Sun, X.; Fang, J. A PTB7-Based Narrow Band-Gap Conjugated Polyelectrolyte as an Efficient Cathode Interlayer in PTB7-Based Polymer Solar Cells. *Chem. Commun.* **2017**, *53* (12), 2005–2008. https://doi.org/10.1039/c6cc09274h.

(72)   Page, Z. A.; Liu, F.; Russell, T. P.; Emrick, T. Tuning the Energy Gap of Conjugated Polymer Zwitterions for Efficient Interlayers and Solar Cells. *J. Polym. Sci. Part A Polym. Chem.* **2015**, *53* (2), 327–336. https://doi.org/10.1002/pola.27349.

(73)   Page, Z. A.; Liu, F.; Russell, T. P.; Emrick, T. Rapid, Facile Synthesis of Conjugated Polymer Zwitterions in Ionic Liquids. *Chem. Sci.* **2014**, *5* (6), 2368–2373. https://doi.org/10.1039/c4sc00475b.

(74)   Reppy, M. A.; Pindzola, B. A. Biosensing with Polydiacetylene Materials: Structures, Optical Properties and Applications. *Chem. Commun.* **2007**, No. 42, 4317. https://doi.org/10.1039/b703691d.

(75)   Fletcher, K.; Bunz, U. H. F.; Dreuw, A. Fluorescence Quenching of Benzaldehyde in Water by Hydrogen Atom Abstraction. *ChemPhysChem* **2016**, *17* (17), 2650–2653. https://doi.org/10.1002/cphc.201501059.

(76)   Birks, J. B. *Photophysics of Aromatic Molecules*; Wiley-Interscience: London, 1970. https://doi.org/10.1016/0022-2313(71)90011-1.

(77)   Watson, W. F.; Livingston, R. Self-Quenching and Sensitization of Fluorescence of Chlorophyll Solutions. *J. Chem. Phys.* **1950**, *18* (6), 802–809. https://doi.org/10.1063/1.1747779.

(78)   TROSPER, T.; PARK, R. B.; SAUER, K. EXCITATION TRANSFER BY CHLOROPHYLL a IN MONOLAYERS AND THE INTERACTION WITH CHLOROPLAST GLYCOLIPIDS*. *Photochem. Photobiol.* **1968**, *7* (5), 451–469. https://doi.org/10.1111/j.1751-1097.1968.tb07406.x.

(79)   BEDDARD, G. S.; PORTER, G. Concentration Quenching in Chlorophyll. *Nature* **1976**, *260* (5549), 366–367. https://doi.org/10.1038/260366a0.

(80)   Iida, A.; Yamaguchi, S. Intense Solid-State Blue Emission with a Small Stokes' Shift: π-Stacking Protection of the Diphenylanthracene Skeleton. *Chem. Commun.* **2009**, *7345* (21), 3002. https://doi.org/10.1039/b901794a.

(81)   Huang, Y.; Xing, J.; Gong, Q.; Chen, L. C.; Liu, G.; Yao, C.; Wang, Z.; Zhang, H. L.; Chen, Z.; Zhang, Q. Reducing Aggregation Caused Quenching Effect through Co-Assembly of PAH Chromophores and Molecular Barriers. *Nat. Commun.* **2019**, *10* (1), 1–9. https://doi.org/10.1038/s41467-018-08092-y.

(82) Xie, Z.; Yang, B.; Li, F.; Cheng, G.; Liu, L.; Yang, G.; Xu, H.; Ye, L.; Hanif, M.; Liu, S.; et al. Cross Dipole Stacking in the Crystal of Distyrylbenzene Derivative: The Approach toward High Solid-State Luminescence Efficiency. *J. Am. Chem. Soc.* **2005**, *127* (41), 14152–14153. https://doi.org/10.1021/ja054661d.

(83) Zhao, C. H.; Wakamiya, A.; Inukai, Y.; Yamaguchi, S. Highly Emissive Organic Solids Containing 2,5-Diboryl-1,4-Phenylene Unit. *J. Am. Chem. Soc.* **2006**, *128* (50), 15934–15935. https://doi.org/10.1021/ja0637550.

(84) Wakamiya, A.; Mori, K.; Yamaguchi, S. 3-Boryl-2,2′-Bithiophene as a Versatile Core Skeleton for Full-Color Highly Emissive Organic Solids. *Angew. Chemie - Int. Ed.* **2007**, *46* (23), 4273–4276. https://doi.org/10.1002/anie.200604935.

(85) Würthner, F.; Thalacker, C.; Diele, S.; Tschierske, C. Fluorescent J-Type Aggregates and Thermotropic Columnar Mesophases of Perylene Bisimide Dyes. *Chem. - A Eur. J.* **2001**, *7* (10), 2245–2253. https://doi.org/10.1002/1521-3765(20010518)7:10<2245::AID-CHEM2245>3.0.CO;2-W.

(86) Luo, J.; Xie, Z.; Lam, J. W. Y.; Cheng, L.; Tang, B. Z.; Chen, H.; Qiu, C.; Kwok, H. S.; Zhan, X.; Liu, Y.; et al. Aggregation-Induced Emission of 1-Methyl-1,2,3,4,5-Pentaphenylsilole. *Chem. Commun.* **2001**, *381* (18), 1740–1741. https://doi.org/10.1039/b105159h.

(87) Peng, Q.; Yi, Y.; Shuai, Z.; Shao, J. Toward Quantitative Prediction of Molecular Fluorescence Quantum Efficiency: Role of Duschinsky Rotation. *J. Am. Chem. Soc.* **2007**, *129* (30), 9333–9339. https://doi.org/10.1021/ja067946e.

(88)   Zhang, T.; Jiang, Y.; Niu, Y.; Wang, D.; Peng, Q.; Shuai, Z. Aggregation Effects on the Optical Emission of 1,1,2,3,4,5-Hexaphenylsilole (HPS): A QM/MM Study. *J. Phys. Chem. A* **2014**, *118* (39), 9094–9104. https://doi.org/10.1021/jp5021017.

(89)   Yin, S.; Peng, Q.; Shuai, Z.; Fang, W.; Wang, Y. H.; Luo, Y. Aggregation-Enhanced Luminescence and Vibronic Coupling of Silole Molecules from First Principles. *Phys. Rev. B - Condens. Matter Mater. Phys.* **2006**, *73* (20), 1–5. https://doi.org/10.1103/PhysRevB.73.205409.

(90)   Chen, J.; Law, C. C. W.; Lam, J. W. Y.; Dong, Y.; Lo, S. M. F.; Williams, I. D.; Zhu, D.; Tang, B. Z. Synthesis, Light Emission, Nanoaggregation, and Restricted Intramolecular Rotation of 1,1-Substituted 2,3,4,5-Tetraphenylsiloles. *Chem. Mater.* **2003**, *15* (7), 1535–1546. https://doi.org/10.1021/cm021715z.

(91)   Liu, J.; Meng, Q.; Zhang, X.; Lu, X.; He, P.; Jiang, L.; Dong, H.; Hu, W. Aggregation-Induced Emission Enhancement Based on 11,11,12,12,-Tetracyano-9,10-Anthraquinodimethane. *Chem. Commun. (Camb).* **2013**, *49* (12), 1199–1201. https://doi.org/10.1039/c2cc38817k.

(92)   Shi, J.; Wu, Y.; Sun, S.; Tong, B.; Zhi, J.; Dong, Y. Tunable Fluorescence Conjugated Copolymers Consisting of Tetraphenylethylene and Fluorene Units: From Aggregation-Induced Emission Enhancement to Dual-Channel Fluorescence Response. *J. Polym. Sci. Part A Polym. Chem.* **2013**, *51* (2), 229–240. https://doi.org/10.1002/pola.26377.

(93)   Wu, W.; Ye, S.; Tang, R.; Huang, L.; Li, Q.; Yu, G.; Liu, Y.; Qin, J.; Li, Z. New Tetraphenylethylene-Containing Conjugated Polymers: Facile Synthesis, Aggregation-Induced Emission Enhanced Characteristics and Application as Explosive Chemsensors

and PLEDs. *Polymer (Guildf).* **2012**, *53* (15), 3163–3171. https://doi.org/10.1016/j.polymer.2012.05.035.

(94)   Dong, W.; Ma, Z.; Chen, P.; Duan, Q. Carbazole and Tetraphenylethylene Based AIE-Active Conjugated Polymer for Highly Sensitive TNT Detection. *Mater. Lett.* **2019**, *236*, 480–482. https://doi.org/10.1016/j.matlet.2018.10.162.

(95)   Gmeiner, J.; Karg, S.; Meier, M.; Rieß, W.; Strohriegl, P.; Schwoerer, M. Synthesis, Electrical Conductivity and Electroluminescence of Poly(P-phenylene Vinylene) Prepared by the Precursor Route. *Acta Polym.* **1993**, *44* (4), 201–205. https://doi.org/10.1002/actp.1993.010440405.

(96)   Lee, D. W.; Kwon, K.-Y.; Jin, J.-I.; Park, Y.; Kim, Y.-R.; Hwang, I.-W. Luminescence Properties of Structurally Modified PPVs: PPV Derivatives Bearing 2-(4- Tert - Butylphenyl)-5-Phenyl-1,3,4-Oxadiazole Pendants. *Chem. Mater.* **2001**, *13* (2), 565–574. https://doi.org/10.1021/cm000794g.

(97)   Sung-Ho, J.; Mock-Yeon, K.; Jin Young, K.; Kwanghee, L.; Yeong-Soon, G. High-Efficiency Poly(p-Phenylenevinylene)-Based Copolymers Containing an Oxadiazole Pendant Group for Light-Emitting Diodes. *J. Am. Chem. Soc.* **2004**, *126* (2), 2474_2480.

(98)   Kim, S. T.; Hwang, D.; Li, X. C.; Grüner, J.; Friend, R. H.; Holmes, A. B.; Shim, H. K. Efficient Green Electroluminescent Diodes Based on Poly (2-Dimethyloctylsilyl-1,4-Phenylenevinylene). *Adv. Mater.* **1996**, *8* (12), 979–982. https://doi.org/10.1002/adma.19960081206.

(99)   Vilbrandt, N.; Gassmann, A.; Von Seggern, H.; Rehahn, M. Blue-Greenish Electroluminescent Poly(p-Phenylenevinylene) Developed for Organic Light-Emitting

Diode   Applications. *Macromolecules* **2016**, *49* (5), 1674–1680. https://doi.org/10.1021/acs.macromol.5b01249.

(100) Burroughes, J. H.; Bradley, D. D. C.; Brown, A. R.; Marks, R. N.; Mackay, K.; Friend, R. H.; Burns, P. L.; Holmes, A. B. Light-Emitting Diodes Based on Conjugated Polymers. *Nature* **1990**, *347* (6293), 539–541. https://doi.org/10.1038/347539a0.

(101) Jakubiak, R.; Collison, C. J.; Wan, W. C.; Rothberg, L. J.; Hsieh, B. R. Aggregation Quenching of Luminescence in Electroluminescent Conjugated Polymers. *J. Phys. Chem. A* **1999**, *103* (14), 2394–2398. https://doi.org/10.1021/jp9839450.

(102) Cole, M. D.; Sheri, M.; Bielicki, C.; Emrick, T. Perylene Diimide-Based Ionene and Zwitterionic Polymers: Synthesis and Solution Photophysical Properties. *Macromolecules* **2017**, *50* (19), 7535–7542. https://doi.org/10.1021/acs.macromol.7b01281.

(103) Liu, Y.; Cole, M. D.; Jiang, Y.; Kim, P. Y.; Nordlund, D.; Emrick, T.; Russell, T. P. Chemical and Morphological Control of Interfacial Self-Doping for Efficient Organic Electronics.   *Adv.   Mater.   **2018**,   *30*   (15),   1705976. https://doi.org/10.1002/adma.201705976.

(104) Li, Y.; Cole, M. D.; Gao, Y.; Emrick, T.; Xu, Z.; Liu, Y.; Russell, T. P. High-Performance Perovskite Solar Cells with a Non-Doped Small Molecule Hole Transporting Layer. *ACS Appl. Energy Mater.* **2019**, *2* (3), 1634–1641. https://doi.org/10.1021/acsaem.9b00164.

SYNTHESIS OF LINEAR POLYELECTROLYTES AND POLYMER ZWITTERIONS CONTAINING PERYLENE DIIMIDES

2.1 Introduction

Ionene polymers, or 'polyionenes', represent a class of polyelectrolytes in which the charged moieties are embedded within the polymer backbone rather than positioned as pendant groups. In general, polyionenes are synthesized by the Menschuktin reaction[1] of bis-tertiary amines or bis-diphenylphosphines with electrophilic dihalides in polar organic solvents as shown in Figure 2.1. Rembaum and coworkers pioneered much of the early work on both aliphatic and aromatic polyionenes.[1–3]

The discovery of high conductivity polyionene-tetracyanoquinodimethane (TCNQ) complexes catalyzed further investigation of theses novel polyelectrolytes.[4] Since these initial
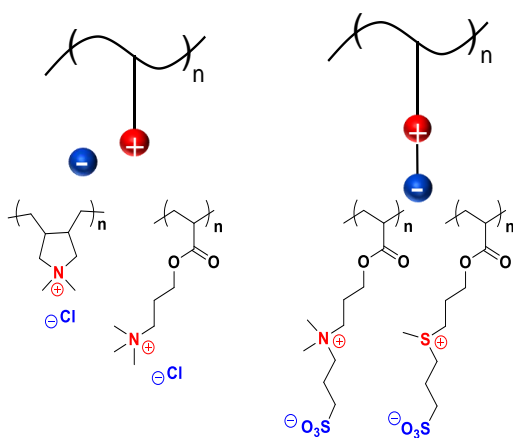
Conventional Polyelectrolytes and Polymer Zwitterions   **Polyionenes and Linear Polymer Zwitterions**
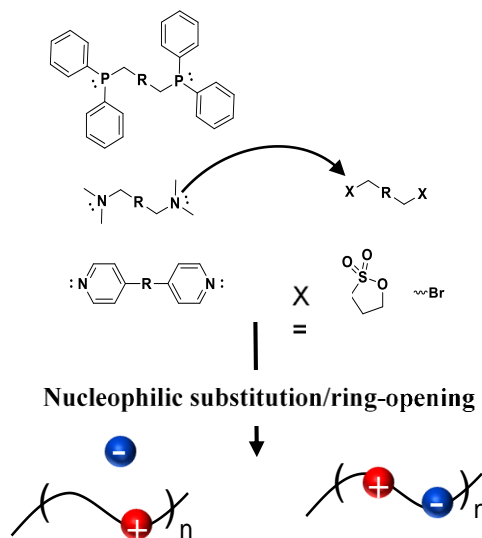
Figure 2.1. Structural comparison of conventional polyelectrolyte and polymer zwitterions to their linear analogs.

reports, there have been several accounts describing the syntheses, structure-property relationships, and mechanical properties of water-soluble ammonium- and phosphonium-based polyionenes.[5,6,7] Some commercially available polyionenes, such as polybrene, have proven useful for enhancing viral transfection.[8] More recently, novel polyionenes have emerged as components of electronically active polymeric and nanocomposite materials.[9,10]

The covalent integration of optoelectronically active components into polyionenes as pendant or main-chain moieties has also been described by Suzuki, who reported the photophysical properties of functional polyionenes containing pendent anthracene groups for probing intra/intermolecular chain dynamics.[11] Additionally, reinforced polymer folding behavior and self-assembly in aromatic polyionenes *via* donor-acceptor interactions in the polymer backbone have been examined.[12]

Zwitterionic polymers are another class of ion-containing macromolecules that have gained significant scientific interest. In these polymers the negative and positive charges are covalently linked, resulting in net neutral structures. Zwitterionic polymers have been extensively studied for their non-fouling properties,[13–15] biocompatibility,[16–18] and electronic properties [19–21]. As with polyelectrolytes, the zwitterionic functionalities in these polymers have predominately been introduced as pendant groups (Figure 2.1). In this chapter the synthetic methodology and characterization of novel polyionenes and linear polymer zwitterions containing perylene diimides (PDIs), in which ionic groups are embedded in the polymer backbone, are detailed.

PDIs are generally interesting for their thermal and chemical stability, as well as their tunable electronic and solution-assembly properties.[22] The primary focus of this work was to develop novel approaches to integrate PDI into functional polymers for photovoltaic applications. The PDI structure allows for simultaneous modification of the solubility and optoelectronic

properties. This is particularly desirable for developing π-conjugated materials for components in organic photovoltaic (OPV) devices. The versatility of PDI-based conjugated polymers was exemplified by its integration into photovoltaic devices as an electron acceptor in all polymer solar cells[23–28] as well as electron-transport layers (ETLs) in organic and perovskite[29,30] photovoltaic devices. While these π-conjugated PDI polymers have garnered significant interest, non-conjugated, main-chain PDI polymers have not been given as much attention.

In contrast to the previously mentioned conjugated polymers, π-conjugation is isolated to single PDI units in the main-chain polymers which holds the potential for unique optoelectronic and photophysical properties. Emerging efforts to prepare hydrophilic PDI-based polymers include water-soluble PDI-containing polyurethanes as fluorescent probes for live cell imaging,[31] and PDI-terpyridine polymers as metal ion sensors.[32] However, in prior reports of polyionenes containing PDI, the PDI monomers lacked functional group versatility at the aromatic core.

It has been shown that through modification of the PDI aromatic core, materials with improved emission properties and solubility can be realized.[33] Here, functionality was introduced at the 1 and 7 positions of the PDI aromatic core to yield 1,7-dibromo- (**PDIBr₂**) and 1,7-diphenyl-substituted (**PDIPh₂**) PDI monomers. Introduction of aromatic functionality resulted in PDI monomers with good solubility for facile incorporation into polymers with cationic or zwitterionic groups into the polymer backbone. The photophysical properties of the ionene and zwitterionic structures were investigated spectroscopically following systematic incorporation of PDI derivatives.

2.2 Synthesis of PDI monomers and polymers

While the aggregation of PDIs can be advantageous for certain applications, PDI monomers with high solubility and low propensity towards aggregation were necessary for the
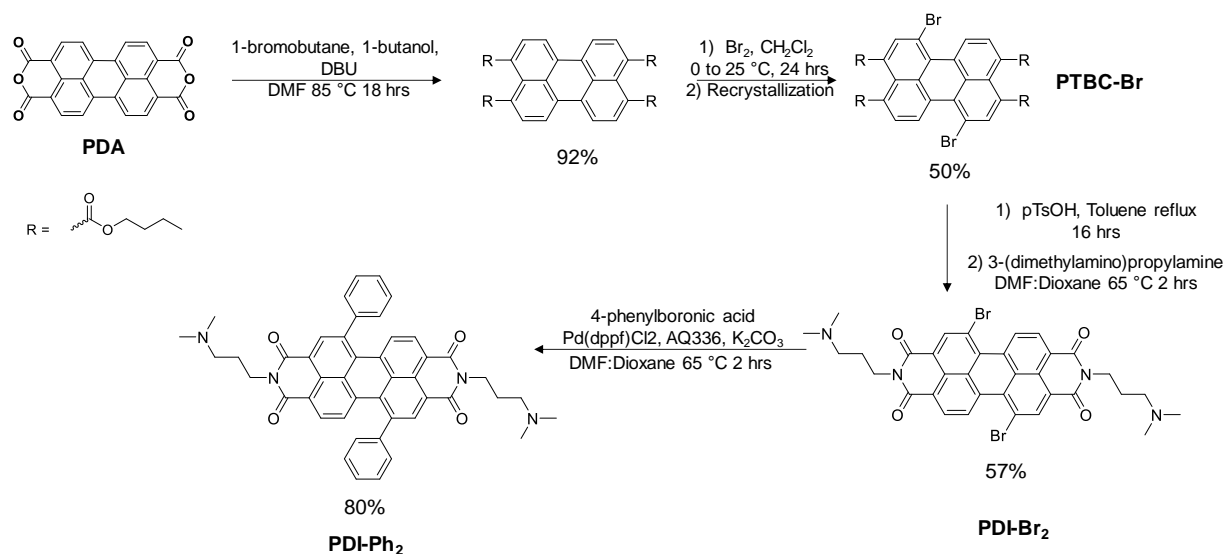
Scheme 2. 1. Synthesis of key perylene precursors and PDI monomers for polymer synthesis.

polymer chemistry discussed here. There are two approaches to attenuate the π-π interactions and increase solubility of PDIs: 1) introduction of sterically hindered groups at the imide position and 2) appending functional groups at the aromatic core. The second approach was employed in this work so that functionality at the imide position could be used for polymerization. A variation of syntheses previously reported by Marder and coworkers was used to prepare aromatic core-functionalized PDI derivatives under mild conditions.[34] As shown in Scheme 2.1, 3,4,9,10-perylene tetracarboxylic dianhydride (**PDA**) is initially reacted with 1-bromobutane and 1-butanol in the presence of 1,8-diazabicyclo[5.4.0]undec-7-ene (DBU), and subsequently treated with molecular bromine under basic conditions. The crude brominated product was recrystallized from an acetonitrile:CH_2Cl_2 mixture to yield regioisomericallly-pure 1,7 perylene tetrabutyl tetracarboxylate (**PTBC-Br**). **PTBC-Br** subsequently underwent an acidic ring-closing step to revert the molecule back to the dianhydride, followed by further reactions to prepare PDI derivatives containing tertiary amine groups at the imide position.

PDIs have traditionally been prepared by reacting the **PDA** with an amine in organic solvent under high temperature conditions (>100 °C) for extended reaction times (>12 hours).[35–37]
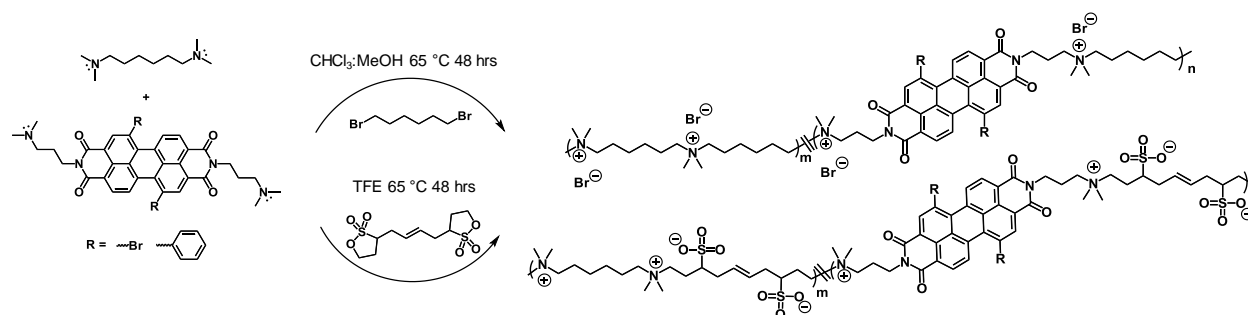
Scheme 2. 2. Synthesis of PDI-based polyionenes and polymer zwitterions.

Here, it was found that the desired tertiary amine groups could be prepared at 65 °C in dimethylformamide (DMF):1,4-dioxane mixtures within 2 hours in appreciable yields (~57%). **PDIBr₂** was converted to the 1,7-diphenyl derivative (**PDIPh₂**) by Suzuki-Miyaura coupling, allowing for a second PDI derivative for polymerization. The resulting PDI monomers were used to prepare PDI-containing polymers.

Polyionenes were synthesized by reacting **PDIBr₂** or **PDIPh₂**, with N,N,N',N'-tetramethyl-1,6-hexanediamine (**TMHDA**) and 1,6-dibromohexane to yield structures of desired PDI incorporation and tailored solubility (Scheme 2.2). The isolated PDI-containing polyionenes exhibited excellent solubility in water, methanol, and 2,2,2-trifluoroethanol (TFE) at >15 mg/mL in all cases. The bromide and phenyl groups in the perylene core attenuated inter-PDI π-π interactions to the benefit of polymer solubility and evolution of appreciable molecular weight, while the tertiary amines at the imide positions provided nucleophilic sites for polymerization. Scheme 2.2 illustrates the addition step-growth polymerization strategy, in which the PDI monomers were reacted with 1,6-dibromohexane to afford the desired ionene polymers respectively. Previous reports of PDI polyionenes employed DMF as the reaction solvent and PDI monomers without aromatic core functionality.[9] Here, attempted polymerizations of **PDIBr₂** and **PDIPh₂** in DMF resulted in low product yields and poor control over PDI incorporation due to the low solubility of the monomers and polymers in DMF. To address this issue, polymerizations of

Table 2.1. PDI incorporation, molecular weights, and yield of the PDI-containing polyionenes.

Polymer[a]	Monomer feed (mole %)	X_{PDI} (mole %)[b]	Mn^c (kDa)	Mw^c (kDa)	Đ[c]	Yield[d] (%)
PDIBr₂-10%	10	9	38.1	56.4	1.5	82
PDIBr₂-50%	50	47	33.7	47.4	1.4	80
PDIBr₂-100%	100	100	18.5	25.5	1.4	43
PDIPh₂-10%	10	8	30.5	46.2	1.5	83
PDIPh₂-50%	50	51	30.3	39.0	1.4	74
PDIPh₂-100%	100	100	18.1	23.0	1.3	48

[a]Polymer nomenclature based on theoretical PDI incorporation; [b] mole percent PDI incorporation determined by ^{1}H NMR spectroscopy; [c]number-average molecular weight estimated by GPC; [d]weight-average molecular weight estimated by GPC.

PDIBr₂ or **PDIPh₂** were conducted in mixture of $CHCl_3$ and methanol, in which the monomer exhibited good solubility. Polymerizations were conducted at an initial total monomer concentration of 0.5 M in a 1:1 mixture of $CHCl_3$ and methanol for 48 hours at 70 °C. Upon cooling, viscous solutions were precipitated into diethyl ether and the polymers were isolated by centrifugation. The crude products were dissolved in methanol then purified by dialysis against a 1:1 methanol:water mixture, followed by pure water, and finally isolated as powders by lyophilization. The purified polymers exhibited red or purple color, indicating incorporation of **PDIBr₂** (red) or **PDIPh₂** (purple), respectively, into the polymer backbone. Polymers were prepared with target PDI incorporation of 10, 50, or 100 mole% PDI which allowed for studying the influence of PDI content on solution and optical properties.The nomenclature in Table 2.1 is based on the selected PDI derivative and its mole% incorporation into the polyionenes. Characterization of the molecular weight and solution photophysical properties of these macromolecules proved highly solvent dependent, with spectral signatures hinging on solvent-induced aggregation.
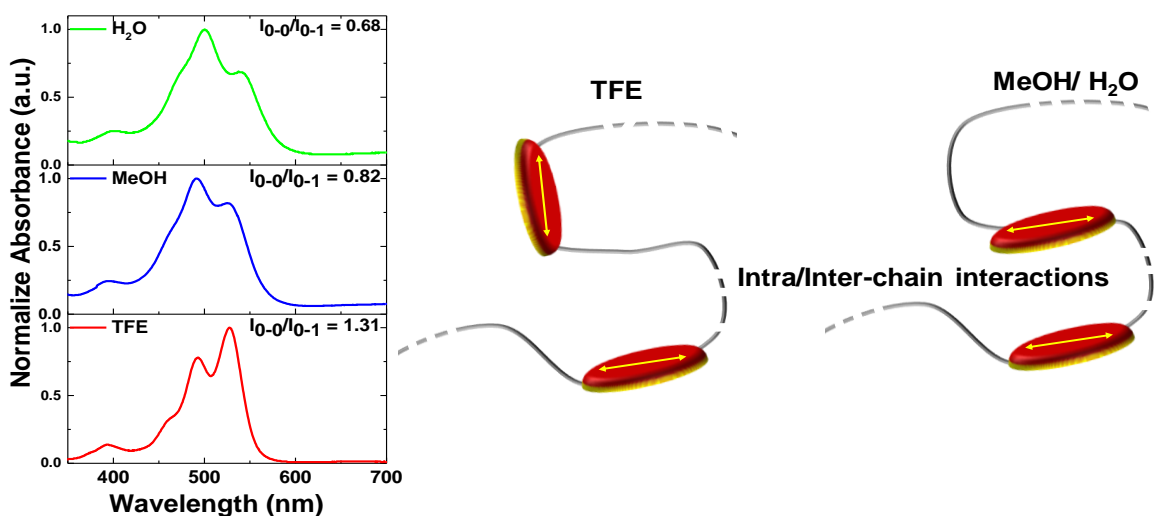
Figure 2.2. (Left) Representative solution UV-Vis spectra of PDIBr2-50% ionene in TFE (green), methanol (blue), and water (red). (Right) Proposed PDI transition dipoles in corresponding solvents.

The molecular weights of previously reported PDI-based polyionenes were estimated by gel-permeation chromatography (GPC) with water as the mobile phase.[9,32] In aqueous environments these polymers aggregate, as reflected by the high intensity S_{0-1} absorbance band and weak vibronic signature observed in their solution UV-Vis absorption spectra.[9,32] Aggregation of the polymer chains in solution could result inaccurate molecular weight estimations. Here, GPC and spectroscopic analyses were conducted in TFE for both the ionene and zwitterionic polymers. Representative UV-Vis spectra of the **PDIBr2-50%** polyionene in TFE, methanol, and water are shown in Figure 2.2. In TFE, the absorption maxima of the polymer were observed at 528 nm; indicative of well-solvated PDI, in which the long-wavelength S_{0-0} vibronic transition is dominant. In water and methanol, the absorption maxima shifted to the shorter wavelength S_{0-1} vibronic transition at 500 nm (in water) and 491 nm (in methanol), indicative of strong H-type aggregate interactions (Figure 2.2). In Figure 2.2 the proposed transition dipole coupling of PDI units corresponding to spectral features observed for each solution is shown. These solution absorption

Table 2. 2. PDI incorporation, molecular weights, and yield of the PDI-containing zwitterionic polymers.

Polymer [a]	Monomer feed (mole %)	X_{PDI} (mole %)[b]	Mn^c (kDa)	Mw^c	Đ [c]	Yield [d] (%)
PDIZBr₂-10%	10	18	8.6	12.5	1.4	86
PDIZBr₂-50%	50	44	7.0	9.0	1.3	80
PDIZBr₂-100%	100	100	4.5	5.0	1.3	40
PDIZPh₂-10%	10	17	13.0	15.0	1.2	84
PDIZPh₂-50%	50	37	8.0	10.0	1.2	82
PDIZPh₂-100%	100	100	6.0	7.0	1.1	40

[a]Polymer nomenclature based on theoretical PDI incorporation, with 'Z' denoting zwitterionic functionality; [b] mole percent PDI incorporation determined by ^{1}H NMR analysis; [c]number-average molecular weight estimated by GPC, [d]weight-average molecular weight estimated by GPC.

spectra suggest TFE as a preferred solvent for characterization and for suppressing the tendency of PDI units to aggregate.

The estimated molecular weights of the PDI polyionenes proved critically dependent on PDI content. As PDI incorporation increased, polymer molecular weights and yields decreased (Table 2.1). This was likely due to the tendency of the charged polymer to aggregate in the CHCl₃:MeOH solvent mixture, resulting in termination of the polymerization due to inaccessibility of the reactive groups. The preparation of **PDI-50%** and **PDI-100%** was attempted in TFE to increase monomer conversion. However, these polymerizations resulted in low molecular weight oligomers, likely due to protonation of the tertiary amines. The ^{1}H NMR spectra of PDI-ionene polymers displayed chemical shifts corresponding to the polymer structure, as shown in Figure 2.3. Signals ranging from 7.60 to 9.65 ppm correspond to protons in the aromatic core of the PDI, confirming successful PDI incorporation. Copolymer compositions were determined by integration of the imide protons of the PDI (4.40 ppm) against the methylene protons of the
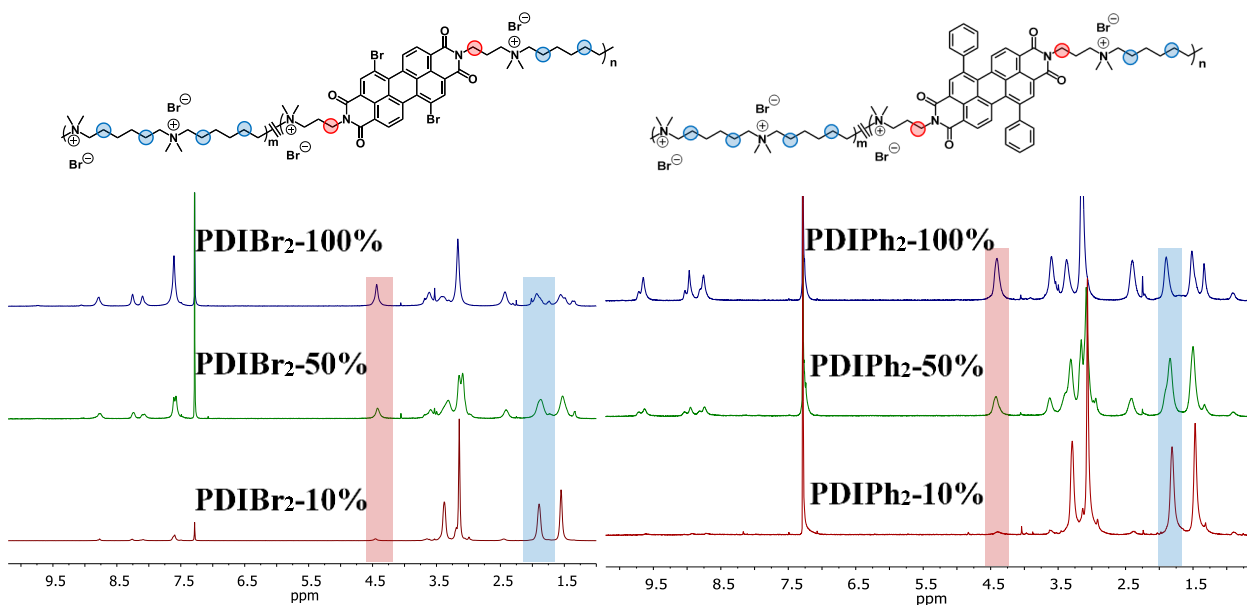
Figure 2. 3. ^{1}H NMR in CDCl3:dTFA of (left) PDIBr2-and (right) PDIPh2-containing polyionenes.

THMDA-based polyionene segments (1.80 ppm). Additionally, the aromatic protons increased in relative intensity as PDI content was increased.

In contrast to the ionene polymers, the PDI polymer zwitterions (**PDIZs**), containing sulfobetaine groups in the polymer backbone, could not be prepared in a CHCl$_3$:MeOH solvent mixture due to premature precipitation. Instead, the **PDIZs** were synthesized by reacting butene bis-sultone (**BBS**) with the appropriate stoichiometric equivalents of **PDIBr$_2$** or **PDIPh$_2$** and **TMHDA** in TFE. The polymerizations were conducted for 48 hours at 70 ˚C, then purified as described for the PDI-ionene polymers, with results shown in Table 2.2. Ring-opening of **BBS** to form the polymer zwitterions was confirmed by the upfield shift of the methylene protons adjacent to the sulfur, from 4.40 ppm to 3.30 ppm, indicative of the sultone-to-sulfobetaine conversion. In contrast to conventional polymer zwitterions,[19,38] the polymers discussed contained the zwitterionic sulfobetaine moiety in the polymer backbone.

Like the trends observed in the polyionenes, the molecular weights and yields of the zwitterionic polymers were influenced by the extent of PDI incorporation. Copolymer

44
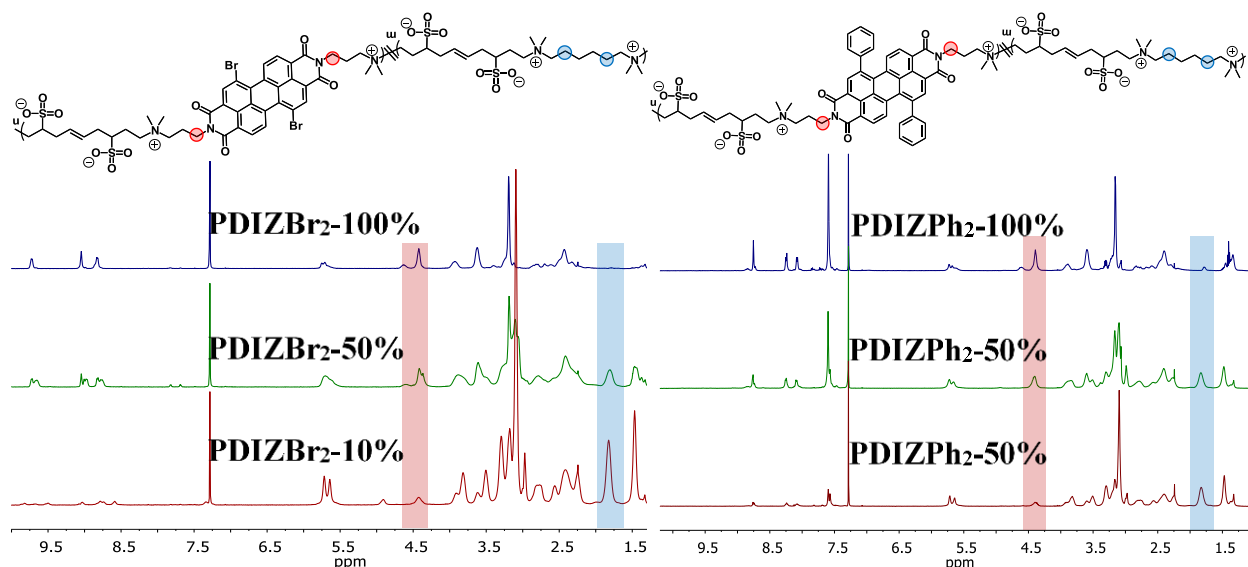
Figure 2. 4. 1H NMR in CDCl3:dTFA of PDIBr2-(top) and PDIPh2-containing (bottom) polymer zwitterions.

composition was calculated using the same method employed for the polyionenes (Figure 2.4). In comparison to the polyionenes, PDI incorporation into the zwitterionic polymers was not as well-controlled. Independent of PDI incorporation, the zwitterionic polymers exhibited lower molecular weights than the ionene polymers, due to the lower reactivity of bis-sultone **3** versus the α,ω-alkyl dihalide and the relative acidity of TFE as solvent. While the PDI-based zwitterionic and ionene polymers exhibited similar solubility properties in water and TFE, their solubilities in methanol were substantially different. Specifically, the solubility of **PDIZs** in methanol was significantly lower (< 1 mg/mL) and independent of the PDI derivative employed for the polymerization. This lower methanol solubility was attributed to dipole-dipole attractive interactions of the zwitterionic groups in the polymer backbone.

2.3 Solution optical properties

The photophysical properties of **PDIBr2** ($\varepsilon = 40{,}400$ M^{-1} cm^{-1}, $\lambda_{abs} = 528$ nm) and **PDIPh2** ($\varepsilon = 25{,}600$ M^{-1} cm^{-1}, $\lambda_{abs} = 525$ nm) were influenced by substituents on the PDI aromatic core. The bromide-substituted PDI exhibited characteristic absorption band corresponding to the S$_0$ to

S_1 electronic transition (transition dipole along molecular axis) with discrete 0-0 (527 nm), 0-1 (493 nm), and 0-2 (460 nm) vibronic bands (Figure 2.5A and 2.5B). Additionally, a low-absorbance peak at 396 nm associated with the S_0 to S_2 electronic transition (transition dipole orthogonal to molecular axis) was also observed.[39] These spectral features correlated well with previously reported 1,7-dibromo substituted PDI derivatives.[34] **PDIPh₂** absorption spectra was redshifted and lacked discrete vibronic structures in comparison to **PDIBr₂**. Simulations of PDI derivatives containing bulky groups at the aromatic core, such as those in **PDIPh₂**, revealed the sterically hindered moieties in these structures interfere with π-π interactions.[39] The suppression of these interactions resulted spectroscopic features of J-type coupling (e.g., band-broadened and red-shifted), similar to the UV-Vis spectra of the **PDIPh₂** and its corresponding polymers. The absorbance spectra of the all polymer samples were recorded as dilute (μM) TFE solutions at equivalent optical densities, allowing for optimized spectral resolution to elucidate the relationship between PDI content, charge density, and the observed spectral signatures. At low PDI incorporation, both the cationic and zwitterionic polymers exhibited similar vibronic signatures to the **PDIBr₂** and **PDI-Ph₂** small molecules. Incorporation of **PDIBr₂** into the polymers resulted in a bathochromic (i.e., red or longer wavelength) shift of the absorption onset, which was most distinct in **PDIBr₂-10%** and diminished with increasing PDI content. This trend was reversed for samples containing **PDIPh₂**, with the homopolymer (i.e., **PDIPh₂-100%**) exhibiting the largest red shift in its absorption spectrum. The details of the absorption spectra are shown in Tables 2.3.

The relative intensity of the S_{0-0} to S_{0-1} vibronic transitions in the absorption spectra, here referred to as I_{0-0}/I_{0-1}, quantified the extent of PDI-PDI interaction in these PDI-based structures. The discrete vibrational modes observed in the absorption spectra of the **PDIBr₂** ionene and zwitterionic polymers allowed for calculation of this ratio and comparison of the zwitterionic and

Table 2. 3. Summary of solution photophysical properties PDIBr$_2$-containing polyionenes and zwitterionic polymers.

Compound	λ_{abs} (nm)	λ_{em} (nm)	$I_{0-0/0-1}$	Φ_f
PDIBr$_2$	527, 493, 460, 392	551, 591	1.43	0.65
PDIBr$_2$-10%	527, 493, 460, 392	551, 591	1.38	0.34
PDIBr$_2$-50%	527, 493, 460, 392	551, 591	1.31	0.20
PDIBr$_2$-100%	527, 493, 460, 392	551, 591	1.10	0.10
PDIZBr$_2$-10%	527, 493, 460, 392	549, 597	1.20	0.30
PDIZBr$_2$-50%	527, 493, 460, 392	553, 591	0.87	0.21
PDIZBr$_2$-100%	527, 493, 460, 392	553, 591	0.83	0.16

ionene derivatives. In TFE, PDI-Br$_2$ exhibited an I_{0-0}/I_{0-1} value of 1.43, indicative of a good solvent environment and low PDI-PDI transition dipole parallel alignment due to aggregation. The moderate decrease of the I_{0-0}/I_{0-1} values as **PDIBr$_2$** was incorporated into the ionene polymers suggested that the PDI units remained solvated when incorporated into the polymer backbone. The zwitterionic polymers containing **PDIBr$_2$** exhibited significantly lower I_{0-0}/I_{0-1} values. Notably, the S$_{0-1}$ absorption band (493 nm) became dominant for **PDIZBr$_2$-50%** and **PDIZBr$_2$-100%** (while **PDIZBr$_2$-10%** exhibit absorption features similar to the **PDIBr$_2$** monomer (i.e., S$_{0-0}$ absorption maxima). The absorption maxima shift from S$_{0-0}$ to S$_{0-1}$ is characteristic of enhanced co-facial alignment of the PDI transition dipoles. This suggested that at 50 and 100 mole% PDI the zwitterionic polymers derivatives have a propensity to aggregate in contrast to the polyionenes.

The proposed aggregation of the zwitterionic polymers was not to an extent that resulted in fluorescence quenching. This is shown in Figure 2.6, using dilute aqueous and TFE solutions of **PDIZBr$_2$-50%**. In TFE, the polymer was emissive upon UV irradiation at 365 nm (Figure 2.6B), while in the aqueous solution no emission was observed (Figure 2.6A). Similar findings were observed for the zwitterionic **PDIZ-100%** derivatives independent of aromatic core

47
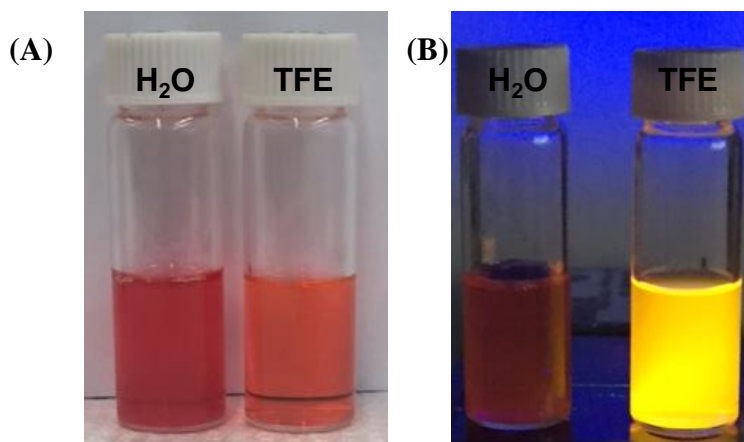
Figure 2. 5. 0.1 mg/mL of PDIZBr$_2$-50% polymer zwitterions (A) in water (left) and TFE (right) in ambient light; (B) under UV irradiation at 365 nm.

functionality. This suggests that the dominant S$_{0-1}$ transition in the absorption spectra of polymers **PDIZBr$_2$-50%** and **PDIZBr$_2$-100%** is facilitated by dipole-dipole interactions of the zwitterions but the π-π interactions are insufficient for quenching. This variation in spectral signatures between cationic and zwitterionic derivatives reflected the influence of these two polymer classes. Specifically, the enhanced H-type spectral features of the **PDIZs** was facilitated by attractive inter-zwitterion interactions, in contrast to the repulsive cation-cation interactions of the PDI-based ionene polymers.

Polymers prepared from PDI-Ph$_2$ lacked well-resolved vibronic signatures necessary for quantitative analysis of I$_{0-0}$/I$_{0-1}$ absorption intensity. The absorption spectra of the ionene polymers containing **PDIPh$_2$** are shown in Figures 2.5C. The vibronic features in the absorption spectra of **PDIPh$_2$** and its resulting polymers could not be resolved. The **PDIZPh$_2$** zwitterionic derivatives displayed a hypsochromic (i.e., blue or shorter wavelength) shift of the absorption maxima relative to the **PDIPh$_2$** small molecule. The absorption maxima of the **PDIZPh$_2$-10%** polymer was the most blue-shifted relative to **PDIPh$_2$** while **PDIZPh$_2$-50%** and **PDIZPh$_2$-100%** displayed

48

maxima closer to the **PDIPh₂** precursor. These spectral observations again support the hypothesis that the zwitterionic functionality facilitates H-type aggregation and enhanced coulombic coupling in solution through dipole-dipole inter/intra zwitterion attractions.

Photoluminescence (PL) quantum yields (Φ_f) of the polymers were studied as a function of PDI incorporation for PDIBr₂ derivatives (Tables 2.4). For both the ionene and zwitterionic polymers, Φ_f was observed to decrease with increasing PDI incorporation. The decrease in quantum yield following PDI incorporation is attributed to self-quenching between PDI units in the polymer backbone. It was postulated that covalently linking PDI units together to prepare the discussed macromolecules, facilitated non-radiative processes. In accord with the UV-Vis results, the similar Φ_f values calculated for both cationic and zwitterionc derivatives of **PDIBr₂**-based polymers suggest that zwitterion-zwitterion interactions influence chain conformation in solution without producing non-emissive, PDI aggregates. Through these studies new class of PDI polymers was developed with solution properties that could be easily tailored through polymer backbone functionality.

Table 2. 4. Summary of solution photophysical properties PDIPh₂-containing polyionenes and zwitterionic polymers.

Compound	λ_{abs}(nm)
PDIPh₂	564, 523, 397
PDIPh₂-10%	564, 523, 397
PDIPh₂-50%	535, 397
PDIPh₂-100%	531, 400
PDIZPh₂-10%	564, 522, 397
PDIZPh₂-50%	535, 397
PDIZPh₂-100%	531, 400

2.4 Conclusion

In summary, cationic (ionene) and zwitterionic (sulfobetaine) PDI-based polymers were synthesized starting from two core-functionalized PDI-diamine monomers. The novel bis-sultone comonomer **BBS** allowed access to linear zwitterionic polymers with solution properties and spectral features distinct from the cationic versions. Bromide and phenyl groups were introduced to the PDI aromatic core to attenuate π-π interactions, which drive self-assembly and diminish solubility. PDI incorporation was well-controlled via the monomer feed ratio and all polymers were synthesized in high yield with appreciable molecular weights. Both the zwitterionic and cationic polymers exhibited good solubility TFE, which will be used to process the polymers into thin films in chapter 3, independent of PDI content or core functionality.

The solution photophysical properties of these novel polymers were studied by UV-Vis absorption and PL spectroscopy, with absorption spectral signatures of the polymer modulated by PDI core functionality and cationic or zwitterionic groups embedded in the polymer backbone. Spectroscopic analysis revealed that PDI-PDI interactions could be modulated through the PDI incorporation in the polymer backbone. Moreover, the polyionene and linear zwitterionic platform offered a method to control π-conjugation density and study the evolution of optoelectronic properties. The knowledge of these materials developed here will be expanded in Chapter 3, in which PDI-based polyionenes and polymer zwitterions are evaluated as charge selective layers in photovoltaic devices.

2.5 References

(1)   Rembaum, A.; Baumgartner, W.; Eisenberg, A. Aliphatic Ionenes. Polym. Lett. 1968, 6, 159–171. https://doi.org/10.1002/pol.1968.110060302.

(2)   Rembaum, A.; Rile, H.; Somoano, R. V. Kinetics of Formation of High Charge Density Ionene Polymers. J. Polym. Sci. Part B Polym. Lett. 1970, 8 (7), 457–466. https://doi.org/10.1002/pol.1970.110080701.

(3)   Rembaum, A.; Singer, S.; Keyzer, H. Ionene Polymers. III. Dicationic Crosslinking Agents (1). J. Polym. Sci. Part B Polym. Lett. 1969, 7 (5), 395–402. https://doi.org/10.1002/pol.1969.110070512.

(4)   Lupinski, J. H.; Kopple, K. D. Electroconductive Polymers. Science (80-.). 1964, 146 (3647), 1038–1039. https://doi.org/10.1126/science.146.3647.1038.

(5)   Hemp, S. T.; Zhang, M.; Tamami, M.; Long, T. E. Phosphonium Ionenes from Well-Defined Step-Growth Polymerization: Thermal and Melt Rheological Properties. Polym. Chem. 2013, 4 (12), 3582. https://doi.org/10.1039/c3py00365e.

(6)   Williams, S. R.; Long, T. E. Recent Advances in the Synthesis and Structure-Property Relationships of Ammonium Ionenes. Prog. Polym. Sci. 2009, 34 (8), 762–782. https://doi.org/10.1016/j.progpolymsci.2009.04.004.

(7)   Tamami, M.; Salas-De La Cruz, D.; Winey, K. I.; Long, T. E. Structure-Property Relationships of Water-Soluble Ammonium-Ionene Copolymers. Macromol. Chem. Phys. 2012, 213 (9), 965–972. https://doi.org/10.1002/macp.201200047.

(8) Han, M.; Yu, D.; Song, Q.; Wang, J.; Dong, P.; He, J. Polybrene: Observations on Cochlear Hair Cell Necrosis and Minimal Lentiviral Transduction of Cochlear Hair Cells. Neurosci. Lett. 2015, 600, 164–170. https://doi.org/10.1016/j.neulet.2015.06.011.

(9) Hu, Z.; Xu, R.; Dong, S.; Lin, K.; Liu, J.; Huang, F.; Cao, Y. Quaternisation-Polymerized N-Type Polyelectrolytes: Synthesis, Characterisation and Application in High-Performance Polymer Solar Cells. Mater. Horiz. 2017, 4 (1), 88–97. https://doi.org/10.1039/C6MH00434B.

(10) Gao, M.; Zhang, X.; Yang, B.; Li, F.; Shen, J. Assembly of Modified CdS Particles /Cationic Polymer Based on Electrostatic Interactions. Thin Solid Films 1996, 285, 242–245.

(11) Suzuki, Y.; Tazuke, S. Functionalized Polyionenes. 1. Synthesis and Photoreaction of Polyionenes Bearing Pendant (9-Anthry1)Methyl Groups. Macromolecules 1980, 8 (13), 25–30.

(12) De, S.; Ramakrishnan, S. Charge-Transfer Reinforced Folding of Novel Ionenes. Macromolecules 2009, 42 (22), 8599–8603. https://doi.org/10.1021/ma901954x.

(13) Van Andel, E.; Lange, S. C.; Pujari, S. P.; Tijhaar, E. J.; Smulders, M. M. J.; Savelkoul, H. F. J.; Zuilhof, H. Systematic Comparison of Zwitterionic and Non-Zwitterionic Antifouling Polymer Brushes on a Bead-Based Platform. Langmuir 2019, 35 (5), 1181–1191. https://doi.org/10.1021/acs.langmuir.8b01832.

(14) Kolewe, K. W.; Dobosz, K. M.; Rieger, K. A.; Chang, C. C.; Emrick, T.; Schiffman, J. D. Antifouling Electrospun Nanofiber Mats Functionalized with Polymer Zwitterions. ACS

Appl. Mater. Interfaces 2016, 8 (41), 27585-27593Kolewe, K. W.; Dobosz, K. M.; Rieger, K. https://doi.org/10.1021/acsami.6b09839.

(15) Leigh, B. L.; Cheng, E.; Xu, L.; Derk, A.; Hansen, M. R.; Guymon, C. A. Antifouling Photograftable Zwitterionic Coatings on PDMS Substrates. Langmuir 2019, 35 (5), 1100–1110. https://doi.org/10.1021/acs.langmuir.8b00838.

(16) Hu, G.; Parelkar, S. S.; Emrick, T. A Facile Approach to Hydrophilic, Reverse Zwitterionic, Choline Phosphate Polymers. Polym. Chem. 2015, 6 (4), 525–530. https://doi.org/10.1039/c4py01292e.

(17) Ko, D. Y.; Patel, M.; Jung, B. K.; Park, J. H.; Jeong, B. Phosphorylcholine-Based Zwitterionic Biocompatible Thermogel. Biomacromolecules 2015, 16 (12), 3853–3862. https://doi.org/10.1021/acs.biomac.5b01169.

(18) Wang, W.; Ji, X.; Kapur, A.; Zhang, C.; Mattoussi, H. A Multifunctional Polymer Combining the Imidazole and Zwitterion Motifs as a Biocompatible Compact Coating for Quantum Dots. J. Am. Chem. Soc. 2015, 137 (44), 14158–14172. https://doi.org/10.1021/jacs.5b08915.

(19) Lee, H.; Puodziukynaite, E.; Zhang, Y.; Stephenson, J. C.; Richter, L. J.; Fischer, D. a; Delongchamp, D. M.; Emrick, T.; Briseno, A. L. Poly(Sulfobetaine Methacrylate)s as Electrode Modi Fi Ers for Inverted Organic Electronics. J. Am. Chem. Soc. 2015, 137, 540–549. https://doi.org/10.1021/ja512148d.

(20) Liu, Y.; Page, Z. A.; Russell, T. P.; Emrick, T. Finely Tuned Polymer Interlayers Enhance Solar Cell Efficiency. Angew. Chemie - Int. Ed. 2015, 54 (39), 11485–11489. https://doi.org/10.1002/anie.201503933.

(21)   Page, Z. A.; Liu, F.; Russell, T. P.; Emrick, T. Tuning the Energy Gap of Conjugated Polymer Zwitterions for Efficient Interlayers and Solar Cells. J. Polym. Sci. Part A Polym. Chem. 2015, 53 (2), 327–336. https://doi.org/10.1002/pola.27349.

(22)   Huang, C.; Barlow, S.; Marder, S. R. Perylene-3,4,9,10-Tetracarboxylic Acid Diimides: Synthesis, Physical Properties, and Use in Organic Electronics. J. Org. Chem. 2011, 76 (8), 2386–2407. https://doi.org/10.1021/jo2001963.

(23)   Jiang, X.; Xu, Y.; Wang, X.; Yang, F.; Zhang, A.; Li, C.; Ma, W.; Li, W. Conjugated Polymer Acceptors Based on Fused Perylene Bisimides with a Twisted Backbone for Non-Fullerene Solar Cells. Polym. Chem. 2017. https://doi.org/10.1039/C7PY00444C.

(24)   Guo, Y.; Li, Y.; Awartani, O.; Zhao, J.; Han, H.; Ade, H.; Zhao, D.; Yan, H. A Vinylene-Bridged Perylenediimide-Based Polymeric Acceptor Enabling Efficient All-Polymer Solar Cells Processed under Ambient Conditions. Adv. Mater. 2016, 28 (38), 8483–8489. https://doi.org/10.1002/adma.201602387.

(25)   Liang, Y.; Lan, S.; Deng, P.; Zhou, D.; Guo, Z.; Chen, H.; Zhan, H. Regioregular and Regioirregular Poly(Selenophene-Perylene Diimide) Acceptors for Polymer-Polymer Solar Cells. ACS Appl. Mater. Interfaces 2018, 10 (38), 32397–32403. https://doi.org/10.1021/acsami.8b09061.

(26)   Zhou, E.; Tajima, K.; Yang, C.; Hashimoto, K. Band Gap and Molecular Energy Level Control of Perylene Diimide-Based Donor–Acceptor Copolymers for All-Polymer Solar Cells. J. Mater. Chem. 2010, 20 (12), 2362. https://doi.org/10.1039/b923452g.

(27)   Liu, W.; Tkachov, R.; Komber, H.; Senkovskyy, V.; Schubert, M.; Wei, Z.; Facchetti, A.; Neher, D.; Kiriy, A. Chain-Growth Polycondensation of Perylene Diimide-Based

Copolymers: A New Route to Regio-Regular Perylene Diimide-Based Acceptors for All-Polymer Solar Cells and n-Type Transistors. Polym. Chem. 2014, 5 (10), 3404. https://doi.org/10.1039/c3py01707a.

(28)   Zhang, Y.; Guo, X.; Su, W.; Guo, B.; Xu, Z.; Zhang, M.; Li, Y. Perylene Diimide-Benzodithiophene D-A Copolymers as Acceptor in All-Polymer Solar Cells. Org. Electron. 2017, 41, 49–55. https://doi.org/10.1016/j.orgel.2016.11.038.

(29)   Zhang, M.; Li, T.; Zheng, G.; Li, L.; Qin, M.; Zhang, S.; Zhou, H.; Zhan, X. An Amino-Substituted Perylene Diimide Polymer for Conventional Perovskite Solar Cells. Mater. Chem. Front. 2017, 1 (10), 2078–2084. https://doi.org/10.1039/C7QM00221A.

(30)   Guo, Q.; Xu, Y.; Xiao, B.; Zhang, B.; Zhou, E.; Wang, F.; Bai, Y.; Hayat, T.; Alsaedi, A.; Tan, Z. Effect of Energy Alignment, Electron Mobility, and Film Morphology of Perylene Diimide Based Polymers as Electron Transport Layer on the Performance of Perovskite Solar Cells. ACS Appl. Mater. Interfaces 2017, 9 (12), 10983–10991. https://doi.org/10.1021/acsami.7b00902.

(31)   Wang, L.; Sun, C.; Li, S.; Jia, N.; Li, J.; Qu, F.; Goh, K.; Chen, Y. Perylene Bisimide-Incorporated Water-Soluble Polyurethanes for Living Cell Fluorescence Labeling. Polym. (United Kingdom) 2016, 82, 172–180. https://doi.org/10.1016/j.polymer.2015.11.037.

(32)   Jin, L.; Liu, C.; An, N.; Zhang, Q.; Wang, J.; Zhao, L.; Lu, Y. Fluorescence Turn-on Detection of Fe 3+ in Pure Water Based on a Cationic Poly(Perylene Diimide) Derivative. RSC Adv. 2016, 6 (63), 58394–58400. https://doi.org/10.1039/C6RA08267J.

(33)   Tian, Z.; Shaller, D.; Li, A. D. Q.; Shaller, A. D.; Li, A. D. Q. Twisted Perylene Dyes
         Enable Highly Fluorescent and Photostable Nanoparticles. Chem. Commun. 2009, No. 2,
         180–182. https://doi.org/10.1039/b815507k.

(34)   Gunbas, D. D.; Grozema, F. C.; Sudho, E. J. R.; Jager, W. F. Synthesis of
         Regioisomerically Pure 1,7-Dibromoperylene-3,4,9,10-Tetracarboxylic Acid Derviatives.
         J. Org. Chem. 2014, 3–10. https://doi.org/10.1021/jo501180a.

(35)   Zhao, Z.; He, J.; Wang, J.; Chen, W.; Wang, N.; Zhang, Y.; Yang, R. A Water/Alcohol-
         Soluble Copolymer Based on Fluorene and Perylene Diimide as a Cathode Interlayer for
         Inverted Polymer Solar Cells. J. Mater. Chem. C 2015, 3, 4515–4521.
         https://doi.org/10.1039/C5TC00450K.

(36)   Eakins, G. L.; Gallaher, J. K.; Keyzers, R. a.; Falber, A.; Webb, J. E. a; Laos, A.; Tidhar,
         Y.; Weissman, H.; Rybtchinski, B.; Thordarson, P.; et al. Thermodynamic Factors
         Impacting the Peptide-Driven Self-Assembly of Perylene Diimide Nanofibers. J. Phys.
         Chem. B 2014, 118 (29), 8642–8651. https://doi.org/10.1021/jp504564s.

(37)   Zhang, S.; Wen, Y.; Zhou, W.; Guo, Y.; Ma, L.; Zhao, X.; Zhao, Z.; Barlow, S.; Marder,
         S. R.; Liu, Y.; et al. Perylene Diimide Copolymers with Dithienothiophene and
         Dithienopyrrole: Use in n-Channel and Ambipolar Field-Effect Transistors. J. Polym. Sci.
         Part A Polym. Chem. 2013, n/a-n/a. https://doi.org/10.1002/pola.26521.

(38)   Chen, X.; Parelkar, S. S.; Henchey, E.; Schneider, S.; Emrick, T. PolyMPC-Doxorubicin
         Prodrugs. Bioconjug. Chem. 2012, 23 (9), 1753–1763. https://doi.org/10.1021/bc200667s.

(39)   Würthner, F.; Thalacker, C.; Diele, S.; Tschierske, C. Fluorescent J-Type Aggregates and
         Thermotropic Columnar Mesophases of Perylene Bisimide Dyes. Chem. - A Eur. J. 2001,

7 (10), 2245–2253. https://doi.org/10.1002/1521-3765(20010518)7:10<2245::AID-CHEM2245>3.0.CO;2-W.

CHAPTER 3

PDI-BASED CATHODE MODIFYING LAYERS

3.1 Introduction

Controlling interfaces has played a pivotal role in the advancement of thin film photovoltaic devices. Within these multi-layered systems, each interface holds the risk of causing device failure while also presenting an opportunity to enhance the device's performance and stability. In thin film photovoltaics, introduction of charge selective layers between the active layer and the metal electrodes has been a promising method of improving device stability, wettability of individual layers, and charge transport.[1,2] An area of particular interest is the development of electron-transporting layer (ETL) materials. Over the last two decades there has been significant advancement in ETL technology for both organic photovoltaic (OPV) and perovskite-based devices, realizing materials that can tailor the active-layer/electrode interface.

As mentioned in chapter 1, low work function, transparent metal oxide materials have been shown enhanced photovoltaic performance as ETLs.[2,3,12,4–11] While these materials efficiently transport electrons and can be fabricated as transparent films in traditional and inverted devices, they have been shown to exhibit limitation that can be detrimental to photovoltaic device performance and commercialization. Firstly, they require costly, high temperature processing conditions and have been shown to be susceptible to photodegredation.[13] Secondly, the electronic properties (conductivity, bandgap, etc.) are fixed making these materials less versatile and applicable to the wide range of active layer materials used in high-performing photovoltaic devices. Moreover, heterogeneous doping in thin films of these materials leads to recombination trap sites limiting maximum photovoltaic performance.[14] To address these issues there has been significant work in developing solution-processable organic ETLs.

58
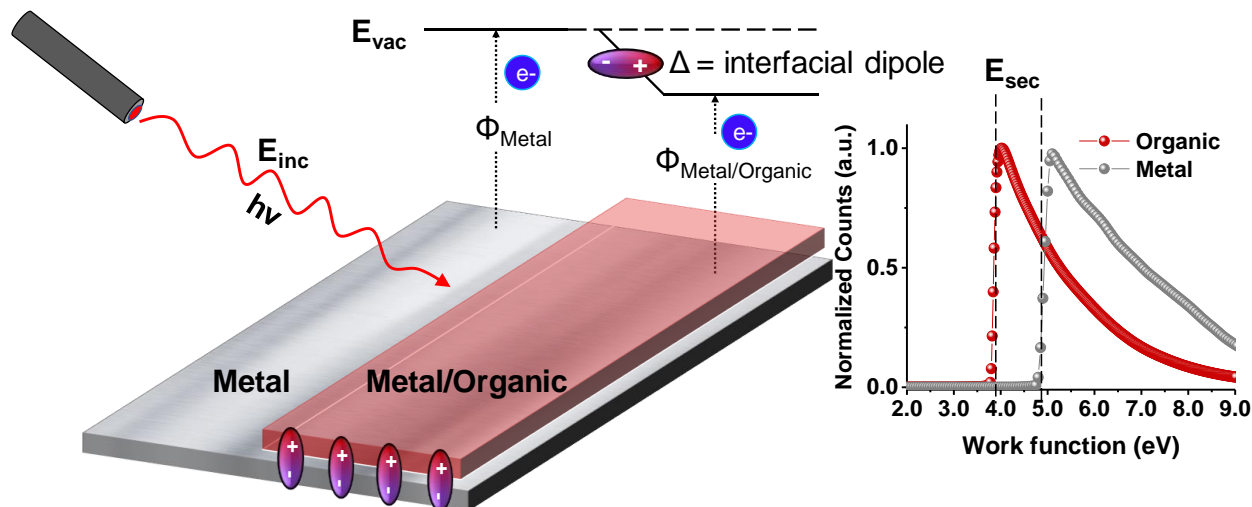
Figure 3. 1. Schematic of observed shift in work function of metal via interfacial dipole of organic layer measured by UPS.

Organic materials as ETLs offer the possibility of low-cost, solution-processing, tailored chemical functionality, and improved energy level compatibility with the active layer. The work-function (Φ), the energy required to extract/inject and electron, is an important materials property for electronics. To efficiently extract electrons and block holes from the active layer, ETLs must exhibit a low Φ. The work function of a bare metal or metal coated with a thin film of organic material can be directly measured by ultraviolet photoelectron spectroscopy (UPS). In UPS the Φ of a substrate is measured by the empirical formula, $\Phi = E_{inc}$ (eV) $-$ E_{SEC} (eV), where E_{inc} is the energy of the incident photon and E_{SEC} is the onset in the secondary electron cutoff region of the spectrum (Figure 3.1). Therefore, the interfacial dipole (Δ) of an inorganic/organic bilayer is simply the difference in the measured work function between the bare metal to the coated metal.

Small molecules and polymers have both been shown to perform as effective ETLs, capable of producing a preferential interfacial dipole at the organic/inorganic interface resulting in a modification of the metal's work function. Depending on the functionality of the molecule this work function modification facilitates injection of a hole of an electron.[2,15,16] In the case of cathode materials in photovoltaic devices, decreasing the work function is preferential for electron

59

injection. Based on this understanding, interest has been given to develop organic materials with proper functionality for modifying the work function of cathode materials. Polyethyleneimine (PEI) has been shown to be a promising ETL due to negative Δ produced by the amine groups in the polymer backbone which lower the work function of metals, such as silver (Ag), but is limited to ultra-thin films. The high resistance of PEI films becomes detrimental to photovoltaic performance at thicknesses exceeding 20 nm.[17]

To address this thickness intolerance research has been conducted to develop organic ETLs able to produce high power conversion efficiencies (PCEs) over a wide range of thicknesses. Through rigorous materials design and characterization, the key features of ETL materials have been elucidated. Specifically, it has been found that conjugated polymers containing tertiary amine, cationic, and zwitterionic pendant groups can preferentially lower the Φ cathodes and efficiently transport electrons with high thickness tolerance (2 to 200 nm) to achieve high performing photovoltaic devices.[18–24] The thickness tolerance of these materials arose from the semiconducting properties of the conjugated polymer, which permitted efficient transport of charge through the layer.
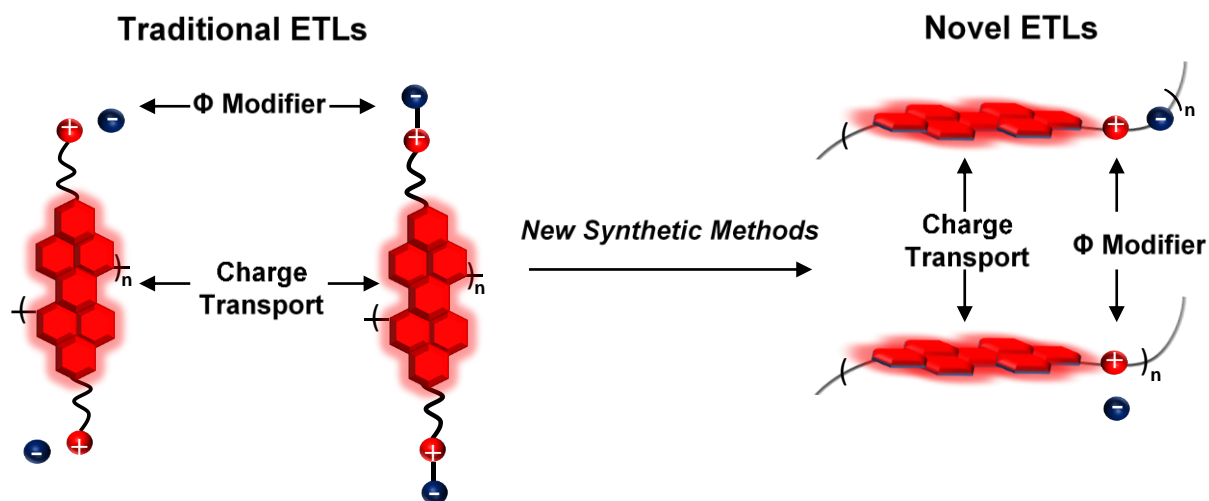
Figure 3. 2. Depiction of traditional π-conjugated polymer ETLs in comparison to novel polymer ETLs with segmented π-conjugation.

60

The results of this work elucidated the key materials properties for thickness tolerant interlayers. Specifically, an ETL should contain a work function modifying moiety (e.g., cationic, zwitterionic, etc.) and a charge transporting component (π-conjugated) (Figure 3.2). While all these components are necessary for an efficient ETL, there has been limited work on understanding how the ETL performance is affected by modifying the molecular architecture. Specifically, it would be of interest to determine if high performing ETLs can be achieved when the work function modifying group is embedded in the polymer backbone and long-range π-conjugation is broken.[25] The thesis work discussed here focused on relating molecular design of linear polyionenes and polymer zwitterions to interfacial properties.

3.2 Interfacial properties of PDI-based polymers

UPS measurements were performed on the PDI-based polyionenes and polymer zwitterions to investigate the interaction between the PDI-based ionene interlayers and Ag electrodes. In UPS, the E_{SEC} in the high binding (low kinetic) energy region probes the effect of the contacting materials on the work function of Ag, where the difference in E_{SEC} for bare Ag vs PDI-based polymer-coated Ag yields Δ values. The UPS spectra of the cationic and zwitterionic PDI polymers are shown in Figure 3.3. In Chapter 2, the optical properties were studied as a function of PDI content in the ionene and zwitterionic polymers. In chapter 3 focus is given to how PDI content as well as zwitterionic or cationic functionality influences Φ modification and photovoltaic device performance.

Ultra-thin (2 – 3 nm) layers of the PDI-based polymer films coated on Ag produced Δ values $\approx$ from 0.7 to -1.4 eV, which corresponds to a significantly reducing the observed Φ ranging from 3.4 to 3.8 eV compared to native Ag (4.3 eV) (Tables 3.1 and 3.2). The work function modification was independent of **PDIBr$_2$** or **PDIPh$_2$** derivative embedded in the polymer
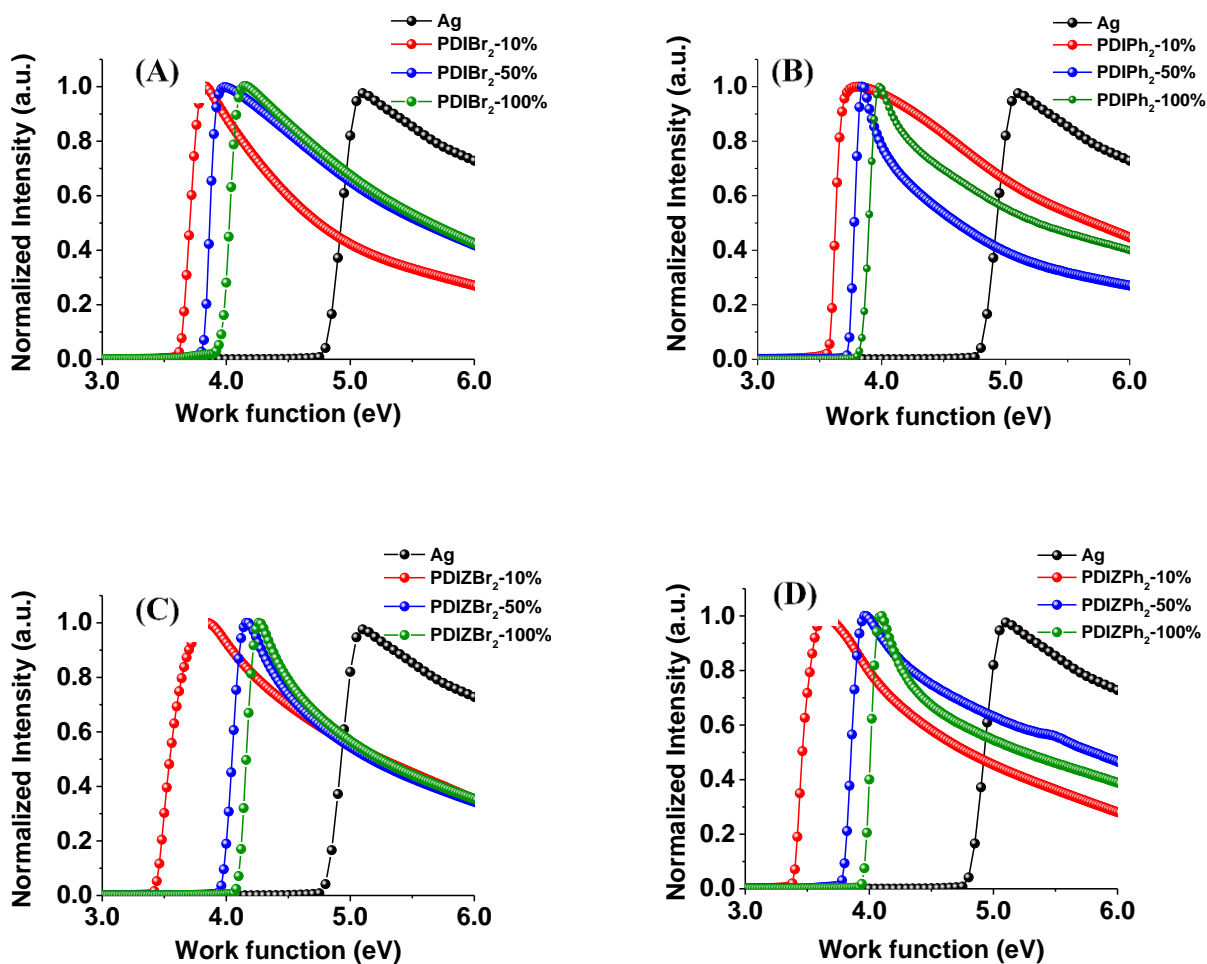
Figure 3. 3. UPS spectra secondary electron region of (A,C) PDIBr$_2$ and (B,D) PDIPh$_2$ polyionenes and polymer zwitterions.

backbone. As PDI content was increased the observed **Δ** decreased in all polymers independent of cationic or zwitterionic functionality. Current interlayer technology has focused on either completely conjugated or aliphatic systems. The influence of conjugation content on work function modification has never been explored. Experimental and theoretical results have shown work function increase in Ag substrates upon adsorption of fused-ring structures, such as perylenes, pyrenes, and coronenes, due to charge-transfer complex formation.[26–28] This is in agreement with

Table 3. 1. Summary of interfacial electronic properties of PDI-based polyionenes.

Polymer	Δ (eV)	Φ_{Ag-PDI}(eV)
PDIBr$_2$-10%	- 1.2	3.6
PDIBr$_2$-50%	-1.0	3.8
PDIBr$_2$-100%	- 0.9	3.9
PDIPh$_2$-10%	- 1.2	3.6
PDIPh$_2$-50%	- 1.1	3.7
PDIPh$_2$-100%	- 1.0	3.8

the results observed here. While the presence of cationic and zwitterionic functionality lowered the Φ of Ag, increasing the PDI content in the polymers attenuated the Φ modification.

The **PDIZ-10%** exhibited slightly larger Δ (1.4 eV) compared to the **PDI-10%** polymers (1.2 eV). Additionally, Δ decreased significantly more in **PDIZ** polymers as the PDI content was increased. These results show that at low PDI content the zwitterionic functionality is more desirable for tailoring the organic/inorganic interface while cationic is preferable at higher PDI content. From the UPS studies it was concluded that the Φ of Ag could be tailored through the introduction of the PDI-based polyionenes and polymer zwitterions. These results suggested that these novel polymers could be used to achieve larger built-in potential, enhanced free charge generation, and extraction efficiency to maximize J$_{SC}$ and FF in photovoltaic devices. Moreover, the Δ increases the anode-cathode work function offset (Φ_{A-C}), which boosts the V$_{OC}$.

Table 3. 2. Summary of interfacial electronic properties of PDI-based polymer zwitterions.

Polymer	Δ (eV)	Φ_{Ag-PDI}(eV)
PDIZBr$_2$-10%	- 1.4	3.4
PDIZBr$_2$-50%	- 0.9	3.9
PDIZBr$_2$-100%	- 0.7	4.1
PDIZPh$_2$-10%	- 1.4	3.4
PDIZPh$_2$-50%	- 1.0	3.8
PDIZPh$_2$-100%	- 0.9	3.9

3.3 ETL performance of PDI-based polymers in OSCs
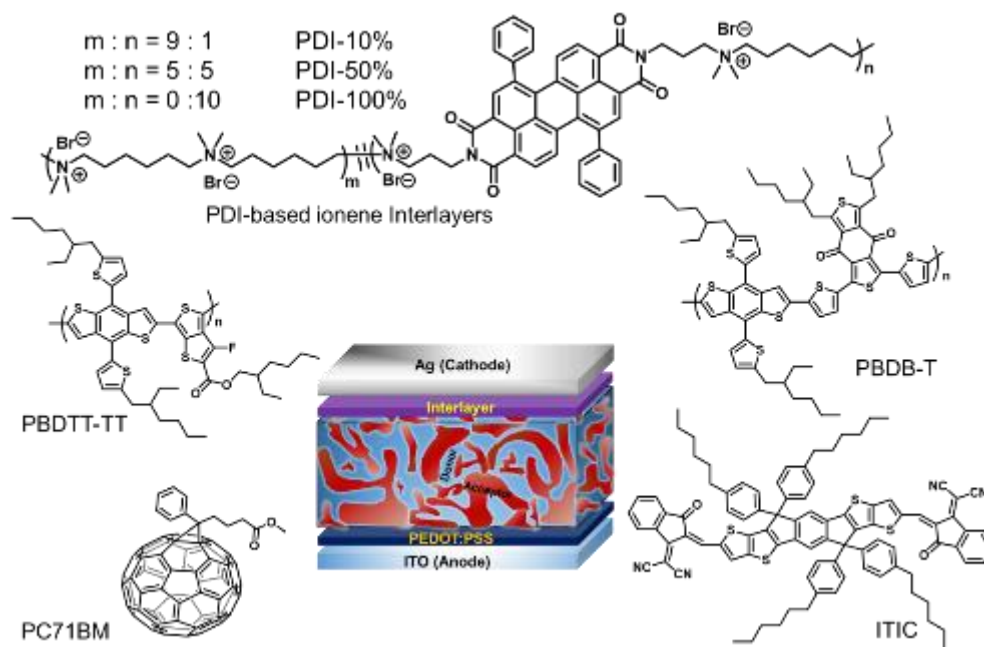
Figure 3. 4. Structure of PDI-based ETL and photoactive components with OSC device architecture.

OPV devices were first fabricated in a bulk heterojunction (BHJ) architecture (Figure 3.4) containing a blend of [6,6]-phenyl C71-butyric acid methyl ester (PC$_{71}$BM) or 3,9-bis(2-methylene-(3-(1,1-dicyanomethylene)-indanone))-5,5,11,11-tetrakis(4-hexylphenyl) dithieno[2,3-d:2',3'-d']-s-indaceno[1,2-b:5,6-b']dithiophene) (ITIC) as the electron acceptor and a low-bandgap conjugated polymer, poly(benzodithiophene-a-thieno[3,4-b]thiophene) with 2-(ethylhexyl)thienyl side chains (PBDTT-TT) or poly[(2,6-(4,8-bis(5-(2-ethylhexyl)thiophen-2-yl)-benzo[1,2-b:4,5-b']dithiophene))-alt-(5,5-(1',3'-di-2-thienyl-5',7'-bis(2-ethylhexyl) benzo[1',2'-c:4',5'-c']dithiophene-4,8-dione))]) (PBDB-T), as the electron donor.[29,30] An ITO/Poly(3,4-ethylenedioxythiophene):polystyrene sulfonate (PEDOT:PSS)/photoactive layer/ PDI-Ph based polymer interlayers/Ag architecture was used for all of the organic solar cells (OSCs).[31] An Ag electrode was selected in place of Al to illustrate the utility of stable, high work function, metal electrodes partnered with **PDIPh₂**-based polyionene interlayers. For OSCs with PBDTT-TT: PC$_{71}$BM active layer, Figure 3.5A and 3.5B compares current density-voltage (J-V) curves with
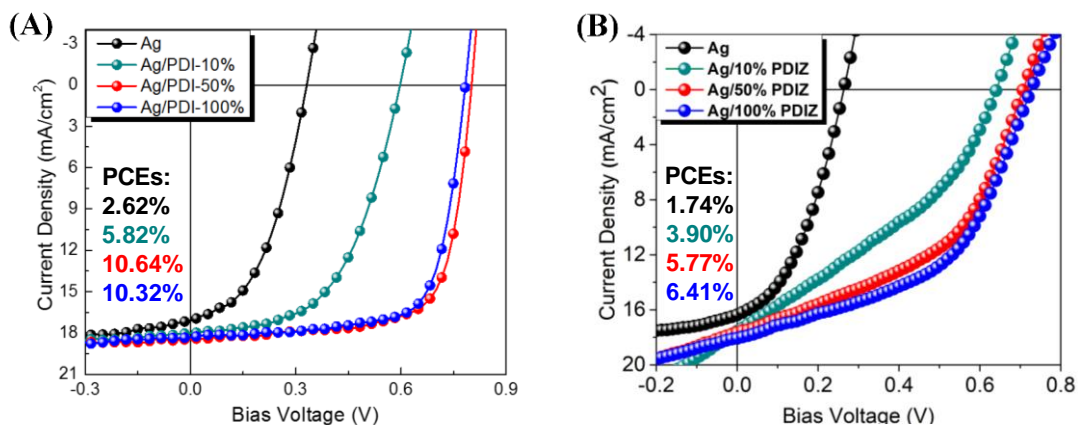
Figure 3. 5. J-V curves of fullerene-based OSC devices employing PDIPh$_2$-containing (A) polyionene and (B) polymer zwitterion interlayers.

devices containing no interlayer (bare Ag control) as well as ionene versus zwitterionic **PDI-10%**, **PDI-50%** and **PDI-100%** interlayers of optimal thickness. The devices without interlayers gave a maximum PCEs of 1.74% (zwitterionic control) and 2.62% (ionene control). Introduction of the PDI polymer interlayers resulted in enhanced photovoltaic performance in comparison to the bare Ag devices. In contrast to trends observed in UPS experiments, increased PDI content corresponded to further enhancement of photovoltaic performance. The photovoltaic metrics of the champion devices with each PDI-based interlayer are shown in Table 3.3. The zwitterionic **PDIZs** containing **PDIPh$_2$** polymers were able to boost the OSC PCEs from 1.74% for the bare device to 3.90% (**PDIZ-10%**), 5.77% (**PDIZ-50%**), and 6.41% (**PDIZ-100%**). These improvements arise from the significant increase in V_{oc} and J_{sc} upon introduction of the interfacial layer. While introduction of the PDIZ interlayers increased the photovoltaic performance, the shape of the J-V provides insight to some of the drawbacks of these materials. PDIZ J-V curves in Figure 3.5B exhibit an "S-shape" distinguishing them from the squarer curves in the ionene PDI J-V curves. The effects of this S-shape were reflected in the significantly lower FF observed in the
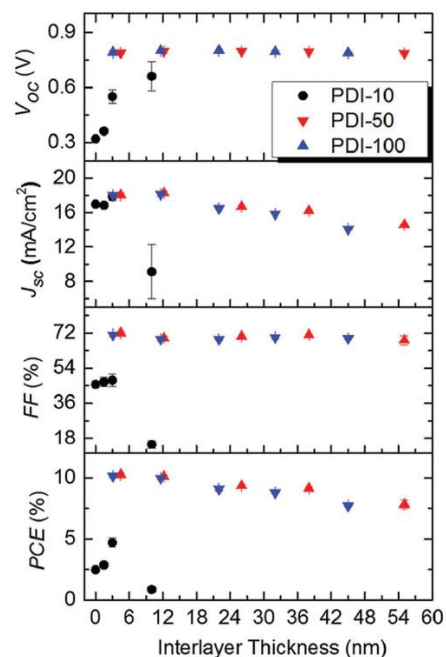
Figure 3. 6. Photovoltaic metrics
as a function of PDI polyionene
interlayer thickness.

zwitterionic interlayer devices. This S-shape was attributed to shunt current loss separate from the

applied bias to rectify the photogenerated current, arising from recombination at the

organic/cathode interface due to trap sites or defects.[32,33] Further investigation was given to the

ionene polymer in which this shunt loss was not observed.

Incorporation of **PDI-10%**, **PDI-50%**, and **PDI-100%** interlayers improved PCEs to

average/maximum values of 5.82%, 10.64% and 10.32%, respectively. This enhanced device

performance resulting from the interlayers is attributed to the increased V_{OC} (~0.33 to 0.80 V), FF

Table 3. 3. Summary of fullerene-based OSC devices employing PDIPh2-containing
polyionene and polymer zwitterion interlayers.

Interlayer	J_{SC} (mA/cm^2)	V_{OC} (V)	FF(%)	PCE(%)
PDI-10%	17.87	0.55	47.73	5.82
PDI-50%	18.02	0.79	71.93	10.64
PDI-100%	18.00	0.79	70.97	10.32
PDIZ-10%	17.56	0.64	34.74	3.90
PDIZ-50%	17.68	0.71	46.17	5.77
PDIZ-100%	18.03	0.73	48.86	6.41
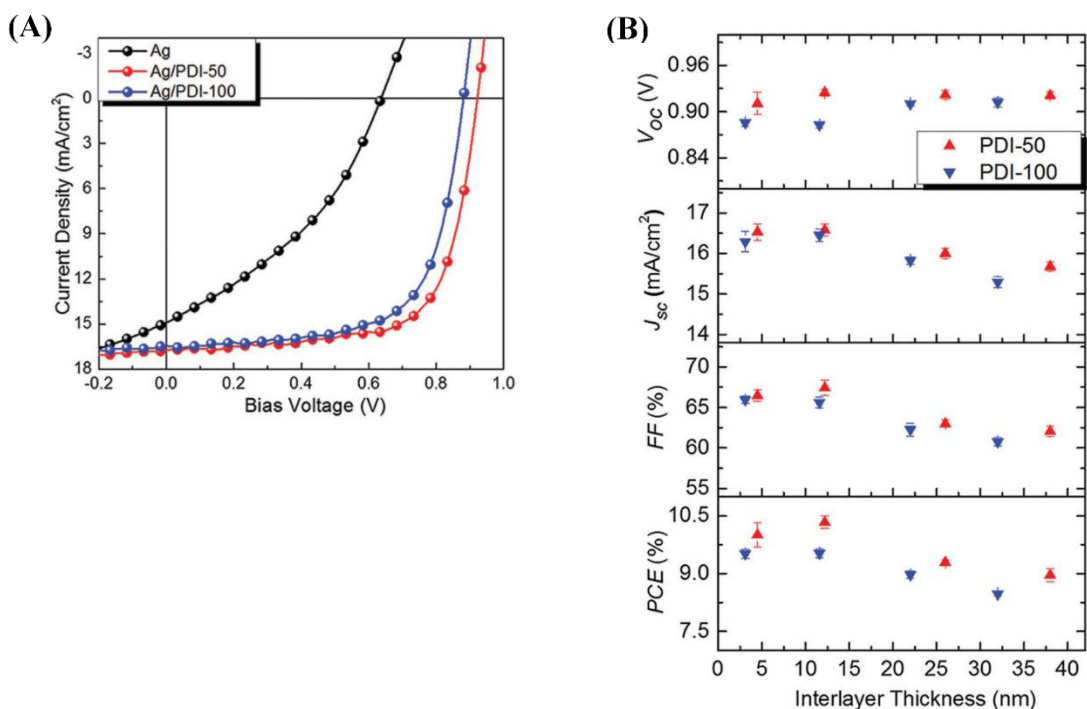
Figure 3. 7. (A) J-V curve of non-fullerene OSCs employing PDI-50% or PDI-100% interlayers; (B) Photovoltaic metrics as function of PDI-50% or PDI-100% thickness.

(~45 to 72%), and J_{SC} (~17.1 to 18.4 mA/cm2) for **PDI-50%** and **PDI-100%** (Table 3.3). The influence of interlayer thickness on device performance was investigated by varying the solution concentration in TFE used for spin-coating onto the BHJ active layer. Devices with interlayer thicknesses varying from ~3 nm to ~55 nm were fabricated. The performance of OPVs containing PDI-10% was sensitive to interlayer thickness, with an appreciable reduction in PCE noted for layers exceeding 5 nm, due to a large decrease of FF and J_{SC} (Figure 3.6). In contrast, the interlayers with larger PDI content (**PDI-50%** and **PDI-100%**) proved to be thickness tolerant, maintaining near peak photovoltaic metric values with V_{OC} (~0.80 V) and FF (~72%) across thicknesses from ~3-55 nm. J_{SC} only exhibited a moderate dependence on interlayer thickness, with values exceeding 14 mA/cm^2 across the entire thickness range. Based on the desirable thickness tolerance of the **PDI-50%** and **PDI-100%**, these interlayers were selected for further studies with non-fullerene acceptor devices.

67

Table 3. 4. Summary of non-fullerene-based OSC devices employing PDIPh2-containing polyionene interlayers.

Interlayer	J_{SC} (mA/cm^2)	V_{OC} (V)	FF (%)	PCE (%)
Bare Ag	11.39	0.57	34.98	3.34
PDI-50%	16.58	0.92	67.43	10.59
PDI-100%	16.45	0.88	65.62	9.68

Non-fullerene-based OSCs hold the potential to achieve enhanced OPVs owing to the more diverse design for both donors and acceptors to achieve maximum light absorption and photocurrent generation.[34,35] In spite of the success of non-fullerene acceptor devices, the proper design of polymer interlayers for non-fullerene-based PSCs has been seldom been reported.[36,37] **PDI-50%** and **PDI-100%** polyione. nes were employed as ETLs in OSCs with a non-fullerene BHJ active layer PBDB-T:ITIC. As shown in Figure 3.7A, the optimized non-fullerene PSCs fabricated with bare Ag cathodes gave PCE values of 3.34%. When **PDI-50%** or **PDI-100%** interlayers were integrated into devices PCE values of 10.34 ± 0.16% (maximum PCE 10.59%), 9.53 ± 0.12% (maximum PCE 9.68%), respectively could be achieved (Figure 3.7 and Table 3.4). This striking improvement in PCE stemmed from higher V_{OC} and FF values, while devices without interlayers suffered from the high intrinsic work function of Ag and the small built-in electrostatic potential difference. As with the fullerene-based devices, interlayers integrated into the non-fullerene devices exhibited excellent thickness tolerance (from ~3 to ~38 nm), and high PCE values were maintained (Figure 3.7B). Thus, the **PDI-50%** and **PDI-100%** polymers proved efficient as cathode interlayer materials for both fullerene- and non-fullerene-based PSCs. It was anticipated that the **PDI-100%** would produce the highest performing devices as its **Δ** could effectively decrease the **Φ** of Ag as it contained the most PDI, which would provide pathways for electron transport. The maximum PCE observed with **PDI-50%** across a wide range of thicknesses was interesting as ETL polymers with controlled π-conjugated component had never been reported.
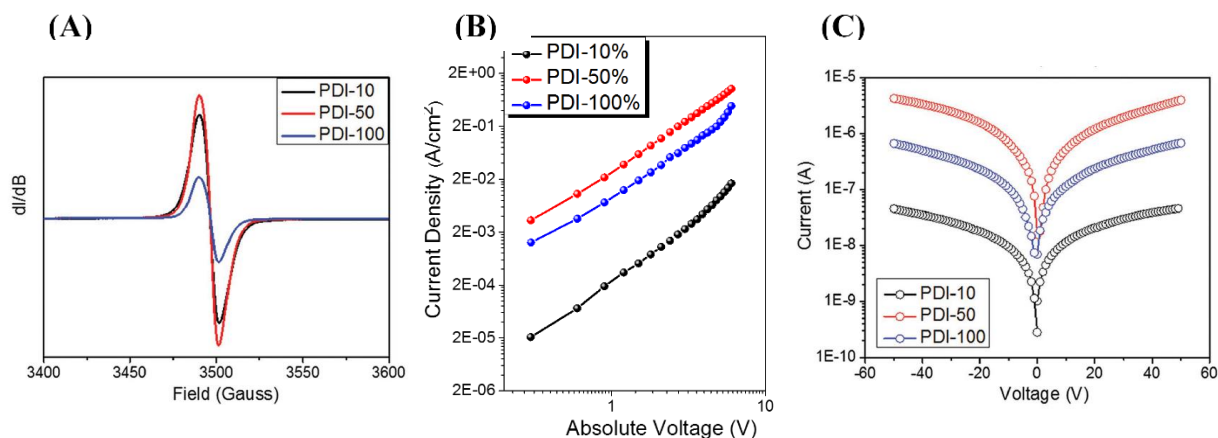
Figure 3. 8. (A) EPR spectra; (B) electron-only devices fabricated in the architecture: ITO/ETL/Ca/Al; and (C) current-voltage (I-V) measurements of PDI-based polyionenes.

The electronic properties of the polyionene interlayers were investigated further by electron paramagnetic resonance (EPR), space charge limited current (SCLC), and conductivity measurements. Self-doping in n-type small molecules and polymers has been shown to improve the charge transporting of ETLs. In previous reports, the self-doping was induced *via* charge transfer from a polar pendant group (cationic, or tertiary amines) to the electron deficient aromatic group.[38–44] In the case of the PDI polyionenes, the self-doping functionality was embedded in the polymer backbone. EPR allowed for the observation of un-paired electrons in samples. As shown in Figure 3.8A an EPR response corresponded to un-paired electrons in the self-doped PDI aromatic core. The EPR spectra of the PDI-based polyionenes shows a single signal centered at 3498 G, indicative of self-doping properties in these polymers through electron transfer from the ammonium bromides to the PDI units. The single peak was assigned to the PDI anions. For each EPR study 10 mg of polymer was used. At these quantities the PDI mole% was inversely related to EPR signal. This could be rationalized by the fact that the for PDI-10% and and PDI-50% there
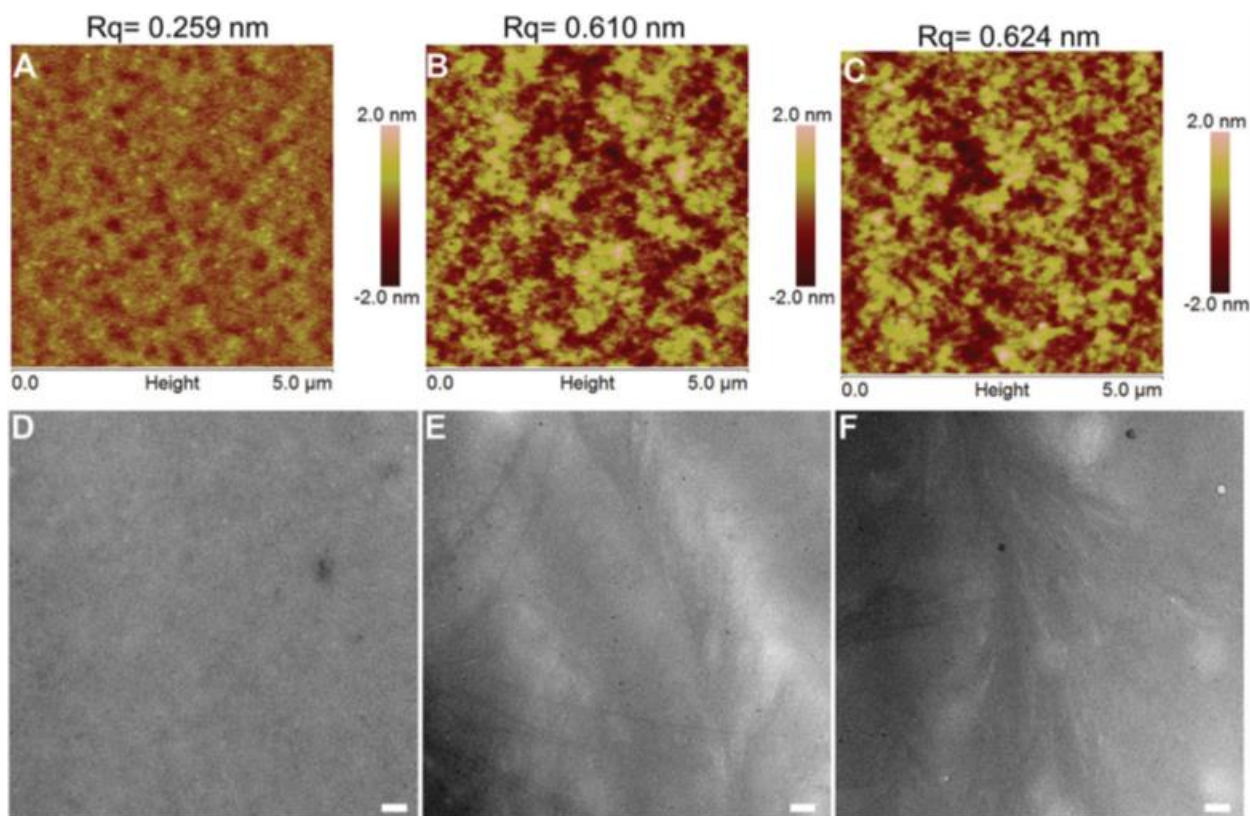
Figure 3. 9. AFM images of: (A) PDI-10% film; (B) PDI-50% film; and (C) PDI-100% film. TEM images of: D) PDI-10% film; E) PDI-50% film; and F) PDI-100% film. (Rq is the root mean square roughness; scale bar is 100 nm).

was significantly more dopant relative to PDI in comparison to the PDI-100%. Therefore, the content of doped PDI was likely larger in polymers with less PDI in the polymer backbone. Duzkho has shown that fullerenes containing zwitterionic sulfobetaine groups do not exhibit self-doping properties, in contrast to those containing cationic functional groups,[41] and require external dopants for improved transport properties.[45] The inability of n-type materials appended with zwitterionic functionality to self-dope may be the cause of the lower device performance in the PDIZ polymers when compared to the PDI ionene polymers. Electron-only SCLC devices were fabricated with the PDI polyionenes to further study their charge transporting properties. PDI-50% and PDI-100% exhibited comparably high electron mobility values of $7.45 \times 10\text{-}4$ cm^2/Vs and $2.54 \times 10\text{-}4$ cm^2/Vs, respectively, while the mobility of PDI-10% was two orders of magnitude

lower at $7.75 \times 10\text{-}6$ cm^2/Vs (Figure 3.8B). The conductivities of the PDI-based polyionenes were measured as thin films coated on parallel gold electrodes. Solutions of PDI-polyionenes in TFE were spin-coated onto the substrates to give a film thickness (T) of ~50 nm. The conductivities calculated from the current-voltage (I-V) curves for thin films of PDI-10%, PDI-50%, and PDI-100% were found to be 2.2×10^{-5}, 2.1×10^{-3}, and 3.3×10^{-4} S/cm (Figure 3.8C). The maximum conductivity observed in PDI-50% can be rationalized by efficient doping of the PDI core observed in the EPR resulting in high thickness tolerance and peak photovoltaic performance in the polymers without complete π-conjugation throughout the polymer backbone.

The influence of thin film morphology on charge transport in these PDI-based ionene interlayers was also investigated by atomic force microscopy (AFM) (Figure 3.9A-C). No large PDI clusters were observed, which makes PDI-based polyionenes suitable for device interfacial modification with a wide range of controllable interlayer thicknesses. Shown in transmission electron microscopy (TEM) (Figure 3.9D-F), fibril-like structures were found for samples of **PDI-50%** and **PDI-100%** but absent from PDI-10%. These structures were hypothesized to be comprised of PDI-aggregates formed through π-π stacking. This was supported by the absence of structures in the PDI-10% (low PDI content) thin film and their prevalence in the **PDI-50%** and **PDI-100%** (high PDI content) thin films. Thus, higher PDI mole% provided more π-π stacked PDI cores to form fibril structures, working as efficient electron transport channels, which afford **PDI-50%** and **PDI-100%** with a higher SCLC electron mobility and conductivity than that of **PDI-10%**. Thus, the PDI ratios in these polymer interlayers play a key role on film morphology and determining charge transporting properties of the materials.

Near edge X-ray absorption fine structure (NEXAFS) characterization was performed to analyze the orientation of these PDI-based polyionene films on top of the active layer. Carbon K-
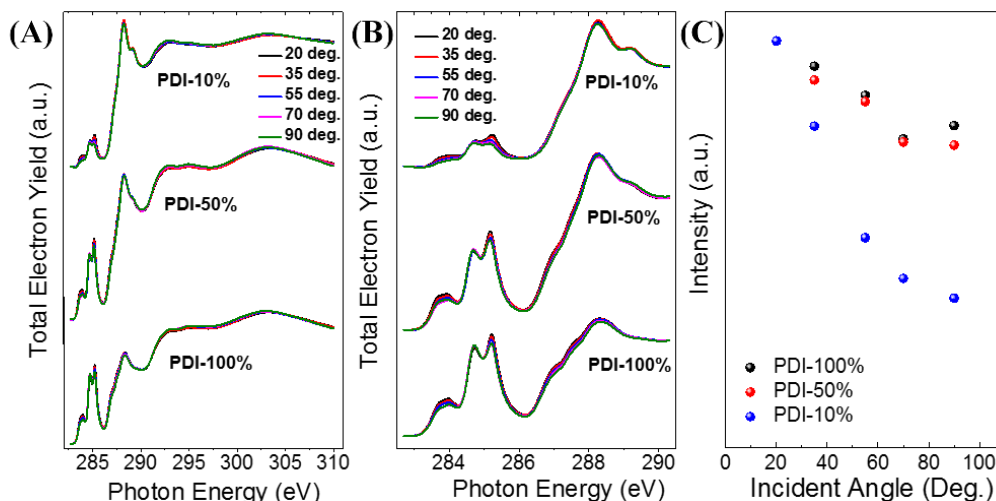
Figure 3. 10. (A) Full experimental region; and (B) π^* zoom-in NEXAFS TEY spectrum of PDI-based ionene interlayer films on top of the photoactive layer (PBDTT-TT: PC71BM); (C) The normalized sum of the PDI peak intensities from the π^* states of the PDI core as a function of incident angle.

edge total electron yield (TEY, ~10 nm) NEXAFS spectra showed the ensemble-averaged orientation at different average depths. Figure 3.10A shows the normalized X-ray absorption structure (XAS) of carbon 1s for PDI-10%, PDI-50%, and PDI-100%, plotted at different incidence x-ray angles (20º, 35º, 55º, 70º, and 90º), along with a zoom-in of the π^* region from 282.7 to 290.3 eV in Figure 3.10B, which corresponds to the states associated with the PDI core. The overall angular dependence was relatively small, but a significant experimental variation of intensities was observed. This was most notably for the π^* states of the aromatic PDI cores. Therefore, the summation of the fitted main π^* state intensities of the PDI cores were plotted as a function of incident angles (Figure 3.10C).

Increases of the incident angles (i.e., increasing the in-plane component of polarization of the incident x-rays) decreased the sum of PDI peak intensities, indicating that the PDI cores in these PDI-based polyionene interlayers preferred a face-on orientation with respect to the underlying photoactive layer. In addition, **PDI-10%** showed a more drastic decrease in intensity with increasing incident angle in Figure 3.10C in comparison to **PDI-50%** and **PDI-100%**. This
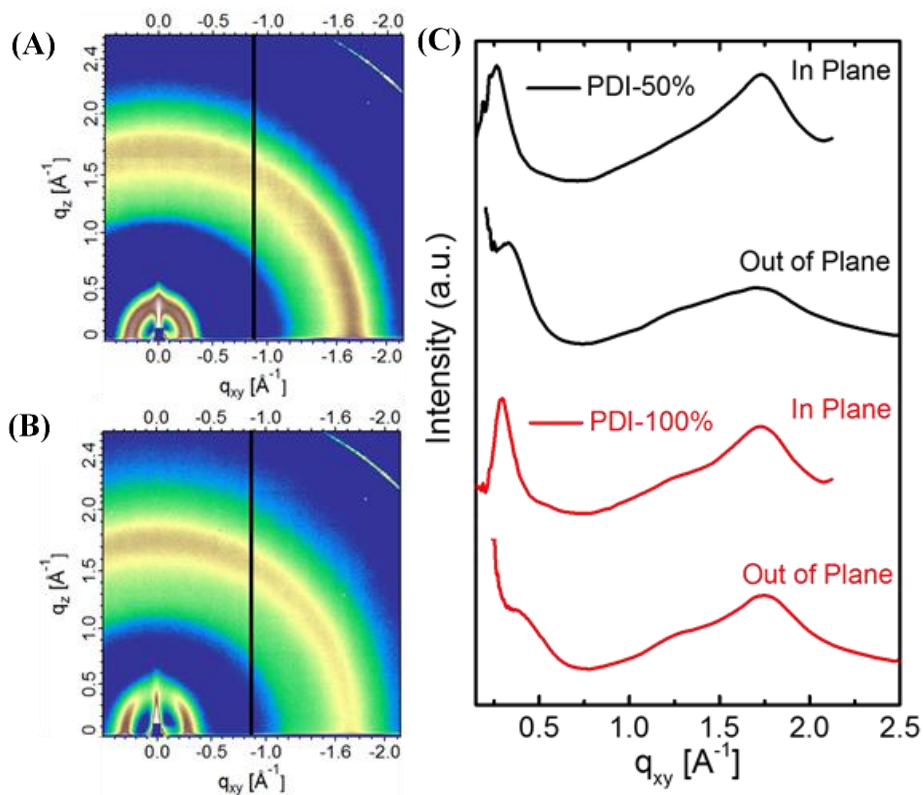
Figure 3. 11. 2D-GIXD patterns of (A) PDI-50%, and (B) PDI-100%;
(C) the corresponding line-cuts of the 2D-GIXD patterns.

difference in incident angle response may arise from the low content of PDI in the film or from stronger alignment with the substrate. These results indicated that the limited PDI content in the **PDI-10%** reduces the formation of PDI-rich charge transporting pathways, which likely played a crucial role in the inferior performance of the devices containing **PDI-10%** as the ETL. Subsequent analyses of morphology focused on the **PDI-50%** and **PDI-100%** which were able to yield high performing photovoltaic devices.

The structural order of the fibrils in **PDI-50%** and **PDI-100%** films was evaluated by grazing incidence X-ray diffraction (GIXD) (Figure 3.11). The diffraction patterns showed a broad peak at q = 1.73 Å-1, corresponding to a d-spacing of 3.63 Å, which is typical of π-π stacking in aromatic compounds.[46] These results compounded with the NEXAFS experiments, provide further evidence of PDI units stacking face-on with a π-interaction distance of 3.63 Å. The low q

diffraction region, PDI-50% showed a peak at q = 0.26 Å^{-1}, corresponding to a d-spacing of 24.17 Å, while PDI-100% gave a peak at q = 0.29 Å^{-1}, pointing to a d-spacing of 21.67 Å. The diffraction peaks at low q value were assigned to the distance between π-stacking PDI units. Interestingly **PDI-50%** and **PDI-100%** exhibited similar diffraction patterns. This was unexpected, as **PDI-50%** contains significantly less PDI to form clusters to produce diffraction. This observation provided additional evidence of a PDI mole% threshold necessary for high performing ETLs. Based on this morphological characterization, it is evident that the PDI mole% in these polymers influence PDI aggregation, and thus the resultant charge transport. While low PDI mole% (**PDI-10%**) produced higher **Δ**, these polymers could not form PDI aggregates (i.e., fibril-like structures) which served as conductive channels for charge transport. Additionally, at the highest PDI mole% ratio (**PDI-100%**) electron mobility, conductivity, doping and work function modification were lower than values observed with **PDI-50%**. Hence, **PDI-50%** proved to be the more effective ETL based on its excellent work function modification properties and formation efficient conductive channels for electron transport.
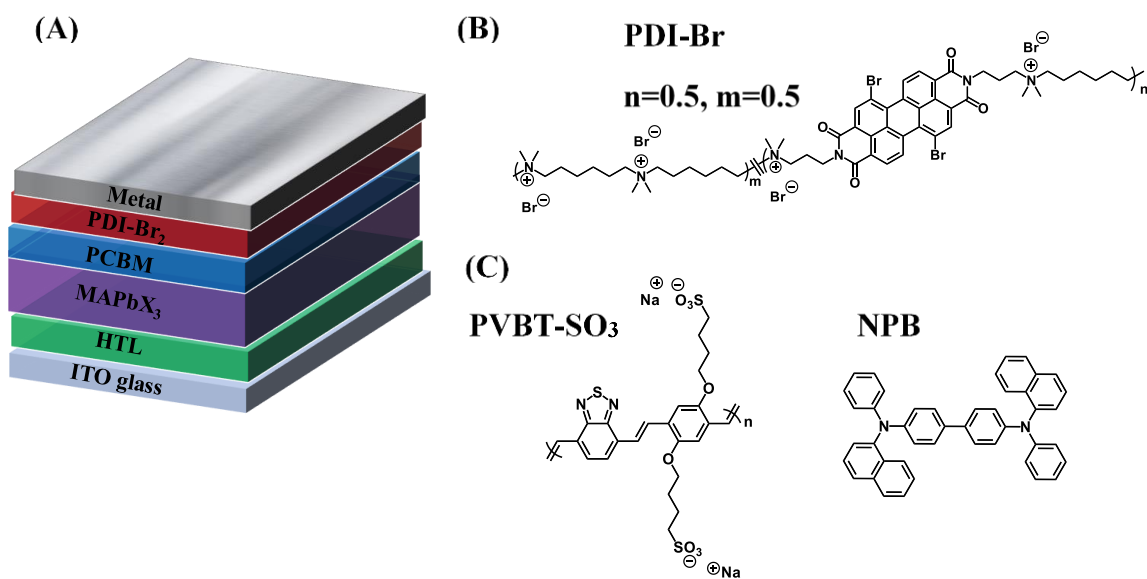
Figure 3. 12. (A) PSC device architecture: ITO anode/HTL/MAPbX3/PCBM/PDI-Br/metal cathode; (B) Structure of PDI-Br interlayer; (C) Structure of PVBT-SO3 and NPB HTLs.

3.4 ETL performance of PDI-based polymers in PSCs

With the knowledge that 50 mole% PDI in the polyionene backbone produced the highest performing OSCs the **PDIBr$_2$-50%** polymer, referred to in this section as **PDI-Br**, was used as an ETL as well as work function modifier in conventional and inverted perovskite solar cells (PSCs).[47] Inverted PSCs with a device architecture of ITO/HTL/CH$_3$NH$_3$PbI$_3$/PC$_{61}$BM/**PDI-Br**/metal cathode were fabricated as shown in Figure 3.12. *N,N'*-bis(naphthalen-1-yl)-*N,N'*-bis(phenyl)benzidine (NPB), or poly(benzothiadiazole vinylene-*alt*-2,5-bis(4-sodium sulfonate)butoxy)-1,4-phenylenevinylene) (PVBT-SO$_3$) were spin-coated onto ITO substrates to serve as the HTL. Devices employing the NPB as the HTL and **PDI-Br** markedly produced a *J$_{SC}$* of 22.92 mA/cm^2, a *V$_{OC}$* of 1.11 V, a FF of 78.4% were able to achieve a maximum PCE of 19.96% (Figure 3.13). This impressive performance can be correlated to the PDI-based interlayer's ability to preferentially modify the work function of Ag and transport electrons. The superior ETL properties of **PDI-Br** partnered with the high hole mobility of NPB (reportedly (6-9)×10^{-4} cm^2/Vs[48,49]) and 5.20 eV HOMO level situated between the work function of indium tin oxide
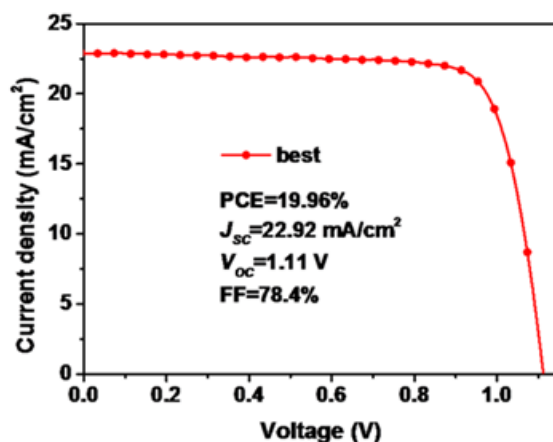
Figure 3. 13. J-V curve of PSC employing the PDI-Br interlayer and NPB as the HTL.

(ITO) and the valence band (VB) of $CH_3NH_3PbI_3$ yielded the observed high performing photovoltaic devices.

Additional studies were conducted with PSCs employing the novel PVBT-SO$_3$ HTL previously reported by Emrick and coworkers[50] and PDI-Br as the ETL. As shown in Figure 3.14A, when using Ag as electrode, the devices showed the highest PCE of 19.12% in the reverse scan with J_{SC} =23.77 mA/cm^2, V_{OC} =1.02 V, FF=78.99%. In the forward scan, the same device gave a PCE of 18.78%, indicative of minor hysteresis. The effects of the **PDI-Br** interlayers on device performance and thickness tolerance were investigated as shown in Table 3.5. The PCEs of
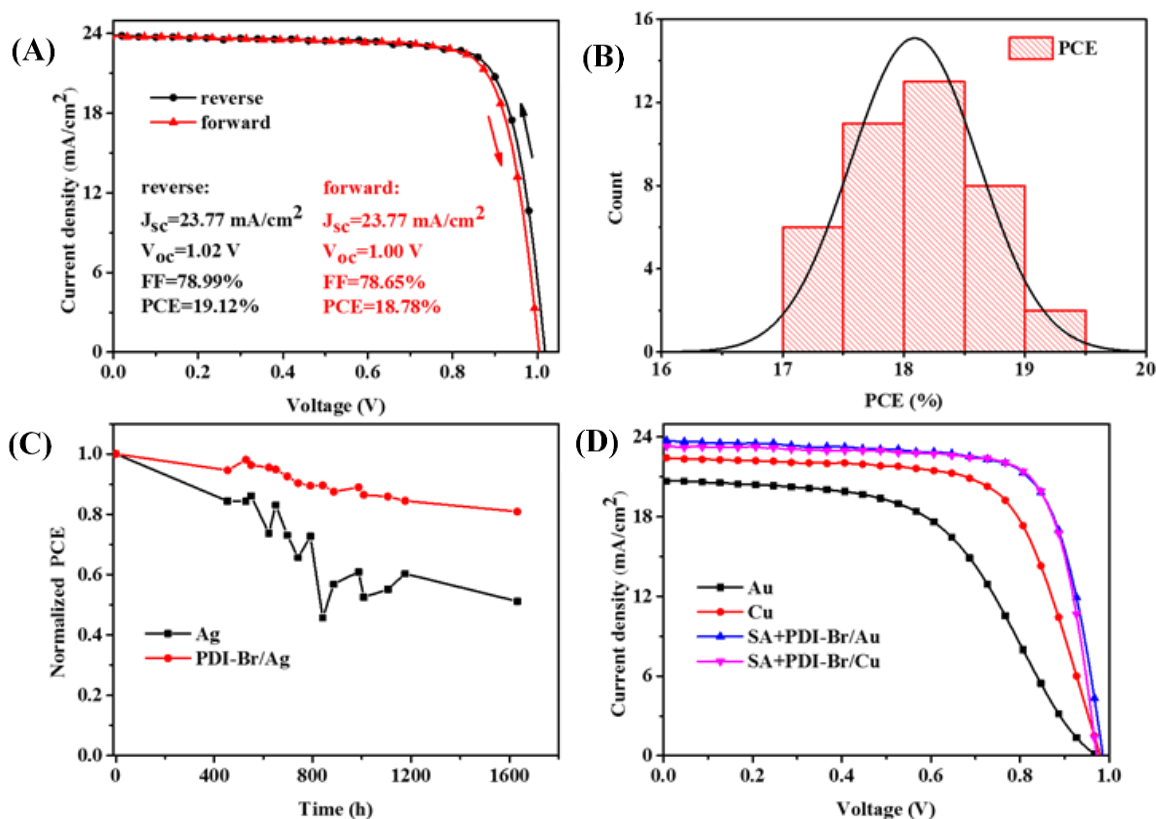
Figure 3. 14. (A) Current density-voltage (J-V) characteristics of the champion PSC measured by reverse and forward modes; (B) PCE histogram of 40 devices with PDI-Br interlayer (measured under reverse scan); (C) Stability performance of the PSCs with and without PDI-Br interlayer, the devices were stored and tested in the glove box without encapsulation; (D) J-V characteristics of PSCs by using Cu and Au as cathode, respectively, the devices were measured under reverse scan.

76

Table 3. 5. Summary of photovoltaic metrics employing PDI-Br interlayer at various thicknesses.

Interlayer	Jsc (mA/cm^2)	Voc (V)	FF (%)	PCE (%)
Bare Ag	21.04	1.02	59.20	12.78
4 nm	20.21	1.01	75.25	15.41
7 nm	20.62	1.03	75.88	16.14
10 nm	21.62	1.00	78.30	16.97
28 nm	20.65	1.00	77.79	16.13

40 devices all exceeded 17% with an average efficiency of 18.08% as shown in Figure 3.14B, suggesting a high reproducibility of the devices fabricated with the **PDI-Br** interlayer. Low FF values were observed in PSC without the **PDI-Br** interlayer. This is attributed to carrier accumulation at the PCBM/Ag interface due to the mismatch between the lowest unoccupied molecular orbital (LUMO) of PCBM and the work function of Ag. When inserting PDI-Br interlayer between PCBM and Ag, the FF shows a desirable rectification from 59.20% to 76.82%. Additionally, all photovoltaic metrics maintained near peak values with interlayer thicknesses ranging from ~4 nm to ~28nm, thus exemplifying the desirable thickness tolerance of **PDI-Br**.

The long-term stability of the devices with and without the **PDI-Br** interlayer was tested in a glove box without encapsulation as shown in Figure 3.14C. The device with the **PDI-Br** interlayer remained at ~80% of the initial PCE after ~1600 hours, while the device without the interlayer decreased by ~50% over the same time frame. The degradation of the PCE mainly arises from the decrease of the FF, as shown in Figure 3.15, especially for the PSC without the PDI-Br. Migration of I$^-$ ions through the perovskite active layer and reaction with metal electrode interface has been shown to lead to irreversible device degradation.[51–53] The use of the PDI-Br interlayer could prevent the direct contact of PCBM and Ag and played an important role in affording effective improvement of device stability. Additionally, **PDI-Br** was shown to improve devices
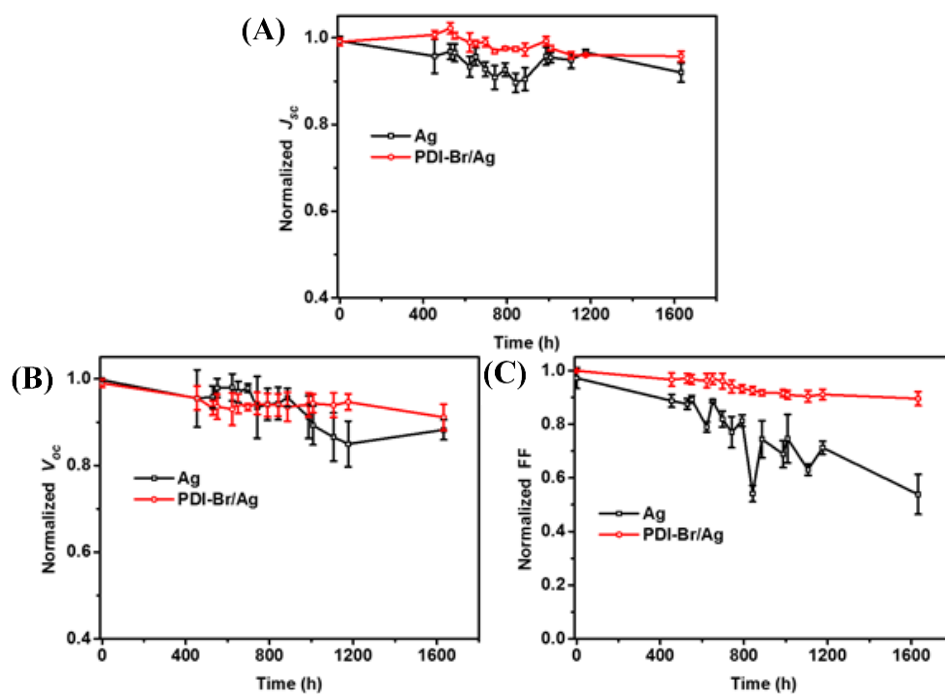
Figure 3. 15. Stability investigation of (A) J_{SC}; (B) V_{OC}; and (C) FF of the PSCs with and without PDI-Br interlayer (3 devices of each type), the devices were stored and tested in the glove box without encapsulation.

employing Cu or Au- cathodes, producing PCEs exceeding 17% (Figure 3.14.D). These results demonstrate the versatility of PDI-Br to enhance perovskite device efficiency and stability. Overall, all PDI-based polyionenes have been shown to improve device performance in both OSCs and PSCs. The main advantage of these systems is the control of the PDI content and the realization of 50 mole% as the threshold for peak device performance. This finding will play a key role in developing cost-effective materials for thin film photovoltaics.

3.5 Small molecule PDI ETLs in perovskite solar cells

While the polymeric PDI structures were able to preferentially modify the work function of metal cathodes and improve electron injection at the active layer/cathode interface, the ETL performance properties of small molecule PDIs was also investigated. (Poly[9,9-bis(3′-(N,N-dimethylamino)- propyl)-2,7-fluorene)-alt-2,7-(9,9-dioctylfluorene) PFN and its derivatives, in
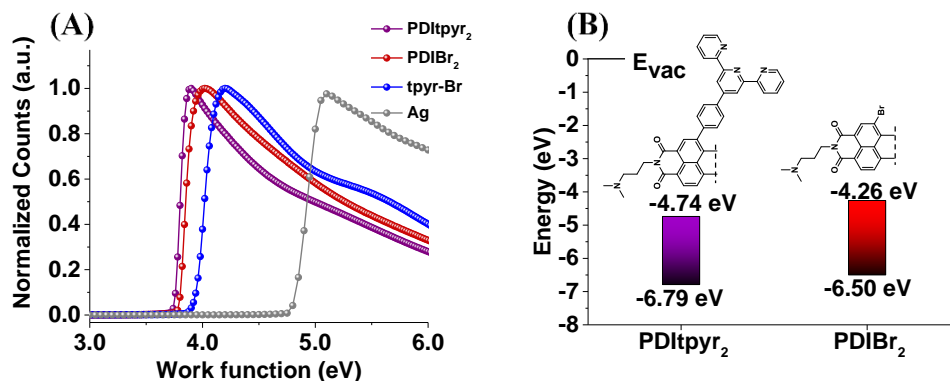
Figure 3. 16. (A) UPS spectra secondary electron region of PDItpyr$_2$, PDIBr$_2$, and tpyr-Br on Ag. (B) Energy level diagram of PDItpyr$_2$ and PDIBr$_2$.

addition to modifying the work function of metal cathodes, can passivate surface defects in the methylammonium lead halide (MAPbX$_3$) perovskite active layer through coordination of the lone pair to the Pb^{2+} atoms, yielding PSCs with enhanced performance and stability.[54–57] Similar effect has been shown with tertiary amine functionalized fullerenes[58] and PDIs.[59] The reported PDI small molecule could improve the performance but also exhibited limited thickness tolerance, likely due to the formation of large aggregates causing charge build-up at the perovskite/cathode interface. Here core-functionalized PDI small molecules were hypothesized to be promising candidates as thickness tolerant small molecule ETLs for PSCs.

The influence of tertiary amines functionality on PSC performance has been well documented, but other kinds of amines could also be advantageous for tailoring interfaces. In addition to the **PDIBr$_2$** mentioned in chapter 1, 4-bromophenyl-terpyridine (**tpyr-Br**) and a PDI derivative containing phenyl-terpyridine groups at the aromatic core (**PDItpyr$_2$**) were integrated into PSCs as interfacial layers. **PDI-tpyr$_2$** was prepared following similar procedures used to synthesize **PDIPh$_2$** *via* Suzuki-Miyaura coupling. UPS studies was used to determine the **Δ** of **tpyr-Br** (-0.51 eV), **PDIBr$_2$** (-0.66 eV), and **PDItpyr$_2$** (-0.70 eV) thin films (~2-5 nm) coated on Ag substrates (Figure 3.16). The **Δ** of these small molecules was significantly smaller than the
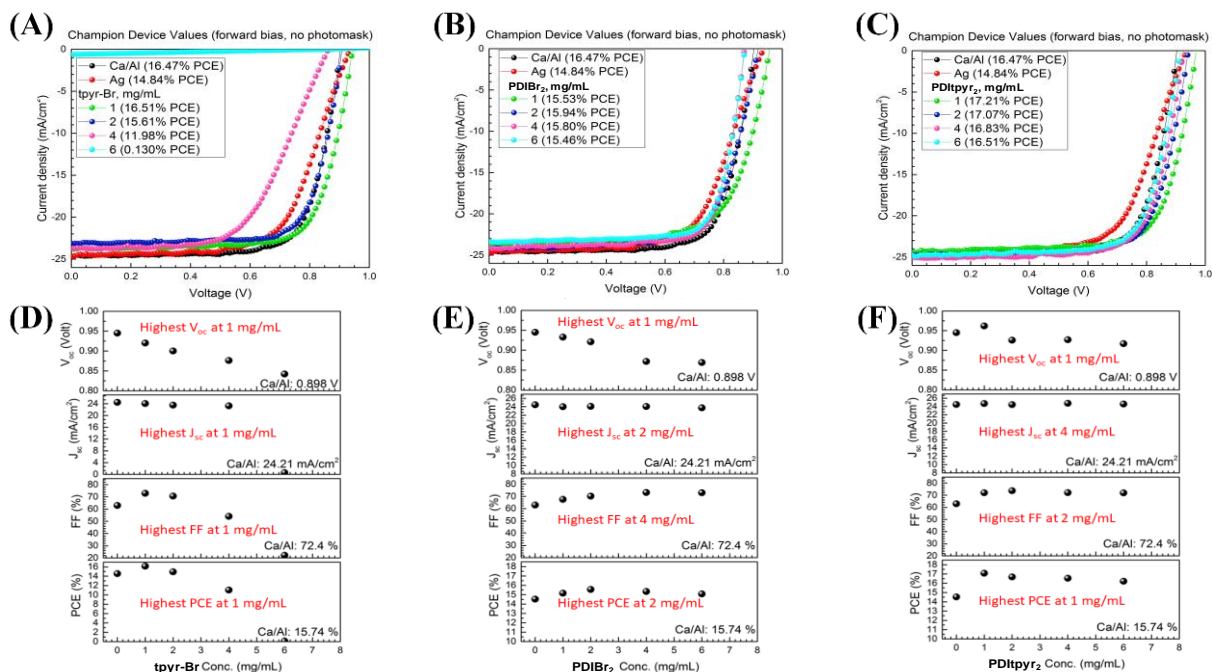
Figure 3. 17. J-V curves and photovoltaic metrics a function of interlayer solution concentration of (A,D) tpyr-Br; (B,E) PDIBr2; and (C,F) PDItpyr2.

polyionenes and polymer zwitterions in the previous section. This difference in **Φ** modification suggests that cationic and zwitterionic functionality possess superior interfacial tailoring properties over tertiary amines. Tpyr-Br on its own produced a **Δ** preferential for electron injection into Ag, while the PDI-tpyr the same interfacial behavior as PDI-Br. This potentially arises due to the orientation of the terpyridine groups relative to the underlying substrate when they conjugated to the PDI core. Based on their desirable work function modification properties, the small molecules were integrated into MAPbX3 PSCs.

The J-V of devices fabricated with the small molecule spin-coated from varying solution concentrations to produce films ranging from 2 to 20 nm by controlling small molecule concentration in TFE with Ag contacts (Figure 3.17). The ETL-containing devices were compared to bare Ag devices and low work function cathode Ca/Al devices. Ca/Al produced higher PCE values than Ag as expected for a low work function metal which allows for high Φ_{A-C} and internal

bias. The J-V curves for champion devices and photovoltaic metrics as a function of interlayer thickness are summarized in Figure 3.17. It was found that all interlayers were able to produce high performing devices ranging from 15.94 to 17.21 % PCE. The **tpyr-Br** small molecule was able to enhance device performance (16.51% PCE) when coated from 1 mg/mL solutions but exhibited low thickness tolerance. In contrast, **PDIBr$_2$** and **PDItpyr$_2$** ETLs were both able to maintain high device performance over all coating concentrations. It is hypothesized that the thickness tolerance of the PDI interlayers discussed here, as opposed to the thickness intolerance of interlayers reported in the literature, was realized through the prevention of large, charge-blocking aggregates by introduction of the bulky bromide or phenyl-terpyridine units at the PDI aromatic core. Additionally, the higher PCE observed in **PDItpyr$_2$** (17.21%) when compared to **PDIBr$_2$** (15.94%) is likely due to the lower lying LUMO of the **PDItpyr$_2$** (-4.74 eV) leading to more efficient extraction of electrons from the perovskite active layer (LUMO = -3.9 eV) (Figure 3.16). These results illustrate the utility of PDI as a small molecule ETL and the necessity of core functionality for enhanced device performance.

3.6 Conclusion

In summary several PDI-containing structures were developed as ETL for organic- and perovskite-based photovoltaic devices and their structure-property relationships were explored. PDI-based polyionenes and polymer zwitterions polymers were observed to preferentially modify the work function of Ag to facilitate electron injection. This work function modification was found to be dependent on the amount of PDI embedded in the polymer backbone. When integrated into OSCs both the cationic polyionenes and polymer zwitterions were able to improve device performance. Devices containing PDI polyionenes outperformed the zwitterionic analogs, likely

due to efficient transportation of charges into the electrode without loss due to interfacial recombination.

The electronic properties of the PDI polyionenes (electron mobility, conductivity, and doping) were all found to be dependent on the content of PDI embedded in the polymer backbone. The combination of fundamental electronic studies, morphological characterization, and device performance analyses revealed that 50 mole% PDI was the threshold for peak device performance. These results transferred to perovskite-based photovoltaic devices as well, in which the **PDI-50%** polymers were again able to improve device performance. Small molecule PDI derivatives were also studied as interfacial layers in PSCs. These small molecules showed aromatic core functionality dependence on work function modification and device performance. Moreover, the small molecule studies revealed that while terpyridine type structures could modify metal work functions, without the presence of a strong n-type component, such as PDI, these materials could not be integrated as thickness tolerant interlayers in PSCs. The results of this work provided greater insight to design of effective charge selective layers in photovoltaic devices and produced a new platform of electronic materials that may provide a pathway towards commercialization of flexible photovoltaics.

3.7 References

(1)   Zhang, W.; Wang, Y. C.; Li, X.; Song, C.; Wan, L.; Usman, K.; Fang, J. Recent Advance in Solution-Processed Organic Interlayers for High-Performance Planar Perovskite Solar Cells. Adv. Sci. 2018, 5 (7). https://doi.org/10.1002/advs.201800159.

(2)   Yin, Z.; Wei, J.; Zheng, Q. Interfacial Materials for Organic Solar Cells: Recent Advances and Perspectives. Adv. Sci. 2016, 3 (8), 1–37. https://doi.org/10.1002/advs.201500362.

(3)   Mohan, M.; Nandal, V.; Paramadam, S.; Reddy, K. P.; Ramkumar, S.; Agarwal, S.; Gopinath, C. S.; Nair, P. R.; Namboothiry, M. A. G. Efficient Organic Photovoltaics with Improved Charge Extraction and High Short-Circuit Current. J. Phys. Chem. C 2017, 121 (10), 5523–5530. https://doi.org/10.1021/acs.jpcc.7b01314.

(4)   Waldauf, C.; Morana, M.; Denk, P.; Schilinsky, P.; Coakley, K.; Choulis, S. A.; Brabec, C. J. Highly Efficient Inverted Organic Photovoltaics Using Solution Based Titanium Oxide as Electron Selective Contact. Appl. Phys. Lett. 2006, 89 (23), 233517. https://doi.org/10.1063/1.2402890.

(5)   Siddiki, M. K.; Venkatesan, S.; Qiao, Q. Nb 2O 5 as a New Electron Transport Layer for Double Junction Polymer Solar Cells. Phys. Chem. Chem. Phys. 2012, 14 (14), 4682–4686. https://doi.org/10.1039/c2cp22627h.

(6)   Trost, S.; Zilberberg, K.; Behrendt, A.; Riedl, T. Room-Temperature Solution Processed SnOxas an Electron Extraction Layer for Inverted Organic Solar Cells with Superior Thermal Stability. J. Mater. Chem. 2012, 22 (32), 16224–16229. https://doi.org/10.1039/c2jm33445c.

(7)   Ling, X.; Yuan, J.; Liu, D.; Wang, Y.; Zhang, Y.; Chen, S.; Wu, H.; Jin, F.; Wu, F.; Shi, G.; et al. Room-Temperature Processed Nb 2 O 5 as the Electron-Transporting Layer for Efficient Planar Perovskite Solar Cells. ACS Appl. Mater. Interfaces 2017, 9 (27), 23181–23188. https://doi.org/10.1021/acsami.7b05113.

(8)   Schulze, P. S. C.; Bett, A. J.; Winkler, K.; Hinsch, A.; Lee, S.; Mastroianni, S.; Mundt, L. E.; Mundus, M.; Würfel, U.; Glunz, S. W.; et al. Novel Low-Temperature Process for Perovskite Solar Cells with a Mesoporous TiO2Scaffold. ACS Appl. Mater. Interfaces 2017, 9 (36), 30567–30574. https://doi.org/10.1021/acsami.7b05718.

(9)   Song, S.; Kang, G.; Pyeon, L.; Lim, C.; Lee, G. Y.; Park, T.; Choi, J. Systematically Optimized Bilayered Electron Transport Layer for Highly Efficient Planar Perovskite Solar Cells (η = 21.1%). ACS Energy Lett. 2017, 2 (12), 2667–2673. https://doi.org/10.1021/acsenergylett.7b00888.

(10)   Jeong, I.; Park, Y. H.; Bae, S.; Park, M.; Jeong, H.; Lee, P.; Ko, M. J. Solution-Processed Ultrathin TiO 2 Compact Layer Hybridized with Mesoporous TiO 2 for High-Performance Perovskite Solar Cells. ACS Appl. Mater. Interfaces 2017, acsami.7b11901. https://doi.org/10.1021/acsami.7b11901.

(11)   Xie, J.; Huang, K.; Yu, X.; Yang, Z.; Xiao, K.; Qiang, Y.; Zhu, X.; Xu, L.; Wang, P.; Cui, C.; et al. Enhanced Electronic Properties of SnO2 via Electron Transfer from Graphene Quantum Dots for Efficient Perovskite Solar Cells. ACS Nano 2017, acsnano.7b04070. https://doi.org/10.1021/acsnano.7b04070.

(12) Guo, Z.; Gao, L.; Zhang, C.; Xu, Z.; Ma, T. Low-Temperature Processed Non-TiO 2
      Electron Selective Layers for Perovskite Solar Cells. J. Mater. Chem. A 2018.
      https://doi.org/10.1039/C7TA10742K.

(13) Constantinou, I.; Shewmon, N. T.; Lo, C. K.; Deininger, J. J.; Reynolds, J. R.; So, F.
      Photodegradation of Metal Oxide Interlayers in Polymer Solar Cells. Adv. Mater.
      Interfaces 2016, 3 (23). https://doi.org/10.1002/admi.201600741.

(14) Ratcliff, E. L.; Zacher, B.; Armstrong, N. R. Selective Interlayers and Contacts in Organic
      Photovoltaic   Cells.   J.   Phys.   Chem.   Lett.   2011,   2   (11),   1337–1350.
      https://doi.org/10.1021/jz2002259.

(15) Yang, D. S.; Bilby, D.; Chung, K.; Wenderott, J. K.; Jordahl, J.; Kim, B. H.; Lahann, J.;
      Green, P. F.; Kim, J. Work Function Modification via Combined Charge-Based Through-
      Space Interaction and Surface Interaction. Adv. Mater. Interfaces 2018, 5 (15), 1800471.
      https://doi.org/10.1002/admi.201800471.

(16) Van Reenen, S.; Kouijzer, S.; Janssen, R. A. J.; Wienk, M. M.; Kemerink, M. Origin of
      Work Function Modification by Ionic and Amine-Based Interface Layers. Adv. Mater.
      Interfaces 2014, 1 (8), 1–11. https://doi.org/10.1002/admi.201400189.

(17) Zhou, Y.; Fuentes-Hernandez, C.; Shim, J.; Meyer, J.; Giordano, A. J.; Li, H.; Winget, P.;
      Papadopoulos, T.; Cheun, H.; Kim, J.; et al. A Universal Method to Produce Low-Work
      Function Electrodes for Organic Electronics. Science (80-.). 2012, 336 (6079), 327–332.
      https://doi.org/10.1126/science.1218829.

(18) Kesters, J.; Govaerts, S.; Pirotte, G.; Drijkoningen, J.; Chevrier, M.; Van Den Brande, N.;
      Liu, X.; Fahlman, M.; Van Mele, B.; Lutsen, L.; et al. High-Permittivity Conjugated

Polyelectrolyte Interlayers for High-Performance Bulk Heterojunction Organic Solar Cells. ACS Appl. Mater. Interfaces 2016, 8 (10), 6309–6314. https://doi.org/10.1021/acsami.6b00242.

(19)   Yang, R.; Zhao, Z.; He, J.; Wang, J.; Chen, W.; Wang, N.; Zhang, Y. A Water/Alcohol-Soluble Copolymer Based on Fluorene and Perylene Diimide as a Cathode Interlayer for Inverted Polymer Solar Cells. J. Mater. Chem. C 2015, 3, 4515–4521. https://doi.org/10.1039/C5TC00450K.

(20)   Chevrier, M.; Houston, J. E.; Kesters, J.; Van Den Brande, N.; Terry, A. E.; Richeter, S.; Mehdi, A.; Coulembier, O.; Dubois, P.; Lazzaroni, R.; et al. Self-Assembled Conjugated Polyelectrolyte-Surfactant Complexes as Efficient Cathode Interlayer Materials for Bulk Heterojunction Organic Solar Cells. J. Mater. Chem. A 2015, 3 (47), 23905–23916. https://doi.org/10.1039/c5ta06966a.

(21)   Subbiah, J.; Mitchell, V. D.; Hui, N. K. C.; Jones, D. J.; Wong, W. W. H. A Green Route to Conjugated Polyelectrolyte Interlayers for High-Performance Solar Cells. Angew. Chemie - Int. Ed. 2017, 56 (29), 8431–8434. https://doi.org/10.1002/anie.201612021.

(22)   Liu, Y.; Page, Z. A.; Russell, T. P.; Emrick, T. Finely Tuned Polymer Interlayers Enhance Solar Cell Efficiency. Angew. Chemie - Int. Ed. 2015, 54 (39), 11485–11489. https://doi.org/10.1002/anie.201503933.

(23)   Page, Z. A.; Liu, F.; Russell, T. P.; Emrick, T. Tuning the Energy Gap of Conjugated Polymer Zwitterions for Efficient Interlayers and Solar Cells. J. Polym. Sci. Part A Polym. Chem. 2015, 53 (2), 327–336. https://doi.org/10.1002/pola.27349.

(24)   Page, Z. A.; Liu, F.; Russell, T. P.; Emrick, T. Rapid, Facile Synthesis of Conjugated Polymer Zwitterions in Ionic Liquids. Chem. Sci. 2014, 5 (6), 2368–2373. https://doi.org/10.1039/c4sc00475b.

(25)   Hu, Z.; Xu, R.; Dong, S.; Lin, K.; Liu, J.; Huang, F.; Cao, Y. Quaternisation-Polymerized N-Type Polyelectrolytes: Synthesis, Characterisation and Application in High-Performance Polymer Solar Cells. Mater. Horiz. 2017, 4 (1), 88–97. https://doi.org/10.1039/C6MH00434B.

(26)   Hofmann, O. T.; Atalla, V.; Moll, N.; Rinke, P.; Scheffler, M. Interface Dipoles of Organic Molecules on Ag(111) in Hybrid Density-Functional Theory. New J. Phys. 2013, 15 (111). https://doi.org/10.1088/1367-2630/15/12/123028.

(27)   Hofmann, O. T.; Glowatzki, H.; Bürker, C.; Rangger, G. M.; Bröker, B.; Niederhausen, J.; Hosokai, T.; Salzmann, I.; Blum, R. P.; Rieger, R.; et al. Orientation-Dependent Work-Function Modification Using Substituted Pyrene-Based Acceptors. J. Phys. Chem. C 2017, 121 (39), 24657–24668. https://doi.org/10.1021/acs.jpcc.7b08451.

(28)   Chen, M. T.; Hofmann, O. T.; Gerlach, A.; Bröker, B.; Bürker, C.; Niederhausen, J.; Hosokai, T.; Zegenhagen, J.; Vollmer, A.; Rieger, R.; et al. Energy-Level Alignment at Strongly Coupled Organic-Metal Interfaces. J. Phys. Condens. Matter 2019, 31 (19). https://doi.org/10.1088/1361-648X/ab0171.

(29)   Page, Z. A.; Liu, Y.; Duzhko, V. V.; Thomas, P.; Russell, T. P.; Emrick, T. Fulleropyrrolidine Interlayers: Tailoring Electrodes to Raise Organic Solar Cell Efficiency. Science (80-.). 2014, 346 (6208), 441–446. https://doi.org/10.1126/science.1255826.

(30)   He, Z.; Xiao, B.; Liu, F.; Wu, H.; Yang, Y.; Xiao, S.; Wang, C.; Russell, T. P.; Cao, Y. Single-Junction Polymer Solar Cells with High Efficiency and Photovoltage. Nat. Photonics 2015, 9 (3), 174–179. https://doi.org/10.1038/nphoton.2015.6.

(31)   Liu, Y.; Cole, M. D.; Jiang, Y.; Kim, P. Y.; Nordlund, D.; Emrick, T.; Russell, T. P. Chemical and Morphological Control of Interfacial Self-Doping for Efficient Organic Electronics. Adv. Mater. 2018, 30 (15), 1705976. https://doi.org/10.1002/adma.201705976.

(32)   Kumar, A.; Sista, S.; Yang, Y. Dipole Induced Anomalous S-Shape I-V Curves in Polymer Solar Cells. J. Appl. Phys. 2009, 105 (9), 094512. https://doi.org/10.1063/1.3117513.

(33)   Wagenpfahl, A.; Rauh, D.; Binder, M.; Deibel, C.; Dyakonov, V. S-Shaped Current-Voltage Characteristics of Organic Solar Devices. Phys. Rev. B 2010, 82 (11), 115306. https://doi.org/10.1103/PhysRevB.82.115306.

(34)   Zhao, W.; Li, S.; Yao, H.; Zhang, S.; Zhang, Y.; Yang, B.; Hou, J. Molecular Optimization Enables over 13% Efficiency in Organic Solar Cells. J. Am. Chem. Soc. 2017, 139 (21), 7148–7151. https://doi.org/10.1021/jacs.7b02677.

(35)   Dai, S.; Zhao, F.; Zhang, Q.; Lau, T. K.; Li, T.; Liu, K.; Ling, Q.; Wang, C.; Lu, X.; You, W.; et al. Fused Nonacyclic Electron Acceptors for Efficient Polymer Solar Cells. J. Am. Chem. Soc. 2017, 139 (3), 1336–1343. https://doi.org/10.1021/jacs.6b12755.

(36)   Sun, C.; Wu, Z.; Hu, Z.; Xiao, J.; Zhao, W.; Li, H. W.; Li, Q. Y.; Tsang, S. W.; Xu, Y. X.; Zhang, K.; et al. Interface Design for High-Efficiency Non-Fullerene Polymer Solar Cells. Energy Environ. Sci. 2017, 10 (8), 1784–1791. https://doi.org/10.1039/c7ee00601b.

(37)   Yin, Q.; Zhang, K.; Zhang, L.; Jia, J.; Zhang, X.; Pang, S.; Xu, Q.-H.; Duan, C.; Huang, F.; Cao, Y. An Efficient Binary Cathode Interlayer for Large-Bandgap Non-Fullerene Organic Solar Cells. J. Mater. Chem. A 2019, 7 (20), 12426–12433. https://doi.org/10.1039/C9TA02844G.

(38)   Reilly, T. H.; Hains, A. W.; Chen, H. Y.; Gregg, B. A. A Self-Doping, O 2-Stable, n-Type Interfacial Layer for Organic Electronics. Adv. Energy Mater. 2012, 2 (4), 455–460. https://doi.org/10.1002/aenm.201100446.

(39)   Tan, Y.; Chen, L.; Wu, F.; Huang, B.; Liao, Z.; Yu, Z.; Hu, L.; Zhou, Y.; Chen, Y. Regulation of the Polar Groups in N-Type Conjugated Polyelectrolytes as Electron Transfer Layer for Inverted Polymer Solar Cells. Macromolecules 2018, 51 (20), 8197–8204. https://doi.org/10.1021/acs.macromol.8b01490.

(40)   Russ, B.; Robb, M. J.; Popere, B. C.; Perry, E. E.; Mai, C. K.; Fronk, S. L.; Patel, S. N.; Mates, T. E.; Bazan, G. C.; Urban, J. J.; et al. Tethered Tertiary Amines as Solid-State n-Type Dopants for Solution-Processable Organic Semiconductors. Chem. Sci. 2016, 7 (3), 1914–1919. https://doi.org/10.1039/c5sc04217h.

(41)   Zhang, J.; Xue, R.; Xu, G.; Chen, W.; Bian, G. Q.; Wei, C.; Li, Y.; Li, Y. Self-Doping Fullerene Electrolyte-Based Electron Transport Layer for All-Room-Temperature-Processed High-Performance Flexible Polymer Solar Cells. Adv. Funct. Mater. 2018, 28 (13), 1–10. https://doi.org/10.1002/adfm.201705847.

(42)   Chen, L.; Tan, Y.; Liu, X.; Chen, Y. Counterion Induced Facile Self-Doping and Tunable Interfacial Dipoles of Small Molecular Electrolytes for Efficient Polymer Solar Cells. Nano Energy 2016, 27, 492–498. https://doi.org/10.1016/j.nanoen.2016.08.005.

(43)   Jia, J.; Fan, B.; Xiao, M.; Jia, T.; Jin, Y.; Li, Y.; Huang, F.; Cao, Y. N-Type Self-Doped Water/Alcohol-Soluble Conjugated Polymers with Tailored Energy Levels for High-Performance Polymer Solar Cells. Macromolecules 2018, 51 (6), 2195–2202. https://doi.org/10.1021/acs.macromol.8b00126.

(44)   Liu, H.; Huang, L.; Cheng, X.; Hu, A.; Xu, H.; Chen, L.; Chen, Y. N-Type Self-Doping of Fluorinate Conjugated Polyelectrolytes for Polymer Solar Cells: Modulation of Dipole, Morphology, and Conductivity. ACS Appl. Mater. Interfaces 2017, 9 (1), 1145–1153. https://doi.org/10.1021/acsami.6b15678.

(45)   Duzhko, V. V.; Dunham, B.; Rosa, S. J.; Cole, M. D.; Paul, A.; Page, Z. A.; Dimitrakopoulos, C.; Emrick, T. N-Doped Zwitterionic Fullerenes as Interlayers in Organic and Perovskite Photovoltaic Devices. ACS Energy Lett. 2017, 957–963. https://doi.org/10.1021/acsenergylett.7b00147.

(46)   Hunter, C. A.; Sanders, J. K. M. The Nature of π-π Interactions. J. Am. Chem. Soc. 1990, 112 (14), 5525–5534. https://doi.org/10.1021/ja00170a016.

(47)   Li, Y.; Cole, M. D.; Gao, Y.; Emrick, T.; Xu, Z.; Liu, Y.; Russell, T. P. High-Performance Perovskite Solar Cells with a Non-Doped Small Molecule Hole Transporting Layer. ACS Appl. Energy Mater. 2019, 2 (3), 1634–1641. https://doi.org/10.1021/acsaem.9b00164.

(48)   Culligan, S. W.; Chen, A. C. A.; Wallace, J. U.; Klubek, K. P.; Tang, C. W.; Chen, S. H. Effect of Hole Mobility through Emissive Layer on Temporal Stability of Blue Organic Light-Emitting Diodes. Adv. Funct. Mater. 2006, 16 (11), 1481–1487. https://doi.org/10.1002/adfm.200500785.

(49)   Deng, Z.; Lee, S. .; Webb, D. .; Chan, Y. .; Gambling, W. . Carrier Transport in Thin Films of Organic Electroluminescent Materials. Synth. Met. 1999, 107 (2), 107–109. https://doi.org/10.1016/S0379-6779(99)00149-6.

(50)   Liu, Y.; Renna, L. A.; Page, Z. A.; Thompson, H. B.; Kim, P. Y.; Barnes, M. D.; Emrick, T.; Venkataraman, D.; Russell, T. P. A Polymer Hole Extraction Layer for Inverted Perovskite Solar Cells from Aqueous Solutions. Adv. Energy Mater. 2016, 1–7. https://doi.org/10.1002/aenm.201600664.

(51)   Lee, J. W.; Kim, S. G.; Yang, J. M.; Yang, Y.; Park, N. G. Verification and Mitigation of Ion Migration in Perovskite Solar Cells. APL Mater. 2019, 7 (4). https://doi.org/10.1063/1.5085643.

(52)   Rivkin, B.; Fassl, P.; Sun, Q.; Taylor, A. D.; Chen, Z.; Vaynzof, Y. Effect of Ion Migration-Induced Electrode Degradation on the Operational Stability of Perovskite Solar Cells. ACS Omega 2018, 3 (8), 10042–10047. https://doi.org/10.1021/acsomega.8b01626.

(53)   Miyano, K.; Yanagida, M.; Tripathi, N.; Shirai, Y. Hysteresis, Stability, and Ion Migration in Lead Halide Perovskite Photovoltaics. J. Phys. Chem. Lett. 2016, 7 (12), 2240–2245. https://doi.org/10.1021/acs.jpclett.6b00579.

(54)   Xue, Q.; Hu, Z.; Liu, J.; Lin, J.; Sun, C.; Chen, Z.; Duan, C.; Wang, J.; Liao, C.; Lau, W. M.; et al. Highly Efficient Fullerene/Perovskite Planar Heterojunction Solar Cells via Cathode Modification with an Amino-Functionalized Polymer Interlayer. J. Mater. Chem. A 2014, 2 (46), 19598–19603. https://doi.org/10.1039/C4TA05352D.

(55)   Jia, X.; Zhang, L.; Luo, Q.; Lu, H.; Li, X.; Xie, Z.; Yang, Y.; Li, Y.; Liu, X.; Ma, C. Power Conversion E Ffi Ciency and Device Stability Improvement of Inverted Perovskite Solar

Cells by Using a ZnO : PFN Composite Cathode Bu Ff Er Layer. ACS Appl. Mater. Interfaces 2016, 8 (28), 18410–18417. https://doi.org/10.1021/acsami.6b03724.

(56)   Yip, H.; Sun, C.; Wu, Z.; Zhang, H.; Jiang, X.; Xue, Q.; Hu, Z.; Hu, Z.; Shen, Y.; Wang, M.; et al. Amino-Functionalized Conjugated Polymer as an Efficient Electron Transport Layer for High-Performance Planar-Heterojunction Perovskite Solar Cells. Adv. Energy Mater. 2015, 1–10. https://doi.org/10.1002/aenm.201501534.

(57)   Tripathi, N.; Shirai, Y.; Yanagida, M.; Karen, A.; Miyano, K. Novel Surface Passivation Technique for Low-Temperature Solution-Processed Perovskite PV Cells. ACS Appl. Mater. Interfaces 2016, 8 (7), 4644–4650. https://doi.org/10.1021/acsami.5b11286.

(58)   Liu, Y.; Page, Z. A.; Zhou, D.; Duzhko, V. V.; Kittilstved, K. R.; Emrick, T.; Russell, T. P. Chemical Stabilization of Perovskite Solar Cells with Functional Fulleropyrrolidines. ACS Cent. Sci. 2018, 4 (2), 216–222. https://doi.org/10.1021/acscentsci.7b00454.

(59)   Zhang, H.; Xue, L.; Han, J.; Fu, Y. Q.; Shen, Y.; Zhang, Z.; Li, Y.; Wang, M. New Generation Perovskite Solar Cells with Solution-Processed Amino-Substituted Perylene Diimide Derivative as Electron-Transport Layer. J. Mater. Chem. A 2016, 4 (22), 8724–8733. https://doi.org/10.1039/c6ta03119f.

(60)   Liu, C.; Li, Z.; Zhang, X.; Guo, W.; Zhang, L.; Ruan, S. Annealing-Free ZnO:PEI Composite Cathode Interfacial Layer for Efficient Organic Solar Cells. ACS Photonics 2017, 4 (11), 2952–2958. https://doi.org/10.1021/acsphotonics.7b01096.

CHAPTER 4

SYNTHESIS AND OPTICAL PROPERTIES OF AGGREGATION-INDUCED

EMISSION CONJUGATED POLYMERS

4.1 Introduction

When chromophores, such as pyrene and perylene, are in dilute solutions (< mM) they can be easily excited by an incident photon and relax back to their ground states through radiative relaxation (Figure 4.1). The solution response to photoexcitation is distinguished from the relaxation observed upon aggregation. Upon photoexcitation of the aggregates, the excited molecules form complexes (excimers) *via* association with ground state molecules through π-π interactions. While these excimers may exhibit emittance, they are predominately "dark" states, especially for the larger exciplex clusters. Due to their planar structure and high affinity towards π-π stacking, most conjugated molecules are susceptible to aggregation-caused quenching (ACQ). The formation of excimers in the aggregated state, leading to dominant non-radiative relaxation
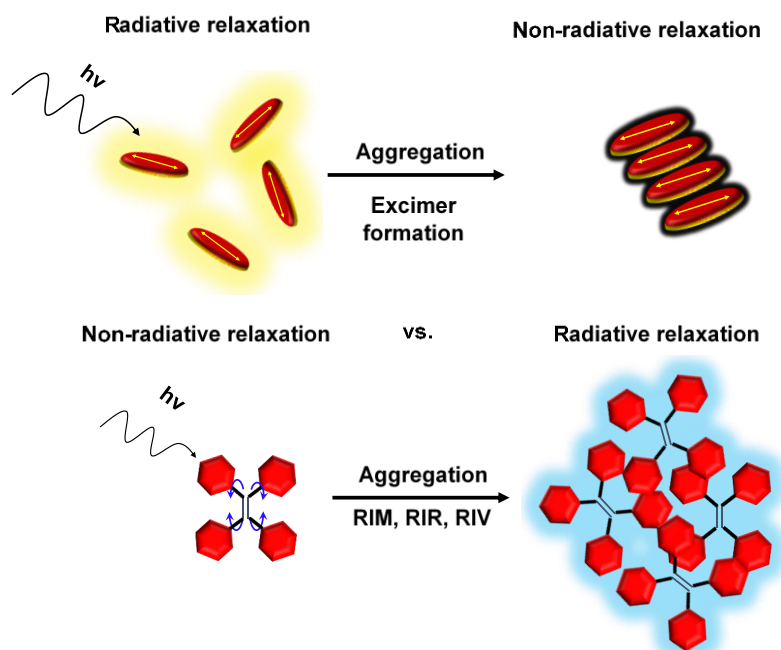
Figure 4.1. Mechanistic comparison of (top) ACQ versus (bottom) AIE.

after excitation, is the predominant theory behind ACQ (Figure 4.1).[1,2] Non-radiative relaxation

can be detrimental to the performance of organic light-emitting diode (OLED) and biological imaging applications. While ACQ can mitigated by introducing bulky side chains to interfere with π-π overlap[3] or embedding the luminescent compounds in a solubilizing matrix to enhance radiative relaxation,[4] these techniques can be synthetically taxing and exhibit limited reproducibility. As an alternative, it would be desirable to design materials that not only were resistant to quenching in the solid state but also gained emission upon aggregation.

Aggregation-induced emission (AIE) molecules stand in stark contrast to many fused aromatic structures that undergo aggregation-caused quenching (ACQ). AIE-active molecules, such as tetraphenylethylene (TPE), consist of propeller-like structures with multiple aromatic rings that rotate freely.[5] In solution, TPE exhibits miniscule emission due to energy dissipation *via* intermolecular rotation and vibration. Restricting this molecular motion, *via* aggregation or other means, results in photoluminescence.[6–8] This unique photophysical property has been employed to prepare fluorescent sensors,[9] dual-functional imaging and photodynamic therapeutics,[10] mechanochromophores,[11] and OLEDs.[12–15]

TPE has been integrated into conjugated polymer frameworks, as seen for example in the work of Tang on TPE homopolymer sensors,[16] and Dong on TPE/fluorene copolymer dual-channel sensors with orthogonal fluorescent responses of the fluorene and TPE components.[17] Related studies were reported by Li for TPE/carbazole-containing polymers.[18,19] Less-studied is the introduction of TPE into polymeric solid-state emitters to further enhance their emission, such as poly(phenylene vinylenes) (PPVs), which are well-known emitters[20–25] that suffer from aggregation-caused quenching (ACQ).[26] Integrating TPE into PPV holds the potential to enrich the optoelectronic properties of PPV without requiring synthetically taxing functionalization with substituents to effect steric repulsion. Horner-Wadsworth-Emmons (HWE) coupling was selected

94

Scheme 4. 1. Synthesis of TPE-based small molecules

to prepare PPVs with embedded TPE groups, and Suzuki-Miyaura (SM) coupling was employed to synthesize comparative TPE polymers containing *para*-phenylene moieties. As described below, this tailoring of polymer backbone chemistry and TPE content dictated the optoelectronic properties of AIE-containing conjugated polymers, while expanding the capabilities of PPV with embedded AIE groups.

4.2 Monomer and polymer synthesis

The synthesis of key TPE derivatives is shown in Scheme 4.1. 4-Bromophenyl-4-ethylhexyloxyphenyl methanone (**1**) was prepared by Friedel-Crafts acylation of 4-bromobenzoyl chloride and anisole, followed by demethylation and substitution with 2-ethylhexyl bromide. **1** was subjected to McMurry coupling conditions to prepare the novel TPE derivative **2**. This reaction produced the expected mixture of E and Z stereoisomers, as reflected in the ^{1}H NMR spectra of **2**. The chemical shifts observed from 7.35 to 6.66 ppm corresponded to both stereoisomers in the isolated product. The mixture of stereoisomers was also observed in the aromatic region of the ^{13}C NMR spectrum from 159 to 114 ppm.

Figure 4. 2. (A) 1H NMR spectra of the aromatic region; (B) MALDI-TOF; and (C) 2D NOESY NMR spectra of (top) E Z isomer and (bottom) Z isomer of **3**.

2 was converted to the diformyl derivative **3** by lithiation at -78 °C, then introduction of dimethylformamide (DMF). The polar aldehyde groups allowed for efficient chromatographic separation of the E and Z isomers, by silica gel chromatography eluting with a mixture of dichloromethane and ethyl acetate. In the aromatic region of the E and Z isomers of **3** (Figure 4.2A), the protons of the aldehyde-substituted phenyls (7.63 and 7.20 ppm) and the ethylhexyloxy-functionalized phenyls (6.93 and 6.70 ppm) are easily distinguished. Molecular weights measured by MALDI-TOF (647.7 m/z) mass spectrometry provided further evidence that the two products isolated by chromatography were the E and Z stereoisomers (Figure 4.2B). Nuclear Overhauser effect spectroscopy (NOSEY) NMR experiments were conducted to confirm the stereochemistry. The presence or absence of cross peaks from 6.70 to 7.63 ppm in the NOESY NMR spectra, due to through-space coupling of the aromatic rings, confirmed the identity of the Z or E isomer (Figure 4.2C). Compounds **4** and **5** were synthesized to compare the influence of phenylene vs. phenylenevinylene appendages on the AIE properties of TPE. These structures were used to provided additional insight to the evolution of AIE properties.
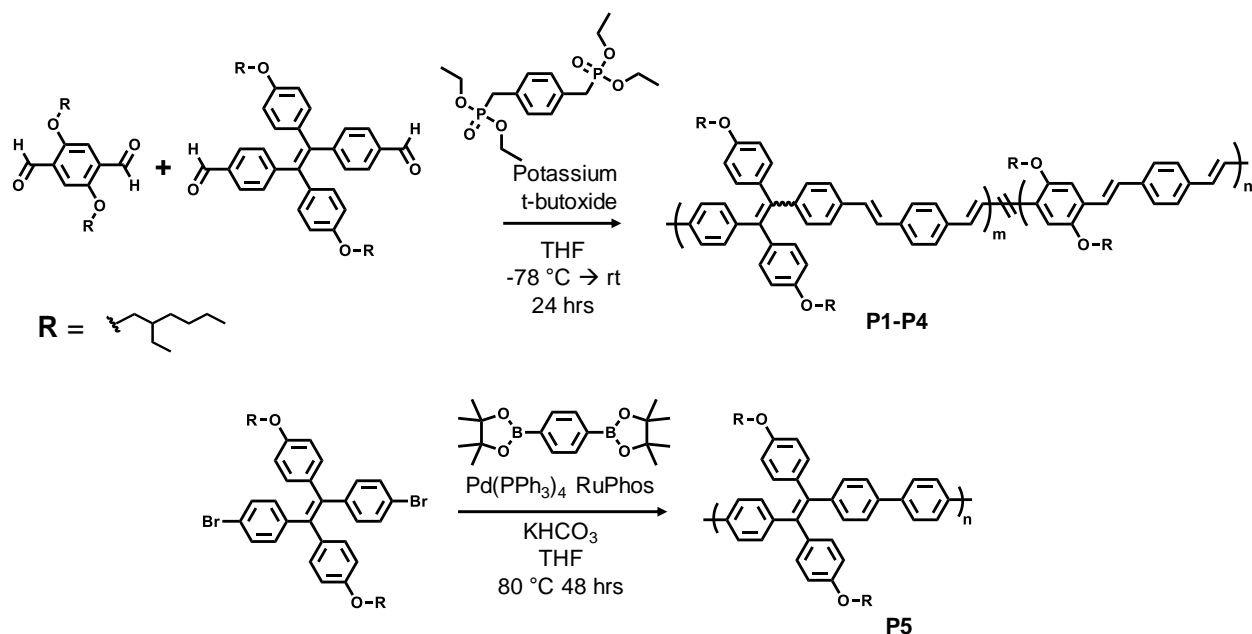
Scheme 4. 2. Synthesis of polymers **P1-P4** (top) by HWE coupling and polymer **P5** (bottom) by SM coupling.

Scheme 4.2 illustrates the synthesis of TPE-based conjugated polymers and the results of these reactions are shown in Table 4.1. The TPE-PPV analog (**P1**) containing phenylene vinylene groups between the TPE units was prepared by reacting the E or Z isomer of **3** with the benzyl bisphosphonate comonomer in the presence of potassium *tert*-butoxide in THF. A PPV homopolymer (**P4**) and copolymers containing 25 mole% (**P3**) or 50 mole% (**P2**) TPE were also prepared under the same conditions. TPE incorporation was determined by ^{1}H NMR as shown in
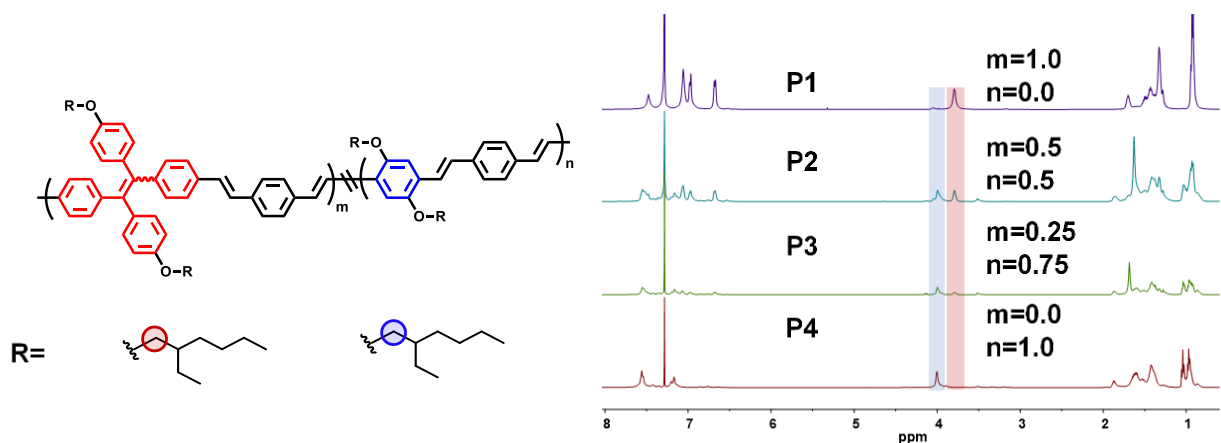
Figure 4. 3. Structure of TPE-PPV copolymers and stacked 1H NMR spectra monitoring TPE content in **P1**-**P4**.

Table 4. 1. TPE incorporation, molecular weight and yield of conjugated polymers.

Polymer[a]	Monomer feed (mole%)	X_{TPE} (mole%)[b]	M_n[c] (kDa)	M_w[c] (kDa)	Đ[c]	Yield (%)
P1Z	100	100	23.0	61.2	2.7	43
P1Z	100	100	11.4	17.3	1.5	46
P2	50	40	22.1	46.6	2.1	68
P3	25	25	54.8	132.3	2.4	90
P4	0	0	45.6	131.7	2.9	60
P5	100	100	4.9	8.1	1.4	48

[a]Polymer nomenclature based on conjugated backbone chemistry, stereochemistry, and side group functionality; [b]mole percent TPE incorporation determined by ^{1}H NMR spectroscopy; [c]number-average molecular weight, weight-average molecular weight, and dispersity estimated by GPC.

Figure 4.3. The TPE polymer containing para-phenylene units between the TPE groups (**P5**) was prepared from **2**, using $Pd(PPh_3)_4$ in the presence of potassium bicarbonate and the 1,4-phenylboronic acid pinacol ester in THF/H_2O mixtures. All polymers were precipitated into acidic methanol and isolated as yellow (**P1-P4**) or green powders (**P5**) yields of 43 to 90%. The optical properties of the synthesized small molecules and polymers are discussed in the proceeding sections.

4.3 Solution and thin film optical properties

The solution absorption and emission spectra of compound **1**, **P5**, and **P1** in DCM are shown in Figure 4.4A. **2** exhibited an absorption onset at 385 nm with maxima at 258 nm and 330 nm corresponding to the phenyl rings and the extended conjugation in the TPE system respectively.[27] The absorption onset of **P5** (430 nm) was red shifted relative to **2**, as expected by extending the conjugation. Increased conjugation and planarization in **P1** resulted in a further bathochromic shift of the absorption onset to 474 nm. **P2**-**P4** exhibited absorption onsets at 517 nm. Embedding TPE in the conjugated polymers afforded them with solution emission, which was not observed for **2**, as reflected in the spectra shown in Figure 3. While the polymer chains remained solvated in the dichloromethane solution, restriction of TPE intermolecular motion by
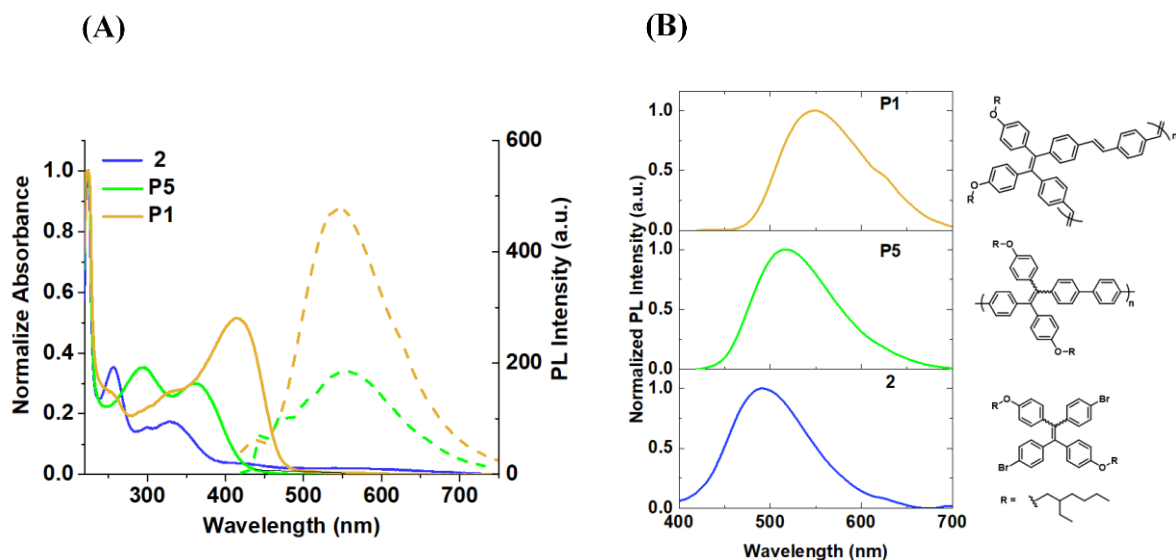
Figure 4. 4. (A) Solution absorption (solid line) and emission (dashed line) spectra in CH$_2$Cl$_2$; (B) Thin films emission spectra on quartz substrates of **2**, **P5**, and **P1** their structures.

embedding the subunits in the π-conjugated backbone allowed for the observed emission. At equivalent optical density, the emission intensity of **P1** was higher relative to the **P5**. This enhanced solution emission was hypothesized to result from additional intramolecular restriction imposed by the vinylene linkers. The thin film emission spectra of the **P1**, **P5**, and **2** are shown in Figure 4.4B. The emission maxima of **2**, **P5**, and **P1** were observed at 491nm (blue), 518 nm (green), and 550 nm (yellow) respectively (Figure 4). These results show the emission color of TPE-containing conjugated polymers can tailored by slight modifications to the backbone chemistry (i.e. phenylene versus phenylene vinylene). The thin film optical properties of the PPV derivatives (**P1**-**P4**) were also compared. Films were prepared by spin coating from pure chlorform solutions or dropcast at 1wt% in PEO (Mn=1900) (Figure 4.5A-D) in THF. Film thicknesses were calculated based on optical densities measured by UV-vis and contact profilometry measurements. The photoluminescence (PL) of **P1** was not influenced by the thin film environment reflected by the nominal blue shift of the emission maxima from 543 for the pure thin film relative to 535 nm when embedded in PEO. **P2**-**P4** all exhibited shifts in ~ 30 nm bathochromic shifts in the emission
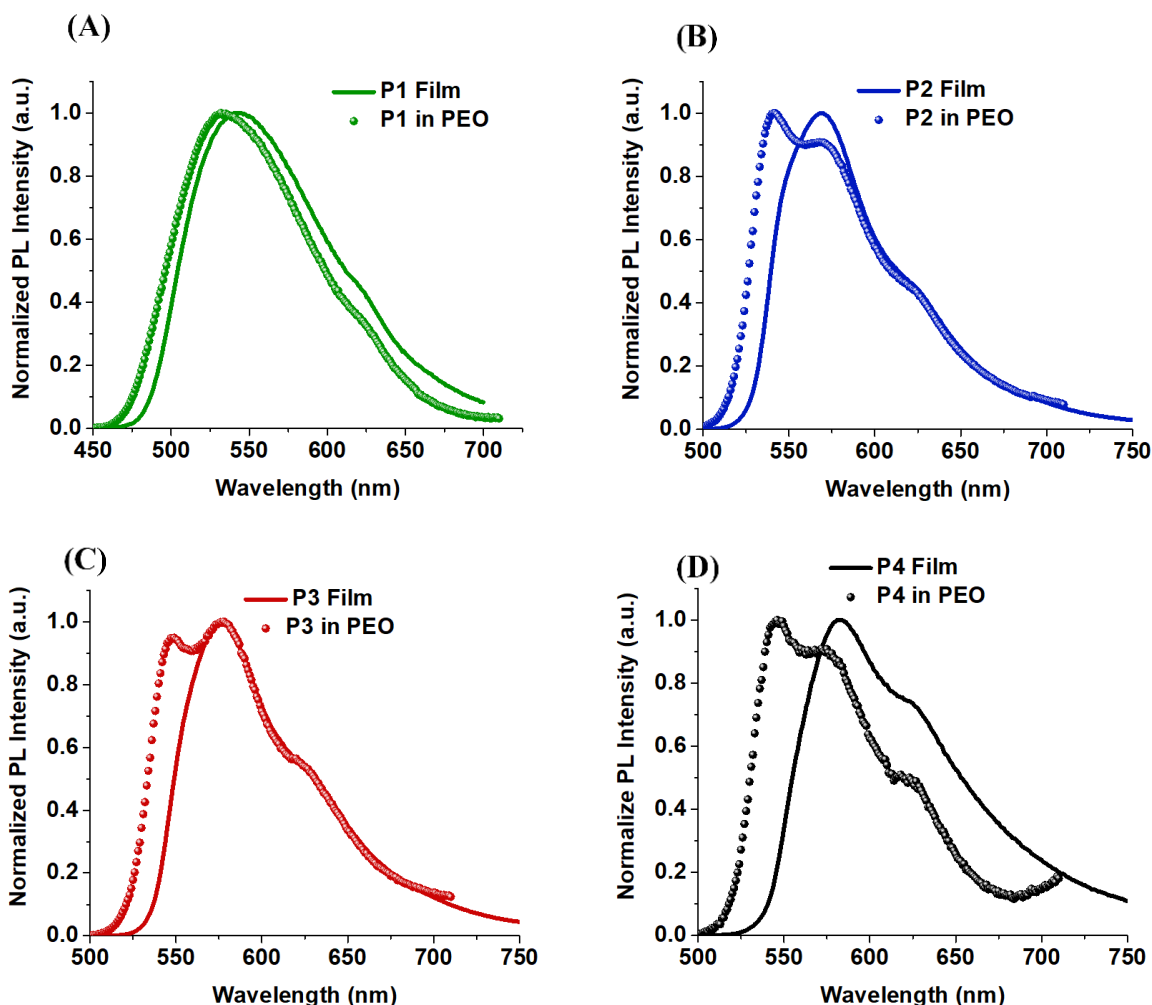
Figure 4. 5. PL spectra of **P1**-**P4** (A-D) as thin films and embedded in PEO.

maxima and variance in vibronic signature when comparing the pure thin to the polymer embedded

in PEO. This observations highlights the influence of TPE content on the optical properties of PPV

structures.

4.4 Aggregation-induced emission properties of novel structures

PL studies in THF:H_2O mixtures allowed for studying how the discussed materials respond

to aggregation. As has been previously reported with other TPE-based small molecules, **2** became

observably emissive at high water content ($> 70\%$ v/v) with ratio of maximum emission intensity

to initial emission intensity (I_{max}/I_0) > 200 indicative of AIE behavior (Figure 4.6). To further

understand the role of extending the conjugation of the TPE structure and the influence of

(A) **(B)**
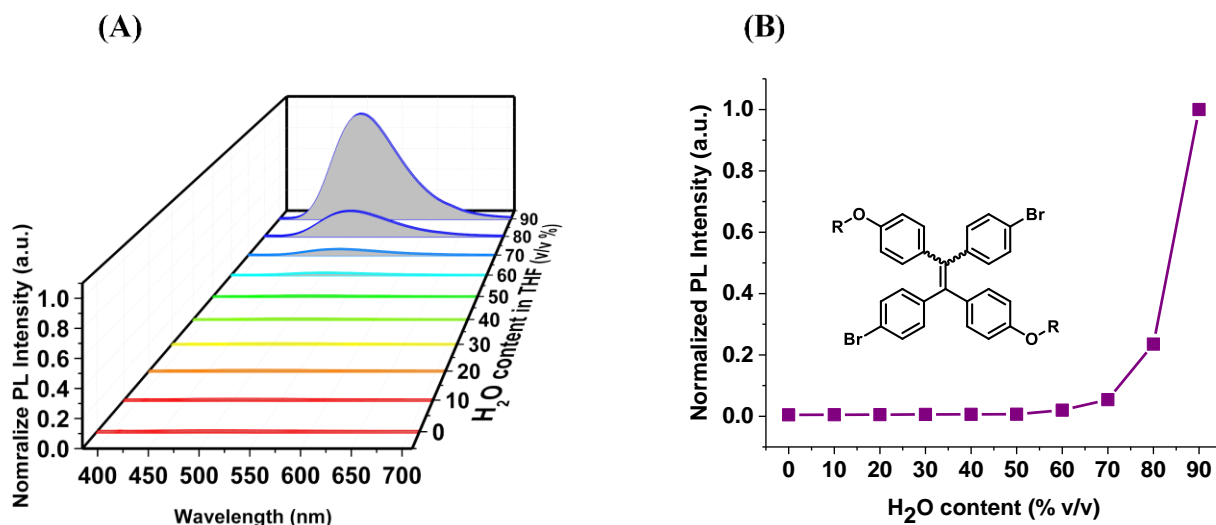
Figure 4. 6. Photoluminescence spectra in THF/H2O solutions with inset of Imax/I0 plotted against v/v% H2O in THF/H2O solutions with molecular structure of 2.

backbone chemistry the AIE properties of small molecules **4** and **5** and polymers **P1** and **P5** were examined (Figure 4.7).   As shown in Figure 4.7, **4**, **5Z**, and **5E** exhibited the strongest emission at the highest water content and large I_{max}/I_0 values of 204.1, 52.9, and 48.2 respectively. Noteworthy was the significant decrease in I_{max}/I_0 with the vinylphenyl functionalized derivatives. I_{max}/I_0 values of 19.6, 11.2, and 8.4 were measured for **P5**, **P1Z**, **P1E**. By increasing the rigidity and/or conjugation of the molecular structure, I_{max}/I_0 values decreased. This is attributed to an increase in restriction of intermolecular motion, giving rise to enhanced solution emission as opposed to diminished aggregate emission. Thus, appending the TPE structure with phenyl or vinylphenyl groups as well as embedding TPE into π-conjugated polymer backbones significantly influences its AIE properties. These results can be used to design future AIE systems with varying sensitivities to aggregation and tailored emission wavelengths.

The PL properties of PPV derivatives **P2**-**P4** in THF:H_2O mixtures are shown in Figure 4.8. These polymers exhibited strong solution emission and clear vibronic structure with emission maxima at 513 and 550 nm. In contrast to **P1**, the emission of the **P4** was strongest in pure THF and became significantly quenched by the addition of water, decreasing by ~10-fold at 90 v/v%
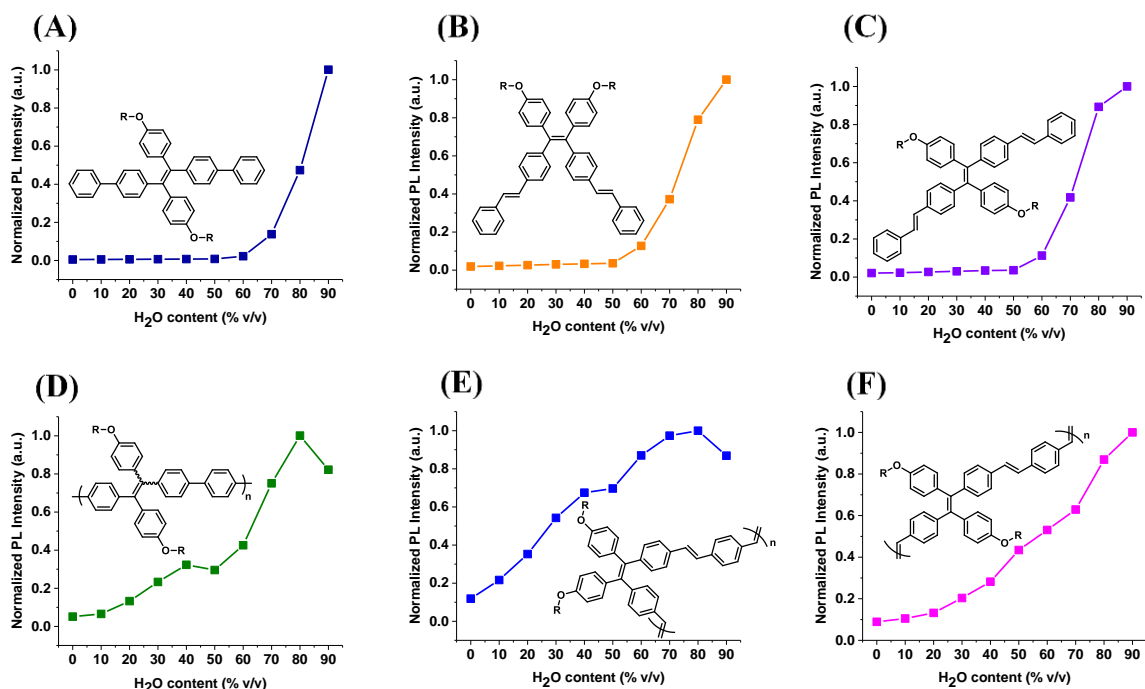
Figure 4. 7. I_{max}/I_0 plotted against v/v% H_2O in THF/H_2O solutions with molecular structure of (A) **4**; (B) **5Z**; (C) **5E**; (D) **P5**; (E) **P1Z**; and (F) **P2Z**.

H_2O. This clearly illustrated the dominant non-radiative relaxation in PPV upon aggregation. Additionally, the emission maximum of **P4** was shifted from the initial 515 nm to 535 nm. While the TPE copolymers, **P2** and **P3**, also exhibited non-radiative relaxation behavior, integration of TPE was found to attenuate ACQ. As shown in Figure 4.8, increasing TPE content in the copolymer resulted in a decrease in fluorescence quenching at high water content relative to emission measured in pure THF. Thus, integration of TPE into PPV can efficiently reduce ACQ behavior in PPV structures, realizing a simple approach to ACQ resistant PPVs.

To further understand the influence of TPE in the PPV structure solution quantum yield experiments and PL studies as a function of film thickness were conducted on **P1** and **P4.** Quantum yields (Φ_{PL}) of **P1**-**P4** were calculated relative to Rhodamine 6G standard (Figure 4.9).[28,29] **P4** exhibited the highest Φ_{PL} value 0.17 ± 0.07. Φ_{PL} was not significantly changed by introducing 25 mole% TPE in **P3**, producing a value of 0.18 ± 0.06. By further increasing the TPE content to 50 mole% in **P2** or with the TPE-PPV homopolymer, **P1**, produced Φ_{PL} values of 0.07 ± 0.03 an 0.03
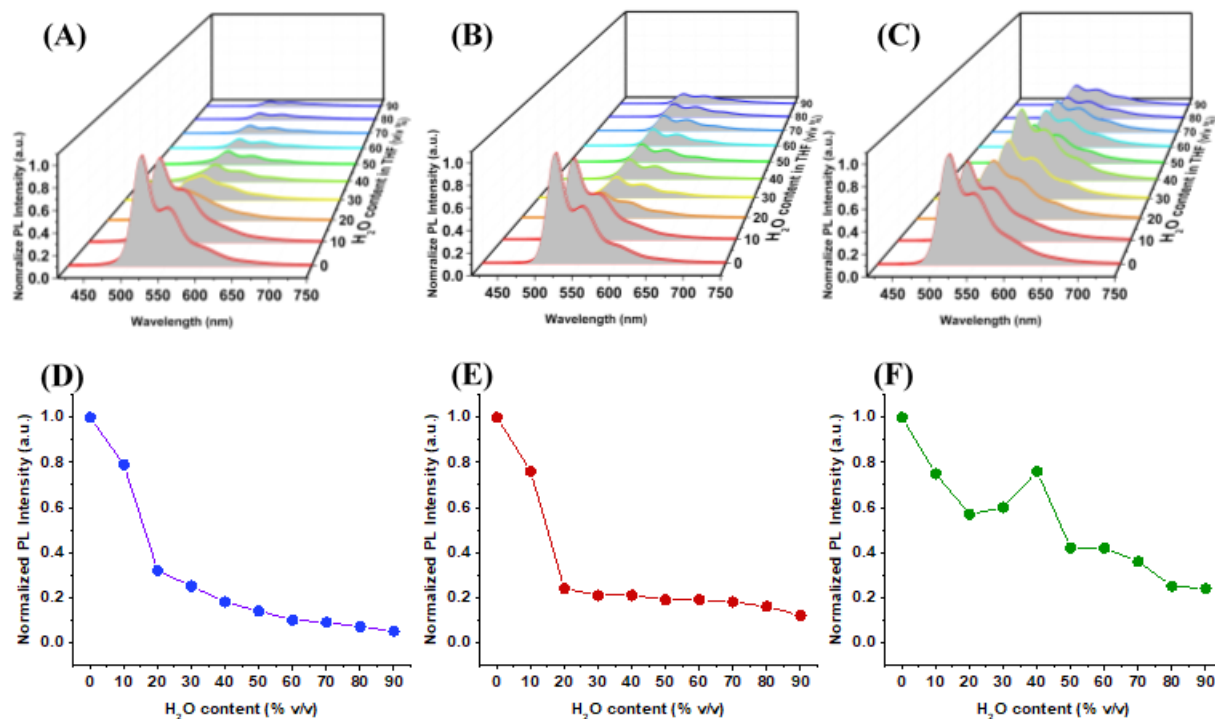
Figure 4. 8. Fluorescence spectra and normalized fluorescence intensity plotted against water content of **P4** (A,D); **P3** (B,E); and **P2** (C,F) solutions.

± 0.01, respectively. These results confirm that introduction of TPE into PPV systems can significantly decrease the influence of ACQ but also impacts the solution quantum yield. For thin film studies solutions of **P1** or **P4** were spin coated onto glass substrates at different concentrations in chloroform solutions. By controlling the concentration of polymer in chloroform the thickness of the film could be controlled. Studying the thickness dependence of the photoluminescence properties of these polymers provided insight into ACQ in the thin films. As shown in Figure 4.10, increasing **P4** thickness from 1 nm to 12 nm resulted in an increase in PL intensity, as is to be expected by increasing the amount of polymer to participate in radiative relaxation. At greater
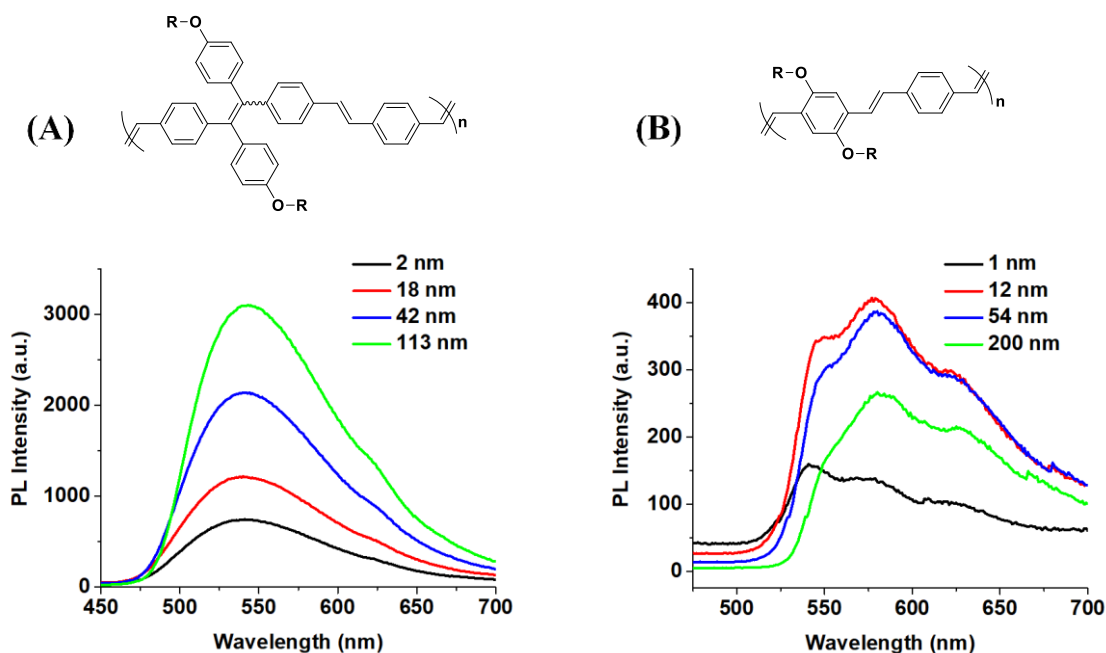
Figure 4. 9. Photoluminescence spectra of thin films prepared at different concentrations of (A) **P1** and (B) **P4**.

thicknesses (54 and 200 nm) the PL intensity was found to decrease. This decrease in PL was attributed to ACQ becoming dominant in the thicker films. PL response of **P1** films was found to scale with thickness, resulting in continuous increasing PL intensity as film thickness increased from 2 to 113. This suggests that in **P1** the PL is sustained as thicker films are formed without significant radiative loss due to quenching which was observed in the **P4**.
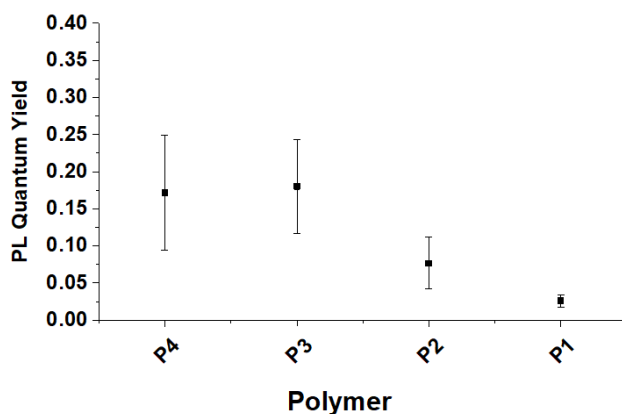
Figure 4. 10. Figure S6. Plot of Φ_{PL} values of **P1**-**P4** with error bars corresponding to one standard deviation.

4.5 Conclusion

Conjugated polymers containing TPE structures were prepared and their optoelectronic properties were studied as a function of TPE content and backbone conjugation chemistry. The TPE-PPV homopolymer, **P1**, displayed optoelectronic properties of both TPE and PPV evident by the observed solution and aggregate emission. **P1** exhibited the lowest I_{max}/I_0 due to the enhanced solution emission. Additionally, emission of the **P1** remained constant upon aggregation in THF/H_2O mixtures, thin films, or embedded in PEO. This distinguished it from **P2**-**P4** which displayed fluctuations in emission wavelength depending on its local electronic environment. This work has shown that TPE can be successfully integrated into a PPV backbone without compromising its advantageous AIE properties. The PPV homopolymer, **P4**, exhibited clear spectral features of aggregation caused quenching in PL studies. By introducing controlled amounts of TPE to the polymer backbone (e.g., **P2** and **P3),** ACQ could be attenuated without modifying the emission maxima (513 nm). Through these studies it was found that the TPE-PPV homopolymer, **P1**, exhibited the highest aggregate emission and stable emission wavelength across all THF/H_2O mixtures. Moreover, the PPV and TPE components worked in synergy to produce the observed optoelectronic characteristics, thus realizing a PPV composition that synergistically combines desirable elements of both AIE and conjugated polymers.

4.6 References

(1)   Hsu, J. H. Fluorescence from Conjugated Polymer Aggregates in Dilute Poor Solution. J. Phys. Chem. A 1999, 103 (14), 2375–2380. https://doi.org/10.1021/jp983921t.

(2)   Birks, J. B. Photophysics of Aromatic Molecules; Wiley-Interscience: London, 1970. https://doi.org/10.1016/0022-2313(71)90011-1.

(3)   Van Severen, I.; Bolink, H. J.; Vanderzande, D.; Lutsen, L.; Cleij, T. J.; Adriaensens, P.; Vandenbergh, J. Tetra-Alkoxy Substituted PPV Derivatives: A New Class of Highly Soluble Liquid Crystalline Conjugated Polymers. Polym. Chem. 2011, 2 (6), 1279. https://doi.org/10.1039/c1py00027f.

(4)   Park, Y. H.; Kim, Y.; Sohn, H.; An, K. S. Concentration Quenching Effect of Organic Light-Emitting Devices Using DCM1-Doped Tetraphenylgermole. J. Phys. Org. Chem. 2012, 25 (3), 207–210. https://doi.org/10.1002/poc.1893.

(5)   Luo, J.; Xie, Z.; Lam, J. W. Y.; Cheng, L.; Tang, B. Z.; Chen, H.; Qiu, C.; Kwok, H. S.; Zhan, X.; Liu, Y.; et al. Aggregation-Induced Emission of 1-Methyl-1,2,3,4,5-Pentaphenylsilole. Chem. Commun. 2001, 381 (18), 1740–1741. https://doi.org/10.1039/b105159h.

(6)   Liu, J.; Meng, Q.; Zhang, X.; Lu, X.; He, P.; Jiang, L.; Dong, H.; Hu, W. Aggregation-Induced Emission Enhancement Based on 11,11,12,12,-Tetracyano-9,10-Anthraquinodimethane. Chem. Commun. (Camb). 2013, 49 (12), 1199–1201. https://doi.org/10.1039/c2cc38817k.

(7)   Chen, J.; Law, C. C. W.; Lam, J. W. Y.; Dong, Y.; Lo, S. M. F.; Williams, I. D.; Zhu, D.; Tang, B. Z. Synthesis, Light Emission, Nanoaggregation, and Restricted Intramolecular

Rotation of 1,1-Substituted 2,3,4,5-Tetraphenylsiloles. Chem. Mater. 2003, 15 (7), 1535–1546. https://doi.org/10.1021/cm021715z.

(8)   Yin, S.; Peng, Q.; Shuai, Z.; Fang, W.; Wang, Y. H.; Luo, Y. Aggregation-Enhanced Luminescence and Vibronic Coupling of Silole Molecules from First Principles. Phys. Rev. B - Condens. Matter Mater. Phys. 2006, 73 (20), 1–5. https://doi.org/10.1103/PhysRevB.73.205409.

(9)   Du, J.; Yu, S.; Huang, Z.; Chen, L.; Xu, Y.; Zhang, G.; Chen, Q.; Yu, X.; Pu, L. Highly Selective Ratiometric Fluorescent Recognition of Histidine by Tetraphenylethene–Terpyridine–Zn(<scp>ii</Scp>) Complexes. RSC Adv. 2016, 6 (30), 25319–25329. https://doi.org/10.1039/C6RA03724K.

(10)   Wu, W.; Feng, G.; Xu, S.; Liu, B. A Photostable Far-Red/Near-Infrared Conjugated Polymer Photosensitizer with Aggregation-Induced Emission for Image-Guided Cancer Cell Ablation. Macromolecules 2016, 49 (14), 5017–5025. https://doi.org/10.1021/acs.macromol.6b00958.

(11)   Wu, H.; Jiang, Y.; Ding, Y.; Meng, Y.; Zeng, Z.; Cabanetos, C.; Zhou, G.; Gao, J.; Liu, J.; Roncali, J. Mechanofluorochromic and Thermochromic Properties of Simple Tetraphenylethylene Derivatives with Fused Fluorine Containing 1,4-Dioxocane Rings. Dye. Pigment. 2017, 146, 323–330. https://doi.org/10.1016/j.dyepig.2017.07.026.

(12)   Li, Y.; Xu, Z.; Zhu, X.; Chen, B.; Wang, Z.; Xiao, B.; Lam, J. W. Y.; Zhao, Z.; Ma, D.; Tang, B. Z. Creation of Efficient Blue AIE Luminogens for High-Performance Nondoped Blue OLEDs and Hybrid White OLEDs. ACS Appl. Mater. Interfaces 2019, acsami.9b03177. https://doi.org/10.1021/acsami.9b03177.

(13)   Li, J.; Han, X.; Bai, Q.; Shan, T.; Lu, P.; Ma, Y. Electropolymerized AIE-Active Polymer Film with High Quantum Efficiency and Its Application in OLED. J. Polym. Sci. Part A Polym. Chem. 2017, 55 (4), 707–715. https://doi.org/10.1002/pola.28414.

(14)   Xie, Y.; Li, Z.; Gong, Y.; Zhang, F.; Peng, Q.; Han, M.; Xie, G. Tetraphenylcyclopentadiene-Based Hyperbranched Polymers: Convenient Syntheses from One Pot "A 4 + B 2 " Polymerization and High External Quantum Yields up to 9.74% in OLED Devices. Macromolecules 2019, 52, 896–903. https://doi.org/10.1021/acs.macromol.8b02051.

(15)   Zhao, Z.; Deng, C.; Chen, S.; Lam, J. W. Y.; Qin, W.; Lu, P.; Wang, Z.; Kwok, H. S.; Ma, Y.; Qiu, H.; et al. Full Emission Color Tuning in Luminogens Constructed from Tetraphenylethene, Benzo-2,1,3-Thiadiazole and Thiophene Building Blocks. Chem. Commun. 2011, 47 (31), 8847–8849. https://doi.org/10.1039/c1cc12775f.

(16)   Hu, R.; Maldonado, J. L.; Rodriguez, M.; Deng, C.; Jim, C. K. W.; Lam, J. W. Y.; Yuen, M. M. F.; Ramos-Ortiz, G.; Tang, B. Z. Luminogenic Materials Constructed from Tetraphenylethene Building Blocks: Synthesis, Aggregation-Induced Emission, Two-Photon Absorption, Light Refraction, and Explosive Detection. J. Mater. Chem. 2012, 22 (1), 232–240. https://doi.org/10.1039/c1jm13556b.

(17)   Shi, J.; Wu, Y.; Sun, S.; Tong, B.; Zhi, J.; Dong, Y. Tunable Fluorescence Conjugated Copolymers Consisting of Tetraphenylethylene and Fluorene Units: From Aggregation-Induced Emission Enhancement to Dual-Channel Fluorescence Response. J. Polym. Sci. Part A Polym. Chem. 2013, 51 (2), 229–240. https://doi.org/10.1002/pola.26377.

(18)   Wu, W.; Ye, S.; Tang, R.; Huang, L.; Li, Q.; Yu, G.; Liu, Y.; Qin, J.; Li, Z. New Tetraphenylethylene-Containing Conjugated Polymers: Facile Synthesis, Aggregation-

Induced Emission Enhanced Characteristics and Application as Explosive Chemsensors and PLEDs. Polymer (Guildf). 2012, 53 (15), 3163–3171. https://doi.org/10.1016/j.polymer.2012.05.035.

(19)   Dong, W.; Ma, Z.; Chen, P.; Duan, Q. Carbazole and Tetraphenylethylene Based AIE-Active Conjugated Polymer for Highly Sensitive TNT Detection. Mater. Lett. 2019, 236, 480–482. https://doi.org/10.1016/j.matlet.2018.10.162.

(20)   Gmeiner, J.; Karg, S.; Meier, M.; Rieß, W.; Strohriegl, P.; Schwoerer, M. Synthesis, Electrical Conductivity and Electroluminescence of Poly(P-phenylene Vinylene) Prepared by the Precursor Route. Acta Polym. 1993, 44 (4), 201–205. https://doi.org/10.1002/actp.1993.010440405.

(21)   Lee, D. W.; Kwon, K.-Y.; Jin, J.-I.; Park, Y.; Kim, Y.-R.; Hwang, I.-W. Luminescence Properties of Structurally Modified PPVs: PPV Derivatives Bearing 2-(4- Tert -Butylphenyl)-5-Phenyl-1,3,4-Oxadiazole Pendants. Chem. Mater. 2001, 13 (2), 565–574. https://doi.org/10.1021/cm000794g.

(22)   Sung-Ho, J.; Mock-Yeon, K.; Jin Young, K.; Kwanghee, L.; Yeong-Soon, G. High-Efficiency Poly(p-Phenylenevinylene)-Based Copolymers Containing an Oxadiazole Pendant Group for Light-Emitting Diodes. J. Am. Chem. Soc. 2004, 126 (2), 2474_2480.

(23)   Kim, S. T.; Hwang, D.; Li, X. C.; Grüner, J.; Friend, R. H.; Holmes, A. B.; Shim, H. K. Efficient Green Electroluminescent Diodes Based on Poly (2-Dimethyloctylsilyl-1,4-Phenylenevinylene). Adv. Mater. 1996, 8 (12), 979–982. https://doi.org/10.1002/adma.19960081206.

(24)   Vilbrandt, N.; Gassmann, A.; von Seggern, H.; Rehahn, M. Blue-Greenish Electroluminescent Poly(p -Phenylenevinylene) Developed for Organic Light-Emitting

Diode Applications. Macromolecules 2016, 49 (5), 1674–1680. https://doi.org/10.1021/acs.macromol.5b01249.

(25) Burroughes, J. H.; Bradley, D. D. C.; Brown, A. R.; Marks, R. N.; Mackay, K.; Friend, R. H.; Burns, P. L.; Holmes, A. B. Light-Emitting Diodes Based on Conjugated Polymers. Nature 1990, 347 (6293), 539–541. https://doi.org/10.1038/347539a0.

(26) Jakubiak, R.; Collison, C. J.; Wan, W. C.; Rothberg, L. J.; Hsieh, B. R. Aggregation Quenching of Luminescence in Electroluminescent Conjugated Polymers. J. Phys. Chem. A 1999, 103 (14), 2394–2398. https://doi.org/10.1021/jp9839450.

(27) Vyas, V. S.; Rathore, R. Preparation of a Tetraphenylethylene-Based Emitter: Synthesis, Structure and Optoelectronic Properties of Tetrakis(Pentaphenylphenyl)Ethylene. Chem. Commun. 2010, 46 (7), 1065–1067. https://doi.org/10.1039/b923915d.

(28) Gettinger, C. L.; Heeger, A. J.; Drake, J. M.; Pine, D. J. The Effect of Intrinsic Rigidity on the Optical Properties of PPV Derivatives. Mol. Cryst. Liq. Cryst. Sci. Technol. Sect. A. Mol. Cryst. Liq. Cryst. 1994, 256 (1), 507–512. https://doi.org/10.1080/10587259408039283.

(29) Crosby, G. A.; Demas, J. N. Measurement of Photoluminescence Quantum Yields. Review. J. Phys. Chem. 1971, 75 (8), 991–1024. https://doi.org/10.1021/j100678a001.

CHAPTER 5

SUMMARY AND OUTLOOK

5.1 PDI-containing ionene and zwitterionic polymers

In Chapter 2 the synthesis and characterization of PDI-based polyionenes and zwitterionic polymers with ammonium and sulfobetaine groups embedded in the polymer backbone was described. PDI monomers containing bromide or phenyl groups at the 1 and 7 positions of the aromatic core were employed for polymer synthesis. Appending bulky groups to the aromatic core imparted the PDI derivatives with solubility properties necessary for polymerizations. Tertiary amine groups at the imide conditions served as active sites for polymerizations when reacted with 1,6-dibromohexane or a novel butene bis-sultone. By employing an aliphatic diamine comonomer, PDI incorporation in both the polyionene and polymer zwitterions could be controlled.

The influence of PDI incorporation was reflected in the yield, molecular weight, and spectral features. The experimental incorporation was in good agreement with the targeted PDI incorporation. The vibronic structure in the UV-vis spectra provided insight into the π-π interactions of the PDI units in the polymers. This was quantitatively studied through the ratio of the S_{0-0} to S_{0-1} absorption bands. The S_{0-1} absorption band was attributed to co-facial interactions of the PDI transition dipole, also associated with H-type aggregation, while the S_{0-0} was associated with well solvated PDI units. The cationic PDI polyionenes were found to maintain S_{0-0}/S_{0-1} values > 1 over across all PDI incorporations while the zwitterionic polymer exhibited ratio values of ~0.8 for the **PDIBr$_2$-50%** and **PDIBr$_2$-100%**. The difference in spectral features arose from the difference in chemical functionality in the polymer backbone. The electrostatic repulsion in the polyionenes created a barrier for inter-or intrachain π-π stacking, distinct from the attractive dipole

coupling observed in zwitterions. Thus, PDI-PDI interactions were facilitated by the presence of sulfobetaine groups in the zwitterionic and attenuated by cationic groups in the polyionenes. The results of this work yielded a novel approach to preparing functional PDI-containing polymers.

While significant work was conducted to elucidate the structure property relationship of these structures, there are still areas of interest left to be explored. This work could be extended by introducing other conjugated monomers. Naphthalene diimides and isoindigos are ideal candidates as they can be easily appended with tertiary amines for polymerization. These aromatic structures are smaller than PDI which may afford them with enhanced solubility without the need of additional functionality at the aromatic core to mitigate π-π stacking. In addition to introducing alternative aromatic component to polyionenes and linear polymer zwitterions, modification of the ionic component would afford novel structures.

The accessibility of PDI permits the integration of a variety of functional groups at the imide position. Organophosphorus compounds containing aryl phosphonium groups have been shown to effectively modify the work function of metal cathodes and improve performance of OPV devices.[1] PDIs containing methyl sulfide or diphenyl phosphine groups could be prepared to achieve ionene and zwitterionic polymers with sulfonium and phosphonium groups in the polymer backbone (Figure 5.1). Additionally, through simple ion exchange methods a large library of polymers with varying cations and counterions can be achieved. The polyionene and linear
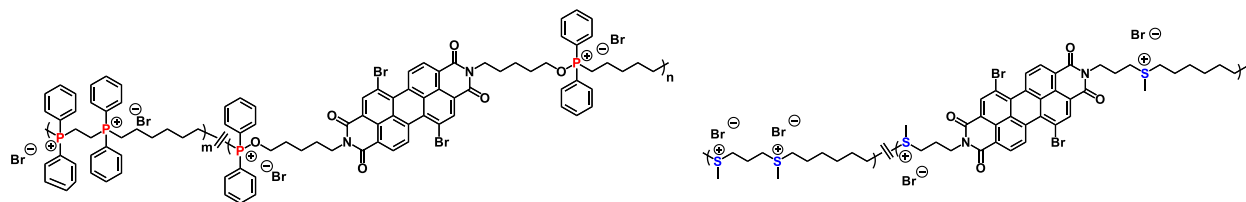
Figure 5. 1. Proposed structures of (left) phosphonium- and (right) sulfonium-based PDI polyionenes

zwitterionic polymer platform is poised for further innovation. The metal-free conditions and facile tunability of these structures are valuable attributes, which will prove integral to advancing their utility beyond academic research and into commercially viable platforms.

5.2 PDI-based photovoltaic interlayers

In Chapter 3 the interfacial properties and photovoltaic performance of PDI-containing structures was detailed. The PDI polyionene and polymer zwitterion platform offered a unique opportunity for a greater understanding of interfacial material design. Organic electron-transporting layers (ETLs) have predominately been either completely aliphatic or conjugated structures, each coming with its own advantages and disadvantages. Conjugated structures have emerged as the more desirable materials due to the ability to improve devices over a wide range of thicknesses. The PDI-based polymers permitted the study of the role of conjugation density in relation to work function modification and charge transporting properties.

UPS experiments were conducted on Ag coated with polyionenes and polymer zwitterions containing controlled amounts of the **PDIBr$_2$** or **PDIPh$_2$**. These studies revealed that increased PDI content resulted in a decrease in the interfacial dipole, resulting in smaller work function modification. This trend held true for both polyionenes and zwitterionic polymers independent of PDI derivative in the polymer backbone. The interfacial dipoles produced by the polymers were larger than those observed for the small molecule analogs containing tertiary amines. Photovoltaic devices were fabricated with the PDI-based materials to determine their efficacy as ETLs.

PDIPh$_2$-containing polyionenes and polymer zwitterions were integrated into OSCs as ETLs to study how PDI content as well as zwitterionic *versus* cationic functionality influenced device performance. Devices containing PDI polymer interlayers exhibited enhanced performance

in comparison to devices fabricated with bare electrodes. The S-shaped J-V curves of devices containing the zwitterionic interlayers distinguished them from polyionene interlayer devices. This S-shape was reflected in the significantly lower fill-factors observed in these devices and attributed to charge build-up at the active layer/cathode interface. In contrast, all ionene polymers exhibited high fill-factors, exceeding 70% with distinct rectification of the current. While the **PDIPh$_2$-10%** polymer produced higher interfacial dipoles and was able moderately increase device performance, it also exhibited low tolerance to interlayer thickness. This was attributed to the insufficient PDI content necessary for effective charge transport as the 50 mole% and homopolymer of **PDI-Ph$_2$** yielded devices with PCEs > 8% over a range of interlayer thicknesses. Noteworthy was the observed peak photovoltaic performance of devices employing **PDIPh$_2$-50%** polyionene.

Additional electronic and morphological studies were conducted on the polyionene interlayers to further understand the trends in photovoltaic performance. **PDIPh$_2$-50%** exhibited superior electron mobilities, conductivity, and doping efficiency in comparison **PDIPh$_2$-10%** and **PDIPh$_2$-100%**. GIXD, TEM, and NEXAFS experiments revealed the morphology of **PDIPh$_2$-50%** to be ideal for efficient charge transport. Based on these results it was concluded that 50 mole% PDI was the threshold to achieve peak ETL performance with high thickness tolerance.

PDIBr$_2$-50% polyionenes were also shown to be successful in perovskite-based photovoltaic devices. With the superior perovskite active layer PCEs > 18% could be achieved over a wider range of interlayer thickness, exemplifying the versatility of these novel materials. The success of the polymers prompted additional investigation of the performance of small molecule interlayers. A PDI derivative containing terpyridine groups at the aromatic core was prepared for these studies and compared to free terpyridine and PDIBr$_2$. The terpyridine-modified

Rigid perovskite device

Metal
Interlayer
ETL
MAPbX$_3$
HTL
ITO glass

Flexible perovskite device

Metal paste

ITO on plastic
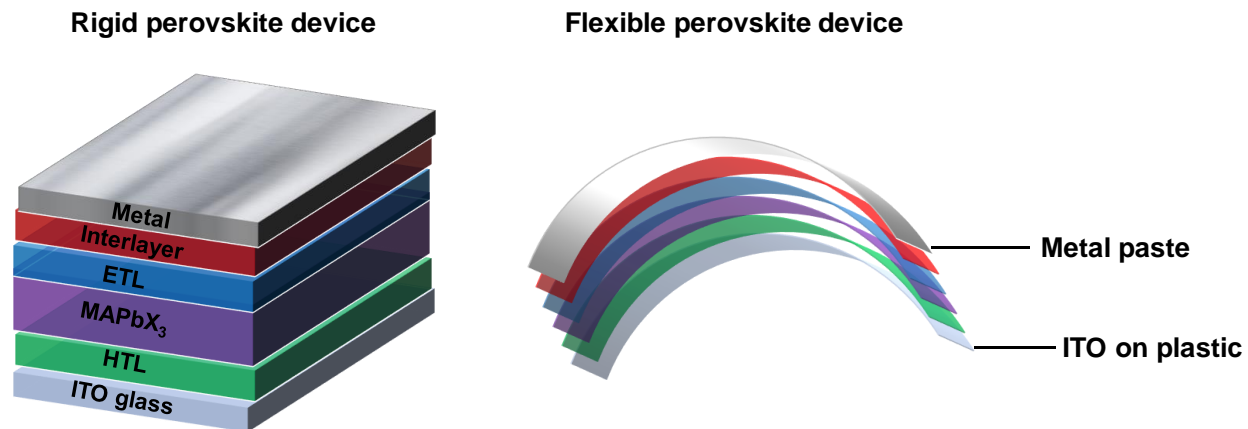
Figure 5. 2. Comparison of (left) rigid and (right) flexible perovskite-based photovoltaic devices. PDI produced the greatest efficiencies over a wide range of thicknesses which had not been previously shown with small molecule PDI interlayers in perovskite devices.

The results of the work discussed in chapter 3 are anticipated to play an integral role in advancing thin film photovoltaic devices. The field has been focused on marginal increases in efficiency without consideration for cost-effective or sustainable materials for fabricating devices. Without greater focus on how materials are made, organic or perovskite photovoltaics will be limited to lab scale studies. This thesis work revealed a threshold for PDI content in polymers for ETLs. PDI or other conjugated structures will be the costly component in fabricating interfacial materials for a photovoltaic device. Developing ways to minimize this cost is imperative to advancing the technology.

An area that was beyond the scope of this work, but should be considered, is the development of flexible devices. One of the staples of thin film photovoltaics is the idea of a malleable system that can be fabricated into a variety of structures (Figure 5.2). While this is the ultimately goal, much of the current research primarily focus fabricating and testing devices employing rigid metal and glass substrates. These rigid systems have remained popular due to higher efficiencies in comparison to flexible substrates. Focusing on peak efficiencies, and not

realistic structures, is preventing the field from achieving the goal of high throughput, flexible photovoltaic devices. Future work should employ flexible substrates with research focused on more critical properties such as device stability.

5.3 Evolution of AIE properties in conjugated polymers

Chapter 4 discussed the synthesis and characterization of conjugated polymers containing TPE. As with the controlled chemistries implemented in Chapter 2, the structure of the polymers in Chapter 4 were modulated to develop a fundamental understanding of AIE-active macromolecular structures. The first approach to tailoring the backbone chemistry was through different coupling chemistries resulting in the presence (**EtHexTPE-PPV**) or absence (**EtHexTPE-PPP**) of vinylene groups in the polymer backbone. This afforded TPE polymers with different backbone rigidity. The second approach used TPE a comonomer in PPV structures as a method to attenuate ACQ.

Integration of TPE into conjugated homopolymers resulted in solution emission which was absent in the small molecules. The solution emission was due to restriction of molecular motion through covalently linking the TPE segments into the polymer. The influence of backbone rigidity was quantitatively determined through photoluminescence experiments conducted in THF/H_2O solutions. The photoluminescence intensity ratio I_{max}/I_0 was observed to be significantly higher for the **EtHexTPE-PPP** than for the **EtHexTPE-PPV**. The lower I_{max}/I_0 observed in **EtHexTPE-PPV** was a result of enhanced solution emission rather than a loss of aggregate emission.

Structural similarity of TPE to the repeat unit of PPV, made it a desirable comonomer to address ACQ without significant modification PPV's intrinsic photoluminescent properties. The EtHex-PPV homopolymer was synthesized and used as a control for photoluminescence studies.

In the absence of TPE in the PPV structure the fluorescence was observed to quench in solutions at high H_2O content. By increasing TPE content in the polymer structure ACQ could be mitigated but not completely impeded. These results highlight the utility of TPE as well as the limitation of native PPV.

While AIE-active polymers have been studied for several years PPV-based systems have seldomly been reported. The structures discussed here hold the potential to innovated current solid-state emitter technology. Current commercial OLEDS are predominately based on heavy metal complexes and processed by evaporative deposition. While solution processing polymer OLEDs are hypothesized to be less costly, infrastructure for evaporative processing has been well establish. Therefore, solution processable polymers must offer additional benefits to compete with the current materials. The resistance to ACQ observed in **EtHexTPE-PPV** make it a viable alternative to conventional OLED materials. Future work should focus on integrating TPE-PPVs into OLEDs and comparing them to pure PPVs. Additionally, introducing functional side chains that would permit solution processing from green solvents and/or allow for modifying the interfaces in OLEDs to prevent non-radiative recombination would be desirable properties for the
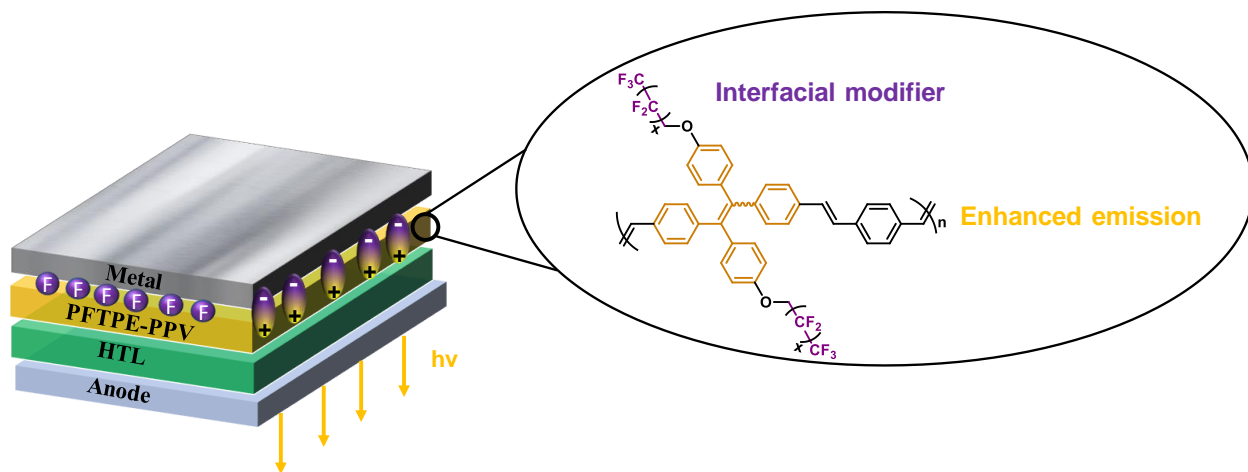
Figure 5. 3. Representative OLED device employing functional TPE-PPV emissive layer.

117

next generation of TPE-PPV materials. Introducing of fluorinated alcohols on top of PPV active layers has been shown to enhance charge injection and reduce interfacial recombination.[2] By introducing fluorinated side chains to TPE-PPV structures, a multi-functional OLED active layer could be achieved (Figure 5.3).

5.4 References

(1)   Gupta, M.; Yan, D.; Yao, J.; Zhan, C. Organophosphorus Derivatives as Cathode Interfacial-Layer Materials for Highly Efficient Fullerene-Free Polymer Solar Cells. ACS Appl. Mater. Interfaces 2018, acsami.8b09313. https://doi.org/10.1021/acsami.8b09313.

(2)   Ng, C. Y. Bin; Yeoh, K. H.; Whitcher, T. J.; Talik, N. A.; Woon, K. L.; Saisopa, T.; Nakajima, H.; Supruangnet, R.; Songsiriritthigul, P. High Efficiency Solution Processed Fluorescent Yellow Organic Light-Emitting Diode through Fluorinated Alcohol Treatment at the Emissive Layer/Cathode Interface. J. Phys. D. Appl. Phys. 2014, 47 (1). https://doi.org/10.1088/0022-3727/47/1/015106.

CHAPTER 6

EXPERIMENTAL

6.1 Materials

1-Butanol, 1-bromobutane, 1,8-diazabicyclo[5.4.0]undec-7-ene, dimethylformamide (DMF) anhydrous 98%, 1,4-dioxane anhydrous 99.8%, bromine, N,N,N',N'-tetramethyl-1,6-hexanediamine (TMHDA), 1,6-dibromohexane, trans-1,4-dibromo-2-butene, 1,3-propanesultone 98%, rhodamine 6G, aliquat 336, phenylboronic acid 95%, 3-(dimethylamino)-1-propylamine 99%, titanium (IV) chloride ReagentPlus©, 99.9%, 4-bromobenzoyl chloride 95%, aluminum(III) chloride 99%, pyridine anhydrous 99.8%, anisole anhydrous 99.7%, 2-ethylhexyl bromide, 2.5M n-butyl lithium in hexanes, sodium hydride 60% dispersion in mineral oil, tetrakis(triphenylphosphine)palladium(0) 99%, [1,1'-bis(diphenyl-phosphino) ferrocene] palladium dichloridewere purchased from MilliporeSigma. 3,4,9,10-perylenetetracarboxylic dianhydride was purchased from Tokyo chemical industry (TCI). 2,2,2-Trifluoroethanol was purchased from Alfa Aesar. Ammonium chloride, sodium bisulfite, potassium carbonate, potassium bicarbonate, diethyl ether, dichloromethane, chloroform, methanol, tetrahydrofuran (THF), acetone, and ethyl acetate were all obtained from Fisher Scientific. Silica powder, neutral alumina, and basic alumina were purchased from Sorbtech. Regenerative cellulose dialysis membranes (MWCO 3,500) were purchased from Spectrum Laboratories. PBDTT-TT was obtained from 1-Material, and PC$_{71}$BM was purchased from Nano-C. PBDB-T and ITIC were obtained from Solarmer. [1,1'-bis(diphenyl-phosphino) ferrocene] palladium dichloride. TEM grids were purchased from Ted Pella.

6.2 Instrumentation

Proton nuclear magnetic resonance (^{1}H NMR) and carbon nuclear magnetic resonance (^{13}C NMR) spectra were recorded on a Bruker Avance-500 (500 MHz) instrument. Chemical shifts are reported in ppm relative to the residual TFE signal in CF_3CD_2OD, $CF_3COCF_3 \cdot 3D_2O$, or the residual $CHCl_3$ signal in $CDCl_3$. Absorption spectra were obtained using a UV-2600 manufactured by Shimadzu. Photoluminescence spectra were obtained using a UV-Vis LS 55 fluorescence spectrophotometers manufactured by Perkin Elmer for the PDI studies and a Shimadzu RF-6000 Spectrofluorophotometer. MALDI-TOF mass spectrometry characterization was conducted on a Bruker MicroFlex working in linear mode employing 2-(4'-hydroxybenzeneazo) benzoic acid (HABA) or trans-2-[3-(4-tert-Butylphenyl)-2-methyl-2-propenylidene]malononitrile as the analyte matrix. Gel permeation chromatography (GPC) characterization of PDI-based polymers was performed using 2,2,2-trifluoroethanol (TFE) (with 0.02 M sodium trifluoroacetate) as the mobile phase, and poly(methyl methacrylate) (PMMA) calibration standards, operating at 0.75 mL/min at 40 °C with three Agilent PL HFIPgel columns (300×7.5 mm) equipped with refractive index (RI) and UV-Vis detection. Polymer freeze drying was performed with LABCONCO® FreeZone 4.5 lyophilizer. characterization of TPE-based polymers was performed using THF mobile phase against polystyrene standard, operating at 1.0 mL/min and 40 °C with an Agilent 1260 isocratic pump, an autosampler, a PLgel guard column (50 x 7.8 mm^2), two PLgel Mixed C columns (300 mm x 7.8 mm x 5μm), one PLgel mixed D column (300 mm x 7.8 mm x 5 μm), and an Agilent 1260 UV detector. UPS measurements were performed on the Omicron Nanotechnology Model ESCA+S, consisting of a helium discharge lamp (He I line, 21.2 eV) as the UV excitation source and a hemispherical SPHERA energy analyzer. The thin film thicknesses were determined using the surface profiler KLA Tencor (model Alpha-Step IQ). Atomic force microscopy (AFM) was performed in tapping mode on a Digital Instruments Dimension 3100. For

all devices *I-V* characteristics were measured under N_2 atmosphere using a Keithley 2400 source-meter under simulated AM1.5G irradiation using a 300 W Xe lamp solar simulator (Newport 91160). The light intensity was adjusted with a National Renewable Energy Laboratory (NREL)-calibrated Si reference solar cell and KG-5 filter. The illuminated area (0.05418 cm^2) was defined by a photomask with an aperture, the area of which was measured at NREL, and used in all of the device measurements. Electrical conductivity measurements were completed using a Keithley 4200 SCS-equipped probe station at ambient atmosphere. Cyclic voltammetry was conducted in glass container employing 3mm platinum working electrode on a BASi Cell stand instrument with Epsilon-EC software.

6.3 Methods

- **Synthesis of tetrabutyl perylene-3,4,9,10-tetracarboxylate (PTBC)**[1]

3,4,9,10-perylenetetracarboxylic dianhydride (5 g, 12.7 mmol) was added to a 500 mL round-bottom flask charge with stir bar and dispersed in 211 mL of acetonitrile. 1-Butanol (9.33 mL, 102 mmol), 1-bromobutane (10.95 mL, 102 mmol), and 1,8-diazabicyclo[5.4.0]undec-7-ene were then injected into the suspension then the reaction vessel was fitted with a condenser. The reaction was heated to 90 °C for 16 hours under nitrogen. The reaction was then cooled to room temperature then concentrated under reduced pressure. The crude product was dissolved in chloroform then extracted with deionized water. The organic layer was separated, dried over Na_2SO_4, filtered, then concentrated under reduced pressure. Finally, the crude product was purified on a silica column eluting with chloroform. The desired fraction was collected and concentrated as a golden yellow powder (6.48 g, 78%). ^{1}H NMR (500 MHz, CDCl$_3$, δ) δ 8.31 (d, J = 7.92 Hz, 4H), 8.06 (d, J = 7.84 Hz, 4H), 4.36 (t, 8H), 1.80 (m, 8H), 1.51 (m, 8H), 1.02 (t, 12H).

- **Synthesis of tetrabutyl 1,7-dibromoperylene-3,4,9,10-tetracarboxylate (PTBC-Br)[1]**

PTBC (3 g, 4.6 mmol) and K_2CO_3 (5.1 g, 36.8 mmol) were dissolved in 67 mL of DCM in a 2-neck round bottom flask fitted with an addition funnel under nitrogen. Bromine (3.7 mL, 73.6 mmol) in 10 mL of DCM was added to the addition funnel then added dropwise to the reaction mixture over an hour then the reaction was stirred overnight at room temperature. The crude mixture was treated with a 10 wt% $NaHSO_3$ aqueous solution to quench toe excess bromine. Then, the organic phase was separated and was extracted three times with the $NaHSO_3$ solution. The organic phase was dried over Na_2SO_4, filtered, and concentrated under reduced pressure. The isolated product was recrystallized twice from a mixture of acetonitrile and DCM to yield orange crystals (1.84 g, 49%). ^{1}H NMR (500 MHz, $CDCl_3$, δ) δ 8.99 (d, J= 7.99 Hz, 2H), 8.32 (s, 2H), 8.12 (d, J=7.96, 2H), 4.36 (t, 8H), 1.80 (m, 8H), 1.51 (m, 8H), 1.02 (t, 12H).

- **Synthesis of 1,7-dibromo-[3-(dimethylamino) propyl] perylene diimide (PDIBr₂)[2]**

Regioisomerically pure 1,7-dibromoperylene-3,4,9,10-tetracarboxylic dianhydride (3.50 g, 6.36 mmol), synthesized according to literature procedure,[3] was suspended in 175 mL of a DMF:1,4-dioxane (3:2) solvent mixture.[1] 3-(Dimethylamino)propyl-1-amine (2.00 mL, 15.9 mmol) was added to the mixture and the reaction was stirred at 65 ˚C for 1.5 hours under N_2. The mixture was concentrated under reduced pressure, then precipitated into diethyl ether and subjected to centrifugation; this process was repeated three times until the supernatant appeared colorless. The product was dissolved in chloroform, washed three times with brine, then washed with DI water and dried over Na_2SO_4. The pure product was isolated as a red powder (2.86 g, 62.6%). ^{1}H NMR (500 MHz, $CDCl_3$, δ) δ 9.51 (d, J = 8.24 Hz, 2H), 8.94 (s, 2H), 8.72 (d, J = 8.24 Hz, 2H), 4.29 (t,

4H), 2.49 (t, 4H), 2.30 (s, 12H), 1.96 (m, 4H). ^{13}C NMR (125 MHz, CDCl$_3$, δ) δ 162.39, 137.98, 133.02, 130.01, 129.26, 128.52, 126.95, 123.17, 122.74, 120.80, 57.26, 45.45, 39.19, 26.09. MALDI-TOF (m/z): [M+H]$^+$ calculated for: C$_{34}$H$_{30}$Br$_2$N$_4$O$_4$: 718.45, found: 718.80

- **Synthesis of 1,7-diphenyl-[3-(dimethylamino) propyl] perylene diimide (PDIPh$_2$)**[2]

PDI-Br (200 mg, 0.278 mmol), potassium fluoride (64 mg, 1.1 mmol), and phenyl boronic acid (89 mg 0.695 mmol) were added to a thick-walled glass pressure vessel followed by 8 mL of DMF:1,4 dioxane (3:2), 800 μL of 2M K$_2$CO$_3$ in water, and 2 drops of Aliquat 336 (AQ336). Then, [1,1'-bis(diphenyl-phosphino) ferrocene] palladium dichloride (6.1 mg, 0.008 mmol) was added to the solution after degassing using a stream of N$_2$ for thirty minutes. The vessel was sealed under a N$_2$ atmosphere and the reaction was stirred at 65 ˚C for 2.5 hours. The reaction was allowed to cool to room temperature and diluted with chloroform (25 mL). The organic phase was subjected to three cycles washing with 50 mL of saturated aqueous LiCl solution (25 mL), brine, and deionized water. The organic phase was dried over anhydrous Na$_2$SO$_4$, filtered, and concentrated under vacuum. The concentrated solution pulled over neutral alumina gel eluting with CHCl$_3$: MeOH (98:2), yielding dark purple crystals after removing solvent (178 mg, 90%). ^{1}H NMR (500 MHz, CDCl$_3$, δ) 8.60 (s, 2H), 8.14 (d, J= 8.24 Hz, 2H), 7.80 (d, J= 7.93 Hz, 2H), 7.54(m broad, 10H), 4.33 (t, 4H), 3.03 (broad, 4H), 2.71 (s, 12H), 2.28 (m, 4). ^{13}C NMR (125 MHz, CDCl$_3$, δ) δ 163.45, 142.04, 135.30, 134.90, 132.61, 130.33, 130.21, 129.44, 129.20, 129.04, 128.74, 127.62, 122.19, 121.85, 57.14, 45.95, 45.22, 38.83, 25.93. MALDI-TOF (m/z): [M+H]$^+$ calculated for: C$_{46}$H$_{40}$Br$_2$N$_4$O$_4$: 712.85, found: 713.30

- **Synthesis of 1,7-diphenylterpyridyl-[3-(dimethylamino) propyl] perylene diimide**

PDIBr$_2$ (100 mg, 0.139 mmol), phenylterpyridine boronic ester (152 mg, 0.349 mmol), and [1,1'-bis(diphenylphosphino)ferrocene]dichloropalladium(II) (3 mg, 0.005 mmol) were added to a pressure vessel. The reagents were dissolve in 4 mL of DMF:dioxane (3:2) mixture, 400 μL of 2M K$_2$CO$_3$ in water, and 2 drops of Aliquat 336 (AQ336). The solution was deoxygenated *via* N$_2$ bubbling then sealed and heated at 110 °C overnight. The crude product was diluted with CHCl$_3$ then extracted with brine three times. The organic layer was separated, dried over Na$_2$SO$_4$, and concentrated under reduced pressure. The crude product was purified on basic alumina eluting with a gradient of pure CHCl$_3$ to 95:5 CHCl$_3$:TEA. The desired fraction was isolated and precipitated into isopropyl alcohol to yield a light purple solid (56 mg, 35%). MALDI-TOF (m/z): [M+H]$^+$ calculated for: C$_{76}$H$_{58}$N$_{10}$O$_4$: 1175.46, found: 1176.6.

- **Synthesis of 3,3'-(bute-2-ene) bis(1,2-oxathiolane-2,2-dioxide) (bis-sultone)**

1,3-Propane sultone (16.5 mmol) was dissolved in THF (80 mL) and cooled to -78 °C. N-butyllithium (2.5 M, 15 mmol) was added slowly, and the mixture was stirred for 30 min. A THF solution of *trans*-1,4-dibromo-2-butene (8.25 mmol) was added drop wise (in THF solution) to the vigorously stirred solution. The mixture was stirred at -78 °C for 2 hrs, and the -78 °C cooling bath was replaced with an ice water bath, and the mixture was stirred for an additional 30 min. Water was added, and the crude product was extracted with ethyl acetate three times. The mixture was dried over anhydrous Na$_2$SO$_4$, and volatiles were removed under reduced pressure. Column chromatography was performed using silica gel, eluting with a 2:8 ethyl acetate:hexanes mixture, affording the product as a white solid (1.2 g, 25%). ^{1}H NMR (500 MHz, CDCl$_3$, δ in ppm): 5.71-5.67 (m, 1H), 4.50-4.35 (m, 2H), 3.35-3.25 (m, 2H), 2.67 (m, 1H), 2.49 (m, 1H), 2.34-2.30 (m, 1H). ^{13}C NMR (125 MHz, CDCl$_3$, δ in ppm): 127.7, 66.1, 54.1, 30.8, 28.1. HRMS. Calcd for C$_{10}$H$_{16}$O$_6$S$_2$ [(M+1)$^+$]: m/z 296.3604. Found: m/z 296.3604.

- **General procedure for preparation PDI-containing ionene polymers** [2]

In a typical procedure, 1,6-dibromohexane (180 μL, 1.18 mmol) and 1.18 mmol of **PDIBr₂** or **PDIPh₂** and N,N,N',N'-tetramethyl-1,6-hexanediamine (TMHDA) to achieve the desired copolymer composition were added to a glass pressure vessel in air dissolved in 1:1 mixture of CHCl₃: MeOH (4.7 mL). This mixture was stirred vigorously for 2 days at 70 ˚C. The crude product was cooled to room temperature and precipitated into diethyl ether. The precipitate was isolated by centrifugation at 5000 rpm for five minutes then the crude product was dissolved in TFE. The product was further purified by dialysis against H₂O:MeOH (1:1) over one day, then pure water for two days using a cellulose dialysis membrane (MWCO 3,500). The purified product was lyophilized and isolated in yields ranging from 43% to 83%.

- **10 mole% PDIBr₂ ionene copolymer (PDIBr₂-10%)**

^{1}H NMR (500 MHz, CF₃COCF₃ · 3D₂O, ppm) δ 9.00- 7.92 (6H ar of PDI-Br₂ polymer), 3.61 (4H of imide ((O=C)₂NC**H₂**CH₂CH₂N⁺(CH₃)₂R) PDI-Br₂ polymer), 2.72 (4H of imide C**H₂** PDI-Br₂ polymer), 2.45 (8H of aliphatic ionene polymer RN⁺(CH₃)₂C**H₂**R), 2.32 (12H of imide R₂N⁺(C**H₃**)₂ of PDI-Br₂ polymer), 2.26 (s, 12 H of aliphatic ionene polymer R₂N⁺(C**H₃**)₂), 1.55 (4H of imide C**H₂** PDI-Br₂ polymer), 1.04 (8H of aliphatic ionene polymer RN⁺(CH₃)₂CH₂C**H₂**R), 0.74 (8H of aliphatic ionene polymer RN⁺(CH₃)₂CH₂CH₂C**H₂**R)

- **50 mole% PDIBr₂ ionene copolymer (PDIBr₂-50%)**

^{1}H NMR (500 MHz, CF₃COCF₃·3D₂O, ppm) δ 9.00- 7.92 (6H ar of PDI-Br₂ polymer), 3.67 (4H of imide C**H₂** PDI-Br₂ polymer), 2.75 (4H of imide C**H₂** PDI-Br₂ polymer), 2.56 (4H C**H₂** of PDI-

Br2 polymer), 2.45 (8H **CH₂** of aliphatic ionene polymer), 2.38- 2.32 (12H of imide $R_2N^+(CH_3)_2$ of PDI-Br$_2$ polymer), 2.26 (12H of $R_2N^+(CH_3)_2$ of aliphatic ionene polymer), 1.54 (4H of imide **CH₂** PDI-Br$_2$ polymer), 1.15 (4H **CH₂** of PDI-Br2 polymer), 1.05 (8H **CH₂** of aliphatic ionene polymer), 0.86 (4H **CH₂** of PDI-Br2 polymer), 0.74 (8H **CH₂** of aliphatic ionene polymer).

- **PDIBr₂ ionene homopolymer (PDIBr₂-100%)**

^{1}H NMR (500 MHz, CF$_3$COCF$_3$·3D$_2$O, ppm) δ 9.00- 7.92 (6H ar), 3.62 (4H of imide **CH₂**), 2.80 (4H of imide), 2.60 (4H **CH₂**), 2.37 (12H of imide $R_2N^+(CH_3)_2$), 1.56 (4H of imide **CH₂**), 1.18 (4H **CH₂**), 0.86 (4H **CH₂**).

- **10 mole% PDIPh₂ ionene copolymer (PDIPh₂-10%)**

^{1}H NMR (500 MHz, CF$_3$COCF$_3$·3D$_2$O, ppm) δ δ 7.97-6.78 (16H ar), 3.65 (4H of imide **CH₂** PDI-Ph$_2$ polyimer), 2.82 (4H of imide **CH₂** PDI-Ph$_2$ polymer), 2.56 (8H **CH₂** of aliphatic ionene polymer), 2.40 (12H of imide $R_2N^+(CH_3)_2$ of PDI-Ph$_2$ polymer) 2.35 (s, 12 H $R_2N^+(CH_3)_2$ of aliphatic ionene polymer), 1.55 (4H of imide **CH₂** PDI-Ph$_2$ polymer), 1.09 (8H **CH₂** of aliphatic ionene polymer), 0.78 (8H **CH₂** of aliphatic ionene polymer)

- **50 mole% PDIPh₂ ionene copolymer (PDIPh₂-50%)**

^{1}H NMR (500 MHz, CF$_3$COCF$_3$·3D$_2$O, ppm) δ 7.97-6.78 (16H ar of PDI-Ph$_2$ polymer), 3.57 (4H of imide **CH₂** PDI-Ph$_2$ polymer), 2.64 (4H of imide **CH₂** PDI-Ph$_2$ polymer), 2.43 (10H **CH₂** of aliphatic ionene polymer and PDI-Ph$_2$ polymer), 2.28 (12H of imide $R_2N^+(CH_3)_2$ of PDI-Ph$_2$ polymer), 2.24 (12H of $R_2N^+(CH_3)_2$ of aliphatic ionene polymer), 1.49 (4H, **CH₂** of PDI-Ph$_2$

ionene polymer imide), 1.02 (10H, C**H₂** of aliphatic ionene polymer and PDI-Ph₂ polymer), 0.72 (10H C**H₂** of aliphatic ionene polymer and PDI-Ph₂ polymer).

- **PDIPh₂ ionene homopolymer (PDIPh₂-100%)**

^{1}H NMR (500 MHz, CF₃COCF₃·3D₂O, ppm) δ 7.97-6.78 (16H ar), 3.57 (4H of imide C**H₂**), 2.68 (4H of imide C**H₂**), 2.45 (4H C**H₂**), 2.07 (12H of imide R₂N⁺(C**H₃**)₂), 1.50 (4H of imide C**H₂**), 1.02 (4H C**H₂**), 0.65 (4H C**H₂**).

- **General procedure for the preparation of PDI-containing zwitterionic polymers**

In a general procedure, **3** (0.05 g, 0.16 mmol) and 0.16 mmol of 1,7-(dibromo/phenyl)-[3-(dimethylamino) propyl] perylene diimide and TMHDA to achieve the desired copolymer composition were added in air to a 7 mL pressure vessel equipped with a magnetic stir bar and dissolved in TFE (0.35 mL) (Scheme 1). The sealed vessel was placed in a preheated oil bath at 70 °C for 48 h. The crude product was cooled to room temperature and precipitated into diethyl ether. The precipitate was isolated by centrifugation at 5000 rpm for five minutes, then redispersed in 2,2,2-trifluoroethanol. The polymerization mixture was dialyzed against water for 2 days using a cellulose dialysis membrane (MWCO 3,500) and lyophilized and isolated in yields ranging from 40% to 85%.

- **10 mole% PDIBr₂ zwitterionic copolymer (PDIZBr₂-10%)**

^{1}H NMR (500 MHz, CF₃CD₂OD, ppm) δ: 9.65-8.39 (6H, Ar of PDI-Br₂ polymer), 5.74-5.65 (2H, RH**C**=**C**HR of aliphatic zwitterionic polymer), 4.32 (4H, R₂NC**H₂**CH₂CH₂ of PDI-Br₂ polymer imide), 3.72 (2H, R₂C**H**(SO₃⁻)), 3.44 (4H, R₂NCH₂C**H₂**CH₂ of PDI-Br₂ polymer imide), 3.26 (4H

of imide CH_2PDI-Br_2), 3.05 (12H, of imide $R_2N(CH_3)_2$), 2.88(12H of imide $R_2N(CH_3)_2$ of PDI-Br_2), 2.78(12H of imide $R_2N(CH_3)_2$ of PDI-Br_2), 2.47 (4H, RCH_2-CH=CHR), 2.35(4H, RCH_2-CH=CHR), 2.15 (4H, CH_2 of aliphatic zwitterionic polymer), 1.85 (4H, CH_2 of 6,6-polyzwitterion), 1.51 (2H, $R_2NCH_2CH_2R$ of 6,6-polyzwitterion), 1.37 (4H CH_2 of PDI-Br_2 polymer).

- **50 mole% PDIBr$_2$ zwitterionic copolymer (PDIZBr$_2$-50%)**

^{1}H NMR (500 MHz, CF_3CD_2OD, ppm) δ 9.53-8.40 (16H; Ar), 5.85-5.65 (2H, $RHC=CHR$), 4.38 (4H, $R_2NCH_2CH_2CH_2$ of imide), 3.68 (2H, $R_2CH(SO_3^-)$), 3.38 (4H, $R_2NCH_2CH_2CH_2$ of imide), 3.21(4H of imide CH_2PDI-Br_2), 3.05 (12H, of imide $R_2N(CH_3)_2$), 2.89(12H of imide $R_2N(CH_3)_2$ of PDI-Br_2), 2.75 (4H, CH_2 of aliphatic zwitterionic polymer), 2.43 (4H, RCH_2-CH=CHR), 2.35 (4H of imide R_2NCH_2PDI-Ph_2 polymer), 2.15 (4H, CH_2 of aliphatic zwitterionic polymer), 1.82 (4H, CH_2 of aliphatic zwitterionic polymer), 1.53 (2H, $R_2NCH_2CH_2R$ of aliphatic zwitterionic polymer), 1.37 (4H CH_2 of PDI-Br_2 polymer).

- **PDIBr$_2$ zwitterionic homopolymer (PDIZBr$_2$-100%)**

^{1}H NMR (500 MHz, $CF_3COCF_3 \cdot 3D_2O$, ppm) δ 8.98-7.75 (6H Ar), 5.12-5.00 (2H, $RHC=CHR$), 3.69 (4H, $R_2NCH_2CH_2CH_2$ of imide), 3.28(2H, $R_2CH(SO_3^-)$), 3.15 (4H, CH_2 of imide), 2.82 (4H of imide CH_2PDI-Br_2), 2.42 (12H, of imide $R_2N(CH_3)_2$), 2.30 (4H of imide $R_2N(CH_3)_2$ of PDI-Br_2), 2.22 (4H, RCH_2-CH=CHR), 1.59 (8H, $R_2NCH_2CH_2R$ of PDI-Br_2 polymer).

- **10 mole% PDI-Ph$_2$ zwitterionic copolymer (PDIZPh$_2$-10%)**

^{1}H NMR (500 MHz, CF$_3$CD$_2$OD, ppm) δ 8.65-7.42 (16H; Ar), 5.74-5.65 (2H, R**H**C=C**H**R), 4.38 (4H, R$_2$NC**H$_2$**CH$_2$CH$_2$ of imide), 3.71 (2H, R$_2$C**H**(SO$_3^-$)), 3.42 (4H, R$_2$NCH$_2$C**H$_2$**CH$_2$ of imide), 3.23(4H of imide C**H$_2$**PDI-Ph$_2$), 3.05 (12H, of imide R$_2$N(C**H$_3$**)$_2$), 2.88(12H of imide R$_2$N(C**H$_3$**)$_2$ of PDI-Ph$_2$), 2.78 (4H, C**H$_2$** of aliphatic zwitterionic polymer), 2.46 (4H, RC**H$_2$**-CH=CHR), 2.35 (4H of imide R$_2$NC**H$_2$**PDI-Ph$_2$ polymer), 2.15 (4H, CH$_2$ of aliphatic zwitterionic polymer1.83 (4H, CH$_2$ of 6,6-polyzwitterion), 1.50 (2H, R$_2$NC**H$_2$**CH$_2$R of aliphatic zwitterionic polymer), 1.37 (4H C**H$_2$** of PDI-Ph$_2$ polymer).

- **50 mole% PDI-Ph$_2$ zwitterionic copolymer (PDIZPh$_2$-50%)**

^{1}H NMR (500 MHz, CF$_3$CD$_2$OD, ppm) δ 9.53-8.40 (16H; Ar), 5.85-5.65 (2H, R**H**C=C**H**R), 4.38 (4H, R$_2$NC**H$_2$**CH$_2$CH$_2$ of imide), 3.68 (2H, R$_2$C**H**(SO$_3^-$)), 3.38 (4H, R$_2$NCH$_2$C**H$_2$**CH$_2$ of imide), 3.21(4H of imide C**H$_2$** PDI-Ph$_2$), 3.05 (12H, of imide R$_2$N(C**H$_3$**)$_2$), 2.89(12H of imide R$_2$N(C**H$_3$**)$_2$ of PDI-Ph$_2$), 2.75 (4H, C**H$_2$** of aliphatic zwitterionic polymer), 2.43 (4H, RC**H$_2$**-CH=CHR), 2.35 (4H of imide R$_2$NC**H$_2$**PDI-Ph$_2$ polymer), 2.15 (4H, CH$_2$ of aliphatic zwitterionic polymer), 1.82 (4H, CH$_2$ of aliphatic zwitterionic polymer), 1.53 (2H, R$_2$NC**H$_2$**CH$_2$R of aliphatic zwitterionic polymer), 1.37 (4H C**H$_2$** of PDI-Br$_2$ polymer).

- **PDI-Ph$_2$ zwitterionic homopolymer (PDIZPh$_2$-100%)**

^{1}H NMR (500 MHz, CF$_3$COCF$_3$·3D$_2$O, ppm) δ 7.65-6.35 (6H Ar), 4.85-4.76 (2H, R**H**C=C**H**R), 3.45 (4H, R$_2$NC**H$_2$**CH$_2$CH$_2$ of imide), 2.95 (2H, R$_2$C**H**(SO$_3^-$)), 2.85 (4H, CH$_2$ of imide), 2.53 (4H of imide C**H$_2$**PDI-Br$_2$), 2.15 (12H, of imide R$_2$N(C**H$_3$**)$_2$), 1.98 (4H of imide R$_2$N(C**H$_3$**)$_2$ of PDI-Br$_2$), 1.83 (4H, RC**H$_2$**-CH=CHR), 1.35 (8H, R$_2$NC**H$_2$**CH$_2$R of PDI-Ph$_2$ polymer).

129

- **UV-vis absorption characterization of PDI small molecules and polymers**

Stock solutions of the PDI small molecules and polymers were prepared at 1 mg/mL in 7 mL glass scintillation vials with TFE. The solutions were diluted to achieve equivalent optical densities of ~0.3. Spectra were collected in quartz cuvettes with 1 cm path length. Absorption spectra were obtained using a UV-2600 from Shimadzu.

- **Quantum yield measurement of PDI small molecules and polymers.**

Solutions of the PDI derivative in TFE were prepared at low concentrations (below 0.005 mg/mL) to achieve optical densities below 0.1 to prevent fluorescence loss due to re-absorption. Photoluminescence spectra were obtained using a UV-Vis LS 55 fluorescence spectrophotometers manufactured by Perkin Elmer. The fluorescence quantum yields (Φ_f) were estimated from the emission and absorption spectra by comparative method at the excitation wavelength of 488 nm using Rhodamine 6G in ethanol ($\Phi_f = 0.95$) as the standard. All spectra were collected in quartz cuvettes with 1 cm path lengths. The quantum yield of the samples (Φ_X) was calculated using the empirical formula: $\Phi_f = \Phi_{standard} (OD_{standard}/OD_x)(I_x/I_{standard})(\eta^2_x/ \eta^2_{standard})$ where $\Phi_{standard}$ is the quantum yield of the standard, OD is the optical density, I is the integrated fluorescence intensity, and η is the refractive index of the solvent.

- **Ultraviolet photoelectron spectroscopy (UPS) characterization of PDI small molecules and polymers**

Samples were dissolved in TFE at 2 mg/mL and 40 °C overnight with stirring. Ag was thermally evaporated on N-doped silicon and interlayers were coated at 1000 RPM for 60 seconds. UPS measurements were performed on the Omicron Nanotechnology Model ESCA+S, consisting of a helium discharge lamp (He I line, 21.2 eV) as the UV excitation source and a hemispherical

SPHERA energy analyzer. All samples were biased by -3V to compensate for the instrument work function difference repelling the low-kinetic energy electrons, shifting the energy scale of experimental graphs by 3 eV.

- **Photovoltaic device fabrication and characterization containing PDI-based interlayers**[4,5]

OSC devices were fabricated by spin-coating PEDOT:PSS (CLEVIOS™ P VP AI 4083) onto pre-cleaned glass substrates (14.7 × 14.7 mm), patterned with ITO film (10 Ω/□, from Thin Film Devices, Inc.). The PEDOT:PSS coated substrates were baked at 150 °C for 15 minutes in air, then transferred to an inert atmosphere glove box (N_2 atmosphere, < 1 ppm O_2, <1 ppm H_2O) for deposition of the photoactive layer, interlayer and top electrode. A mixture of PBDTT-TT and $PC_{71}BM$ (1:1.8 weight ratio) in chlorobenzene (CB):1,8-diiodooctane (3.2 v% DIO), or a mixture of PBDB-T and ITIC (1:1 weight ratio) in CB: DIO (0.5 v% DIO), was stirred at 55 °C for ~12 hours. The photoactive layers were deposited by spin-coating the solution onto the PEDOT:PSS layer. The thickness of the active layer film was ~100 nm as determined by profilometry. DIO was removed under vacuum, followed by spin-coating of interlayers from solutions with different concentrations at constant spin-coating speed of 4000 rpm. The interlayer thicknesses were determined using the surface profiler KLA Tencor (model Alpha-Step IQ) and AFM. Thermal evaporation of Ag electrodes was performed through a shadow mask, defining the maximum available device area of 0.06 cm^2.

For PSC devices all the pre-cleaned ITO substrates were treated by UV-ozone for 15 min to remove the last traces of the organic residues before the device fabrication. Then $PVBT-SO_3$ water solution (2 mg/ml) was spin-coated onto ITO substrates at 3500 revolutions per minute (rpm)

for 40 s without any post-treatment. The perovskite film was made by anti-solvent method [25] inside a glove box (N_2 atmosphere, < 1 ppm O_2, < 1 ppm H_2O) , the perovskite precursor solution of $CH_3NH_3PbI_3$ was composed of PbI_2 and CH_3NH_3I (1:1 molar ratio) in a mixture of dimethyl sulfoxide (DMSO):γ-butyrolactone (GBL) (3:7, v/v) with a total concentration of ~43 w%, then the precursor solution was deposited onto PVBT-SO_3/ITO substrate by a consecutive two-step spin-coating process at 1500 rpm and 4000 rpm for 20 s and 60 s, respectively, and the chlorobenzene in final spin-stage was dripped onto the substrate during spin coating. For thermally annealed devices, the perovskite films were next annealed at 100 °C for 5 minutes. For solvent annealed devices, the perovskite films were put into the bottom of a glass petri dish, and 10 μl *N,N*-dimethylformamide (DMF) solvent was added at the edge of the petri dish, then the perovskite films were covered by the lid of the petri dish and put on top of a hot plate with a temperature of 100 °C for different annealing time. Afterwards, a thin layer of $PC_{61}BM$ was then spin-coated inside the glove box (N_2 atmosphere, < 1 ppm O_2, < 1 ppm H_2O) from a solution in chlorobenzene (15 mg/ml) at 1000 rpm for 60 s. PDI-Br interlayer was dissolved in 2,2,2-trifluoroethanol (TFE) and spin-coated onto $PC_{61}BM$ surface at 4000 rpm for 30 s with different concentrations. Finally, 100 nm Ag electrode was deposited (device area of 0.06, 0.09, or 0.27 cm^2 was defined by a metal shadow mask) on the active layer under high vacuum (4×10^{-6} mbar) using a thermal evaporator. For all devices *I-V* characteristics were measured under N_2 atmosphere using a Keithley 2400 source-meter under simulated AM1.5G irradiation using a 300 W Xe lamp solar simulator (Newport 91160). The light intensity was adjusted with a National Renewable Energy Laboratory (NREL)-calibrated Si reference solar cell and KG-5 filter. The illuminated area (0.05418 cm^2) was defined by a photomask with an aperture, the area of which was measured at NREL, and used in all of the device measurements.

- **Grazing incident X-ray diffraction (GIXD) of PDI-based polyionenes**[4]

Polymer thin films were prepared silicon substrates employing conditions described by photovoltaic device fabrication. An X-ray beam impinged onto the sample at a grazing angle above and below the critical angle of the polymer film ($\alpha c = 0.16$) but below the critical angle of the silicon substrate ($\alpha c = 0.22$). The wavelength of X-rays used was 1.240 Å, and the scattered intensity was detected by a PILATUS 1M detector.

Near edge X-ray absorption fine structure (NEXAFS)[4]

Angular dependent X-ray Absorption Spectroscopy (XAS) was acquired at BL 8-2 at Stanford Synchrotron Radiation Light Source (SSRL), a bending magnet beamline with a linear polarization of about 0.9 and a spherical grating monochromator, operated in this study at a resolution of around 0.3eV, providing around 1×1010ph/s onto a 1 mm 2 beam spot. The samples were mounted onto an aluminum sample holder with double sided carbon tape, and the incidence angle was varied relative to the incoming beam, using the same convention of the geometry as Stöhr and Outka.[S1]The spectra were background subtracted and normalized to the atomic cross-section (at higher energies) and energy aligned to adventitious carbon (285.3eV) from a reference sample mounted upstream. The peak intensities were analyzed using IGOR Pro software version 7. The energy positions for the aromatic pi* states were established in spectra with stronger contributions, and thereafter fixed in position and width for the full dataset that was batch fitted with the same constraints for most rigid results. Both the individual and averaged angular dependence for the major pi-states contributing to the angular dependence was extracted for each sample and fitted to the function for angular dependence for an azimuthally averaged vector states according to Stöhr and Outka, to extract the ensemble-averaged angle of the aromatic backbone with respect to the substrate.

- **Conductivity measurements of PDI polyionenes**[4]

Parallel gold electrodes (thickness =50 nm) were patterned on silicon dioxide substrates using standard photolithographic procedures. The length of the gold electrode (W) was 4000 μm and the separation distance (L) between the two electrodes was 500 μm. Solutions of PDI polyionenes in TFE were spin coated onto the substrates to give a film thickness (T) of ≈50 nm. Electrical characterization was completed using a Keithley 4200 SCS-equipped probe station at ambient atmosphere. The conductivity was extracted from the equation of $\sigma = I \times L/(V \times W \times T)$.

- **Synthesis of (4-bromophenyl)(4-methoxyphenyl)methanone**

Aluminum (III) chloride (36.4 g, 0.27 mol) was added to a flame-dried 1L round-bottom flask charge with a stir bar and fitted with an addition funnel under argon and dispersed in 150 mL of anhydrous dichloromethane. The slurry was cooled to 0 °C then a solution of 4-bromobenzoyl chloride (50 g, 0.23 mol) in 125 mL of anhydrous dichloromethane was added dropwise. The reaction was stirred for one hour at 0 °C then a solution of anisole (28 mL, 0.273 mol) in 125 mL of dichloromethane over 30 minutes. The reaction was warmed to room temperature and stirred for 16 hours. The crude mixture was quenched by addition of 100 mL of methanol dropwise at 0 °C. The precipitate was separated by filtration and washed with additional methanol. The filtrate was concentrated then precipitated into methanol again to yield white crystalline solid (64 g, 96%). ^{1}H NMR (500 mHz, DMSO, δ) δ 7.75 (m, 4H), δ 7.64 (d, J = 8.2, 2H), δ 7.10 (d, J = 8.5 Hz, 2H), δ 3.87 (s, 3H). ^{13}C NMR (125 MHz, DMSO-d_6, δ) 193.93, 163.62, 137.26, 132.69, 132.00, 131.77, 129.48, 114.47, 56.09.

- **Synthesis of (4-bromophenyl)(4-hydroxyphenyl)methanone**

Aluminum (III) chloride (9.14 g, 0.07 mol) was added to a flame-dried round bottom flask fitted with an addition funnel and reflux condenser under nitrogen and dissolved in 50 mL of anhydrous toluene and cooled to 0 °C. A solution of **1** in 200 mL of anhydrous toluene was added to the reaction dropwise then the reaction as heated to reflux for 2 hours. The crude mixture was cooled to room temperature then quenched into 100 mL of 2M hydrochloric and extracted diethyl ether. The organic layer was washed with 2M hydrochloric acid and then saturated $KHCO_3$. The organic layer was separated, dried over Na_2SO_4, filtered, then concentrated under reduced pressure. The   product was diluted with diethyl ether, precipitated into hexanes and filtered to yield the pure product as tan crystals (6.87 g, 73%). ^{1}H NMR (500 mHz, DMSO, δ) δ10.49 (s, 1H), δ 7.76 (d, J = 8.45, 2H), δ 7.67 (d, J = 8.70), 2H), δ 7.62 (d, J = 8.5, 2H); ^{13}C NMR (125 MHz, DMSO-d[6], δ) 193.76, 162.67, 137.58, 133.02, 131.91, 131.65, 127.98, 126.12, 115.81.

- **Synthesis of (4-bromophenyl)(4-((2-ethylhexyl)oxy)phenyl)methanone (1)**

60 wt% dispersion of NaH in mineral oil (0.55 g, 16.2 mmol) was added to a flame-dried round bottom flask charged with stir bar and dispersed in 5 mL of anhydrous DMF under nitrogen. Then a solution of **4** (3.0 g, 10.8 mmol) in 5 mL of anhydrous DMF was added to the suspension dropwise. The reaction was allowed to stir for 10 minutes then 2-ethylhexylbromide (2.9 mL, 16.2 mmol) was added dropwise and the reaction was heated to 60 °C for 3 hours. The solution was cooled to room temperature, poured into 2 wt% LiCl (aq.) and extracted with diethyl ether. The organic layer was extracted several times with the LiCl solution, dried over Na_2SO_4, filtered and concentrated under reduced pressure. The crude residue was purified through a silica plug eluting with 1:1 dichloromethane:hexanes mixture to yield an off white solid (3.04 g, 72%). ^{1}H NMR (500 mHz, DMSO, δ) 7.76 (q, 4H), 7.63 (d, J = 8.5 Hz, 2H), 7.10 (d, J = 8.5 Hz, 2H), 3.97 (d, J = 5.8 Hz, 2H), 1.72 (m, 1H), 1.43 (m, 4H), 1.30 (m, 4H), 0.90 (m, 6H). ^{13}C NMR (125 MHz, DMSO-

d$_6$, δ) 193.90, 163.29, 137.31, 132.70, 131.99, 131.75, 129.31, 126.41, 114.90, 70.86, 30.32, 28.87, 23.72, 22.97, 14.42, 11.35.

- **Synthesis of 1,2-bis(4-bromophenyl)-1,2-bis(4-((2-ethylhexyl)oxy)phenyl)ethene (2)**

3 (3.52 g, 9.04 mmol) and zinc dust (0.5 g, 7.71 mol) were added to a flame-dried round bottom, fitted with a condenser and charged with a stir bar. The reaction vessel was evacuated then back-filled with nitrogen three times. The reagents were dispersed in 25 mL of anhydrous THF, treated with pyridine (2.2 mL, 27.1 mmol), then cooled to -78 °C with a dry ice/acetone bath. Titanium (IV) chloride (2.96 mL, 7.71 mmol) was added dropwise to the cooled suspension and the reaction was slowly warmed to room temperature over two hours then refluxed for 14 hours. The reaction was cooled to 0 °C and quenched with 2M hydrochloric acid then extracted with diethyl ether. The organic layer was separated and washed with additional 2M hydrochloric acid then dried over Na$_2$SO$_4$, filtered, and concentrated under reduced pressure. The concentrated residue was purified on basic alumina eluting with 1 to 5% CH$_2$Cl$_2$ in hexanes then recrystallized from 9:1 mixture of methanol to diethyl ether as a white crystalline solid. The desired fraction was concentrated then precipitated to yield a mixture of the E and Z isomers as a white powder (1.94 g, 58%). ^{1}H NMR (500 mHz, DMSO, δ) 7.35 (m, 4H), 6.90 (m, 4H), 6.84 (m, 4H), 6.72 (m, 4H), 3.77 (d, J = 5.2 Hz, 4H), 1.61 (m, 2H), 1.33 (m, 16H), 0.87 (m, 12H). ^{13}C NMR (125 MHz, DMSO d$_6$, δ) 158.17, 158.08, 143.13, 142.98, 138.97, 138.93 135.35, 135.15, 133.05, 133.01, 132.45, 132.45, 132.38, 130.97, 130.88, 120.41, 120.28, 113.92, 113.85, 70.46, 39.42, 30.53, 29.12, 23.84, 23.05, 14.11, 11.15. MALDI-TOF (m/z): [M+H]$^+$ calculated for: C$_{42}$H$_{50}$Br$_2$O$_2$: 746.67, found: 747.7.

- **4,4'-(1,2-bis(4-((2-ethylhexyl)oxy)phenyl)ethene-1,2-diyl)dibenzaldehyde (EtHexTPE-CHO) (3)**

EtHexTPE-Br (0.29 g, 0.52 mmol) was added to a flame-dried round bottom flask charged with stir bar under argon and dissolved in 10 mL of anhydrous THF. The solution was cooled to -78 °C then 2.5 M n-butyl lithium in hexanes (0.7 mL, 1.75 mmol) was added dropwise and the reaction was stirred for ten minutes. The reaction was then treated with DMF (1.5 mL, 19.5 mmol) and allowed to warm to room temperature over twenty minutes. The reaction was quenched with a saturated NH_4Cl solution then extracted with diethyl ether. The organic layer was washed with 2M hydrochloric acid several times then dried over Na_2SO_4, filtered and concentrated under reduced pressure. The crude product was purified on silica eluting with a solvent gradient of hexane:CH_2Cl_2 (70:40) to pure CH_2Cl_2 and the pure product was isolated as a bright yellow viscous oil of the E and Z isomers (0.22 g, 87%). Z isomer: ^{1}H NMR (500 mHz, DMSO d_6, δ) 9.92 (s, 2H), 7.63 (d, J = 8.2 Hz, 4H), 7.20 (d, J = 8.2 Hz, 4H), 6.93 (d, J = 8.7 Hz), 6.70 (d, J = 8.8, 4H), 3.80 (d, J = 5.9 Hz, 4H), 1.71 (m, 2H), 1.41 (m, 16H), 0.92 (m, 12H). ^{13}C NMR (125 MHz, DMSO-d_6, δ) 193.00, 158.33, 150.39, 140.53, 134.74, 132.58, 131.98, 129.58, 114.57, 70.32, 30.34, 28.90, 23.71, 22.94, 14.40, 11.38. E isomer: ^{1}H NMR (500 mHz, DMSO d_6, δ) 9.95 (s, 2H), 7.66 (d, J = 8.4 Hz, 4H), 7.24 (d, J = 8.2 Hz, 4H), 6.87 (d, J = 8.7 Hz), 6.66 (d, J = 8.8, 4H), 3.77 (d, J = 5.9 Hz, 4H), 1.74 (m, 2H), 1.31 (m, 16H), 0.89 (m, 16H). ^{13}C NMR (125 MHz, DMSO-d_6, δ) 193.00, 158.24, 150.18, 140.47, 134.78, 132.45, 132.07, 129.59, 114.53, 70.30, 30.36, 28.91, 23.74, 22.96, 14.40, 11.40. MALDI-TOF (m/z): $[M+H]^+$ calculated for: $C_{44}H_{52}O_4$: 644.90, found: 645.7.

- **Synthesis of TPE conjugated polymer with para-phenylene spacer (P5)**

EtHexTPE-Br (0.21 g, 0.28 mmol) and 1,4-benzene diboronic acid bis(pinacol)ester (0.09 g, 0.28 mmol) were added to a 15 mL pressure vessel and dissolved in 5 mL of THF and deoxygenated via nitrogen bubbling for 30 minutes. Potassium bicarbonate (0.17 g, 1.68 mmol) was added to a separate vial, dissolved in 1 mL deionized water and deoxygenated via nitrogen

bubbling for 30 minutes. Pd(PPh₃)₄ (0 .016 g, 0.014 mmol) and RuPhos (0.019 g, 0.42 mmol) were dissolved in THF inside a glovebox then added to the pressure vessel along with a drop of Aliquat 336 under nitrogen. The reaction vessel was capped and heated to 70 °C for 48 hours. The crude reaction was cooled to room temperature, diluted in chloroform, then precipitated into methanol with 5 v/v% acetic acid several times. The isolated green precipitate was dried under vacuum and subjected to no further purification. M_w = 8.1 kDa, M_n = 4.9, Đ = 1.6; 0.120 g, 65%). ^{1}H NMR (500 mHz, CDCl₃, δ) 7.64, 7.43, 7.16, 7.02, 6.70, 3.81, 1.71, 1.45, 1.34, 0.93

- **Synthesis of EtHexTPE-based poly(phenylenevinylene) (P1)**

    EtHexTPE-CHO (66 mg, 0.102 mmol) and tetraethyl (1,4 phenylenebis(methylene))bis(phosphonate) (39 mg, 0.102 mmol) was added to a 7 mL scintillation vial charged with stir bar and dissolved in 2 mL of anhydrous THF. The solution was cooled to -78 °C and then a solution of potassium tert-butoxide (46 mg, 0.41 mmol) in 1 mL tert-butanol was added in one portion then the reaction was warmed to room temperature and stirred for 16 hours under nitrogen. The crude mixture was dilute with chloroform then precipitated into methanol with 5 v/v% acetic acid several times then hexanes. The isolated orange solid was dried under vacuum and subjected to no further purification Z isomer (M_w = 61.2 kDa, M_n = 23.0, Đ = 2.7, 0.045 g, 43%). ^{1}H NMR (500 mHz, CDCl₃, δ) 7.48, 7.06, 6.97, 6.67, 3.79, 1.70, 1.44, 1.33, 0.92. E Isomer (M_w = 17.3 kDa, M_n = 11.4, Đ = 1.5, 0.079 46%.). ^{1}H NMR (500 mHz, CDCl₃, δ) 7.44, 7.05, 6.97, 6.68, 3.80, 1.71, 1.44, 1.33, 0.93.

- **Synthesis of 1,2-di([1,1'-biphenyl]-4-yl)-1,2-bis(4-((2-ethylhexyl)oxy)phenyl)ethene (4)**

Following procedure described for **EtHexTPE-PPP** and purified on silica eluting with mixture of hexanes and CH_2Cl_2 (88 mg, 40%). ^{1}H NMR (500 mHz, $CDCl_3$, δ) 7.59 (m, 4H), 7.39 (m, 10H), 7.15 (m, 4H), 7.00 (m, 4H), 6.69 (m, 4H), 3.80 (m, 4H), 1.71, 2H), 1.43 (m, 16H), 0.93 (m, 12H). ^{13}C NMR (125 MHz, $CDCl_3$, δ) 157.94, 157.87, 143.56, 143.45, 140.77, 140.72, 139.41, 138.63, 138.51, 136.09, 132.62, 132.59, 131.93, 131.91, 128.70, 128.67, 127.09, 126.88, 126.85, 126.18, 113.75, 113.73, 70.43, 70.41, 39.46, 30.55, 29.13, 23.86, 23.07, 14.12, 11.16. MALDI-TOF (m/z): $[M]^+$ calculated for: $C_{54}H_{60}O_2$: 741.07, found: 740.1.

- **Synthesis of 1,2-bis(4-((2-ethylhexyl)oxy)phenyl)-1,2-bis(4-styryl)phenyl)ethene (5)**

Following procedure described for EtHexTPE-PPV purified on silica eluting with mixture of hexanes and CH_2Cl_2 (11 mg, 29%). ^{1}H NMR (500 mHz, $CDCl_3$, δ) 7.50 (d, J = 7.7 Hz, 4H), 7.37 (m, 4H), 7.28, 7.06 (m, 8H), 6.97 (d, J = 8.3 Hz), 3.79 (d, J= 5.7 Hz, 4H), 1.70 (m, 2H), 1.43 (m, 16H), 0.93 (m, 12H). ^{13}C NMR (125 MHz, $CDCl_3$, δ) 157.99, 144.04, 139.47, 137.49, 136.03, 135.03, 132.63, 131.86, 128.67, 128.57, 128.18, 127.49, 126.44, 125.90, 113.76, 70.42, 39.44, 30.53, 29.12, 23.84, 23.05, 14.11, 11.16. MALDI-TOF (m/z): $[M]^+$ calculated for: $C_{54}H_{60}O_2$: 793.15, found: 793.3.

- **Synthesis of ethylhexyloxy poly(phenylenevinylene) (P4)[6]**

Following procedure described for **EtHexTPE-PPV** (M_w = 131.7, M_n = 45.6, Đ = 2.9 39 mg, 60%). ^{1}H NMR (500 MHz, $CDCl_3$, δ) 7.56, 7.17, 4.00, 1.86, 1.58, 1.40, 0.97.

- **Synthesis of 25 mole% EtHexTPE poly(pphenylenevinylene) (P3)**

Following procedure described for EtHexTPE-PPV (M_w = 132.3, M_n = 54.8, Đ = 2.4 45 mg, 90%). ^{1}H NMR (500 MHz, $CDCl_3$, δ) 7.55, 7.16, 7.07, 6.97, 6.67, 4.00, 3.79, 1.87, 1.42, 0.96.

- **Synthesis of 50 mole% EtHexTPE poly(pphenylenevinylene) (P2)**

Following procedure described for EtHexTPE-PPV ($M_w = 46.6$, $M_n = 22.1$, Đ = 2.1 38 mg, 68%). ^{1}H NMR (500 MHz, CDCl$_3$, δ) 7.53, 7.16, 7.06, 6.97, 6.67, 4.00, 3.79, 1.85, 1.42, 0.95.

- **Aggregation-induced emission studies with TPE- and PPV-based structures**

  Stock solutions of TPE- and PPV-based small molecules and polymers were prepared in THF at concentrations of 1 mg/mL. 10 μL of the stock solution was then added to 2 mL of THF/H$_2$O mixtures ranging from 0 to 90% H$_2$O in 7 mL scintillation vials. The mixtures were vortexed for 10 seconds prior to photoluminescence characterizations. Each solution was added to a 1 cm x 1 cm quartz cuvette with a Teflon stopper. Spectra were collected at wavelengths ranging from 400 to 750 nm at excitation wavelengths of 365 nm or 405 nm. Excitation and emission bandwidths were held constant at 3 nm and automatic sensitivity was used for all samples characterized on the Shimadzu RF-6000 spectrofluorophotometer.

6.3 References

(1)   Gunbas, D. D.; Grozema, F. C.; Sudho, E. J. R.; Jager, W. F. Synthesis of Regioisomerically Pure 1,7-Dibromoperylene-3,4,9,10-Tetracarboxylic Acid Derviatives. J. Org. Chem. 2014, 3–10. https://doi.org/10.1021/jo501180a.

(2)   Cole, M. D.; Sheri, M.; Bielicki, C.; Emrick, T. Perylene Diimide-Based Ionene and Zwitterionic Polymers: Synthesis and Solution Photophysical Properties. Macromolecules 2017, 50 (19), 7535–7542. https://doi.org/10.1021/acs.macromol.7b01281.

(3)   Alvino, A.; Franceschin, M.; Cefaro, C.; Borioni, S.; Ortaggi, G.; Bianco, A. Synthesis and Spectroscopic Properties of Highly Water-Soluble Perylene Derivatives. Tetrahedron 2007, 63 (33), 7858–7865. https://doi.org/10.1016/j.tet.2007.05.096.

(4)   Liu, Y.; Cole, M. D.; Jiang, Y.; Kim, P. Y.; Nordlund, D.; Emrick, T.; Russell, T. P. Chemical and Morphological Control of Interfacial Self-Doping for Efficient Organic Electronics. Adv. Mater. 2018, 30 (15), 1705976. https://doi.org/10.1002/adma.201705976.

(5)   Li, Y.; Cole, M. D.; Gao, Y.; Emrick, T.; Xu, Z.; Liu, Y.; Russell, T. P. High-Performance Perovskite Solar Cells with a Non-Doped Small Molecule Hole Transporting Layer. ACS Appl. Energy Mater. 2019, 2 (3), 1634–1641. https://doi.org/10.1021/acsaem.9b00164.

(6)   Page, Z. A.; Liu, Y.; Puodziukynaite, E.; Russell, T. P.; Emrick, T. Hydrophilic Conjugated Polymers Prepared by Aqueous Horner-Wadsworth-Emmons Coupling. Macromolecules 2016, 49 (7), 2526–2532. https://doi.org/10.1021/acs.macromol.5b02501.

BIBLIOGRAPHY

Albery, W. J. Development of Photogalvanic Cells for Solar Energy Conversion. Acc. Chem. Res. 1982, 15 (5), 142–148. https://doi.org/10.1021/ar00077a003.

Albery, W. J.; Archer, M. D. Optimum Efficiency of Photogalvanic Cells for Solar Energy Conversion. Nature 1977, 270 (5636), 399–402. https://doi.org/10.1038/270399a0.

Beddard, G. S.; Porter, G. Concentration Quenching in Chlorophyll. Nature 1976, 260 (5549), 366–367. https://doi.org/10.1038/260366a0.

Birks, J. B. Photophysics of Aromatic Molecules; Wiley-Interscience: London, 1970. https://doi.org/10.1016/0022-2313(71)90011-1.

Birks, J. B. Photophysics of Aromatic Molecules; Wiley-Interscience: London, 1970. https://doi.org/10.1016/0022-2313(71)90011-1.

Burroughes, J. H.; Bradley, D. D. C.; Brown, A. R.; Marks, R. N.; Mackay, K.; Friend, R. H.; Burns, P. L.; Holmes, A. B. Light-Emitting Diodes Based on Conjugated Polymers. Nature 1990, 347 (6293), 539–541. https://doi.org/10.1038/347539a0.

Burroughes, J. H.; Bradley, D. D. C.; Brown, A. R.; Marks, R. N.; Mackay, K.; Friend, R. H.; Burns, P. L.; Holmes, A. B. Light-Emitting Diodes Based on Conjugated Polymers. Nature 1990, 347 (6293), 539–541. https://doi.org/10.1038/347539a0.

Chang, C. Y.; Chang, Y. C.; Huang, W. K.; Lee, K. T.; Cho, A. C.; Hsu, C. C. Enhanced Performance and Stability of Semitransparent Perovskite Solar Cells Using Solution-Processed Thiol-Functionalized Cationic Surfactant as Cathode Buffer Layer. Chem. Mater. 2015, 27 (20), 7119–7127. https://doi.org/10.1021/acs.chemmater.5b03137.

Chen, H. C.; Hsu, C. P.; Reek, J. N. H.; Williams, R. M.; Brouwer, A. M. Highly Soluble Benzo[Ghi]Perylenetriimide Derivatives: Stable and Air-Insensitive Electron Acceptors for Artificial Photosynthesis. ChemSusChem 2015, 8 (21), 3639–3650. https://doi.org/10.1002/cssc.201500950.

Chen, H. Z.; Ling, M. M.; Mo, X.; Shi, M. M.; Wang, M.; Bao, Z. Air Stable N-Channel Organic Semiconductors for Thin Film Transistors Based on Fluorinated Derivatives of Perylene Diimides. Chem. Mater. 2007, 19 (4), 816–824. https://doi.org/10.1021/cm062352w.

Chen, J.; Law, C. C. W.; Lam, J. W. Y.; Dong, Y.; Lo, S. M. F.; Williams, I. D.; Zhu, D.; Tang, B. Z. Synthesis, Light Emission, Nanoaggregation, and Restricted Intramolecular Rotation of 1,1-Substituted 2,3,4,5-Tetraphenylsiloles. Chem. Mater. 2003, 15 (7), 1535–1546. https://doi.org/10.1021/cm021715z.

Chen, L.; Tan, Y.; Liu, X.; Chen, Y. Counterion Induced Facile Self-Doping and Tunable Interfacial Dipoles of Small Molecular Electrolytes for Efficient Polymer Solar Cells. Nano Energy 2016, 27, 492–498. https://doi.org/10.1016/j.nanoen.2016.08.005.

Chen, M. T.; Hofmann, O. T.; Gerlach, A.; Bröker, B.; Bürker, C.; Niederhausen, J.; Hosokai, T.; Zegenhagen, J.; Vollmer, A.; Rieger, R.; et al. Energy-Level Alignment at Strongly Coupled Organic-Metal Interfaces. J. Phys. Condens. Matter 2019, 31 (19). https://doi.org/10.1088/1361-648X/ab0171.

Chen, X.; Parelkar, S. S.; Henchey, E.; Schneider, S.; Emrick, T. PolyMPC-Doxorubicin Prodrugs. Bioconjug. Chem. 2012, 23 (9), 1753–1763. https://doi.org/10.1021/bc200667s.

Chen, Y.; Feng, Y.; Gao, J.; Bouvet, M. Self-Assembled Aggregates of Amphiphilic Perylene Diimide-Based Semiconductor Molecules: Effect of Morphology on Conductivity. J. Colloid Interface Sci. 2012, 368 (1), 387–394. https://doi.org/10.1016/j.jcis.2011.10.076.

Chen, Z.; Hu, Z.; Wu, Z.; Liu, X.; Jin, Y.; Xiao, M. Polyelectrolytes for the Interface Engineering of e Ffi Cient Polymer Solar Cells †. J. Mater. Chem. A Mater. energy Sustain. 2017, 5, 19447–19455. https://doi.org/10.1039/C7TA05246D.

Chevrier, M.; Houston, J. E.; Kesters, J.; Van Den Brande, N.; Terry, A. E.; Richeter, S.; Mehdi, A.; Coulembier, O.; Dubois, P.; Lazzaroni, R.; et al. Self-Assembled Conjugated Polyelectrolyte-Surfactant Complexes as Efficient Cathode Interlayer Materials for Bulk Heterojunction Organic Solar Cells. J. Mater. Chem. A 2015, 3 (47), 23905–23916. https://doi.org/10.1039/c5ta06966a.

Cole, M. D.; Sheri, M.; Bielicki, C.; Emrick, T. Perylene Diimide-Based Ionene and Zwitterionic Polymers: Synthesis and Solution Photophysical Properties. Macromolecules 2017, 50 (19), 7535–7542. https://doi.org/10.1021/acs.macromol.7b01281.

Coleman, L. B.; Cohen, M. J.; Sandman, D. J.; Yamagishi, F. G.; Garito, A. F.; Heeger, A. J. Superconducting Fluctuations and the Peierls Instability in an Organic Solid. Solid State Commun. 1973, 12 (11), 1125–1132. https://doi.org/10.1016/0038-1098(73)90127-0.

Constantinou, I.; Shewmon, N. T.; Lo, C. K.; Deininger, J. J.; Reynolds, J. R.; So, F. Photodegradation of Metal Oxide Interlayers in Polymer Solar Cells. Adv. Mater. Interfaces 2016, 3 (23). https://doi.org/10.1002/admi.201600741.

Culligan, S. W.; Chen, A. C. A.; Wallace, J. U.; Klubek, K. P.; Tang, C. W.; Chen, S. H. Effect of Hole Mobility through Emissive Layer on Temporal Stability of Blue Organic Light-

Emitting Diodes. Adv. Funct. Mater. 2006, 16 (11), 1481–1487. https://doi.org/10.1002/adfm.200500785.

Dai, S.; Zhao, F.; Zhang, Q.; Lau, T. K.; Li, T.; Liu, K.; Ling, Q.; Wang, C.; Lu, X.; You, W.; et al. Fused Nonacyclic Electron Acceptors for Efficient Polymer Solar Cells. J. Am. Chem. Soc. 2017, 139 (3), 1336–1343. https://doi.org/10.1021/jacs.6b12755.

Daik, R.; James Feast, W.; Batsanov, A. S.; Howard, J. a. K. Stereochemical Outcome of McMurry Coupling. New J. Chem. 1998, 22 (10), 1047–1049. https://doi.org/10.1039/a805208e.

De, S.; Ramakrishnan, S. Charge-Transfer Reinforced Folding of Novel Ionenes. Macromolecules 2009, 42 (22), 8599–8603. https://doi.org/10.1021/ma901954x.

Deng, Z.; Lee, S. .; Webb, D. .; Chan, Y. .; Gambling, W. . Carrier Transport in Thin Films of Organic Electroluminescent Materials. Synth. Met. 1999, 107 (2), 107–109. https://doi.org/10.1016/S0379-6779(99)00149-6.

Dong, W.; Ma, Z.; Chen, P.; Duan, Q. Carbazole and Tetraphenylethylene Based AIE-Active Conjugated Polymer for Highly Sensitive TNT Detection. Mater. Lett. 2019, 236, 480–482. https://doi.org/10.1016/j.matlet.2018.10.162.

Dong, W.; Ma, Z.; Chen, P.; Duan, Q. Carbazole and Tetraphenylethylene Based AIE-Active Conjugated Polymer for Highly Sensitive TNT Detection. Mater. Lett. 2019, 236, 480–482. https://doi.org/10.1016/j.matlet.2018.10.162.

Du, J.; Yu, S.; Huang, Z.; Chen, L.; Xu, Y.; Zhang, G.; Chen, Q.; Yu, X.; Pu, L. Highly Selective Ratiometric Fluorescent Recognition of Histidine by Tetraphenylethene–Terpyridine–Zn(

<scp>ii</Scp>) Complexes. RSC Adv. 2016, 6 (30), 25319–25329. https://doi.org/10.1039/C6RA03724K.

Duzhko, V. V.; Dunham, B.; Rosa, S. J.; Cole, M. D.; Paul, A.; Page, Z. A.; Dimitrakopoulos, C.; Emrick, T. N-Doped Zwitterionic Fullerenes as Interlayers in Organic and Perovskite Photovoltaic Devices. ACS Energy Lett. 2017, 957–963. https://doi.org/10.1021/acsenergylett.7b00147.

Eakins, G. L.; Gallaher, J. K.; Keyzers, R. a.; Falber, A.; Webb, J. E. a; Laos, A.; Tidhar, Y.; Weissman, H.; Rybtchinski, B.; Thordarson, P.; et al. Thermodynamic Factors Impacting the Peptide-Driven Self-Assembly of Perylene Diimide Nanofibers. J. Phys. Chem. B 2014, 118 (29), 8642–8651. https://doi.org/10.1021/jp504564s.

Elumalai, N. K.; Uddin, A. Open Circuit Voltage of Organic Solar Cells: An in-Depth Review. Energy Environ. Sci. 2016, 9 (2), 391–410. https://doi.org/10.1039/c5ee02871j.

Everett, T. A.; Higgins, D. A. Electrostatic Self-Assembly of Ordered Perylene-Diimide/Polyelectrolyte Nanofibers in Fluidic Devices: From Nematic Domains to Macroscopic Alignment. Langmuir 2009, 25 (22), 13045–13051. https://doi.org/10.1021/la9019298.

Fakharuddin, A.; Schmidt-Mende, L.; Garcia-Belmonte, G.; Jose, R.; Mora-Sero, I. Interfaces in Perovskite Solar Cells. Adv. Energy Mater. 2017, 7 (22). https://doi.org/10.1002/aenm.201700623.

Fang, X.; Zhang, Y. M.; Chang, K.; Liu, Z.; Su, X.; Chen, H.; Zhang, S. X. A.; Liu, Y.; Wu, C. Facile Synthesis, Macroscopic Separation, E/Z Isomerization, and Distinct AIE Properties

of Pure Stereoisomers of an Oxetane-Substituted Tetraphenylethene Luminogen. Chem. Mater. 2016, 28 (18), 6628–6636. https://doi.org/10.1021/acs.chemmater.6b02746.

Fletcher, K.; Bunz, U. H. F.; Dreuw, A. Fluorescence Quenching of Benzaldehyde in Water by Hydrogen Atom Abstraction. ChemPhysChem 2016, 17 (17), 2650–2653. https://doi.org/10.1002/cphc.201501059.

Gao, M.; Zhang, X.; Yang, B.; Li, F.; Shen, J. Assembly of Modified CdS Particles /Cationic Polymer Based on Electrostatic Interactions. Thin Solid Films 1996, 285, 242–245.

Garnier, F. Organic-Based Electronics a La Carte. Acc. Chem. Res. 1999, 32 (3), 209–215. https://doi.org/10.1021/ar9800340.

Gebers, J.; Rolland, D.; Marty, R.; Suàrez, S.; Cervini, L.; Scopelliti, R.; Brauer, J. C.; Frauenrath, H. Solubility and Crystallizability: Facile Access to Functionalized π-Conjugated Compounds with Chlorendylimide Protecting Groups. Chem. - A Eur. J. 2015, 21 (4), 1542–1553. https://doi.org/10.1002/chem.201403623.

Gmeiner, J.; Karg, S.; Meier, M.; Rieß, W.; Strohriegl, P.; Schwoerer, M. Synthesis, Electrical Conductivity and Electroluminescence of Poly(P-phenylene Vinylene) Prepared by the Precursor Route. Acta Polym. 1993, 44 (4), 201–205. https://doi.org/10.1002/actp.1993.010440405.

Gmeiner, J.; Karg, S.; Meier, M.; Rieß, W.; Strohriegl, P.; Schwoerer, M. Synthesis, Electrical Conductivity and Electroluminescence of Poly(P-phenylene Vinylene) Prepared by the Precursor Route. Acta Polym. 1993, 44 (4), 201–205. https://doi.org/10.1002/actp.1993.010440405.

Grill, I.; Aygüler, M. F.; Bein, T.; Docampo, P.; Hartmann, N. F.; Handloser, M.; Hartschuh, A. Charge Transport Limitations in Perovskite Solar Cells: The Effect of Charge Extraction Layers. ACS Appl. Mater. Interfaces 2017, acsami.7b09567. https://doi.org/10.1021/acsami.7b09567.

Gunbas, D. D.; Grozema, F. C.; Sudho, E. J. R.; Jager, W. F. Synthesis of Regioisomerically Pure 1,7-Dibromoperylene-3,4,9,10-Tetracarboxylic Acid Derviatives. J. Org. Chem. 2014, 3–10. https://doi.org/10.1021/jo501180a.

Guo, Q.; Xu, Y.; Xiao, B.; Zhang, B.; Zhou, E.; Wang, F.; Bai, Y.; Hayat, T.; Alsaedi, A.; Tan, Z. Effect of Energy Alignment, Electron Mobility, and Film Morphology of Perylene Diimide Based Polymers as Electron Transport Layer on the Performance of Perovskite Solar Cells. ACS Appl. Mater. Interfaces 2017, 9 (12), 10983–10991. https://doi.org/10.1021/acsami.7b00902.

Guo, Y.; Li, Y.; Awartani, O.; Zhao, J.; Han, H.; Ade, H.; Zhao, D.; Yan, H. A Vinylene-Bridged Perylenediimide-Based Polymeric Acceptor Enabling Efficient All-Polymer Solar Cells Processed under Ambient Conditions. Adv. Mater. 2016, 28 (38), 8483–8489. https://doi.org/10.1002/adma.201602387.

Guo, Y.; Sato, W.; Shoyama, K.; Nakamura, E. Sulfamic Acid-Catalyzed Lead Perovskite Formation for Solar Cell Fabrication on Glass or Plastic Substrates. J. Am. Chem. Soc. 2016, 138 (16), 5410–5416. https://doi.org/10.1021/jacs.6b02130.

Guo, Z.; Gao, L.; Zhang, C.; Xu, Z.; Ma, T. Low-Temperature Processed Non-TiO 2 Electron Selective Layers for Perovskite Solar Cells. J. Mater. Chem. A 2018. https://doi.org/10.1039/C7TA10742K.

Guo, Z.; Gao, L.; Zhang, C.; Xu, Z.; Ma, T. Low-Temperature Processed Non-TiO 2 Electron Selective Layers for Perovskite Solar Cells. J. Mater. Chem. A 2018. https://doi.org/10.1039/C7TA10742K.

Gupta, M.; Yan, D.; Yao, J.; Zhan, C. Organophosphorus Derivatives as Cathode Interfacial-Layer Materials for Highly Efficient Fullerene-Free Polymer Solar Cells. *ACS Appl. Mater. Interfaces* **2018**, acsami.8b09313. https://doi.org/10.1021/acsami.8b09313.

Han, M.; Yu, D.; Song, Q.; Wang, J.; Dong, P.; He, J. Polybrene: Observations on Cochlear Hair Cell Necrosis and Minimal Lentiviral Transduction of Cochlear Hair Cells. Neurosci. Lett. 2015, 600, 164–170. https://doi.org/10.1016/j.neulet.2015.06.011.

He, Z.; Xiao, B.; Liu, F.; Wu, H.; Yang, Y.; Xiao, S.; Wang, C.; Russell, T. P.; Cao, Y. Single-Junction Polymer Solar Cells with High Efficiency and Photovoltage. Nat. Photonics 2015, 9 (3), 174–179. https://doi.org/10.1038/nphoton.2015.6.

Heek, T.; Nikolaus, J.; Schwarzer, R.; Fasting, C.; Welker, P.; Licha, K.; Herrmann, A.; Haag, R. An Amphiphilic Perylene Imido Diester for Selective Cellular Imaging. Bioconjug. Chem. 2013, 24 (2), 153–158. https://doi.org/10.1021/bc3005655.

Heimel, G.; Romaner, L.; Zojer, E.; Bredas, J. L. The Interface Energetics of Self-Assembled Monolayers on Metals. Acc. Chem. Res. 2008, 41 (6), 721–729. https://doi.org/10.1021/ar700284q.

Hemp, S. T.; Zhang, M.; Tamami, M.; Long, T. E. Phosphonium Ionenes from Well-Defined Step-Growth Polymerization: Thermal and Melt Rheological Properties. Polym. Chem. 2013, 4 (12), 3582. https://doi.org/10.1039/c3py00365e.

Herbst, W.; Hunger, K.; Wilker, G.; Ohleier, H.; Winter, R. Industrial Organic Pigments; 2004; Vol. Third Edit. https://doi.org/10.1002/3527602429.

Hestand, N. J.; Spano, F. C. Interference between Coulombic and CT-Mediated Couplings in Molecular Aggregates: H- to J-Aggregate Transformation in Perylene-Based π-Stacks. J. Chem. Phys. 2015, 143 (24), 244707. https://doi.org/10.1063/1.4938012.

Hofmann, O. T.; Atalla, V.; Moll, N.; Rinke, P.; Scheffler, M. Interface Dipoles of Organic Molecules on Ag(111) in Hybrid Density-Functional Theory. New J. Phys. 2013, 15 (111). https://doi.org/10.1088/1367-2630/15/12/123028.

Hofmann, O. T.; Glowatzki, H.; Bürker, C.; Rangger, G. M.; Bröker, B.; Niederhausen, J.; Hosokai, T.; Salzmann, I.; Blum, R. P.; Rieger, R.; et al. Orientation-Dependent Work-Function Modification Using Substituted Pyrene-Based Acceptors. J. Phys. Chem. C 2017, 121 (39), 24657–24668. https://doi.org/10.1021/acs.jpcc.7b08451.

Hsieh, B. R.; Yu, Y.; VanLaeken, A. C.; Lee, H. General Methodology toward Soluble Poly(p - Phenylenevinylene) Derivatives. Macromolecules 1997, 30 (25), 8094–8095. https://doi.org/10.1021/ma9713771.

Hsu, J. H. Fluorescence from Conjugated Polymer Aggregates in Dilute Poor Solution. J. Phys. Chem. A 1999, 103 (14), 2375–2380. https://doi.org/10.1021/jp983921t.

Hu, G.; Parelkar, S. S.; Emrick, T. A Facile Approach to Hydrophilic, Reverse Zwitterionic, Choline Phosphate Polymers. Polym. Chem. 2015, 6 (4), 525–530. https://doi.org/10.1039/c4py01292e.

Hu, R.; Maldonado, J. L.; Rodriguez, M.; Deng, C.; Jim, C. K. W.; Lam, J. W. Y.; Yuen, M. M. F.; Ramos-Ortiz, G.; Tang, B. Z. Luminogenic Materials Constructed from Tetraphenylethene Building Blocks: Synthesis, Aggregation-Induced Emission, Two-Photon Absorption, Light Refraction, and Explosive Detection. J. Mater. Chem. 2012, 22 (1), 232–240. https://doi.org/10.1039/c1jm13556b.

Hu, Z.; Xu, R.; Dong, S.; Lin, K.; Liu, J.; Huang, F.; Cao, Y. Quaternisation-Polymerized N-Type Polyelectrolytes: Synthesis, Characterisation and Application in High-Performance Polymer Solar Cells. Mater. Horiz. 2017, 4 (1), 88–97. https://doi.org/10.1039/C6MH00434B.

Hu, Z.; Xu, R.; Dong, S.; Lin, K.; Liu, J.; Huang, F.; Cao, Y. Quaternisation-Polymerized N-Type Polyelectrolytes: Synthesis, Characterisation and Application in High-Performance Polymer Solar Cells. Mater. Horiz. 2017, 4 (1), 88–97. https://doi.org/10.1039/C6MH00434B.

Huang, C.; Barlow, S.; Marder, S. R. Perylene-3,4,9,10-Tetracarboxylic Acid Diimides: Synthesis, Physical Properties, and Use in Organic Electronics. J. Org. Chem. 2011, 76 (8), 2386–2407. https://doi.org/10.1021/jo2001963.

Huang, C.; Barlow, S.; Marder, S. R. Perylene-3,4,9,10-Tetracarboxylic Acid Diimides: Synthesis, Physical Properties, and Use in Organic Electronics. J. Org. Chem. 2011, 76 (8), 2386–2407. https://doi.org/10.1021/jo2001963.

Huang, Y.; Xing, J.; Gong, Q.; Chen, L. C.; Liu, G.; Yao, C.; Wang, Z.; Zhang, H. L.; Chen, Z.; Zhang, Q. Reducing Aggregation Caused Quenching Effect through Co-Assembly of PAH

Chromophores and Molecular Barriers. Nat. Commun. 2019, 10 (1), 1–9. https://doi.org/10.1038/s41467-018-08092-y.

Hunter, C. A.; Sanders, J. K. M. The Nature of π-π Interactions. J. Am. Chem. Soc. 1990, 112 (14), 5525–5534. https://doi.org/10.1021/ja00170a016.

Iida, A.; Yamaguchi, S. Intense Solid-State Blue Emission with a Small Stokes' Shift: π-Stacking Protection of the Diphenylanthracene Skeleton. Chem. Commun. 2009, 7345 (21), 3002. https://doi.org/10.1039/b901794a.

Ishii, B. H.; Sugiyama, K.; Ito, E.; Seki, K. Energy Level Alignment and Interfacial Electronic Structures at Organic / Metal and Organic / Organic Interfaces **. Adv. Mater. 1999, 11 (8), 605–625. https://doi.org/10.1002/(SICI)1521-4095(199906)11:8<605::AID-ADMA605>3.0.CO;2-Q.

Ishii, H.; Seki, K. Energy Level Alignment at Organic/Metal Interfaces Studied by UV Photoemission: Breakdown of Traditional Assumption of a Common Vacuum Level at the Interface. IEEE Trans. Electron Devices 1997, 44 (8), 1295–1301. https://doi.org/10.1109/16.605471.

Jakubiak, R.; Collison, C. J.; Wan, W. C.; Rothberg, L. J.; Hsieh, B. R. Aggregation Quenching of Luminescence in Electroluminescent Conjugated Polymers. J. Phys. Chem. A 1999, 103 (14), 2394–2398. https://doi.org/10.1021/jp9839450.

Jakubiak, R.; Collison, C. J.; Wan, W. C.; Rothberg, L. J.; Hsieh, B. R. Aggregation Quenching of Luminescence in Electroluminescent Conjugated Polymers. J. Phys. Chem. A 1999, 103 (14), 2394–2398. https://doi.org/10.1021/jp9839450.

Jen, K.; Miller, G. G.; Elsenbaumer, R. L. Highly Conducting, Soluble, and Environmentally-Stable Poly(3-Alkylthiophenes). J. Chem. Soc. Chem. Commun. 1986, 5 (17), 1346. https://doi.org/10.1039/c39860001346.

Jeong, I.; Park, Y. H.; Bae, S.; Park, M.; Jeong, H.; Lee, P.; Ko, M. J. Solution-Processed Ultrathin TiO 2 Compact Layer Hybridized with Mesoporous TiO 2 for High-Performance Perovskite Solar Cells. ACS Appl. Mater. Interfaces 2017, acsami.7b11901. https://doi.org/10.1021/acsami.7b11901.

Jeong, I.; Park, Y. H.; Bae, S.; Park, M.; Jeong, H.; Lee, P.; Ko, M. J. Solution-Processed Ultrathin TiO 2 Compact Layer Hybridized with Mesoporous TiO 2 for High-Performance Perovskite Solar Cells. ACS Appl. Mater. Interfaces 2017, acsami.7b11901. https://doi.org/10.1021/acsami.7b11901.

Jia, J.; Fan, B.; Xiao, M.; Jia, T.; Jin, Y.; Li, Y.; Huang, F.; Cao, Y. N-Type Self-Doped Water/Alcohol-Soluble Conjugated Polymers with Tailored Energy Levels for High-Performance Polymer Solar Cells. Macromolecules 2018, 51 (6), 2195–2202. https://doi.org/10.1021/acs.macromol.8b00126.

Jia, X.; Zhang, L.; Luo, Q.; Lu, H.; Li, X.; Xie, Z.; Yang, Y.; Li, Y.; Liu, X.; Ma, C. Power Conversion E Ffi Ciency and Device Stability Improvement of Inverted Perovskite Solar Cells by Using a ZnO : PFN Composite Cathode Bu Ff Er Layer. ACS Appl. Mater. Interfaces 2016, 8 (28), 18410–18417. https://doi.org/10.1021/acsami.6b03724.

Jiang, X.; Xu, Y.; Wang, X.; Yang, F.; Zhang, A.; Li, C.; Ma, W.; Li, W. Conjugated Polymer Acceptors Based on Fused Perylene Bisimides with a Twisted Backbone for Non-Fullerene Solar Cells. Polym. Chem. 2017. https://doi.org/10.1039/C7PY00444C.

Jin, L.; Liu, C.; An, N.; Zhang, Q.; Wang, J.; Zhao, L.; Lu, Y. Fluorescence Turn-on Detection of Fe 3+ in Pure Water Based on a Cationic Poly(Perylene Diimide) Derivative. RSC Adv. 2016, 6 (63), 58394–58400. https://doi.org/10.1039/C6RA08267J.

Kaiser, T. E.; Stepanenko, V.; Würthner, F. Fluorescent J-Aggregates of Core-Substituted Perylene Bisimides: Studies on Structure-Property Relationship, Nucleation-Elongation Mechanism, and Sergeants-and-Soldiers Principle. J. Am. Chem. Soc. 2009, 131 (19), 6719–6732. https://doi.org/10.1021/ja900684h.

Kesters, J.; Govaerts, S.; Pirotte, G.; Drijkoningen, J.; Chevrier, M.; Van Den Brande, N.; Liu, X.; Fahlman, M.; Van Mele, B.; Lutsen, L.; et al. High-Permittivity Conjugated Polyelectrolyte Interlayers for High-Performance Bulk Heterojunction Organic Solar Cells. ACS Appl. Mater. Interfaces 2016, 8 (10), 6309–6314. https://doi.org/10.1021/acsami.6b00242.

Kesters, J.; Govaerts, S.; Pirotte, G.; Drijkoningen, J.; Chevrier, M.; Van Den Brande, N.; Liu, X.; Fahlman, M.; Van Mele, B.; Lutsen, L.; et al. High-Permittivity Conjugated Polyelectrolyte Interlayers for High-Performance Bulk Heterojunction Organic Solar Cells. ACS Appl. Mater. Interfaces 2016, 8 (10), 6309–6314. https://doi.org/10.1021/acsami.6b00242.

Kim, S. T.; Hwang, D.; Li, X. C.; Grüner, J.; Friend, R. H.; Holmes, A. B.; Shim, H. K. Efficient Green Electroluminescent Diodes Based on Poly (2-Dimethyloctylsilyl-1,4-Phenylenevinylene). Adv. Mater. 1996, 8 (12), 979–982. https://doi.org/10.1002/adma.19960081206.

Kim, S. T.; Hwang, D.; Li, X. C.; Grüner, J.; Friend, R. H.; Holmes, A. B.; Shim, H. K. Efficient Green Electroluminescent Diodes Based on Poly (2-Dimethyloctylsilyl-1,4-

Phenylenevinylene). Adv. Mater. 1996, 8 (12), 979–982. https://doi.org/10.1002/adma.19960081206.

Ko, D. Y.; Patel, M.; Jung, B. K.; Park, J. H.; Jeong, B. Phosphorylcholine-Based Zwitterionic Biocompatible Thermogel. Biomacromolecules 2015, 16 (12), 3853–3862. https://doi.org/10.1021/acs.biomac.5b01169.

Kolewe, K. W.; Dobosz, K. M.; Rieger, K. A.; Chang, C. C.; Emrick, T.; Schiffman, J. D. Antifouling Electrospun Nanofiber Mats Functionalized with Polymer Zwitterions. ACS Appl. Mater. Interfaces 2016, 8 (41), 27585-27593Kolewe, K. W.; Dobosz, K. M.; Rieger, K. https://doi.org/10.1021/acsami.6b09839.

Krieg, E.; Shirman, E.; Weissman, H.; Shimoni, E.; Wolf, S. G.; Pinkas, I.; Rybtchinski, B. Supramolecular Gel Based on a Perylene Diimide Dye: Multiple Stimuli Responsiveness, Robustness, and Photofunction. J. Am. Chem. Soc. 2009, 131 (40), 14365–14373. https://doi.org/10.1021/ja903938g.

Kumar, A.; Sista, S.; Yang, Y. Dipole Induced Anomalous S-Shape I-V Curves in Polymer Solar Cells. J. Appl. Phys. 2009, 105 (9), 094512. https://doi.org/10.1063/1.3117513.

Lee, D. W.; Kwon, K.-Y.; Jin, J.-I.; Park, Y.; Kim, Y.-R.; Hwang, I.-W. Luminescence Properties of Structurally Modified PPVs: PPV Derivatives Bearing 2-(4- Tert -Butylphenyl)-5-Phenyl-1,3,4-Oxadiazole Pendants. Chem. Mater. 2001, 13 (2), 565–574. https://doi.org/10.1021/cm000794g.

Lee, D. W.; Kwon, K.-Y.; Jin, J.-I.; Park, Y.; Kim, Y.-R.; Hwang, I.-W. Luminescence Properties of Structurally Modified PPVs: PPV Derivatives Bearing 2-(4- Tert -Butylphenyl)-5-

Phenyl-1,3,4-Oxadiazole Pendants. Chem. Mater. 2001, 13 (2), 565–574. https://doi.org/10.1021/cm000794g.

Lee, H.; Puodziukynaite, E.; Zhang, Y.; Stephenson, J. C.; Richter, L. J.; Fischer, D. a; Delongchamp, D. M.; Emrick, T.; Briseno, A. L. Poly(Sulfobetaine Methacrylate)s as Electrode Modi Fi Ers for Inverted Organic Electronics. J. Am. Chem. Soc. 2015, 137, 540–549. https://doi.org/10.1021/ja512148d.

Lee, H.; Puodziukynaite, E.; Zhang, Y.; Stephenson, J. C.; Richter, L. J.; Fischer, D. A.; Delongchamp, D. M.; Emrick, T.; Briseno, A. L. Poly(Sulfobetaine Methacrylate)s as Electrode Modi Fi Ers for Inverted Organic Electronics. J. Am. Chem. Soc. 2015, 137, 540–549. https://doi.org/10.1021/ja512148d.

Lee, H.; Stephenson, J. C.; Richter, L. J.; McNeill, C. R.; Gann, E.; Thomsen, L.; Park, S.; Jeong, J.; Yi, Y.; DeLongchamp, D. M.; et al. The Structural Origin of Electron Injection Enhancements with Fulleropyrrolidine Interlayers. Adv. Mater. Interfaces 2016, 3 (10), 1500852. https://doi.org/10.1002/admi.201500852.

Lee, J. W.; Kim, S. G.; Yang, J. M.; Yang, Y.; Park, N. G. Verification and Mitigation of Ion Migration in Perovskite Solar Cells. APL Mater. 2019, 7 (4). https://doi.org/10.1063/1.5085643.

Leigh, B. L.; Cheng, E.; Xu, L.; Derk, A.; Hansen, M. R.; Guymon, C. A. Antifouling Photograftable Zwitterionic Coatings on PDMS Substrates. Langmuir 2019, 35 (5), 1100–1110. https://doi.org/10.1021/acs.langmuir.8b00838.

Li, J.; Han, X.; Bai, Q.; Shan, T.; Lu, P.; Ma, Y. Electropolymerized AIE-Active Polymer Film with High Quantum Efficiency and Its Application in OLED. J. Polym. Sci. Part A Polym. Chem. 2017, 55 (4), 707–715. https://doi.org/10.1002/pola.28414.

Li, Y.; Cole, M. D.; Gao, Y.; Emrick, T.; Xu, Z.; Liu, Y.; Russell, T. P. High-Performance Perovskite Solar Cells with a Non-Doped Small Molecule Hole Transporting Layer. ACS Appl. Energy Mater. 2019, 2 (3), 1634–1641. https://doi.org/10.1021/acsaem.9b00164.

Li, Y.; Cole, M. D.; Gao, Y.; Emrick, T.; Xu, Z.; Liu, Y.; Russell, T. P. High-Performance Perovskite Solar Cells with a Non-Doped Small Molecule Hole Transporting Layer. ACS Appl. Energy Mater. 2019, 2 (3), 1634–1641. https://doi.org/10.1021/acsaem.9b00164.

Li, Y.; Xu, Z.; Zhu, X.; Chen, B.; Wang, Z.; Xiao, B.; Lam, J. W. Y.; Zhao, Z.; Ma, D.; Tang, B. Z. Creation of Efficient Blue AIE Luminogens for High-Performance Nondoped Blue OLEDs and Hybrid White OLEDs. ACS Appl. Mater. Interfaces 2019, acsami.9b03177. https://doi.org/10.1021/acsami.9b03177.

Liang, J.; Shi, H.; Kwok, R. T. K.; Gao, M.; Yuan, Y.; Zhang, W.; Tang, B. Z.; Liu, B. Distinct Optical and Kinetic Responses from E/Z Isomers of Caspase Probes with Aggregation-Induced Emission Characteristics. J. Mater. Chem. B 2014, 2 (27), 4363–4370. https://doi.org/10.1039/c4tb00405a.

Liang, Y.; Lan, S.; Deng, P.; Zhou, D.; Guo, Z.; Chen, H.; Zhan, H. Regioregular and Regioirregular Poly(Selenophene-Perylene Diimide) Acceptors for Polymer-Polymer Solar Cells. ACS Appl. Mater. Interfaces 2018, 10 (38), 32397–32403. https://doi.org/10.1021/acsami.8b09061.

Ling, X.; Yuan, J.; Liu, D.; Wang, Y.; Zhang, Y.; Chen, S.; Wu, H.; Jin, F.; Wu, F.; Shi, G.; et al. Room-Temperature Processed Nb 2 O 5 as the Electron-Transporting Layer for Efficient Planar Perovskite Solar Cells. ACS Appl. Mater. Interfaces 2017, 9 (27), 23181–23188. https://doi.org/10.1021/acsami.7b05113.

Ling, X.; Yuan, J.; Liu, D.; Wang, Y.; Zhang, Y.; Chen, S.; Wu, H.; Jin, F.; Wu, F.; Shi, G.; et al. Room-Temperature Processed Nb 2 O 5 as the Electron-Transporting Layer for Efficient Planar Perovskite Solar Cells. ACS Appl. Mater. Interfaces 2017, 9 (27), 23181–23188. https://doi.org/10.1021/acsami.7b05113.

Liu, C.; Li, Z.; Zhang, X.; Guo, W.; Zhang, L.; Ruan, S. Annealing-Free ZnO:PEI Composite Cathode Interfacial Layer for Efficient Organic Solar Cells. ACS Photonics 2017, 4 (11), 2952–2958. https://doi.org/10.1021/acsphotonics.7b01096.

Liu, H.; Huang, L.; Cheng, X.; Hu, A.; Xu, H.; Chen, L.; Chen, Y. N-Type Self-Doping of Fluorinate Conjugated Polyelectrolytes for Polymer Solar Cells: Modulation of Dipole, Morphology, and Conductivity. ACS Appl. Mater. Interfaces 2017, 9 (1), 1145–1153. https://doi.org/10.1021/acsami.6b15678.

Liu, J.; Meng, Q.; Zhang, X.; Lu, X.; He, P.; Jiang, L.; Dong, H.; Hu, W. Aggregation-Induced Emission Enhancement Based on 11,11,12,12,-Tetracyano-9,10-Anthraquinodimethane. Chem. Commun. (Camb). 2013, 49 (12), 1199–1201. https://doi.org/10.1039/c2cc38817k.

Liu, W.; Tkachov, R.; Komber, H.; Senkovskyy, V.; Schubert, M.; Wei, Z.; Facchetti, A.; Neher, D.; Kiriy, A. Chain-Growth Polycondensation of Perylene Diimide-Based Copolymers: A New Route to Regio-Regular Perylene Diimide-Based Acceptors for All-Polymer Solar

Cells and n-Type Transistors. Polym. Chem. 2014, 5 (10), 3404.
https://doi.org/10.1039/c3py01707a.

Liu, Y.; Cole, M. D.; Jiang, Y.; Kim, P. Y.; Nordlund, D.; Emrick, T.; Russell, T. P. Chemical and
Morphological Control of Interfacial Self-Doping for Efficient Organic Electronics. Adv.
Mater. 2018, 30 (15), 1705976. https://doi.org/10.1002/adma.201705976.

Liu, Y.; Cole, M. D.; Jiang, Y.; Kim, P. Y.; Nordlund, D.; Emrick, T.; Russell, T. P. Chemical and
Morphological Control of Interfacial Self-Doping for Efficient Organic Electronics. Adv.
Mater. 2018, 30 (15), 1705976. https://doi.org/10.1002/adma.201705976.

Liu, Y.; Page, Z. A.; Russell, T. P.; Emrick, T. Finely Tuned Polymer Interlayers Enhance Solar
Cell Efficiency. Angew. Chemie - Int. Ed. 2015, 54 (39), 11485–11489.
https://doi.org/10.1002/anie.201503933.

Liu, Y.; Page, Z. A.; Russell, T. P.; Emrick, T. Finely Tuned Polymer Interlayers Enhance Solar
Cell Efficiency. Angew. Chemie - Int. Ed. 2015, 54 (39), 11485–11489.
https://doi.org/10.1002/anie.201503933.

Liu, Y.; Page, Z. A.; Zhou, D.; Duzhko, V. V.; Kittilstved, K. R.; Emrick, T.; Russell, T. P.
Chemical Stabilization of Perovskite Solar Cells with Functional Fulleropyrrolidines. ACS
Cent. Sci. 2018, 4 (2), 216–222. https://doi.org/10.1021/acscentsci.7b00454.

Liu, Y.; Page, Z.; Ferdous, S.; Liu, F.; Kim, P.; Emrick, T.; Russell, T. Dual Functional
Zwitterionic Fullerene Interlayer for Efficient Inverted Polymer Solar Cells. Adv. Energy
Mater. 2015, 5 (14), 1–6. https://doi.org/10.1002/aenm.201500405.

Liu, Y.; Renna, L. A.; Page, Z. A.; Thompson, H. B.; Kim, P. Y.; Barnes, M. D.; Emrick, T.; Venkataraman, D.; Russell, T. P. A Polymer Hole Extraction Layer for Inverted Perovskite Solar Cells from Aqueous Solutions. Adv. Energy Mater. 2016, 1–7. https://doi.org/10.1002/aenm.201600664.

Liu, Y.; Renna, L. A.; Page, Z. A.; Thompson, H. B.; Kim, P. Y.; Barnes, M. D.; Emrick, T.; Venkataraman, D.; Russell, T. P. A Polymer Hole Extraction Layer for Inverted Perovskite Solar Cells from Aqueous Solutions. Adv. Energy Mater. 2016, 1–7. https://doi.org/10.1002/aenm.201600664.

Luo, J.; Xie, Z.; Lam, J. W. Y.; Cheng, L.; Tang, B. Z.; Chen, H.; Qiu, C.; Kwok, H. S.; Zhan, X.; Liu, Y.; et al. Aggregation-Induced Emission of 1-Methyl-1,2,3,4,5-Pentaphenylsilole. Chem. Commun. 2001, 381 (18), 1740–1741. https://doi.org/10.1039/b105159h.

Luo, J.; Xie, Z.; Lam, J. W. Y.; Cheng, L.; Tang, B. Z.; Chen, H.; Qiu, C.; Kwok, H. S.; Zhan, X.; Liu, Y.; et al. Aggregation-Induced Emission of 1-Methyl-1,2,3,4,5-Pentaphenylsilole. Chem. Commun. 2001, 381 (18), 1740–1741. https://doi.org/10.1039/b105159h.

Lupinski, J. H.; Kopple, K. D. Electroconductive Polymers. Science (80-.). 1964, 146 (3647), 1038–1039. https://doi.org/10.1126/science.146.3647.1038.

Ma, X.; Zhang, Y.; Zhang, Y.; Peng, C.; Che, Y.; Zhao, J. Stepwise Formation of Photoconductive Nanotubes through a New Top-Down Method. Adv. Mater. 2015, 27 (47), 77467751. https://doi.org/10.1002/adma.201503771.

Meiss, J.; Riede, M. K.; Leo, K. Towards Efficient Tin-Doped Indium Oxide (ITO)-Free Inverted Organic Solar Cells Using Metal Cathodes. Appl. Phys. Lett. 2009, 94 (1), 013303. https://doi.org/10.1063/1.3059552.

Miyano, K.; Yanagida, M.; Tripathi, N.; Shirai, Y. Hysteresis, Stability, and Ion Migration in Lead Halide Perovskite Photovoltaics. J. Phys. Chem. Lett. 2016, 7 (12), 2240–2245. https://doi.org/10.1021/acs.jpclett.6b00579.

Mohan, M.; Nandal, V.; Paramadam, S.; Reddy, K. P.; Ramkumar, S.; Agarwal, S.; Gopinath, C. S.; Nair, P. R.; Namboothiry, M. A. G. Efficient Organic Photovoltaics with Improved Charge Extraction and High Short-Circuit Current. J. Phys. Chem. C 2017, 121 (10), 5523–5530. https://doi.org/10.1021/acs.jpcc.7b01314.

Mohan, M.; Nandal, V.; Paramadam, S.; Reddy, K. P.; Ramkumar, S.; Agarwal, S.; Gopinath, C. S.; Nair, P. R.; Namboothiry, M. A. G. Efficient Organic Photovoltaics with Improved Charge Extraction and High Short-Circuit Current. J. Phys. Chem. C 2017, 121 (10), 5523–5530. https://doi.org/10.1021/acs.jpcc.7b01314.

Ng, C. Y. Bin; Yeoh, K. H.; Whitcher, T. J.; Talik, N. A.; Woon, K. L.; Saisopa, T.; Nakajima, H.; Supruangnet, R.; Songsiriritthigul, P. High Efficiency Solution Processed Fluorescent Yellow Organic Light-Emitting Diode through Fluorinated Alcohol Treatment at the Emissive Layer/Cathode Interface. *J. Phys. D. Appl. Phys.* **2014**, *47* (1). https://doi.org/10.1088/0022-3727/47/1/015106.

Page, Z. A.; Liu, F.; Russell, T. P.; Emrick, T. Rapid, Facile Synthesis of Conjugated Polymer Zwitterions in Ionic Liquids. Chem. Sci. 2014, 5 (6), 2368–2373. https://doi.org/10.1039/c4sc00475b.

Page, Z. A.; Liu, F.; Russell, T. P.; Emrick, T. Rapid, Facile Synthesis of Conjugated Polymer Zwitterions in Ionic Liquids. Chem. Sci. 2014, 5 (6), 2368–2373. https://doi.org/10.1039/c4sc00475b.

Page, Z. A.; Liu, F.; Russell, T. P.; Emrick, T. Tuning the Energy Gap of Conjugated Polymer Zwitterions for Efficient Interlayers and Solar Cells. J. Polym. Sci. Part A Polym. Chem. 2015, 53 (2), 327–336. https://doi.org/10.1002/pola.27349.

Page, Z. A.; Liu, F.; Russell, T. P.; Emrick, T. Tuning the Energy Gap of Conjugated Polymer Zwitterions for Efficient Interlayers and Solar Cells. J. Polym. Sci. Part A Polym. Chem. 2015, 53 (2), 327–336. https://doi.org/10.1002/pola.27349.

Page, Z. A.; Liu, F.; Russell, T. P.; Emrick, T. Tuning the Energy Gap of Conjugated Polymer Zwitterions for Efficient Interlayers and Solar Cells. J. Polym. Sci. Part A Polym. Chem. 2015, 53 (2), 327–336. https://doi.org/10.1002/pola.27349.

Page, Z. A.; Liu, Y.; Duzhko, V. V.; Thomas, P.; Russell, T. P.; Emrick, T. Fulleropyrrolidine Interlayers: Tailoring Electrodes to Raise Organic Solar Cell Efficiency. Science (80-.). 2014, 346 (6208), 441–446. https://doi.org/10.1126/science.1255826.

Page, Z. A.; Liu, Y.; Duzhko, V. V.; Thomas, P.; Russell, T. P.; Emrick, T. Fulleropyrrolidine Interlayers: Tailoring Electrodes to Raise Organic Solar Cell Efficiency. Science (80-.). 2014, 346 (6208), 441–446. https://doi.org/10.1126/science.1255826.

Page, Z. A.; Liu, Y.; Puodziukynaite, E.; Russell, T. P.; Emrick, T. Hydrophilic Conjugated Polymers Prepared by Aqueous Horner-Wadsworth-Emmons Coupling. Macromolecules 2016, 49 (7), 2526–2532. https://doi.org/10.1021/acs.macromol.5b02501.

Park, Y. H.; Kim, Y.; Sohn, H.; An, K. S. Concentration Quenching Effect of Organic Light-Emitting Devices Using DCM1-Doped Tetraphenylgermole. J. Phys. Org. Chem. 2012, 25 (3), 207–210. https://doi.org/10.1002/poc.1893.

Peng, H.-Q.; Zheng, X.; Han, T.; Kwok, R. T. K.; Lam, J. W. Y.; Huang, X.; Tang, B. Z. Dramatic Differences in Aggregation-Induced Emission and Supramolecular Polymerizability of Tetraphenylethene-Based Stereoisomers. J. Am. Chem. Soc. 2017, 139 (29), 10150–10156. https://doi.org/10.1021/jacs.7b05792.

Peng, Q.; Yi, Y.; Shuai, Z.; Shao, J. Toward Quantitative Prediction of Molecular Fluorescence Quantum Efficiency: Role of Duschinsky Rotation. J. Am. Chem. Soc. 2007, 129 (30), 9333–9339. https://doi.org/10.1021/ja067946e.

Peumans, P.; Yakimov, A.; Forrest, S. R. Small Molecular Weight Organic Thin-Film Photodetectors and Solar Cells. J. Appl. Phys. 2003, 93 (7), 3693–3723. https://doi.org/10.1063/1.1534621.

Ratcliff, E. L.; Zacher, B.; Armstrong, N. R. Selective Interlayers and Contacts in Organic Photovoltaic Cells. J. Phys. Chem. Lett. 2011, 2 (11), 1337–1350. https://doi.org/10.1021/jz2002259.

Ratcliff, E. L.; Zacher, B.; Armstrong, N. R. Selective Interlayers and Contacts in Organic Photovoltaic Cells. J. Phys. Chem. Lett. 2011, 2 (11), 1337–1350. https://doi.org/10.1021/jz2002259.

Reilly, T. H.; Hains, A. W.; Chen, H. Y.; Gregg, B. A. A Self-Doping, O 2-Stable, n-Type Interfacial Layer for Organic Electronics. Adv. Energy Mater. 2012, 2 (4), 455–460. https://doi.org/10.1002/aenm.201100446.

Rembaum, A.; Baumgartner, W.; Eisenberg, A. Aliphatic Ionenes. Polym. Lett. 1968, 6, 159–171. https://doi.org/10.1002/pol.1968.110060302.

Rembaum, A.; Rile, H.; Somoano, R. V. Kinetics of Formation of High Charge Density Ionene Polymers. J. Polym. Sci. Part B Polym. Lett. 1970, 8 (7), 457–466. https://doi.org/10.1002/pol.1970.110080701.

Rembaum, A.; Singer, S.; Keyzer, H. Ionene Polymers. III. Dicationic Crosslinking Agents (1). J. Polym. Sci. Part B Polym. Lett. 1969, 7 (5), 395–402. https://doi.org/10.1002/pol.1969.110070512.

Reppy, M. A.; Pindzola, B. A. Biosensing with Polydiacetylene Materials: Structures, Optical Properties and Applications. Chem. Commun. 2007, No. 42, 4317. https://doi.org/10.1039/b703691d.

Rivkin, B.; Fassl, P.; Sun, Q.; Taylor, A. D.; Chen, Z.; Vaynzof, Y. Effect of Ion Migration-Induced Electrode Degradation on the Operational Stability of Perovskite Solar Cells. ACS Omega 2018, 3 (8), 10042–10047. https://doi.org/10.1021/acsomega.8b01626.

Russ, B.; Robb, M. J.; Popere, B. C.; Perry, E. E.; Mai, C. K.; Fronk, S. L.; Patel, S. N.; Mates, T. E.; Bazan, G. C.; Urban, J. J.; et al. Tethered Tertiary Amines as Solid-State n-Type Dopants for Solution-Processable Organic Semiconductors. Chem. Sci. 2016, 7 (3), 1914–1919. https://doi.org/10.1039/c5sc04217h.

Saliba, M.; Matsui, T.; Seo, J.-Y.; Domanski, K.; Correa-Baena, J.-P.; Nazeeruddin, M. K.; Zakeeruddin, S. M.; Tress, W.; Abate, A.; Hagfeldt, A.; et al. Cesium-Containing Triple Cation Perovskite Solar Cells: Improved Stability, Reproducibility and High Efficiency. Energy Environ. Sci. 2016, 9 (6), 1989–1997. https://doi.org/10.1039/C5EE03874J.

Schulze, P. S. C.; Bett, A. J.; Winkler, K.; Hinsch, A.; Lee, S.; Mastroianni, S.; Mundt, L. E.; Mundus, M.; Würfel, U.; Glunz, S. W.; et al. Novel Low-Temperature Process for

Perovskite Solar Cells with a Mesoporous TiO2Scaffold. ACS Appl. Mater. Interfaces 2017, 9 (36), 30567–30574. https://doi.org/10.1021/acsami.7b05718.

Schulze, P. S. C.; Bett, A. J.; Winkler, K.; Hinsch, A.; Lee, S.; Mastroianni, S.; Mundt, L. E.; Mundus, M.; Würfel, U.; Glunz, S. W.; et al. Novel Low-Temperature Process for Perovskite Solar Cells with a Mesoporous TiO2Scaffold. ACS Appl. Mater. Interfaces 2017, 9 (36), 30567–30574. https://doi.org/10.1021/acsami.7b05718.

Shi, J.; Wu, Y.; Sun, S.; Tong, B.; Zhi, J.; Dong, Y. Tunable Fluorescence Conjugated Copolymers Consisting of Tetraphenylethylene and Fluorene Units: From Aggregation-Induced Emission Enhancement to Dual-Channel Fluorescence Response. J. Polym. Sci. Part A Polym. Chem. 2013, 51 (2), 229–240. https://doi.org/10.1002/pola.26377.

Shi, J.; Wu, Y.; Sun, S.; Tong, B.; Zhi, J.; Dong, Y. Tunable Fluorescence Conjugated Copolymers Consisting of Tetraphenylethylene and Fluorene Units: From Aggregation-Induced Emission Enhancement to Dual-Channel Fluorescence Response. J. Polym. Sci. Part A Polym. Chem. 2013, 51 (2), 229–240. https://doi.org/10.1002/pola.26377.

Shirakawa, H.; Macdiarmid, A. G.; Chiang, C. K.; Fincher Jr., C. R.; Park, Y. W.; Heeger, A. J.; Louis, E. J.; Gau, S. C. Electical Conductivity in Doped Polyacetylene. Phys. Rev. Lett. 1977, 39 (17), 1098–1101. https://doi.org/10.1103/PhysRevLett.39.1098.

Siddiki, M. K.; Venkatesan, S.; Qiao, Q. Nb 2O 5 as a New Electron Transport Layer for Double Junction Polymer Solar Cells. Phys. Chem. Chem. Phys. 2012, 14 (14), 4682–4686. https://doi.org/10.1039/c2cp22627h.

Siddiki, M. K.; Venkatesan, S.; Qiao, Q. Nb 2O 5 as a New Electron Transport Layer for Double Junction Polymer Solar Cells. Phys. Chem. Chem. Phys. 2012, 14 (14), 4682–4686. https://doi.org/10.1039/c2cp22627h.

Siddiqui, S.; Spano, F. H- and J-Aggregates of Conjugated Polymers and Oligomers. Chem. Phys. Lett. 1999, 308 (1–2), 99–105. https://doi.org/10.1016/S0009-2614(99)00577-1.

Song, S.; Kang, G.; Pyeon, L.; Lim, C.; Lee, G. Y.; Park, T.; Choi, J. Systematically Optimized Bilayered Electron Transport Layer for Highly Efficient Planar Perovskite Solar Cells (η = 21.1%). ACS Energy Lett. 2017, 2 (12), 2667–2673. https://doi.org/10.1021/acsenergylett.7b00888.

Song, S.; Kang, G.; Pyeon, L.; Lim, C.; Lee, G. Y.; Park, T.; Choi, J. Systematically Optimized Bilayered Electron Transport Layer for Highly Efficient Planar Perovskite Solar Cells (η = 21.1%). ACS Energy Lett. 2017, 2 (12), 2667–2673. https://doi.org/10.1021/acsenergylett.7b00888.

Spano, F. C.; Introduction, I. The Spectral Signatures of Frenkel Polarons in H and J Aggregates. Acc. Chem. Res. 2009, 43 (3), 429–439.

Subbiah, J.; Mitchell, V. D.; Hui, N. K. C.; Jones, D. J.; Wong, W. W. H. A Green Route to Conjugated Polyelectrolyte Interlayers for High-Performance Solar Cells. Angew. Chemie - Int. Ed. 2017, 56 (29), 8431–8434. https://doi.org/10.1002/anie.201612021.

Subbiah, J.; Mitchell, V. D.; Hui, N. K. C.; Jones, D. J.; Wong, W. W. H. A Green Route to Conjugated Polyelectrolyte Interlayers for High-Performance Solar Cells. Angew. Chemie - Int. Ed. 2017, 56 (29), 8431–8434. https://doi.org/10.1002/anie.201612021.

Sun, C.; Wu, Z.; Hu, Z.; Xiao, J.; Zhao, W.; Li, H. W.; Li, Q. Y.; Tsang, S. W.; Xu, Y. X.; Zhang, K.; et al. Interface Design for High-Efficiency Non-Fullerene Polymer Solar Cells. Energy Environ. Sci. 2017, 10 (8), 1784–1791. https://doi.org/10.1039/c7ee00601b.

Sung-Ho, J.; Mock-Yeon, K.; Jin Young, K.; Kwanghee, L.; Yeong-Soon, G. High-Efficiency Poly(p-Phenylenevinylene)-Based Copolymers Containing an Oxadiazole Pendant Group for Light-Emitting Diodes. J. Am. Chem. Soc. 2004, 126 (2), 2474_2480.

Sung-Ho, J.; Mock-Yeon, K.; Jin Young, K.; Kwanghee, L.; Yeong-Soon, G. High-Efficiency Poly(p-Phenylenevinylene)-Based Copolymers Containing an Oxadiazole Pendant Group for Light-Emitting Diodes. J. Am. Chem. Soc. 2004, 126 (2), 2474_2480.

Suzuki, Y.; Tazuke, S. Functionalized Polyionenes. 1. Synthesis and Photoreaction of Polyionenes Bearing Pendant (9-Anthry1)Methyl Groups. Macromolecules 1980, 8 (13), 25–30.

Tamami, M.; Salas-De La Cruz, D.; Winey, K. I.; Long, T. E. Structure-Property Relationships of Water-Soluble Ammonium-Ionene Copolymers. Macromol. Chem. Phys. 2012, 213 (9), 965–972. https://doi.org/10.1002/macp.201200047.

Tan, Y.; Chen, L.; Wu, F.; Huang, B.; Liao, Z.; Yu, Z.; Hu, L.; Zhou, Y.; Chen, Y. Regulation of the Polar Groups in N-Type Conjugated Polyelectrolytes as Electron Transfer Layer for Inverted Polymer Solar Cells. Macromolecules 2018, 51 (20), 8197–8204. https://doi.org/10.1021/acs.macromol.8b01490.

Tan, Y.; Chen, L.; Wu, F.; Huang, B.; Liao, Z.; Yu, Z.; Hu, L.; Zhou, Y.; Chen, Y. Regulation of the Polar Groups in N-Type Conjugated Polyelectrolytes as Electron Transfer Layer for

Inverted Polymer Solar Cells. Macromolecules 2018, 51 (20), 8197–8204. https://doi.org/10.1021/acs.macromol.8b01490.

Tatemichi, S.; Ichikawa, M.; Koyama, T.; Taniguchi, Y. High Mobility N-Type Thin-Film Transistors Based on N,N′-Ditridecyl Perylene Diimide with Thermal Treatments. Appl. Phys. Lett. 2006, 89 (11), 2004–2007. https://doi.org/10.1063/1.2349290.

Tian, Z.; Shaller, D.; Li, A. D. Q.; Shaller, A. D.; Li, A. D. Q. Twisted Perylene Dyes Enable Highly Fluorescent and Photostable Nanoparticles. Chem. Commun. 2009, No. 2, 180–182. https://doi.org/10.1039/b815507k.

Tripathi, N.; Shirai, Y.; Yanagida, M.; Karen, A.; Miyano, K. Novel Surface Passivation Technique for Low-Temperature Solution-Processed Perovskite PV Cells. ACS Appl. Mater. Interfaces 2016, 8 (7), 4644–4650. https://doi.org/10.1021/acsami.5b11286.

Trosper, T.; Park, R. B.; Sauer, K. Excitation Transfer by Chlorophyll a in Monolayers and the Interaction with Chloroplast Glycolipids*. Photochem. Photobiol. 1968, 7 (5), 451–469. https://doi.org/10.1111/j.1751-1097.1968.tb07406.x.

Trost, S.; Zilberberg, K.; Behrendt, A.; Riedl, T. Room-Temperature Solution Processed SnOxas an Electron Extraction Layer for Inverted Organic Solar Cells with Superior Thermal Stability. J. Mater. Chem. 2012, 22 (32), 16224–16229. https://doi.org/10.1039/c2jm33445c.

Trost, S.; Zilberberg, K.; Behrendt, A.; Riedl, T. Room-Temperature Solution Processed SnOxas an Electron Extraction Layer for Inverted Organic Solar Cells with Superior Thermal Stability. J. Mater. Chem. 2012, 22 (32), 16224–16229. https://doi.org/10.1039/c2jm33445c.

Van Andel, E.; Lange, S. C.; Pujari, S. P.; Tijhaar, E. J.; Smulders, M. M. J.; Savelkoul, H. F. J.; Zuilhof, H. Systematic Comparison of Zwitterionic and Non-Zwitterionic Antifouling Polymer Brushes on a Bead-Based Platform. Langmuir 2019, 35 (5), 1181–1191. https://doi.org/10.1021/acs.langmuir.8b01832.

Van Reenen, S.; Kouijzer, S.; Janssen, R. A. J.; Wienk, M. M.; Kemerink, M. Origin of Work Function Modification by Ionic and Amine-Based Interface Layers. Adv. Mater. Interfaces 2014, 1 (8), 1–11. https://doi.org/10.1002/admi.201400189.

Van Reenen, S.; Kouijzer, S.; Janssen, R. A. J.; Wienk, M. M.; Kemerink, M. Origin of Work Function Modification by Ionic and Amine-Based Interface Layers. Adv. Mater. Interfaces 2014, 1 (8), 1–11. https://doi.org/10.1002/admi.201400189.

Van Severen, I.; Bolink, H. J.; Vanderzande, D.; Lutsen, L.; Cleij, T. J.; Adriaensens, P.; Vandenbergh, J. Tetra-Alkoxy Substituted PPV Derivatives: A New Class of Highly Soluble Liquid Crystalline Conjugated Polymers. Polym. Chem. 2011, 2 (6), 1279. https://doi.org/10.1039/c1py00027f.

Vilbrandt, N.; Gassmann, A.; Von Seggern, H.; Rehahn, M. Blue-Greenish Electroluminescent Poly(p-Phenylenevinylene) Developed for Organic Light-Emitting Diode Applications. Macromolecules 2016, 49 (5), 1674–1680. https://doi.org/10.1021/acs.macromol.5b01249.

Vilbrandt, N.; Gassmann, A.; Von Seggern, H.; Rehahn, M. Blue-Greenish Electroluminescent Poly(p-Phenylenevinylene) Developed for Organic Light-Emitting Diode Applications. Macromolecules 2016, 49 (5), 1674–1680. https://doi.org/10.1021/acs.macromol.5b01249.

Vyas, V. S.; Rathore, R. Preparation of a Tetraphenylethylene-Based Emitter: Synthesis, Structure and Optoelectronic Properties of Tetrakis(Pentaphenylphenyl)Ethylene. Chem. Commun. 2010, 46 (7), 1065–1067. https://doi.org/10.1039/b923915d.

Wagenpfahl, A.; Deibel, C.; Dyakonov, V. Organic Solar Cell Efficiencies under the Aspect of Reduced Surface Recombination Velocities. IEEE J. Sel. Top. Quantum Electron. 2010, 16 (6), 1759–1763. https://doi.org/10.1109/JSTQE.2010.2042142.

Wagenpfahl, A.; Rauh, D.; Binder, M.; Deibel, C.; Dyakonov, V. S-Shaped Current-Voltage Characteristics of Organic Solar Devices. Phys. Rev. B 2010, 82 (11), 115306. https://doi.org/10.1103/PhysRevB.82.115306.

Wagenpfahl, A.; Rauh, D.; Binder, M.; Deibel, C.; Dyakonov, V. S-Shaped Current-Voltage Characteristics of Organic Solar Devices. Phys. Rev. B 2010, 82 (11), 115306. https://doi.org/10.1103/PhysRevB.82.115306.

Wakamiya, A.; Mori, K.; Yamaguchi, S. 3-Boryl-2,2′-Bithiophene as a Versatile Core Skeleton for Full-Color Highly Emissive Organic Solids. Angew. Chemie - Int. Ed. 2007, 46 (23), 4273–4276. https://doi.org/10.1002/anie.200604935.

Waldauf, C.; Morana, M.; Denk, P.; Schilinsky, P.; Coakley, K.; Choulis, S. A.; Brabec, C. J. Highly Efficient Inverted Organic Photovoltaics Using Solution Based Titanium Oxide as Electron Selective Contact. Appl. Phys. Lett. 2006, 89 (23), 233517. https://doi.org/10.1063/1.2402890.

Waldauf, C.; Morana, M.; Denk, P.; Schilinsky, P.; Coakley, K.; Choulis, S. A.; Brabec, C. J. Highly Efficient Inverted Organic Photovoltaics Using Solution Based Titanium Oxide as

Electron Selective Contact. Appl. Phys. Lett. 2006, 89 (23), 233517. https://doi.org/10.1063/1.2402890.

Wang, J.; Mei, J.; Hu, R.; Sun, J. Z.; Qin, A.; Tang, B. Z. Click Synthesis, Aggregation-Induced Emission, E/Z Isomerization, Self-Organization, and Multiple Chromisms of Pure Stereoisomers of a Tetraphenylethene-Cored Luminogen. J. Am. Chem. Soc. 2012, 134 (24), 9956–9966. https://doi.org/10.1021/ja208883h.

Wang, L.; Sun, C.; Li, S.; Jia, N.; Li, J.; Qu, F.; Goh, K.; Chen, Y. Perylene Bisimide-Incorporated Water-Soluble Polyurethanes for Living Cell Fluorescence Labeling. Polym. (United Kingdom) 2016, 82, 172–180. https://doi.org/10.1016/j.polymer.2015.11.037.

Wang, W.; Ji, X.; Kapur, A.; Zhang, C.; Mattoussi, H. A Multifunctional Polymer Combining the Imidazole and Zwitterion Motifs as a Biocompatible Compact Coating for Quantum Dots. J. Am. Chem. Soc. 2015, 137 (44), 14158–14172. https://doi.org/10.1021/jacs.5b08915.

Watson, W. F.; Livingston, R. Self-Quenching and Sensitization of Fluorescence of Chlorophyll Solutions. J. Chem. Phys. 1950, 18 (6), 802–809. https://doi.org/10.1063/1.1747779.

Williams, S. R.; Long, T. E. Recent Advances in the Synthesis and Structure-Property Relationships of Ammonium Ionenes. Prog. Polym. Sci. 2009, 34 (8), 762–782. https://doi.org/10.1016/j.progpolymsci.2009.04.004.

Wu, H.; Jiang, Y.; Ding, Y.; Meng, Y.; Zeng, Z.; Cabanetos, C.; Zhou, G.; Gao, J.; Liu, J.; Roncali, J. Mechanofluorochromic and Thermochromic Properties of Simple Tetraphenylethylene

Derivatives with Fused Fluorine Containing 1,4-Dioxocane Rings. Dye. Pigment. 2017, 146, 323–330. https://doi.org/10.1016/j.dyepig.2017.07.026.

Wu, H.; Xie, Z.; Xiao, B.; He, Z.; Zhang, W.; Wu, X.; Würthner, F.; Wang, C.; Xie, F.; Liu, L.; et al. Self-Assembled Perylene Bisimide J-Aggregates as Promising Cathode Modifier for Highly Efficient Inverted Polymer Solar Cells. Mater. Horiz. 2015, 514–518. https://doi.org/10.1039/C5MH00056D.

Wu, W.; Feng, G.; Xu, S.; Liu, B. A Photostable Far-Red/Near-Infrared Conjugated Polymer Photosensitizer with Aggregation-Induced Emission for Image-Guided Cancer Cell Ablation. Macromolecules 2016, 49 (14), 5017–5025. https://doi.org/10.1021/acs.macromol.6b00958.

Wu, W.; Ye, S.; Tang, R.; Huang, L.; Li, Q.; Yu, G.; Liu, Y.; Qin, J.; Li, Z. New Tetraphenylethylene-Containing Conjugated Polymers: Facile Synthesis, Aggregation-Induced Emission Enhanced Characteristics and Application as Explosive Chemsensors and PLEDs. Polymer (Guildf). 2012, 53 (15), 3163–3171. https://doi.org/10.1016/j.polymer.2012.05.035.

Wu, W.; Ye, S.; Tang, R.; Huang, L.; Li, Q.; Yu, G.; Liu, Y.; Qin, J.; Li, Z. New Tetraphenylethylene-Containing Conjugated Polymers: Facile Synthesis, Aggregation-Induced Emission Enhanced Characteristics and Application as Explosive Chemsensors and PLEDs. Polymer (Guildf). 2012, 53 (15), 3163–3171. https://doi.org/10.1016/j.polymer.2012.05.035.

Wu, Y.; Chen, W.; Yue, Y.; Liu, J.; Bi, E.; Yang, X.; Islam, A.; Han, L. Consecutive Morphology Controlling Operations for Highly Reproducible Mesostructured Perovskite Solar Cells.

ACS Appl. Mater. Interfaces 2015, 7 (37), 20707–20713. https://doi.org/10.1021/acsami.5b05576.

Würthner, F.; Thalacker, C.; Diele, S.; Tschierske, C. Fluorescent J-Type Aggregates and Thermotropic Columnar Mesophases of Perylene Bisimide Dyes. Chem. - A Eur. J. 2001, 7 (10), 2245–2253. https://doi.org/10.1002/1521-3765(20010518)7:10<2245::AID-CHEM2245>3.0.CO;2-W.

Würthner, F.; Thalacker, C.; Diele, S.; Tschierske, C. Fluorescent J-Type Aggregates and Thermotropic Columnar Mesophases of Perylene Bisimide Dyes. Chem. - A Eur. J. 2001, 7 (10), 2245–2253. https://doi.org/10.1002/1521-3765(20010518)7:10<2245::AID-CHEM2245>3.0.CO;2-W.

Xie, J.; Huang, K.; Yu, X.; Yang, Z.; Xiao, K.; Qiang, Y.; Zhu, X.; Xu, L.; Wang, P.; Cui, C.; et al. Enhanced Electronic Properties of SnO2 via Electron Transfer from Graphene Quantum Dots for Efficient Perovskite Solar Cells. ACS Nano 2017, acsnano.7b04070. https://doi.org/10.1021/acsnano.7b04070.

Xie, J.; Huang, K.; Yu, X.; Yang, Z.; Xiao, K.; Qiang, Y.; Zhu, X.; Xu, L.; Wang, P.; Cui, C.; et al. Enhanced Electronic Properties of SnO2 via Electron Transfer from Graphene Quantum Dots for Efficient Perovskite Solar Cells. ACS Nano 2017, acsnano.7b04070. https://doi.org/10.1021/acsnano.7b04070.

Xie, Y.; Li, Z.; Gong, Y.; Zhang, F.; Peng, Q.; Han, M.; Xie, G. Tetraphenylcyclopentadiene-Based Hyperbranched Polymers: Convenient Syntheses from One Pot "A 4 + B 2 " Polymerization and High External Quantum Yields up to 9.74% in OLED Devices. Macromolecules 2019, 52, 896–903. https://doi.org/10.1021/acs.macromol.8b02051.

Xie, Z.; Yang, B.; Li, F.; Cheng, G.; Liu, L.; Yang, G.; Xu, H.; Ye, L.; Hanif, M.; Liu, S.; et al. Cross Dipole Stacking in the Crystal of Distyrylbenzene Derivative: The Approach toward High Solid-State Luminescence Efficiency. J. Am. Chem. Soc. 2005, 127 (41), 14152–14153. https://doi.org/10.1021/ja054661d.

Xue, Q.; Hu, Z.; Liu, J.; Lin, J.; Sun, C.; Chen, Z.; Duan, C.; Wang, J.; Liao, C.; Lau, W. M.; et al. Highly Efficient Fullerene/Perovskite Planar Heterojunction Solar Cells via Cathode Modification with an Amino-Functionalized Polymer Interlayer. J. Mater. Chem. A 2014, 2 (46), 19598–19603. https://doi.org/10.1039/C4TA05352D.

Yang, D. S.; Bilby, D.; Chung, K.; Wenderott, J. K.; Jordahl, J.; Kim, B. H.; Lahann, J.; Green, P. F.; Kim, J. Work Function Modification via Combined Charge-Based Through-Space Interaction and Surface Interaction. Adv. Mater. Interfaces 2018, 5 (15), 1800471. https://doi.org/10.1002/admi.201800471.

Yang, D. S.; Bilby, D.; Chung, K.; Wenderott, J. K.; Jordahl, J.; Kim, B. H.; Lahann, J.; Green, P. F.; Kim, J. Work Function Modification via Combined Charge-Based Through-Space Interaction and Surface Interaction. Adv. Mater. Interfaces 2018, 5 (15), 1800471. https://doi.org/10.1002/admi.201800471.

Yang, G.; Wang, C.; Lei, H.; Zheng, X.; Qin, P.; Xiong, L.; Zhao, X.; Yan, Y.; Fang, G. Interface Engineering in Planar Perovskite Solar Cells: Energy Level Alignment, Perovskite Morphology Control and High Performance Achievement. J. Mater. Chem. A 2017, 5 (4), 1658–1666. https://doi.org/10.1039/C6TA08783C.

Yang, R.; Wu, H.; Cao, Y.; Bazan, G. C. Control of Cationic Conjugated Polymer Performance in Light Emitting Diodes by Choice of Counterion. J. Am. Chem. Soc. 2006, 128 (45), 14422–14423. https://doi.org/10.1021/ja063723c.

Yang, R.; Zhao, Z.; He, J.; Wang, J.; Chen, W.; Wang, N.; Zhang, Y. A Water/Alcohol-Soluble Copolymer Based on Fluorene and Perylene Diimide as a Cathode Interlayer for Inverted Polymer Solar Cells. J. Mater. Chem. C 2015, 3, 4515–4521. https://doi.org/10.1039/C5TC00450K.

Yang, R.; Zhao, Z.; He, J.; Wang, J.; Chen, W.; Wang, N.; Zhang, Y. A Water/Alcohol-Soluble Copolymer Based on Fluorene and Perylene Diimide as a Cathode Interlayer for Inverted Polymer Solar Cells. J. Mater. Chem. C 2015, 3, 4515–4521. https://doi.org/10.1039/C5TC00450K.

Yang, W. S.; Park, B.-W.; Jung, E. H.; Jeon, N. J. Iodide Management in Formamidinium-Lead-Halide – Based Perovskite Layers for Efficient Solar Cells. Science (80-.). 2017, 356 (6345), 1376–1379. https://doi.org/10.1126/science.aan2301.

Yin, Q.; Zhang, K.; Zhang, L.; Jia, J.; Zhang, X.; Pang, S.; Xu, Q.-H.; Duan, C.; Huang, F.; Cao, Y. An Efficient Binary Cathode Interlayer for Large-Bandgap Non-Fullerene Organic Solar Cells. J. Mater. Chem. A 2019, 7 (20), 12426–12433. https://doi.org/10.1039/C9TA02844G.

Yin, S.; Peng, Q.; Shuai, Z.; Fang, W.; Wang, Y. H.; Luo, Y. Aggregation-Enhanced Luminescence and Vibronic Coupling of Silole Molecules from First Principles. Phys. Rev. B - Condens. Matter Mater. Phys. 2006, 73 (20), 1–5. https://doi.org/10.1103/PhysRevB.73.205409.

Yin, Z.; Wei, J.; Zheng, Q. Interfacial Materials for Organic Solar Cells: Recent Advances and Perspectives. Adv. Sci. 2016, 3 (8), 1–37. https://doi.org/10.1002/advs.201500362.

Yin, Z.; Wei, J.; Zheng, Q. Interfacial Materials for Organic Solar Cells: Recent Advances and Perspectives. Adv. Sci. 2016, 3 (8), 1–37. https://doi.org/10.1002/advs.201500362.

Yip, H.; Sun, C.; Wu, Z.; Zhang, H.; Jiang, X.; Xue, Q.; Hu, Z.; Hu, Z.; Shen, Y.; Wang, M.; et al. Amino-Functionalized Conjugated Polymer as an Efficient Electron Transport Layer for High-Performance Planar-Heterojunction Perovskite Solar Cells. Adv. Energy Mater. 2015, 1–10. https://doi.org/10.1002/aenm.201501534.

Yuan, Z.; Lee, S. L.; Chen, L.; Li, C.; Mali, K. S.; De Feyter, S.; Müllen, K. Processable Rylene Diimide Dyes up to 4 Nm in Length: Synthesis and STM Visualization. Chem. - A Eur. J. 2013, 19 (36), 11842–11846. https://doi.org/10.1002/chem.201302086.

Zhang, H.; Xue, L.; Han, J.; Fu, Y. Q.; Shen, Y.; Zhang, Z.; Li, Y.; Wang, M. New Generation Perovskite Solar Cells with Solution-Processed Amino-Substituted Perylene Diimide Derivative as Electron-Transport Layer. J. Mater. Chem. A 2016, 4 (22), 8724–8733. https://doi.org/10.1039/c6ta03119f.

Zhang, J.; Xue, R.; Xu, G.; Chen, W.; Bian, G. Q.; Wei, C.; Li, Y.; Li, Y. Self-Doping Fullerene Electrolyte-Based Electron Transport Layer for All-Room-Temperature-Processed High-Performance Flexible Polymer Solar Cells. Adv. Funct. Mater. 2018, 28 (13), 1–10. https://doi.org/10.1002/adfm.201705847.

Zhang, M.; Li, T.; Zheng, G.; Li, L.; Qin, M.; Zhang, S.; Zhou, H.; Zhan, X. An Amino-Substituted Perylene Diimide Polymer for Conventional Perovskite Solar Cells. Mater. Chem. Front. 2017, 1 (10), 2078–2084. https://doi.org/10.1039/C7QM00221A.

Zhang, S.; Wen, Y.; Zhou, W.; Guo, Y.; Ma, L.; Zhao, X.; Zhao, Z.; Barlow, S.; Marder, S. R.; Liu, Y.; et al. Perylene Diimide Copolymers with Dithienothiophene and Dithienopyrrole: Use in n-Channel and Ambipolar Field-Effect Transistors. J. Polym. Sci. Part A Polym. Chem. 2013, n/a-n/a. https://doi.org/10.1002/pola.26521.

Zhang, T.; Jiang, Y.; Niu, Y.; Wang, D.; Peng, Q.; Shuai, Z. Aggregation Effects on the Optical Emission of 1,1,2,3,4,5-Hexaphenylsilole (HPS): A QM/MM Study. J. Phys. Chem. A 2014, 118 (39), 9094–9104. https://doi.org/10.1021/jp5021017.

Zhang, W.; Li, Y.; Zhu, L.; Liu, X.; Song, C.; Li, X.; Sun, X.; Fang, J. A PTB7-Based Narrow Band-Gap Conjugated Polyelectrolyte as an Efficient Cathode Interlayer in PTB7-Based Polymer Solar Cells. Chem. Commun. 2017, 53 (12), 2005–2008. https://doi.org/10.1039/c6cc09274h.

Zhang, W.; Wang, Y. C.; Li, X.; Song, C.; Wan, L.; Usman, K.; Fang, J. Recent Advance in Solution-Processed Organic Interlayers for High-Performance Planar Perovskite Solar Cells. Adv. Sci. 2018, 5 (7). https://doi.org/10.1002/advs.201800159.

Zhang, Y.; Guo, X.; Su, W.; Guo, B.; Xu, Z.; Zhang, M.; Li, Y. Perylene Diimide-Benzodithiophene D-A Copolymers as Acceptor in All-Polymer Solar Cells. Org. Electron. 2017, 41, 49–55. https://doi.org/10.1016/j.orgel.2016.11.038.

Zhang, Z.-G.; Qi, B.; Jin, Z.; Chi, D.; Qi, Z.; Li, Y.; Wang, J. Perylene Diimides: A Thickness-Insensitive Cathode Interlayer for High Performance Polymer Solar Cells. Energy Environ. Sci. 2014, 7 (6), 1966. https://doi.org/10.1039/c4ee00022f.

Zhao, C. H.; Wakamiya, A.; Inukai, Y.; Yamaguchi, S. Highly Emissive Organic Solids Containing 2,5-Diboryl-1,4-Phenylene Unit. J. Am. Chem. Soc. 2006, 128 (50), 15934–15935. https://doi.org/10.1021/ja0637550.

Zhao, D.; Wu, Q.; Cai, Z.; Zheng, T.; Chen, W.; Lu, J.; Yu, L. Electron Acceptors Based on α-Substituted Perylene Diimide (PDI) for Organic Solar Cells. Chem. Mater. 2016, 28 (4), 1139–1146. https://doi.org/10.1021/acs.chemmater.5b04570.

Zhao, W.; Li, S.; Yao, H.; Zhang, S.; Zhang, Y.; Yang, B.; Hou, J. Molecular Optimization Enables over 13% Efficiency in Organic Solar Cells. J. Am. Chem. Soc. 2017, 139 (21), 7148–7151. https://doi.org/10.1021/jacs.7b02677.

Zhao, Z.; Deng, C.; Chen, S.; Lam, J. W. Y.; Qin, W.; Lu, P.; Wang, Z.; Kwok, H. S.; Ma, Y.; Qiu, H.; et al. Full Emission Color Tuning in Luminogens Constructed from Tetraphenylethene, Benzo-2,1,3-Thiadiazole and Thiophene Building Blocks. Chem. Commun. 2011, 47 (31), 8847–8849. https://doi.org/10.1039/c1cc12775f.

Zhao, Z.; He, J.; Wang, J.; Chen, W.; Wang, N.; Zhang, Y.; Yang, R. A Water/Alcohol-Soluble Copolymer Based on Fluorene and Perylene Diimide as a Cathode Interlayer for Inverted Polymer Solar Cells. J. Mater. Chem. C 2015, 3, 4515–4521. https://doi.org/10.1039/C5TC00450K.

Zhong, Y.; Trinh, M. T.; Chen, R.; Wang, W.; Khlyabich, P. P.; Kumar, B.; Xu, Q.; Nam, C. Y.; Sfeir, M. Y.; Black, C.; et al. Efficient Organic Solar Cells with Helical Perylene Diimide Electron Acceptors. J. Am. Chem. Soc. 2014, 136 (43), 15215–15221. https://doi.org/10.1021/ja5092613.

Zhou, E.; Tajima, K.; Yang, C.; Hashimoto, K. Band Gap and Molecular Energy Level Control of Perylene Diimide-Based Donor–Acceptor Copolymers for All-Polymer Solar Cells. J. Mater. Chem. 2010, 20 (12), 2362. https://doi.org/10.1039/b923452g.

Zhou, Y.; Fuentes-hernandez, C.; Shim, J.; Meyer, J.; Giordano, A. J.; Li, H.; Winget, P.; Papadopoulos, T.; Cheun, H.; Kim, J.; et al. A Universal Method to Produce Low–Work Function Electrodes for Organic Electronics. Science (80-.). 2012, 873 (April), 327–332. https://doi.org/10.1126/science.1218829.

Zhou, Y.; Fuentes-Hernandez, C.; Shim, J.; Meyer, J.; Giordano, A. J.; Li, H.; Winget, P.; Papadopoulos, T.; Cheun, H.; Kim, J.; et al. A Universal Method to Produce Low-Work Function Electrodes for Organic Electronics. Science (80-.). 2012, 336 (6079), 327–332. https://doi.org/10.1126/science.1218829.

Zhu, Z.; Chueh, C. C.; Lin, F.; Jen, A. K. Y. Enhanced Ambient Stability of Efficient Perovskite Solar Cells by Employing a Modified Fullerene Cathode Interlayer. Adv. Sci. 2016, 3 (9), 1–7. https://doi.org/10.1002/advs.201600027.